DISCOVERY AND CHARACTERIZATION OF NOVEL BETA-LACTAMASE INHIBITORS

DISCOVERY AND CHARACTERIZATION OF NOVEL BETA-LACTAMASE INHIBITORS

By ANDREW M. KING, B.Sc.

A thesis submitted to the school of graduate studies in partial fulfillment of the requirements for the degree of Doctor of Philosophy.

McMaster University © Andrew M. King, May 2016.

DESCRIPTIVE NOTE

DOCTOR OF PHILOSOPHY (2016) McMaster University

(Chemistry and Chemical Biology) Hamilton, Ontario, Canada

TITLE: Discovery and Characterization of Novel Beta-lactamase Inhibitors

AUTHOR: Andrew M. King, B.Sc. (McMaster University)

SUPERVISOR: Dr. Gerard D. Wright

NUMBER OF PAGES: xiii, 228

ABSTRACT

The discovery of antibiotics and their subsequent clinical use has had a tremendous and beneficial impact on human health. The β-lactam antibiotics, which include penicillins, cephalosporins, carbapenems, and monobactams, constitute over half of the global antibiotic market. However, like all antibiotics, the β-lactams are susceptible to bacterial antibiotic resistance. One of the most disconcerting manifestations of bacterial resistance to β-lactam antibiotics is the evolution and dissemination of β-lactamases, enzymes able to chemically inactivate β-lactam antibiotics. These resistance determinants are the key contributing factor to extensively-drug resistant Gram-negative pathogens, for which we are already bereft of chemotherapeutic treatment options in some cases.

The coadministration of a β-lactamase inhibitor (BLI) with a β-lactam antibiotic is a proven therapeutic strategy to counter β-lactamase expression. Unfortunately, the emergence of both serine β-lactamases (SBLs) that are resistant to BLIs and metallo-β-lactamases (MBLs), which are intrinsically resistant to BLIs due to a discrete mechanism of β-lactam hydrolysis, threaten the efficacy of combination therapy. Notwithstanding this bacterial adaptation, the discovery and development of novel BLIs is an attractive strategy to evade resistance, as evidenced by the recent clinical approval of the diazabicyclooctane (DBO) SBL inhibitor, avibactam.

Herein, I describe efforts directed at understanding the mechanism of avibactam SBL inhibition. Furthermore, DBO derivatives are shown to display bifunctional properties in inhibiting both β-lactamases and the targets of β-lactam antibiotics, the penicillin-binding proteins. In addition to understanding the enzymology and chemical biology of DBOs, I describe two screening campaigns directed towards discovering inhibitors of MBLs, an unmet clinical need. Using target and cell-based screening of both synthetic and natural product chemical libraries, a fungal natural product inhibitor of clinically relevant MBLs was discovered and characterized.

This study expands our understanding of the mechanisms by which DBOs can be used to combat extensively drug-resistant Gram-negative pathogens. It also describes the discovery of a new natural product MBL inhibitor using a workflow that should be amenable to other resistance determinants. It's hoped that these studies can contribute meaningfully to countering antibiotic resistance observed in clinical settings.

ACKNOWLEDGEMENTS

My PhD supervisor, Dr. Gerry Wright, has been a constant source of inspiration and guidance for me during the tenure of graduate study. I've had the privilege of meeting a number of creative, learned, motivated, and passionate people since I decided to pursue a career in science. However, in addition to these qualities, you possess an uncompromising work ethic and integrity coupled with raw intelligence that I've always admired. Thank you for giving me the opportunity to be a part of your lab and for always pushing multidisciplinary science. It's no surprise that the members of the Wright lab past and present have been an absolute pleasure to work alongside as well. I'm indebted to you all for discussion, collaboration, and guidance. I'm particularly grateful to members of the lab and Institute for Infectious Disease Research who contributed to my early learning and skills development. To Dr. Kalinka Koteva and Dr. Wenliang Wang, for always being available to help with equipment and methodology associated with synthetic and natural products chemistry. To Linda Ejim, who has always been incredibly helpful with any questions I have in the lab. To Dr. Geoff Tranmer, for showing me the practicals of organic chemistry and for insightful discussions. I would also like to thank the members of my committee, Dr. Fred Capretta and Dr. Nathan Magarvey, for their guidance through graduate studies. A special thanks must go to Dr. Murray Junop, whose love and excitement for science got me hooked early on in undergrad, no doubt setting me on my current path.

I've had the good fortune to be blessed with a number of collaborations and in particular would like to thank my 'brother', Dr. Dustin King. I only hope that my future collaborations can be as productive and enjoyable as ours during these past few years. I must thank Dr. Tom Parr, Jr. for getting the both of us involved in the avibactam project. I also thank the other people and professors with whom I've had the chance to collaborate significantly: Dr. Kalinka Koteva, Dr. Wenliang Wang, Dr. Sarah Reid-Yu, Sarah Lal, Dr. Shawn French, Dr. Brian Coombes, Dr. Eric Brown, Dr. Fred Capretta, and Dr. Natalie Strynadka. I would like to thank the Canadian Institutes for Health Research for awarding me a doctoral fellowship.

Graduate school has only taken up 99% of my time and the other 1% has been important in shaping who I am as a person and complementing the science life. Thanks to all my friends in Hamilton but in particular the people I've played soccer and music with. Honeybadgers, we never won the championships but we did beat the Red Devils. 'nuff said. Too many thanks must go out to all the musicians I've had the chance to record, perform, and get down with. The past five years wouldn't have been half as exciting and fulfilling without you all!

Finally and most importantly, I'd like to thank my family for their love and support through my whole life. My brother, David, and sister, Sandra, who I don't get to see as much as I used to but never feel the time between. To my father, Stephen, for always motivating me to do better and my mother, Susan, for her unconditional love and encouragement. I dedicate this work to you all.

TABLE OF CONTENTS

LIST OF FIGURES

Chapter 1

Chapter 2

Chapter 3

Chapter 4

Chapter 5

Chapter 6

LIST OF TABLES

Chapter 1

Chapter 2

Chapter 3

Chapter 4

Chapter 5

LIST OF ABBREVIATIONS

6-APA	6-aminopenicillanic acid
7-ACA	7-aminocephalosporanic acid
AADC	Aromatic L-amino acid decarboxylase
ACE	Angiotensin-converting enzyme
AMA	Aspergillomarasmine A
ASU	Asymmetric unit
BLI	β-lactamase inhibitor
BSA	Bovine serum albumin
CRE	Carbapenem-resistant Enterobacteriaceae
CCC	Canadian Compound Collection
CHAPS	3-[(3-cholamidopropyl)dimethylammonio]-1-propanesulfonate
CLS	Canadian Light Source
CLSI	Clinical Laboratory Standards Institute
DCM	Dichloromethane
DMSO	Dimethyl sulfoxide
EDTA	Ethylenediaminetetraaceticacid
ESBL	Extended-spectrum β-lactamase
FIC	Fractional inhibitory concentration
FPI	Fedora Pharmaceuticals Inc.
HEPES	4-(2-hydroxyethyl)-1-piperazineethanesulfonic acid
HNA	L-Histidine β-naphthylamide
HTS	High-throughput screening
IPTG	Isopropyl β-D-1-thiogalactopyranoside
ICP-MS	Inductively coupled mass spectrometry
LC-MS	Liquid chromatography-mass spectrometry
L-DOPA	L-3,4-dihydroxyphenylalanine
MBL	Metallo-β-lactamase
MES	2-(N-morpholino)ethanesulfonic acid
MIC	Minimum inhibitory concentration
PAINS	Pan Assay INterference compoundS

PG	Peptidoglycan
PBP	Penicillin binding protein
PCR	Polymerase chain reaction
PDB	Protein Data Bank
PMB	Para-methoxybenzoate
RND	Resistance-Nodulation-Division
SBL	Serine β-lactamase
SAR	Structure-activity relationship
WT	Wild-type

CHAPTER ONE

INTRODUCTION

A Preamble on Antibiotic Resistance

Antibiotic resistance has emerged as a multifaceted and ever-changing threat facing the modern world. Defined simply, antibiotic resistance is the ability of a microorganism to overcome an antimicrobial drug that was originally effective for treatment of infections caused by it. While this is a useful functional definition in the context of human health, its anthropocentric view skirts acknowledging the powerful forces of evolution, microbial physiology, and chemistry that underpin what we observe as the phenomenon of antibiotic resistance. Microorganisms, in particular the soil-dwelling actinomycetes, are prolific producers of antimicrobial compounds and humans have exploited this propensity in the discovery of many life-saving drugs, particularly during the "golden era" of antibiotic discovery (Figure 1-1) (Brown and Wright, 2016). Indeed, antibiotics and associated resistance determinants have existed long before we knew of them (D'Costa et al., 2011). This is a consequence of the link between microbial biosynthesis of antibiotics and the expression of genes able to confer a resistance phenotype to any given antibiotic, usually found clustered together in the genome of producing bacteria (Cimermancic et al., 2014). Furthermore, the abundance of proto-resistance elements (direct precursors to resistance elements) that must exist in nature ensures that microbes have a vast reservoir of chemical transformations at their disposal even if they are not linked to biosynthetic gene clusters (Morar and Wright, 2010; Spanogiannopoulos et al., 2014). Spellberg summarized the situation appropriately: "We will never 'defeat' microbes with antibiotics. There is no 'endgame' - resistance is inevitable." (Spellberg, 2014).

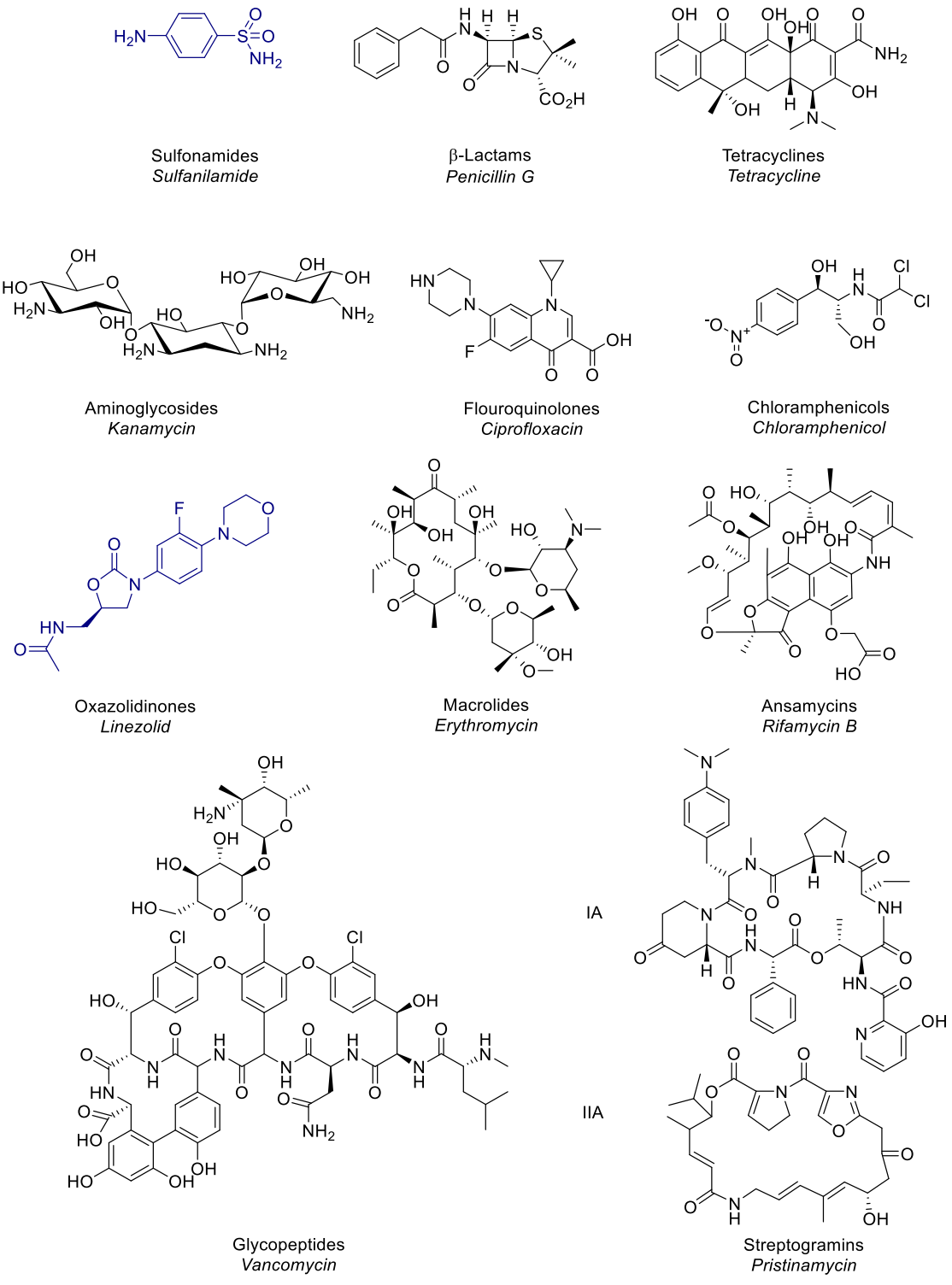

Figure 1-1. Antibiotic scaffolds discovered during the "golden era" of antibiotic discovery. Classes of synthetic origin coloured in blue, all others are natural products. Adapted from (Brown and Wright, 2016)

There may be no endgame in this struggle, however there are most certainly strategies and tactics we can adopt to minimize casualties on our side of the conflict. While it may be argued that we cannot unambiguously link mass transfer of resistance determinants from environmental to pathogenic bacteria we encounter in hospital- or community-acquired infections, evidence is mounting to support this notion (Forsberg et al., 2012). Accordingly, the agricultural misuse of antibiotics should give pause for thought; in 2010, the United States administered 13 million kilograms of antibiotics to animals (Spellberg et al., 2013). There is, without question, the need for antibiotic use in agriculture, however the amount and selection of antibiotic used must be chosen judiciously. The recent reports of a colistin resistance determinant, *mcr-1*, discovered in animals and human beings serves to underline this point (Liu et al., 2015). Colistin is an antibiotic of last resort in the treatment of life-threatening extensively drug-resistant Gram-negative pathogens but the global agricultural use is estimated at over 11 million kilograms. It is perhaps unsurprising that we have observed widespread resistance only several years after colistin was introduced as an antibiotic of last resort for human disease.

Although the amounts of antibiotics administered to people is a fraction of that given to animals at 3 million kilograms (Spellberg et al., 2013), this too has consequences. Antibiotics acting as selective pressures on microorganisms in hospital settings (and sometime community settings) has led to the emergence of an assortment of different pathogenic bacteria able to evade antibiotics, notably the "ESKAPE" pathogens: ***E****nterococcus faecium*, ***S****taphylococcus aureus*, ***K****lebsiella pneumoniae*, ***A****cinetobacter baumannii*, ***P****seudomonas aeruginosa*, and ***E****nterobacter spp.* (Boucher et al., 2009). The

extent of mortality and morbidity associated with ESKAPE infections in modern times stands in sharp contrast to the opinions of many medical professionals in the mid-twentieth century (although it would seem that the famous William H. Stewart "close the book on infectious diseases" urban myth has been debunked) (Spellberg and Taylor-Blake, 2013). The relative contributions of shifting policies, pharmaceutical industry withdrawal, and medical hubris to our current quagmire of resistance is beyond the scope of this work but has been reviewed by Spellberg, as referenced above.

Given that we are locked in an arms race with bacteria for the foreseeable future it is imperative to both understand the molecular mechanisms by which bacteria acquire and utilize resistance determinants and to go one step further to test the hypothesis of whether we can leverage molecular understanding to generate chemotherapeutic solutions (De Pascale and Wright, 2010; Wright, 2011). As demonstrated by the diverse chemical structures shown in Figure 1-1, there exists a dizzying array of mechanisms by which bacteria can evade the toxic effects of antibiotics. There is much to be learned and exploited from any given antibiotic family and paired array of resistance determinants.

Having laid the larger contextual framework of antibiotic resistance and its implications, the specific topic of this dissertation will now be discussed: the β-lactam antibiotics and β-lactamases. β-lactam antibiotics (Figure 1-2) are far and away the most widely consumed antibiotic class in the world with cephalosporins and broad-spectrum penicillins alone comprising 55% of global consumption (Figure 1-3) (Van Boeckel et al., 2014). Accordingly, the number of unique β-lactamases, enzymes able to confer resistance

to β-lactam antibiotics, discovered in the clinic have been increasing exponentially since the 1980s and now number over 1300 (Bush, 2013c).

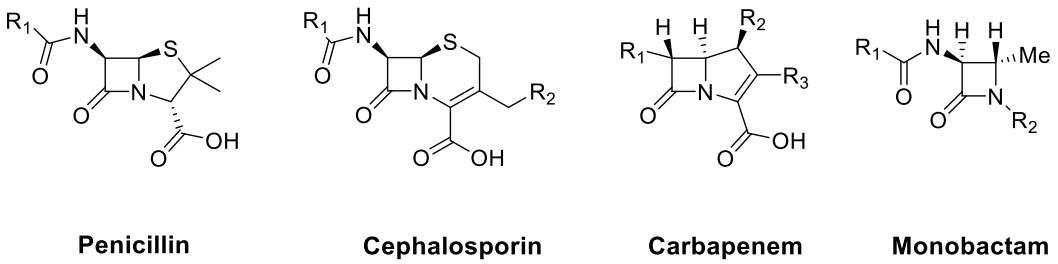

Figure 1-2. Chemical scaffolds of the main β-lactam families.

Therefore the pertinent questions to ask are: why are the β-lactam antibiotics so successful? Why do such an overwhelming number of β-lactamases exist in the clinic? Lastly, what can be done to counter the emergence of β-lactamase-mediated resistance to this class of antibiotic?

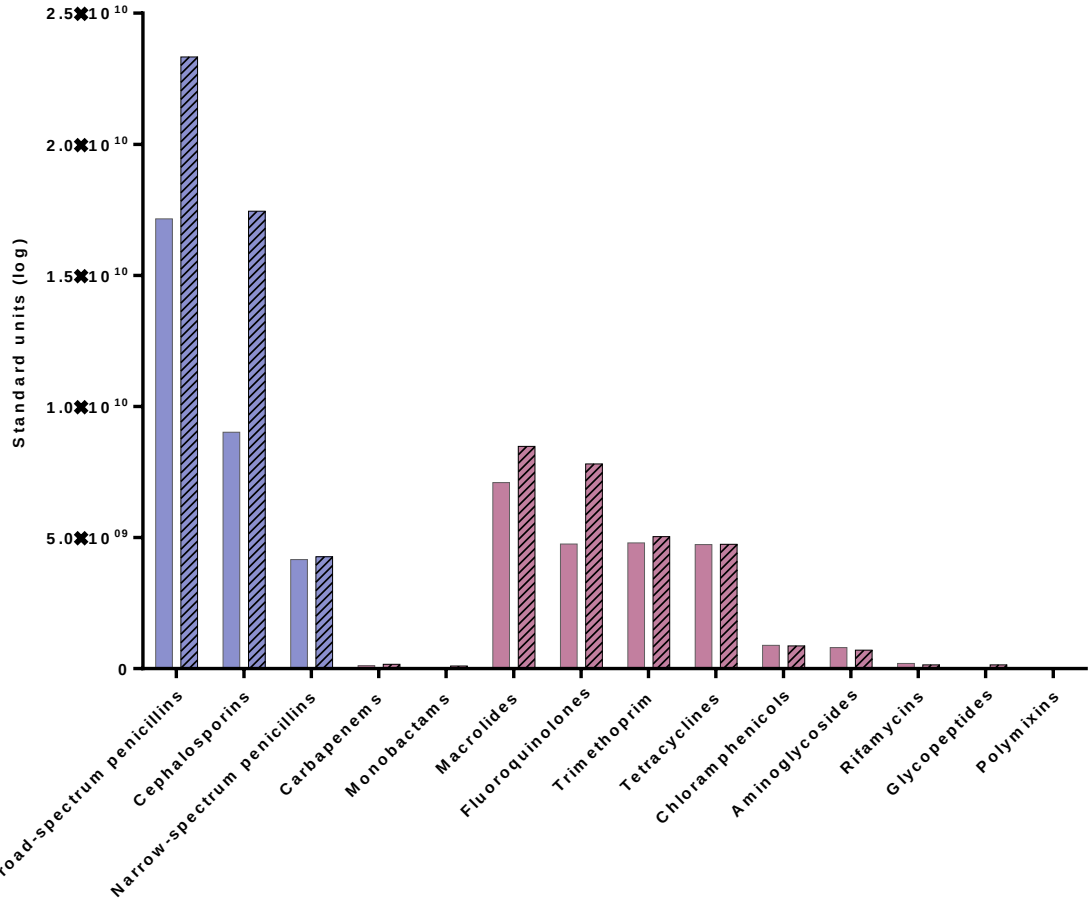

Figure 1-3. Global antibiotic consumption. Standard units are defined as a single dose unit. Clear bars are data for 2000, patterned bars for 2010. Shaded in blue are the β-lactam antibiotics, all others are in red. Adapted from Van Boeckel *et al.* (2014).

A brief history of penicillin

The penicillin story begins with the Alexander Fleming, then working in London, serendipitously discovering that a *Penicillium* mold contaminant (originally identified as *Penicillium notatum* but later classified as *Penicillium chrysogenum* (Samson et al., 1977)) could create zones of growth inhibition on plates of *Staphylococcus.* Having studied the effects of bacterial lysis extensively (Fleming, 1922), he realized that the mold must have been producing a lytic substance, which he named 'penicillin'. Fleming subsequently showed in a 1929 publication that the mold could be subcultured and fermentation broths yielded bacteriolytic activity with low toxicity when injected in mice (Fleming, 1929). However, it wasn't until the early 1940s that Ernst Chain, Howard Florey, and associates working at the University of Oxford published methods for preparation of suitable quantities for small human clinical trials (Abraham et al., 1941; Chain et al., 1940). Even with a suitable method of preparation it took almost another decade for the structure of penicillin G to be solved via x-ray crystallography and eventually published (Figure 1-4A) (Crowfoot, 1949). It should be noted here that those working in Oxford had been isolating penicillin F (Figure 1-4C) while those in America were working with penicillin G. The different products were a result of fermentative growth additives; in this case the Americans added corn steep liquor, which contained phenylacetic acid (Abraham, 1987). The instability of penicillin F may have been a contributing factor to Fleming's early difficulties in purification.

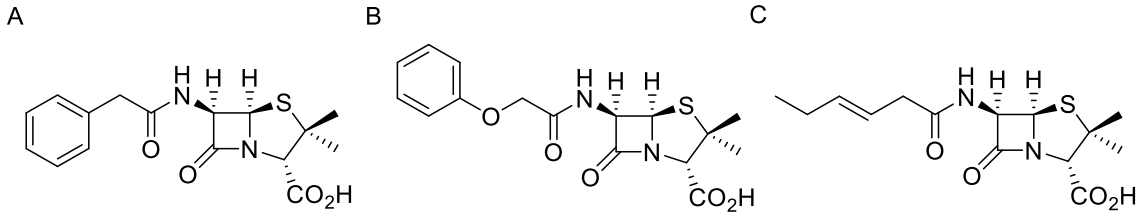

Figure 1-4. Chemical structures of A) penicillin G, B) penicillin V, and C) penicillin F

The importance of penicillin to the history of medicine cannot be understated. It was the first example of a chemotherapy able to kill bacteria *in vivo* while avoiding significant metabolism and toxicity. Penicillin paved the way for the antibiotic era, in which the rates of death attributed to infection dropped from ~ 30 % to 4 % (Kardos and Demain, 2011). The semisynthetic expansion of penicillin coupled with related scaffold discovery (and analogous semisynthetic expansions) led to what we now know as the β-lactam antibiotic class.

Scaffold discovery and semisynthetic modifications of β-lactam antibiotics

Optimization of penicillin fermentation conditions was underway during the 1950s at Beecham Research Laboratories. Co-discoverer of penicillin Ernst Chain, acting as a consultant, suggested that useful derivatives of penicillin could be generated by the modification of the acyl side chain of penicillin. He also suggested that the fermentation of a precursor lacking the acyl chain, which could then be modified chemically, was a logical method to obtain derivatives as well. The same researchers at Beecham were able to identify a deacylase from *Streptomyces lavendulae* that acted on penicillin V (Figure 1-

4), which enabled the generation of 6-aminopenicillanic acid (6-APA). This discovery enabled the generation of nearly 30 semisynthetic penicillins, including methicillin, ampicillin, and piperacillin (Figure 1-5) (Rolinson, 1998). Some of these, like methicillin, have been categorized as "narrow spectrum", meaning they have activity against a select number of pathogens, or vice versa as "broad spectrum".

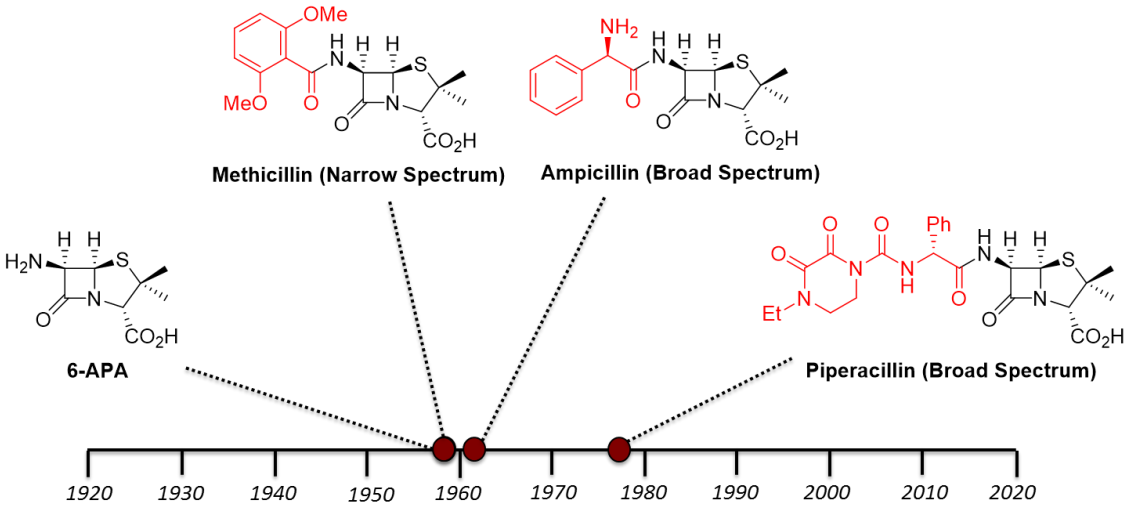

Figure 1-5. A representative timeline of semisynthetic penicillin development. Colored sections of molecules indicate sites of semisynthesis. Circles marks the approximate dates when penicillins were first reported.

This process was not limited to the penicillins. The discovery of cephalosporin C and its structural elucidation (Figure 1-6) (Abraham and Newton, 1961; Newton and Abraham, 1956) naturally prompted the generation of 7-aminocephalosporanic acid (7-ACA) (Morin et al., 1962)

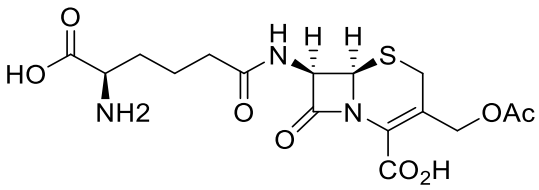

Figure 1-6. Chemical structure of cephalosporin C

Semisynthetic modification of 7-ACA has led to similar expansions of the cephalosporin class (Figure 1-7) (Clarke et al., 1985; Heymes et al., 1977; Nagarajan et al., 1971). These have been categorized as "generations", with each generation generally having expanded spectra of activity and resistance to hydrolysis by β-lactamases, enzymes able to inactivate β-lactam antibiotics, while taking into account safety and stability (Bryskier, 2000)

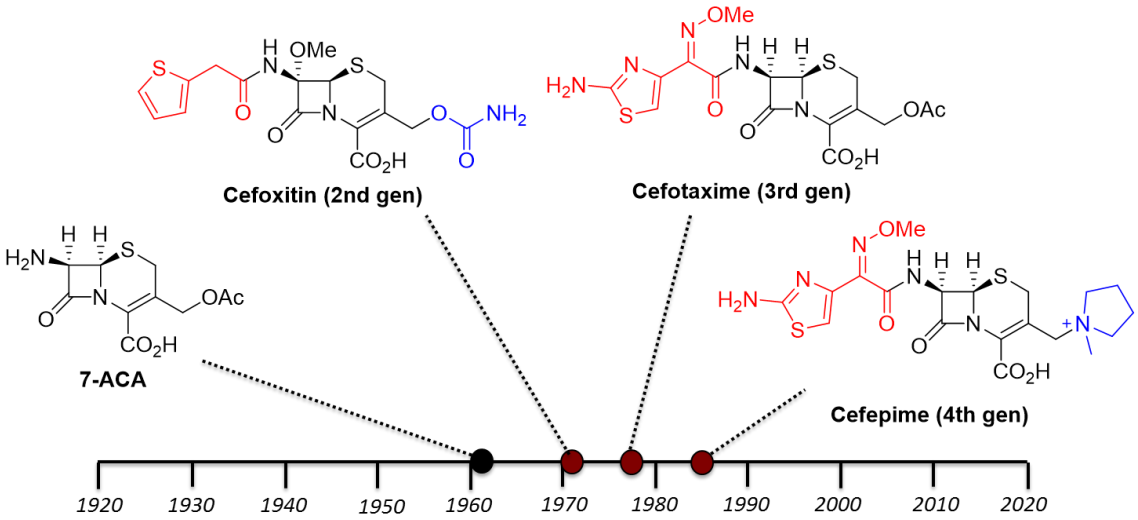

Figure 1-7. A representative timeline of semisynthetic cephalosporin development. Colored sections of molecules indicate sites of semisynthesis. Circles marks the approximate dates when cephalosporins were first reported.

The discovery of the carbapenem, thienamycin (Kahan et al., 1979), the monobactam, nocardicin A (Matsuura et al., 1993b) (Figure 1-8), and subsequent semisynthesis on these natural product scaffolds completed the set of the four main families of β-lactam antibiotics in current clinical use (Figure 1-1).

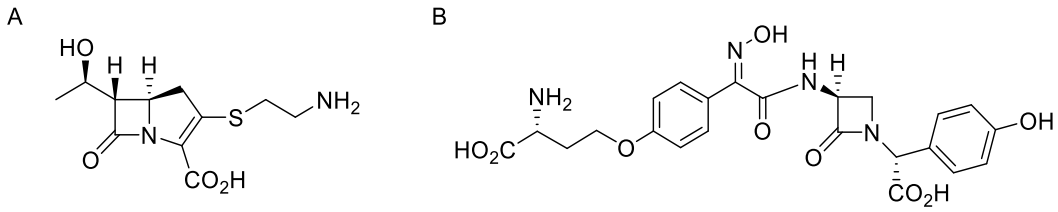

Figure 1-8. Chemical structures of A) thienamycin and B) nocardicin A

Penicillin-binding proteins: Sensitivity and resistance

Although it had been suggested in 1946 that penicillin might target cell wall integrity, it was Tipper and Strominger who posited that the antibiotic mechanism of action lay in the structural similarity of the molecule to acyl-D-alanyl-D-alanine (Figure 1-9), lending it properties as an inhibitor of cell wall biosynthesis (Tipper and Strominger, 1965).

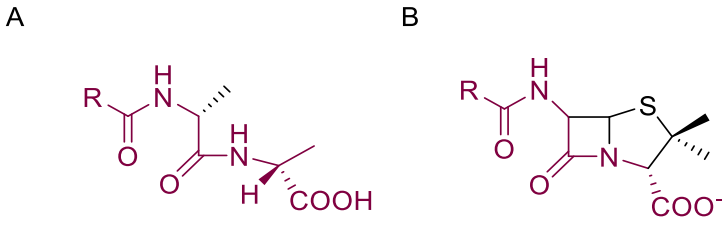

Figure 1-9. Chemical structures of A) D-alanyl-D-alanine and B) penicillin. Colored sections of molecules indicate structural similarity

Later, it was shown that penicillins and cephalosporins covalently modify bacterial transpeptidases, enzymes responsible for cross-linking peptidoglycan in the cell wall (Waxman et al., 1980). It was also demonstrated that penicillins bind multiple enzymes, the so-called "penicillin-binding proteins" (PBPs) (Spratt, 1980). We now know that all bacteria possess multiple PBPs, which are numbered sequentially based on observed molecular weight (high to low). Some PBPs are monofunctional transpeptidases and others are bifunctional, possessing a penicillin-insensitive transglycosylase domain in addition to a penicillin-sensitive transpeptidase domain (Ghuysen, 1991). It is also clear that different β-lactam antibiotics possess varying specificities for PBPs, leading to predictable morphological defects based on the specific cell wall biosynthetic role of any given PBP (Tipper, 1985). More recently, it has been shown that the arrest of cell wall synthesis via PBP inhibition leads to a complex cascade of events, including futile cycling of cell wall synthesis and degradation that depletes cell resources (Cho et al., 2014).

Bacteria have evolved numerous mechanisms of resistance to β-lactams, including: altered PBP expression (for example *S. aureus* PBP2a, a PBP insensitive to β-lactams), porin deletion (a broad range of Gram-negative pathogens), and expression of efflux systems (for example MexAB-OprM) (Fisher et al., 2005). However, it is the evolution and spread of β-lactamases that poses the greatest threat to the utility of the β-lactam antibiotics.

β-lactamases: Past to present

Problems with bacterial contamination ruining large scale fermentations of *Penicillium* in the late 1930s prompted investigation into these "penicillin-destroying cultures" (McQuarrie et al., 1944). Abraham and Chain took these cultures of *Bacillus coli,* now known as *Escherichia coli* (*E. coli*) that were not killed by penicillin and determined the activity to be enzymatic, therefore naming the protein "penicillinase" and publishing these results in *Nature* well before penicillin was available for use as a drug (Abraham and Chain, 1940). Since that initial discovery more than 1300 β-lactamases have been reported (Bush). Currently two main systems are used for classification of β-lactamases, one first proposed by Richard Ambler in 1980 (Ambler, 1980) and the other by Karen Bush in 1988 (Bush, 1988). The Ambler system uses amino acid sequence to define molecular phylogenies and groups β-lactamases into four broad classes: A, B, C, and D. The A, C, and D classes are serine β-lactamases (SBLs) while the class B enzymes are metallo-β-lactamases (MBLs). All MBLs use one or two zinc ions to activate bulk solvent as nucleophile (Figure 1-10A) while SBLs use an active site serine as nucleophile (Figure 1-10B). Both mechanisms converge on a ring opened inactivated drug product.

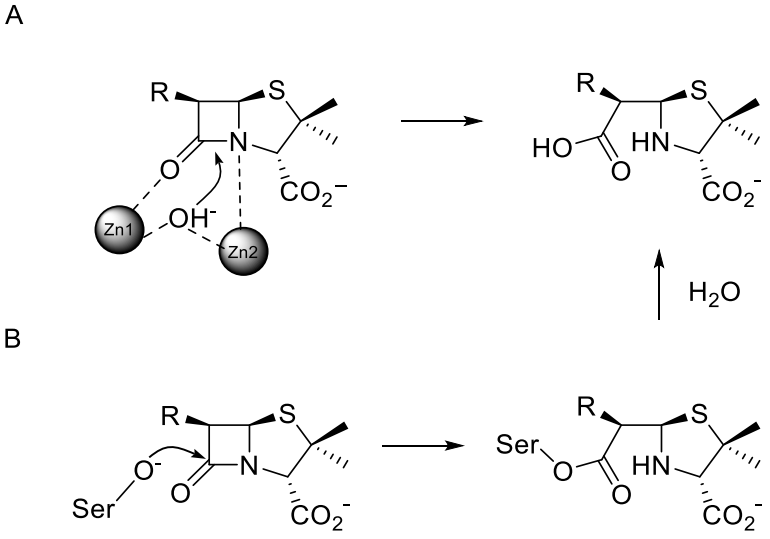

Figure 1-10. Generalized mechanisms of β-lactamase-mediated hydrolysis of penicillin. A) Metallo-β-lactamases utilize two (sometimes one) zinc ions and bulk solvent as nucleophile. B) SBLs utilize an active site serine as nucleophile. Both mechanisms converge on production of a ring-opened penicilloic acid.

Table 1-1. Representative enzymes grouped according to Ambler and Bush-Jacoby classification schemes.

Ambler Class	Bush-Jacoby Group	Penicillinase activity	Cephalosporinase activity	ESBL activity	Carbapenemase activity	Monobactamase activity	Clavulanic acid sensitive	Enzyme
A	2a	Y	N	N	N	N	Y	PC1
	2b	Y	Y	N	N	N	Y	TEM-1
	2be	Y	Y	Y	N	Y	Y	CTX-M-15
	2br	Y	Y	N	N	N	N	TEM-30
	2c	Y	N	N	N	V	V	PSE-4
	2ce	Y	N	N	N	N	Y	RTG-4
	2e	Y	Y	Y	N	V	Y	L2
	2f	Y	Y	Y	Y	Y	Y	KPC-2
B	3a	Y	Y	Y	Y	N	N	NDM-1
	3b	Y	N	N	Y	N	N	CphA
C	1	N	Y	N	N	N	N	AmpC
	1e	N	Y	Y	N	N	N	CMY-37
D	2d	Y	N	N	N	N	V	OXA-10
	2de	Y	Y	V	N	N	V	OXA-11
	2df	Y	N	Y	N	N	N	OXA-48

*Adapted from (Bush, 2013a). Y = yes, N = no, V = variable

The Bush-Jacoby system (as it is now known) rather uses substrate and inhibitor profiles to define groups and subgroups. Table 1-1 shows how both classifications organize the many different types of β-lactamase we know. More complete details can be found in a recent review (Bush, 2013a). Table 1.1 also serves as a useful reference for understanding the substrate/inhibition profiles of certain clinically relevant β-lactamases. For instance, the extended-spectrum β-lactamases (ESBLs) are enzymes able to hydrolyze oximino-cephalosporins (cefotaxime, ceftriaxone, ceftazidime) (Bradford, 2001), amongst other substrates, and fall under Group 2be. Serine carbapenemases and metallo-carbapenemases fall under Groups 2f and 3a, respectively (Bush, 2013b).

Each Ambler class will be discussed separately, beginning with an overview of structure and mechanism. This will then be followed by epidemiology and clinical relevance, a logical order since it is often subtle structural changes leading to distinct substrate profiles that bring certain β-lactamase variants to our attention.

Ambler class A β-lactamases

The best known class A β-lactamase is TEM-1 (Figure 1-11), so-called because it was first isolated in 1965 from a Greek patient named "Temoniera" (Datta and Kontomichalou, 1965). Since that initial isolation, at least 223 TEM variants have been observed in the clinic as of 2015. Together with the closely related SHV (sulfhydryl-variable, 193 variants) they comprise the best characterized SBL group and are predominantly found in *E. coli* and *K. pneumoniae* (Bush). Ultrahigh resolution structures for representatives of both enzymes have been published (Minasov et al., 2002; Nukaga et al., 2003). These structures exhibit the canonical class A fold consisting of an α/β domain and an α domain (Figure 1-10A). The substrate binding site is located at the domain interface and contains common motifs found in class A enzymes (TEM numbering): Ser70XaaXaaLys, Ser130XaaGln, Glu166XaaXaaLeuGln, Lys234ThrGly (Figure 1-10B) (Bush, 2013a). These residues are required for both half reactions involved in SBL-mediated β-lactam hydrolysis; the first being acylation and second, deacylation. Ser70 is the nucleophilic serine acylated by β-lactams and catalysis is driven by the coordination of other invariant active site residues: Lys73, Ser130, and Glu166. Lys234 acts to coordinate the substrate carboxyl through electrostatic interactions while the backbone amides of

residues Ser70 and Ala237 (the "oxyanion hole") provide hydrogen bonding interactions with the β-lactam carbonyl (Figure 1-11) (Fink and Page, 2012).

There are two proposed mechanisms for the acylation half reaction of class A β-lactamases. The first envisions Glu166 acting as general base to abstract a proton from Ser70 via a bridging water molecule (Nukaga et al., 2003) while the second gives Lys73 the role of general base in direct activation of Ser70 (Strynadka et al., 1992). Collapse of the tetrahedral intermediate is dependent upon N-protonation and Ser130 is widely accepted as the general acid responsible for this (Figure 1-12). It is possible that both mechanisms act in concert and may contribute to the diversity of substrates these enzymes can hydrolyze (Meroueh et al., 2005).

Deacylation occurs via Glu166 again acting as general base to deprotonate a water molecule, which then attacks the acyl-enzyme intermediate. Collapse of the tetrahedral intermediate likely comes about with Ser130 shuttling the proton from Lys73 (Figure 1-13). Alternatively it may be Lys234 shuttling the proton from Lys73, or both acting in concert (Fink and Page, 2012).

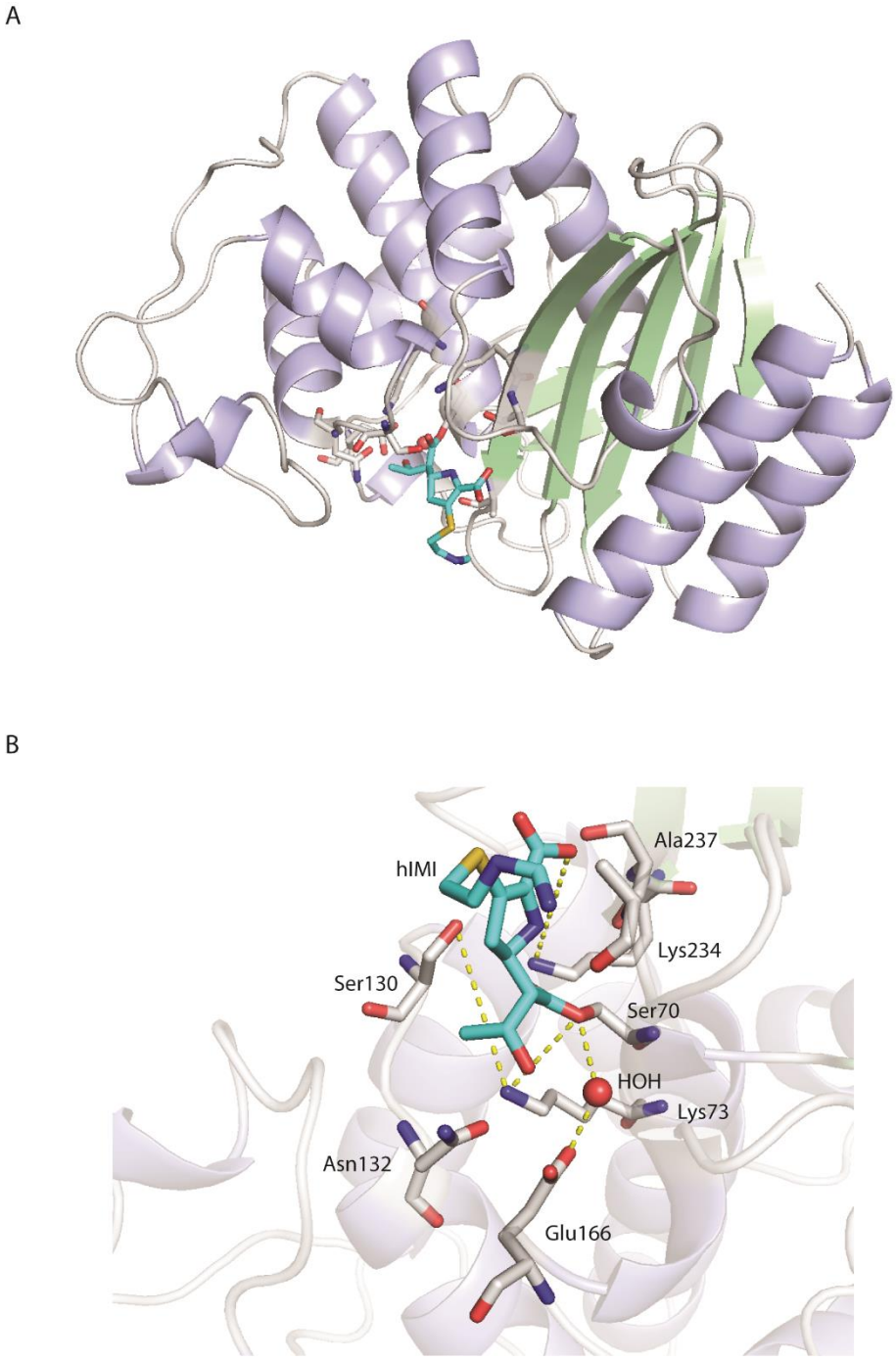

Figure 1-11. Structure of TEM-1, a class A SBL, in complex with hydrolyzed imipenem. A) Overall fold and B) active site are shown. Active site residues are show in white sticks and hydrolyzed imipenem as teal sticks for the carbon backbone. Individual atoms are colored red (oxygen), blue (nitrogen), and yellow (sulfur). PDB code 1bt5.

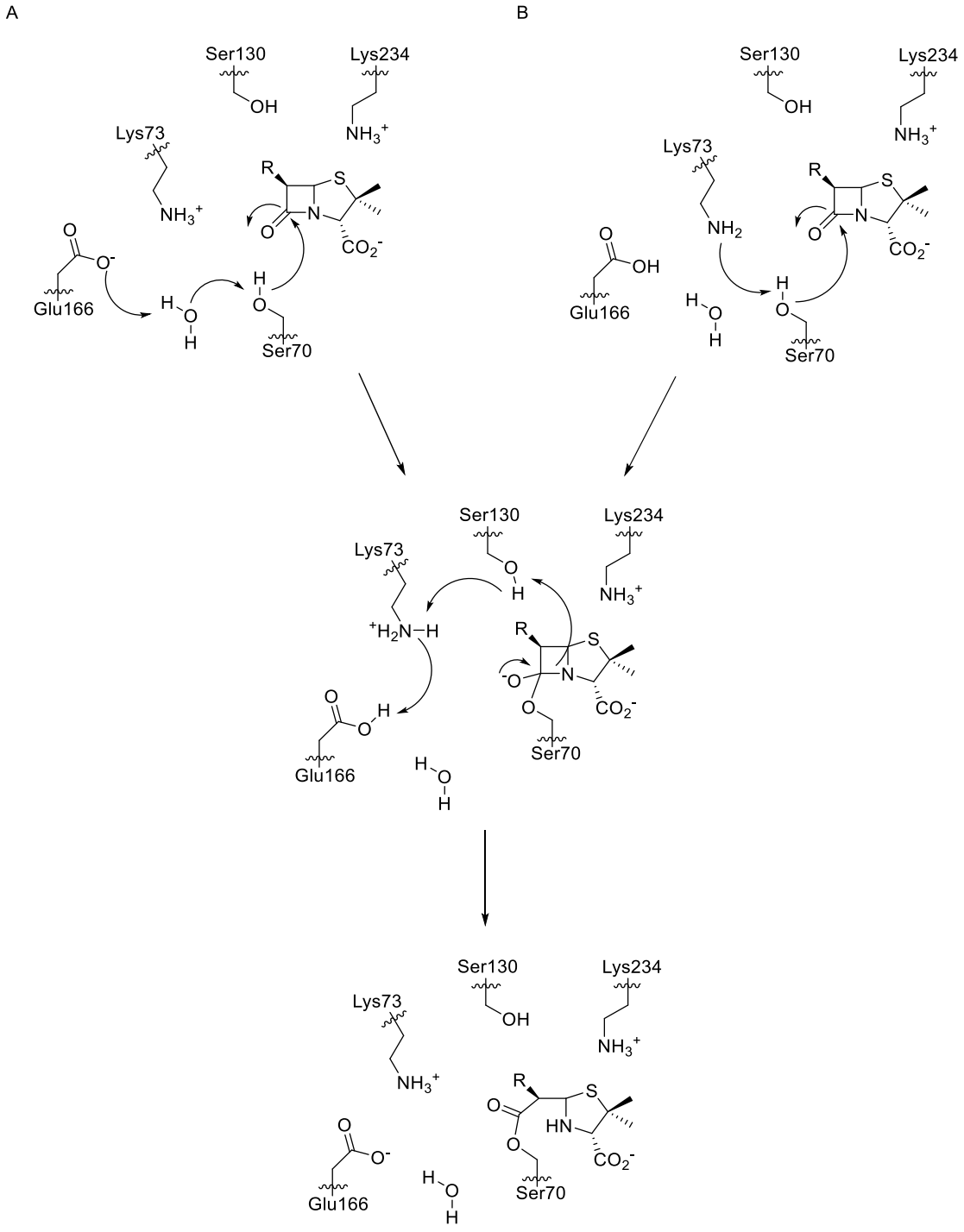

Figure 1-12. Proposed mechanisms for class A SBL acylation half reaction. A) Glu166 acts as general base to deprotonate Ser70 via a water molecule or B) Lys73 acts as general base to deprotonate Ser70 directly. Adapted from (Meroueh, Fisher et al. 2005).

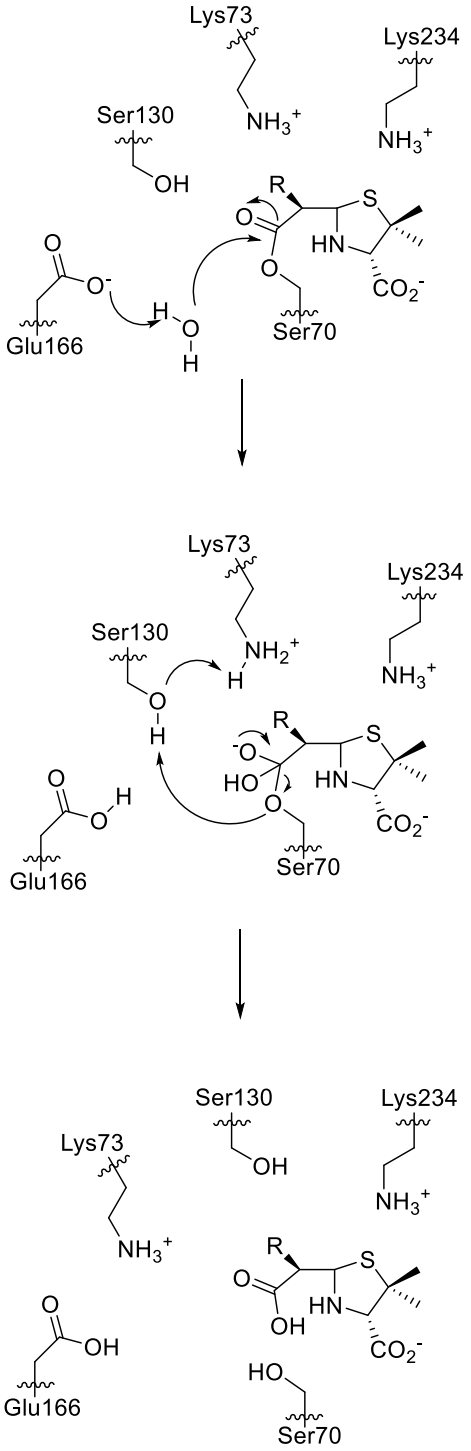

Figure 1-13. Proposed mechanisms for class A SBL deacylation half reaction.

The development and widespread use of expanded-spectrum cephalosporins like the oximino-cephalosporins that are stable against TEM-1 and SHV-1 (Neu, 1982) led predictably to the enrichment of ESBL alleles in bacterial populations. The first instance of a ESBL can be traced back to 1985 with the discovery of SHV-2 from a *K. pneumoniae* strain isolated in Germany (Kliebe et al., 1985). The other clinically significant class A ESBLs are the CTX-M-type, which did not arise from point mutations in other plasmid-borne β-lactamases but rather mobilized from environmental *Kluyvera spp.* (Canton et al., 2012). In 1989, CTX-M-1 was isolated in Germany and was named for its activity against cefotaxime (Bauernfeind et al., 1990). Since then, this class, too, has exploded in number with 172 variants reported (Bush). The CTX-M enzymes have become a global problem due to their ability to hydrolyze a wide range of β-lactam substrates, genetically associated resistance determinants, and the rapidity with which they evolve and spread under antibiotic pressure (Hawkey and Jones, 2009). The global emergence of a clonal isolate of *E. coli* (ST131) expressing CTX-M-15 is a particularly alarming development in ESBLs (Peirano and Pitout, 2010).

The other class A enzymes garnering attention are the serine carbapenemases, enzymes able to hydrolyze and confer resistance to carbapenems (Queenan and Bush, 2007). In particular, the KPC-type enzymes pose significant threats due to their rapid international spread and association with high mortality rates (Munoz-Price et al., 2013). KPC-1 was first discovered in the United States but later renamed KPC-2 as it was discovered that the KPC-1 sequence contained an error (Yigit et al., 2001b, 2008). The KPC enzymes have broad substrate specificity, are found on plasmids with broad host

range, and pathogens expressing them are often only treatable by polymyxins or tigecycline (Bush and Fisher, 2011).

Ambler class C β-lactamases

The original "penicillinase" reported by Abraham and Chain in 1940 was, in fact, what we now refer to as AmpC in *E. coli*. This class of enzyme is found chromosomally-expressed in a wide range of bacteria spanning two phyla, three classes, and 6 orders, although predominantly proteobacterial (Jacoby, 2009). Like Class A enzymes, class C SBLs like AmpC possess two domains, one α domain and one α/β domain (Figure 1-14A). They similarly possess active site motifs including: Ser64XaaXaaLys, Tyr150XaaGln, and Lys315SerGly (Figure 1-14B) (Bush, 2013a). Crystal structures of hydrolyzed substrate in the active site clearly show that Ser64 is the nucleophile that undergoes acylation but subsequent steps in the mechanism are not as well understood as in the class A enzymes. For the acylation half reaction, it's thought that Tyr150 acts as general base, via activation of a neutral Lys67 and perhaps the participation of Asn152 in a hydrogen bonding network, to deprotonate Ser64 (Chen et al., 2009; Wouters and Bauvois, 2012). The deacylation step is thought to proceed in similar fashion with Tyr150 and/or Lys67 active as general base but there is also the possibility for the participation of a charge relay between Asn152, Lys67, Tyr150, and Lys315 (Fink and Page, 2012).

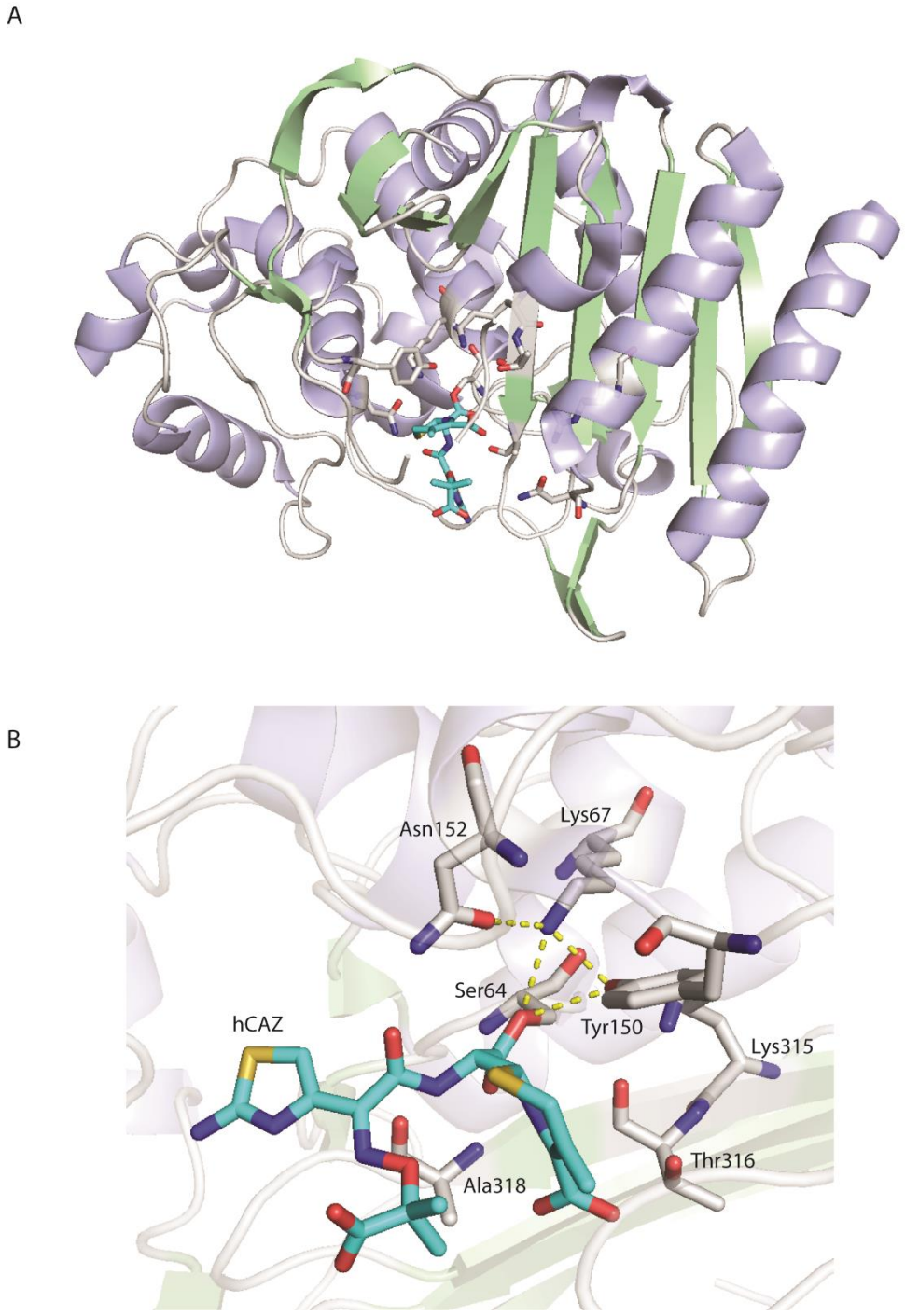

Figure 1-14. Structure of AmpC from *E. coli*, a class C SBL, in complex with hydrolyzed ceftazidime. A) Overall fold and B) active site are shown. Active site residues are show in white sticks and hydrolyzed ceftazidime as teal sticks for the carbon backbone. Individual atoms are colored red (oxygen), blue (nitrogen), and yellow (sulfur). PDB code 1iel.

In terms of clinical relevance, when chromosomal AmpC-expressing *E. cloacae* acquire mutations leading to the hyperproduction of this enzyme, increased mortality and morbidity is observed (Cosgrove et al., 2002). The same trend is observed in *E. coli*, *Acinetobacter spp.*, and *P. aeruginosa*: mutations or insertions that affect the regulation and lead to overexpression of normally modestly expressed AmpC leads to heightened and stable resistance phenotypes (Jacoby, 2009). AmpC overproduction coupled with overexpression of Resistance-Nodulation-Division (RND) efflux pumps and OprD porin loss can even lead to carbapenem resistance (Rodríguez-Martínez et al., 2009).

Plasmid-borne class C enzymes are also becoming commonplace. CMY-type β-lactamases are most commonly found in Enterobacteriaceae are widespread internationally, confer similar resistance phenotypes to ESBLs, and are not inhibited by typical β-lactamase inhibitors (Sidjabat et al., 2009). More worrying is the increasing frequency of CMY enzymes, like CTX-M, being found associated with resistance to quinolones and aminoglycosides (Hawkey and Jones, 2009); most alarming of all is finding them being associated with $bla_{\text{NDM-1}}$-carrying plasmids (Kumarasamy et al., 2010).

Ambler class D β-lactamases

The class D OXA (originally named for the ability to hydrolyze oxacillin) enzymes are a massive and diverse family, with over 498 sequence variants described (Bush). Despite this variation one can still define common folds and active site motifs as in the class A and C β-lactamases. OXA-type enzymes exhibit a similar fold as other SBLs, possessing one predominantly α domain and one α/β domain (Figure 1-15A). The active site lies in between the two domains and has common sequence motifs of Ser67XaaXaaLys, Ser115XaaVal, and Lys205ThrGly (OXA-10 numbering) (Figure 1-15B) (Kerff et al., 2012). The OXA enzymes are distinguished from other SBLs by the presence of a carbamylated ("carboxylated") Lys67 (Golemi et al., 2001). This residue likely acts as general base in deprotonating Ser67 for attack on the β-lactam carbonyl. In analogous fashion to the class A enzymes, Ser115 protonates the lactam nitrogen, leading to cleavage. Carbamylated Lys67 likely acts as general base by deprotonating water in the deacylation step as well. This mechanism has practical implications as assays must be set up such that Lys67 is fully carboxylated, else biphasic kinetics can be observed (Golemi et al., 2001). With such structural variation it's difficult to keep track of the molecular properties and significance of certain variants. The largest group of OXA enzymes are the OXA-51-like β-lactamases. Unlike the early identified OXA enzymes, which were plasmid encoded and found in Gram-negative bacteria (Sykes and Matthew, 1976), these enzymes are found chromosomally in *A. baumannii*, with at least 95 variants identified (Evans and Amyes, 2014).

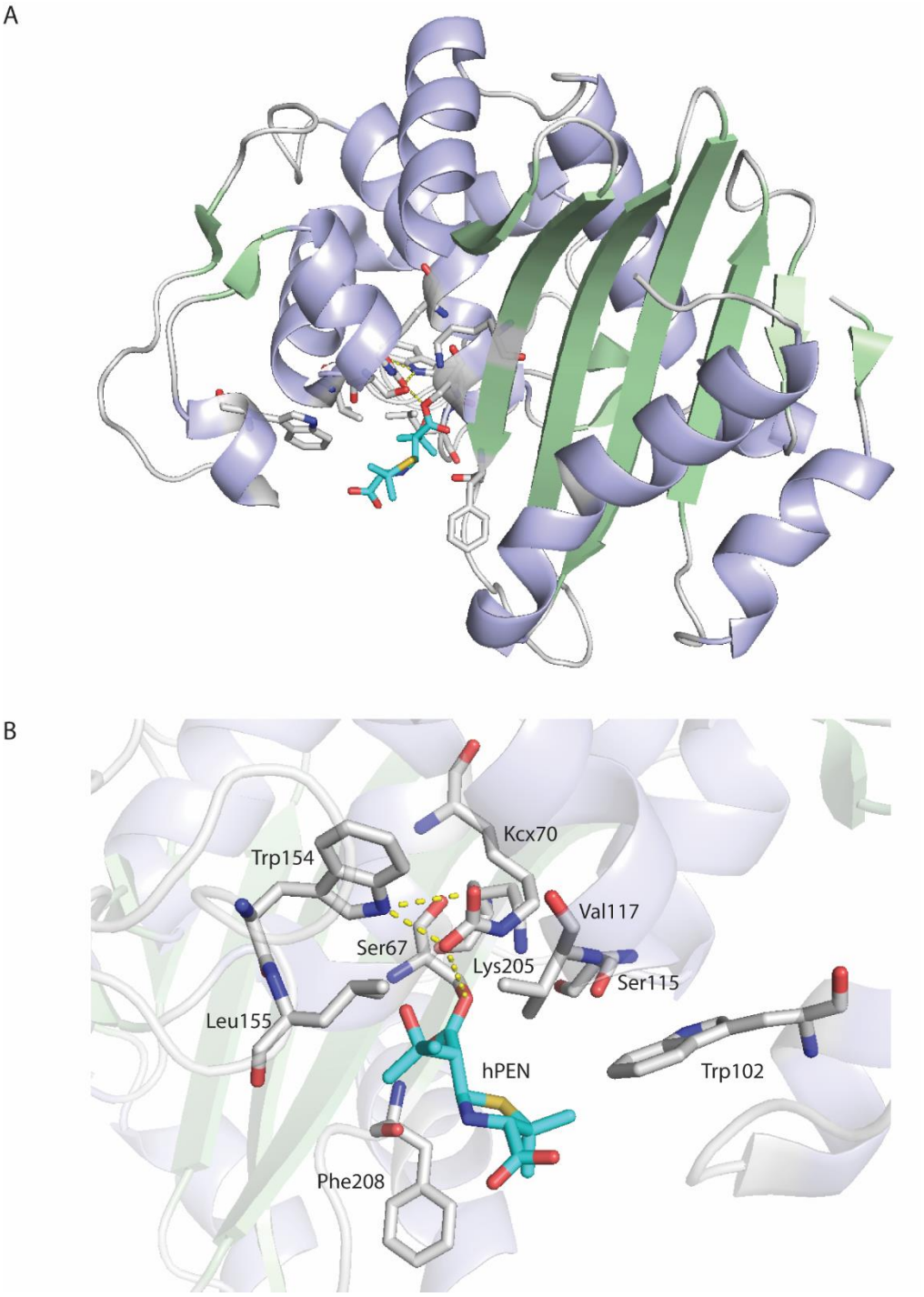

Figure 1-15. Structure of OXA-10, a class D SBL, in complex with hydrolyzed penicillin. A) Overall fold and B) active site are shown. Active site residues are show in white sticks and hydrolyzed penicillin as teal sticks for the carbon backbone. Individual atoms are colored red (oxygen), blue (nitrogen), and yellow (sulfur). PDB code 1k54.

Here, representatives from the three Bush-Jacoby subgroups will be discussed (Table 1-1). OXA-10 belongs to group 2d and like other members, has increased activity against methicillin and oxacillin and is poorly inhibited by clavulanic acid; these enzymes also possess rather narrow substrate specificity. This enzyme, found on plasmids in *P. aeruginosa* was originally named PSE-2 (*P*-specific enzyme) but then renamed OXA-10 after its discovery in Enterobacteriaceae (Hall et al., 1993). The same publication also reported the discovery of OXA-11, which through two point mutations had acquired ESBL spectrum. This enzyme is joined by many others in group 2de and their molecular epidemiology and phylogenetic groupings has been well summarized in a comprehensive review on OXA-type β-lactamases (Evans and Amyes, 2014). The last functional group, 2df, will be discussed in the context of OXA-48, a carbapenemase that was first identified in a strain of *K. pneumoniae*. The detection of this plasmid-borne OXA-type carbapenemase stood in sharp contrast to the other carbapenemases in this family, which had remained chromosomally encoded in *A. baumannii* (Poirel et al., 2004). The recent publication of the structure of OXA-48 also shows that it shares more in common with OXA-10-type β-lactamases than other OXA carbapenemases, suggesting a distinct evolutionary route. In particular, the lack of a hydrophobic bridge across its active site, suggesting, as with most β-lactamases, that it is subtle changes in active site architecture that confer substrate specificity (Docquier et al., 2009).

Ambler class B β-lactamases

The first class B β-lactamase, or MBL, identified was BcII from *Bacillus cereus*. Differential penicillinase and cephalosporinase activity had been observed during preparations of the enzyme from this organism. The varying activity remained poorly understood until Kuwabara and Abraham reported the isolation of two different aptly named β-lactamases, BcI and BcII with penicillinase and cephalosporinase activity, respectively (Kuwabara and Abraham, 1967). BcII belongs to the MBL subclass B1, to which other MBL families like IMP (Resistance to imipenem), NDM (New Delhi MBL), SPM (Sao Paolo MBL), and VIM (Verona integron-encoded MBL) also belong. There are two other subclasses, B2 and B3, and these are summarized in Table 2-1 (Bush, 2013a).

Table 1-2. Ambler class B subclasses

Subclass	Substrates	Number of Zn^{2+} active site atoms	Zn1 coordinating residues	Zn2 coordinating residues	Representative families
B1a	All β-lactams except monobactams	2	His His His	Asp Cys His	BcII, IMP, VIM SPM, CcrA
B1b	All β-lactams except monobactams	2	His His His	Asp Cys His	NDM[a]
B2	Carbapenems	1	N/A	Asp Cys His	CphA, Sfh-1
B3	All β-lactams except monobactams	2	His His His	Asp His His	L1, FEZ-1 CAU-1

[a] Based on low sequence homology to other class B1 enzymes

*Adapted from (Bush, 2013a).

BcII has since been the model enzyme for studying MBLs but as a whole the class B enzymes had remained something of an academic pursuit (despite incredibly broad substrate hydrolysis profiles) because they were chromosomally confined and not often a clinical concern. This changed in 1991 when IMP-1, a plasmid-borne MBL, was isolated from *P. aeruginosa* in Japan (Watanabe et al., 1991). The subsequent discoveries of other acquired resistance determinants VIM-1 (Lauretti et al., 1999) and NDM-1 (Kumarasamy et al., 2010) in Gram-negative pathogens have brought us to a new era where MBLs are perhaps the most ominous threat to our arsenal of β-lactam antibiotics (Cornaglia et al., 2011). For this reason, focus here will be on subclass B1 in terms of structure, mechanism, and clinical relevance.

All MBLs possess an αβ/βα fold and at the interface of the β sheets a catalytic center with one or two zinc ions (Figure 1-16A). In B1 MBLs, there are two zinc binding sites, with the first zinc, Zn1, coordinated by three His residues and the second, Zn2, coordinated by Asp, Cys, and His residues (Figure 1-16B). The active site cleft is flanked by loop regions that modulate the conformational shape of the cleft and this flexibility no doubt affords the enzymes broad substrate specificity by allowing for variable side chains (Bebrone et al., 2012; King and Strynadka, 2011). The actual mechanism by which B1 MBLs catalyze lactam ring hydrolysis is still a matter of open debate. The single most confounding factor in mechanistic studies is the simple question: what is the occupancy of zinc-binding sites in these enzymes?

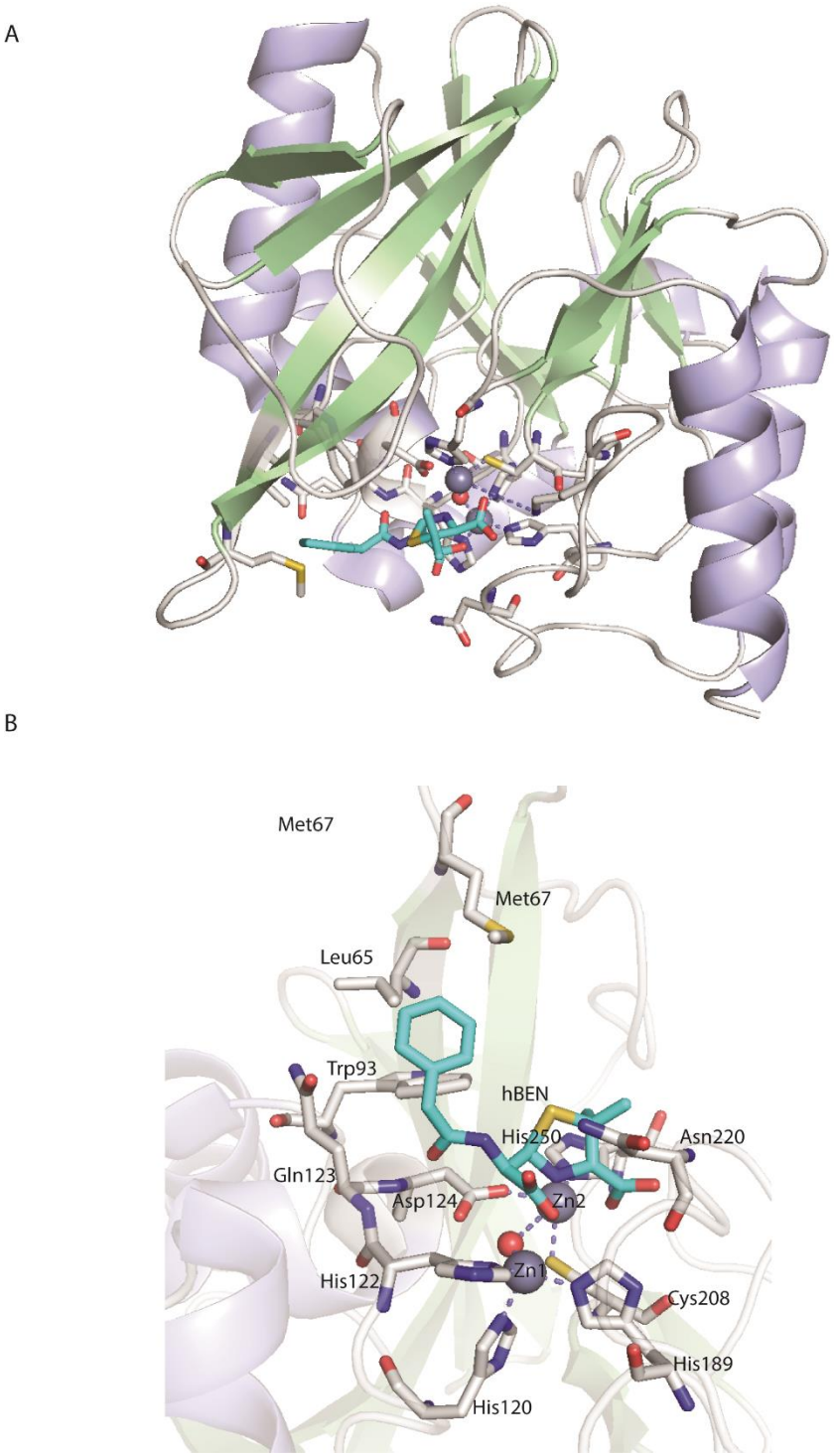

Figure 1-16. Structure of NDM-1, a class B MBL, in complex with hydrolyzed benzylpenicillin. A) Overall fold and B) active site are shown. Active site residues are show in white sticks and hydrolyzed imipenem as teal sticks for the carbon backbone. Individual atoms are colored red (oxygen), blue (nitrogen), and yellow (sulfur). PDB code 4eyf

One of the earliest studies showed some critical properties of the BcII enzyme. The enzyme could be substituted with different metal cofactors (Co^{2+}, Cd^{2+}, Mn^{2+}, Hg^{2+}) and retain activity, albeit reduced. Furthermore, the enzyme displayed zinc-dependent activity profiles, with a maximum rate of hydrolysis for both benzylpenicillin and cephalosporin C requiring millimolar $ZnSO_4$ concentrations (Davies and Abraham, 1974). The variation in rate with respect to Zn^{2+} concentrations is intriguing when one considers that NDM-1 activity is affected likewise (Thomas et al., 2011), however IMP-1 is not significantly affected by Zn^{2+} (Laraki et al., 1999). Furthermore, the two zinc binding sites in BcII have been shown to have different dissociation constants: Zn1 is in the picomolar range whilst Zn2 is in the micromolar range (Wommer et al., 2002). Taken together, these data suggest that either the IMP-1 enzyme is active as a mono-zinc variant or that the Zn2 site has a significantly lower dissociation constant relative to BcII or NDM enzymes. A crystal structure for IMP-1 shows two zinc ions in the active site (Concha et al., 2000), however, the closely related SPM-1 displayed a similar kinetic profile and bound 1.5 equivalents of Zn^{2+} (Murphy et al., 2003) but then was later crystallized with a single Zn^{2+} in the active site (Murphy et al., 2006). It comes as no surprise that the literature is replete with mechanisms proposing one and/or two zinc ions in catalysis, and/or the additional involvement of an active site Asp residue acting as general base (Badarau and Page, 2006; Bebrone et al., 2012; Tioni et al., 2008; Wommer et al., 2002). Recently, the Vila group suggested that the evolution of a Cys ligand tunes metal binding affinity in the zinc-deficient environment of the bacterial periplasm, asserting that the di-zinc variant is active (Gonzalez et al., 2012).

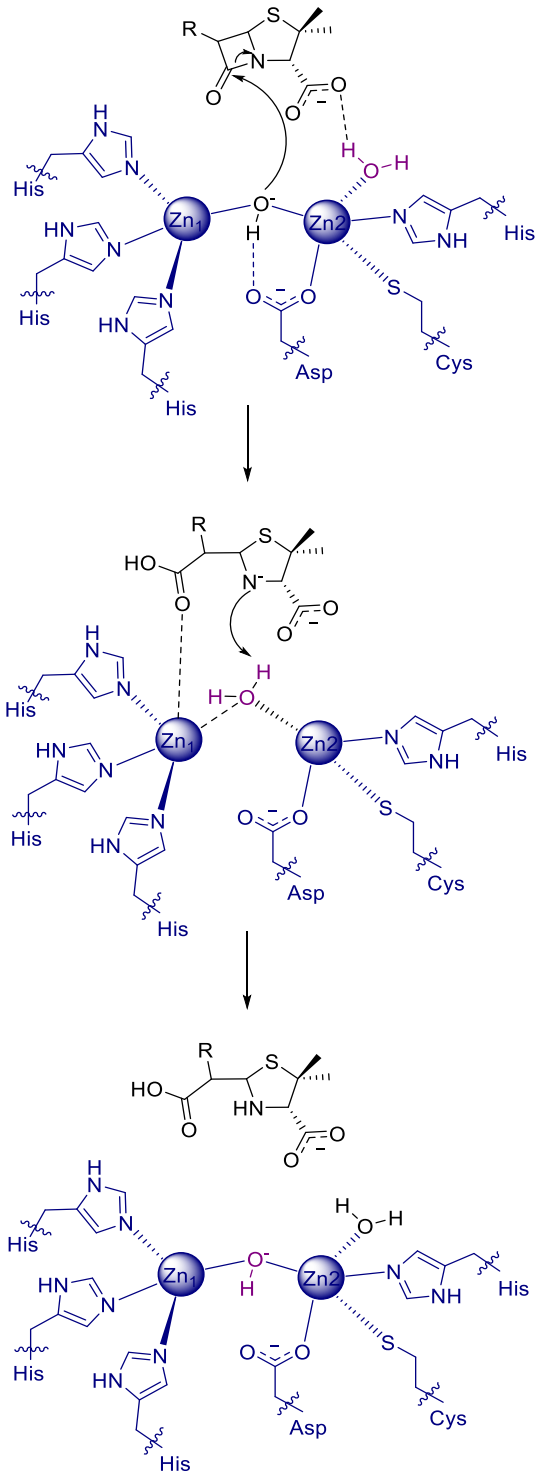

Figure 1-17. Proposed mechanisms for class B1 MBL hydrolysis of β-lactams. Adapted from (Simona, Magistrato et al. 2009)

Taken together, a likely mechanism for MBL hydrolysis is shown in Figure 1-17 (Llarrull et al., 2007; Simona et al., 2009). Zn2 participates in substrate carboxylate binding via a water molecule to orient the substrate optimally for binding (although the presence of a water molecule may vary between substrates, and could rather be direct interaction). Zn1 is responsible for activation of the nucleophilic water (hydroxide) in addition to acting as a Lewis acid coordinating to the carbonyl oxygen and lowering electron density at the carbonyl carbon, facilitating nucleophilic addition. Evidence for the generation of a negatively charged nitrogen stabilized by Zn acting as a Lewis acid has been published, albeit with the resonance stabilized, chromogenic substrate, nitrocefin (Wang et al., 1999; Yang et al., 2012). N-protonation, likely from the water molecule originally bound by Zn2 (now shifted to bridge the zincs), then completes the catalytic cycle (Meini et al., 2015).

At the time of writing there have been 52 IMP, 46 VIM, and 16 NDM variants reported (Bush). A recent review provides a thorough presentation of countries and organisms where acquired MBL variants were first detected (Cornaglia et al., 2011); here a brief summary of the IMP, VIM and NDM variants will be presented. In terms of molecular epidemiology, bla_{IMP} genes have been detected in a wide range of Gram-negative pathogens, in particular *P. aeruginosa*. These enzymes have traditionally been largely found in Japan and other East Asian regions, with IMP-1 being the most common variant (Zhao and Hu, 2011). VIM-type enzymes were originally endemic to Europe, in particular Mediterranean countries where they've been associated with nosocomial outbreaks (Mazzariol et al., 2011). The VIM variants have since spread throughout the rest of Europe, for instance nosocomial outbreaks of VIM-1-expressing *P. aeruginosa* in France (Corvec

et al., 2006). The two major variants, VIM-1 and VIM-2, seem to be more commonly associated with Enterobacteriaceae and *P. aeruginosa*, respectively (Mojica et al., 2015). The last major subgroup of acquired MBLs is the NDM family, which was first discovered in Enterobacteriaceae in the Indian subcontinent (Yong et al., 2009). Subsequent widespread detection in multiple strains of Enterobacteriaceae in clinical (Kumarasamy et al., 2010) and community (Walsh et al., 2011) settings was cause for international concern. Like other B1 enzymes, NDM-1 is able to hydrolyze a broad range of β-lactams, including carbapenems, but what was particularly striking with NDM-1 was the pan-resistant profile observed in isolates. This is a consequence of its association with multiple resistance determinants on both narrow and broad host-range plasmids, leading to rapid dissemination amongst a number of Gram-negative pathogens (Poirel et al., 2011). The lack of MBL inhibitors in clinical development makes the situation all the more frightening (Buynak, 2013). It stands to reason, however, that the development of an inhibitor effective against IMP, VIM, and NDM MBLs expressed in *A. baumannii*, *P. aeruginosa*, and Enterobacteriaceae could be combined with a carbapenem antibiotic for successful treatment of these extreme-drug resistant infections.

β-lactamase inhibitors

The first of two strategies to counter the expression of β-lactamases has culminated in the impressive array of β-lactam antibiotics, as described above. The second strategy involves the co-administration of a β-lactamase inhibitor (BLI) that can neutralize the function of β-lactamase activity. There are currently four BLIs approved for clinical use in the United States (Figure 1-18).

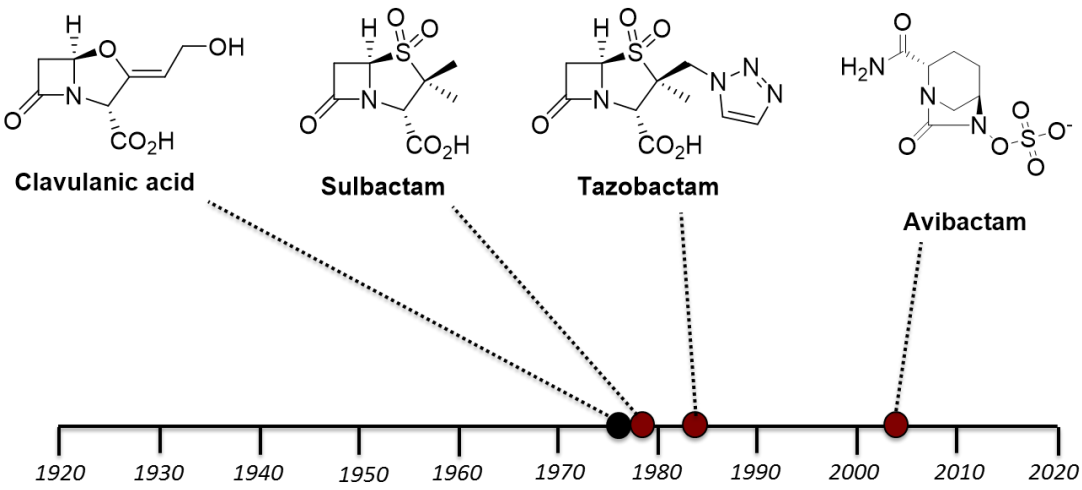

Figure 1-18. Timeline of BLI development. Circles marks the approximate dates when BLIs were first reported.

The early inhibitors, clavulanic acid, sulbactam, and tazobactam were discovered and developed in very similar fashion to the β-lactam antibiotics decades before. Clavulanic acid was discovered at Beecham pharmaceuticals as a natural product produced by *Streptomyces clavuligeris* (Reading and Cole, 1977). This molecule had poor antimicrobial activity but excellent inhibitory activity against penicillinases, displaying synergy with partner penicillin antibiotics (Neu and Fu, 1978). Soon after, it was

formulated with amoxicillin and marketed as Augmentin and has been a success in terms of treating patients and commercial revenue through to the 21st century (Walsh, 2003). The mechanism by which this "suicide inhibitor" irreversibly acylates its target has been reviewed elsewhere (Drawz and Bonomo, 2010b) but is summarized in Figure 1-20.

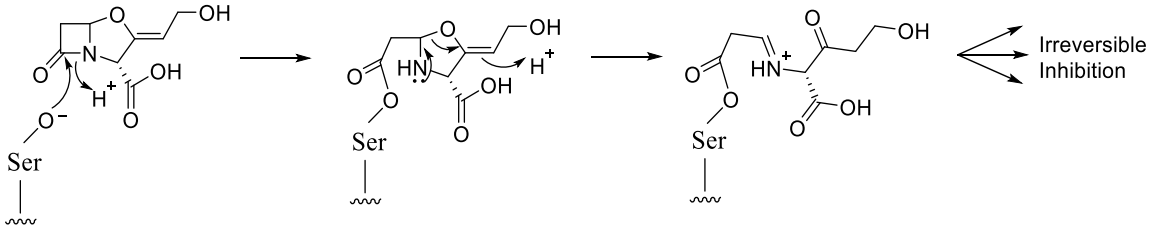

Figure 1-19. Simplified mechanism of SBL inhibition by clavulanic acid. Adapted from (Drawz and Bonomo, 2010b)

The success of clavulanic acid prompted the development of semisynthetic sulbactam and tazobactam (Figure 1-18) (Aronoff et al., 1984; English et al., 1978). Both have similar inhibition profiles of SBLs as clavulanic acid, however these derivatives, in particular tazobactam, did display better profiles of inhibition against class C enzymes, perhaps at the expense of ESBL TEM inhibition (Bush et al., 1993). Sulbactam is combined with ampicillin under the trade name Unasyn, which was developed in the late 1980s whereas tazobactam is combined with piperacillin under the trade name Zosyn in the United States.

There had been a significant gap in the development of BLIs until recently, with the clinical approval of avibactam, formerly NXL-104 (aka AVE1330A) (Figure 1-18). This BLI has modest antimicrobial activity but potent β-lactamase inhibitory properties. The

aim in developing NXL-104 was to develop an inhibitor with activity against class C β-lactamases and restore efficacy of 3rd generation cephalosporins (Pratt, 2012). Avibactam was indeed able to restore efficacy of ceftazidime against a panel of class A and class C-expressing Enterobacteriaceae (Bonnefoy et al., 2004). Avibactam was also shown to inhibit its targets through a unique covalent, reversible mechanism (Figure 1-20) (Ehmann et al., 2012a).

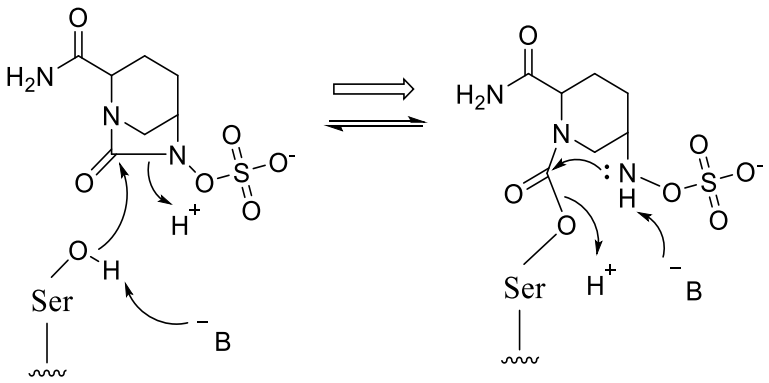

Figure 1-20. Simplified mechanism of SBL inhibition by avibactam. Adapted from (Ehmann et al., 2013b)

The same group at Astra Zeneca went on to characterize the inhibitory properties against a panel of SBLs from all three Ambler classes (Ehmann et al., 2013b). Avibactam demonstrated excellent inhibition of class A enzymes, although was slowly hydrolyzed by KPC-2, an observation that should be kept in mind when testing this and derivative molecules against other SBLs. It also displayed some good activity against class C enzymes, however the class D inhibition profiles were far more varied. On- and off-rates for the OXA enzymes were very slow, although this lead to an overall favorable

dissociation constant. Avibactam was recently approved for clinical use in combination with ceftazidime (Avycaz).

Discovery and characterization of novel β-lactamase inhibitors

Efforts to discover and bring to clinic novel β-lactamase inhibitors have intensified in recent years, highlighted by the recent approval of Avycaz (Buynak, 2013). It's clear that the rising tide of antibiotic resistance, in particular to the valuable β-lactam antibiotics, necessitates the discovery and optimization of new scaffolds. For nearly a century the combination of microbiology, natural product and synthetic chemistry, and enzymology has led to the development of life-saving β-lactam antibiotics and partner BLIs. It stands to reason that new inhibitor scaffolds can be discovered from natural products sources or from newly developed synthetic libraries. In particular, scaffolds with activity against Gram-negative pathogens expressing ESBLs and MBLs that are widely disseminated are needed to counter new resistance phenotypes. In this workflow new scaffolds require careful characterization of both *in vitro* enzymology and cell-based activity to inform subsequent derivatization. Therefore, this thesis aims to:

Research Aims

1. Characterize the mechanism of SBL inhibition of avibactam (Chapter 2)
2. Investigate synthetic derivatives of avibactam for their SBL and PBP inhibitory properties (Chapter 3)
3. Discover clinically relevant inhibitors of NDM-1 and associated MBLs (Chapters 4 and 5).

CHAPTER 2

MOLECULAR MECHANISM OF AVIBACTAM-MEDIATED BETA-LACTAMASE INHIBITION

CHAPTER 2 PREFACE

The work presented in this chapter was previously published in:

King, D.T.*, King, A.M.*, Lal, S.M., Wright, G.D. & Strynadka, N.C.J. Molecular Mechanism of Avibactam-Mediated β-Lactamase Inhibition. ACS Infectious Diseases 1, 175-184 (2015).

* These authors contributed equally

Copyright © American Chemical Society.

I co-authored this work with Dustin T. King. I conducted cloning, site-directed mutagenesis, protein purification, enzyme kinetics, and dynamic light scattering. S.M. Lal also conducted site-directed mutagenesis and protein purification of CTX-M-15 constructs.

Acknowledgements:

We thank beamline personnel of CMCF-2 at the Canadian Light Source synchrotron facility (Saskatoon, SK) for their assistance with data collection. We would also like to thank Dr. Alba Guarné, Monica Pillon, and Jeremy Caron for their assistance with DLS experiments.

ABSTRACT

Emerging β-lactamase-mediated resistance is threatening the clinical utility of the single most prominent class of antibacterial agents used in medicine, the β-lactams. The diazabicyclooctane avibactam is able to inhibit a wider range of serine-β-lactamases than has been previously observed with β-lactamase inhibitors such as the widely prescribed clavulanic acid. However, despite its broad-spectrum activity, variable levels of inhibition have been observed for the molecular class D β-lactamases. In order to better understand the molecular basis and spectrum of inhibition by avibactam we provide structural and mechanistic analysis of the compound in complex with important Class A and D SBLs. Herein, we reveal the 1.7 and 2.0Å resolution crystal structures of avibactam covalently bound to the class D β-lactamases OXA-10 and OXA-48. Furthermore, a kinetic analysis of key active site mutants for the class A β-lactamase CTX-M-15 allows us to propose a validated mechanism for avibactam mediated β-lactamase inhibition including a unique role for Ser130, which acts as a general base. This study provides molecular insights that will aid in the design and development of avibactam-based chemotherapeutic agents effective against emerging drug-resistant microorganisms

INTRODUCTION

The β-lactam antibiotics target the final synthetic step in peptidoglycan (PG) biogenesis, whereby they act as substrate analogues of the penultimate D-Ala-D-Ala on the PG stem peptide to inhibit the PBP-catalyzed transpeptidation of adjacent PG strands. The most clinically prevalent resistance mechanism to the β-lactams in Gram-negative bacteria is the expression of β-lactamase enzymes that hydrolyze the four membered lactam ring,

yielding an inactivated product. These enzymes are often encoded on readily transferable plasmids that facilitate their transmission throughout microbial populations (Bush, 2010).

The β-lactamases are often grouped into four distinct classes (A-D) based upon sequence homology (Bush, 2013a). The class A, C and D SBLs evolved from the PBP transpeptidases, and are the most clinically prevalent and employ an active site serine as a nucleophile in β-lactam hydrolysis. In contrast, the class B MBLs utilize active site zinc ions to mediate lactam bond fission. SBL catalyzed β-lactam hydrolysis occurs via the formation and subsequent hydrolysis of a serine-bound acyl enzyme intermediate. Despite having low overall sequence identity, amino acid sequence comparisons and structural analysis has identified three common active site motifs among the SBLs: motif (i) harbors the nucleophilic serine required for acylation (SXXK), motif (ii) is required for protonation of the β-lactam N4 nitrogen leaving group upon acylation (S/Y-X-N/V), and motif (iii) is involved in activation of the motif ii S/Y proton donor, and in substrate recognition and oxyanion stabilization (K/R-T/S-G) (Bush, 2013a). The class A enzymes have a conserved Glu166 (thought to be the general base required for activation of the catalytic water during hydrolytic deacylation), located in a region known as the Ω loop (residues 161-179). In contrast, the class D (OXA) enzymes lack the Ω loop Glu166 and instead involve a carboxylated lysine (i.e. lysine is reversibly modified with CO_2 at the ε amino group) in a SXXK motif, which is thought to play a dual role as the general base involved in both serine activation during acylation and in activation of the catalytic water during hydrolytic deacylation (Delmas et al., 2008; Golemi et al., 2001; Schneider et al., 2009).

To overcome SBL mediated resistance, three β-lactam-based inhibitors have been introduced into clinical practice in the late seventies and early eighties: clavulanic acid, sulbactam and tazobactam (Drawz and Bonomo, 2010b). These compounds are mechanism based, covalent inactivators that form a stable acyl-enzyme intermediate with the catalytic serine. At clinically used concentrations, the bound inhibitor hydrolytically deacylates, either directly or through a series of covalent intermediates, resulting in the eventual turnover of inactivated inhibitor and catalytically active enzyme (Helfand et al., 2003). Traditionally, these inhibitors target the class A β-lactamases and are clinically ineffective against strains harboring the emerging class C, and D SBL enzymes (Bebrone et al., 2010). Furthermore, there are now several class A β-lactamases that have evolved resistance to these compounds (e.g. inhibitor-resistant TEM and complex mutant TEM) (Cantón et al., 2008; Drawz and Bonomo, 2010b), making the development of novel inhibitors paramount.

Perhaps of greatest promise for the immediate future comes from the novel class of non-β-lactam based β-lactamase inhibitors termed diazobicyclooctanes (DBOs). These were originally designed in the late 1990's and display remarkably potent and broad-spectrum inhibition of SBLs. The DBO compound avibactam is currently in phase III clinical development as part of a combination therapy in conjunction with ceftazidime to treat complicated urinary-tract and intra-abdominal infections (Lagacé-Wiens et al., 2014). Ceftazidime-avibactam is active against the majority of Enterobacteriaceae, including multi-drug resistant strains, and importantly is effective against *P. aeruginosa* (Coleman, 2011). In animal models, avibactam-ceftazidime has been utilized to effectively treat ceftazidime-resistant Gram-negative bacterial septicemia, meningitis, pneumonia and

pyelonephritis. The avibactam-ceftazidime safety and tolerability in clinical trials has been outstanding, and there have been relatively few adverse drug affects documented (Coleman, 2011).

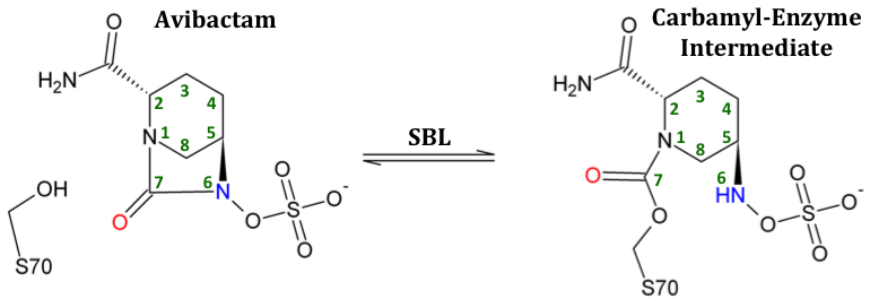

Figure 2-1. Avibactam-mediated reversible SBL inhibition

Although avibactam displays excellent inhibitory activity against the class A and C enzymes, more variable levels of inhibition have been observed towards the class D SBLs (Ehmann et al., 2013b). Avibactam forms a unique carbamyl linkage with the catalytic serine, which does not decompose via a hydrolytic mechanism as is true for the β-lactam based SBL inhibitors (Figure 2-1). Instead decarbamylation of avibactam occurs via recyclization of the DBO fused ring structure, re-forming the intact inhibitor that can then either re-carbamylate the same active site or be released into solution to inactivate subsequent SBLs (Ehmann et al., 2012b). The most common mechanism of resistance to ceftazidime-avibactam is the expression of β-lactamases that are unhindered by avibactam (for example, the MBLs and the majority of class D SBLs). Crystal structures of avibactam bound to the class A enzymes BlaC and CTX-M-15, the class C enzyme AmpC have recently been released (Lahiri et al., 2013), (Xu et al., 2012). Additionally, Lahiri and

colleagues recently reported the crystal structures of OXA-24 and OXA-48 bound to avibactam at 2.3 and 2.4Å resolution (Lahiri et al., 2014). However, the mechanism and roles of individual amino acids in SBLs that contribute to avibactam activity remain largely unresolved.

To address the underlying molecular details of avibactam inhibition, we have undertaken a multifaceted structural, kinetic and mutagenesis study on known targets. We have utilized the class A enzyme CTX-M-15 which is the most widely distributed extended-spectrum β-lactamase (ESBL) globally (Poirel et al., 2013) as a model enzyme. The universally conserved Ser130 acts both as a general acid during carbamylation and a general base during de-carbamylation in the avibactam recycling pathway. We further reveal the 2.0 and 1.7Å resolution crystal structures of avibactam covalently bound to the catalytic serine of the clinical variants, OXA-48 and OXA-10. The narrow spectrum oxacillinase OXA-10 is among the most prevalent class D enzymes in *P. aeruginosa* (Antunes et al., 2014), and the carbapenem hydrolyzing OXA-48 is prevalent in the emerging carbapenem resistant Enterobacteriaceae (CRE) (Ehmann et al., 2013b; Zhang et al., 2013). The data elucidate the active site features likely responsible for the variable inhibition observed for this class of SBL enzymes that uniquely relies on a post-translationally modified (carboxylated) lysine during catalysis.

MATERIALS AND METHODS

DNA manipulations and plasmid construction.

Primers used for polymerase chain reaction (PCR) DNA amplification and site-directed mutagenesis were purchased from MOBIX lab (McMaster University, Hamilton, ON, Canada) or Integrated DNA Technologies (IDT; Coralville, IA). The list of primer sequences used can be found in Supplemental Table 2-2. pET-28b(CTX-M-15), encoding mature CTX-M-15 (Q26-L288) was constructed by amplifying the *bla*$_{\text{CTX-M-15}}$ gene from *K. pneumoniae* strain H0142423 (Mt. Sinai hospital, New York, NY) using CTX-M-15 F and CTX-M-15 R primers and cloning into pET-28b. pET-28b(KPC-2) and pET-28b(OXA-48) were constructed by cloning the mature genes into pET-28b. Genes were synthesized by IDT.

Site-directed mutagenesis of CTX-M-15.

A two-primer, two-stage PCR method[36] was used to engineer CTX-M-15 variants harboring the following point mutations (Lys73Ala, ASAsn104AlaLA, Ser130Ala, Asn132Ala, Glu166Gln, Lys234Ala). pET-28b(CTX-M-15) was used as template in mutagenesis experiments to generate the listed pET-28b(CTX-M-15) variants for protein expression and purification.

Protein expression and purification.

For kinetics studies, an *E. coli* BL21(DE3) colony transformed with its respective β-lactamase construct, CTX-M-15 (wild type (WT), Lys73Ala, Asn104Ala, Ser130Ala, Asn132Ala, Glu166Gln, Lys234Ala), KPC-2 or OXA-48, was inoculated into LB medium containing 50 µg/mL kanamycin and grown at 37°C. Protein expression was induced with

1 mM IPTG at OD_{600} 0.7 and cultures were incubated overnight at 16°C. Cells were harvested by centrifugation and cell paste from 1 L of culture expressing β-lactamase was washed with 8 mL 0.85 % NaCl, resuspended in buffer containing 50 mM HEPES pH 7.5, 350 mM NaCl, and 20 mM imidazole then lysed by cell disruption at 20,000 PSI. Lysate was centrifuged using a Beckman JA 25.50 rotor at 20 000 RPM (48 254 x g) for 45 min at 4°C. The supernatant was applied to a 5-mL HiTrap Ni-NTA column (GE Lifesciences) at a constant flow rate of 3 mL/min. The column was washed with 5 column volumes of the same buffer and step gradients of increasing imidazole were used for wash and elution steps. Fractions containing purified β-lactamase, based on SDS-PAGE, were pooled and dialyzed overnight at 4°C in buffer containing 50 mM HEPES pH 7.5, 150 mM NaCl, and 20% glycerol. All purified enzymes were verified to be >95% pure as assessed by SDS-PAGE and stored at -20°C.

CTX-M-15 enzyme assays.

Nitrocefin was synthesized as reported previously (Lee et al., 2005b). Kinetic parameters of purified mutant CTX-M-15 β-lactamase hydrolysis of nitrocefin were determined at 30°C in 50 mM HEPES buffer (pH 7.5). Rates of hydrolysis were measured in 96-well microplate format at 490 nm using a Spectramax reader (Molecular Dynamics). Enzyme concentrations were adjusted so as to yield the following concentrations in 200 µL: WT (0.5 nM), Lys73Ala (5 nM), Asn104Ala (0.1 nM), Ser130Ala (0.1 nM), Asn132Ala (0.5 nM), Glu166Gln (100 nM), Lys234Ala (20 nM). All enzyme dilutions were done in 100 ng/µl bovine serum albumin (BSA). Nitrocefin concentrations ranged from 320 µM to 2.5 µM.

WT, Asn104Ala, and Asn132Ala carbamylation experiments were carried out using a Bio-Logic SFM-4 Stopped-Flow/Quench-Flow instrument using a cuvette with 2 mm path length. A four-syringe method was used to give a constant final concentration of 20 nM enzyme and 200 µM nitrocefin in 50 mM HEPES pH 7.5 with 0.01% Tween20. The maximum concentration of avibactam used was 10 µM. Total flow rate was adjusted to 3 mL/s. Absorbance was read continuously at 490 nm. For data analysis, the offset between reaction initiation and the first absorbance read was 700 ms. For Glu166Gln and Lys234Ala acylation experiments were carried out in 96-well microplate format monitored continuously at 490 nm using a Spectramax reader (Molecular Dynamics). Enzyme concentrations were adjusted so as to yield the following final concentrations in 200 µL wells: 200 nM Glu166Gln, 10 nM Lys234Ala. For Glu166Gln on-rate assays the maximum concentration of avibactam used was 1 µM with 100 µM nitrocefin as reporter substrate. For Lys234Ala on-rate assays the maximum concentration of avibactam used was 256 µM with 200 µM nitrocefin as reporter substrate.

Data were fit to a two-step reversible inhibition model as described previously (Ehmann et al., 2013a),

$$E + I \underset{k_{-1}}{\overset{k_1}{\rightleftharpoons}} EI \underset{k_{-2}}{\overset{k_2}{\rightleftharpoons}} EI^*$$

where

$$K_\mathrm{i} = \frac{k_{-1}}{k_1}$$

and

$$K_{\mathrm{i}}^{*} = \frac{K_{\mathrm{i}} k_{-2}}{k_2 + k_{-2}}$$

Time courses were fit to Equation 4 to obtain the pseudo first-order rate constant for enzyme inactivation, k_{obs} (Morrison and Walsh, 1988).

$$\mathrm{P} = \mathrm{v_s t} + (\mathrm{v_0} - \mathrm{v_s}) \frac{(1 - \mathrm{e}^{-k\mathrm{t}})}{k}$$

Where P, v_s, v_0, and t are the amount of product formed, the steady state rate (approximated by a no enzyme control), the initial rate (approximated by a no inhibitor control), and time. Equation 5 was used to derive k_2/K_i, the second-order rate constant for enzyme carbamylation,

$$k_{\mathrm{obs}} = k_{-2} + \frac{k_2}{K_{\mathrm{i}}} \frac{[\mathrm{I}]}{\left(1 + \frac{[\mathrm{S}]}{K_{\mathrm{m}}}\right)}$$

where [I], [S], and K_m are the concentration of avibactam, nitrocefin, and the K_m value of each enzyme for nitrocefin (see Supplemental Table 2-3). Error values reported are the standard errors of the fit.

For Lys73Ala and Ser130Ala on-rate assays, discontinuous sampling was employed from samples incubated at 30°C for 120 and 20 hours, respectively. Enzyme concentrations were adjusted so as to yield 5 nM Lys73Ala and 0.5 nM Ser130Ala final. The maximum concentration of avibactam used was 320 µM and 64 µM for Lys73Ala and Ser130Ala, respectively. Rates were measured periodically as above by adding 180 µL of the above and adding 20 µL of nitrocefin (final concentration 50 µM) and fit to Equation 6 to obtain

the pseudo first-order rate constant for enzyme inactivation, k_{obs} (Morrison and Walsh, 1988).

$$v = v_s + (v_0 - v_s) * e^{-kt}$$

where v is the rate of sample taken at time, t. Equation 5 was used to derive k_2/K_i, the second-order rate constant for enzyme carbamylation as above. Since the samples were incubated in the absence of nitrocefin, the concentration of substrate used in calculations was 0.

WT, Asn104Ala, and Asn132Ala decarbamylation experiments were performed using the jump dilution method (Copeland et al., 2011). Enzyme (1 µM) was incubated with avibactam (10 µM) for 20 minutes at 30°C and diluted 1/400 in buffer and 20 µL was added to 180 µL of nitrocefin for final concentrations of enzyme (0.25 nM), avibactam (5 nM) and nitrocefin (400 µM). For Glu166Gln and Lys234Ala, decarbamylation experiments were performed using a PD-10 desalting column (GE Healthcare) according to the manufacturer's gravity protocol. Glu166Gln (200 nM) or Lys234Ala (20 nM) were incubated with avibactam (5 µM) at 30°C for 0.5 and 2 hours, respectively. After desalting via PD-10 column (1.4x dilution), 180 µL was added to 20 µL nitrocefin (final concentration 400 µM for Lys234Ala and 200 µM for Glu166Gln). For WT, Asn104Ala, Asn132Ala, Glu166Gln, and Lys234Ala experiments were carried out in 96-well microplate format monitored continuously at 490 nm using a Spectramax reader (Molecular Dynamics). Data were fit to Equation 4 to obtain k_{off}. In the off-rate experiment, v_s was approximated by a no inhibitor control and v_0 by a no enzyme control. Error values reported are the standard deviation of three technical replicates.

For Lys73Ala and Ser130Ala, decarbamylation experiments were performed using a PD-10 spin column as above. Lys73Ala (5 nM) or Ser130Ala (1 nM) were incubated with avibactam (256 µM and 128 µM, respectively) at 30°C for 60 hours (Lys73Ala) or 3 hours (Ser130Ala). After removal of excess avibactam via PD-10 column (1.4x dilution), discontinuous sampling of the mixtures was done by taking 90 µL of the above into 10 µL of nitrocefin (final concentration 100 µM). Data were fit to Equation 6 to obtain k_{off} (Morrison and Walsh, 1988). In the off-rate experiment, v_s was approximated by a no inhibitor control and v_0 by a no enzyme control. Error values reported are the standard deviation of three technical replicates.

Crystallization, data collection, and structure determination.

Avibactam bound CTX-M-15, OXA-10 (Paetzel et al., 2000) and OXA-48 crystals were grown using the sitting drop vapor diffusion method at 25 °C. For CTX-M-15, drops contained 2µL of 30mg/mL CTX-M-15 in an equal volume of precipitant (0.2M ammonium sulphate, 0.1M MES pH 6.5, 30% PEG 5K MME, 5mM avibactam). For OXA-10, drops contained 3µL of 10 mg/mL protein in an equal volume of precipitant (1.8 M $(NH_4)_2SO_4$, 0.1 M MES pH 6.5, 10 mM $CoCl_2$, 2mM avibactam). For the OXA-48 crystal structures, drops contained 2uL of 50 mg/mL protein in an equal volume of precipitant [(i) OXA-48-AVI6.5: 0.1M sodium cacodylate pH 6.5, 40% v/v MPD, 5% wt/v PEG 8K, 2mM avibactam, (ii) OXA-48-AVI7.5: 200 mM Tris pH 7.5, 0.1M ammonium chloride, 40% MPD, 5% PEG 8K, 100 mM NaCl, 2 mM avibactam, (iii) Native OXA-48: The OXA-48-AVI7.5 precipitant minus avibactam, and (iv) and OXA-48-AVI8.5: 0.1M TRIS pH 8.5,

20% ethanol, 2mM avibactam]. Crystallization mother liquor plus 25% glycerol was used as a cryo-protectant and the crystals were flash frozen in liquid nitrogen. The CTX-M-15-AVI, OXA-48-AVI7.5, OXA-48-AVI8.5, native OXA-48 and OXA-10-AVI crystals diffracted to 1.6, 2.1, 2.0, 1.7, and 2.0Å at beamline CMCF-2 at the Canadian Light Source (CLS). The OXA-48-AVI6.5 crystals diffracted to 2.5Å at our in house x-ray machine. At the CLS and x-ray home source, data was collected at a wavelength of 1.0 and 1.54Å, at a temperature of 100K.

Data were processed using iMOSFLM (Battye et al., 2011), and the CCP4(Winn et al., 2011) program suite. For cross-validation purposes, a total of 5% of reflections were set aside. The avibactam bound CTX-M-15, OXA-48 and OXA-10 structures were solved by molecular replacement using the program Phaser (McCoy et al., 2007), with chain A of the native (CTX-M-14, OXA-48 and OXA-10) crystal structures as starting models [PDB ID: 1YLT (Chen et al., 2005a), 3HBR (Docquier et al., 2009), 1FOF (Paetzel et al., 2000)]. Several cycles of manual rebuilding in coot (Emsley et al., 2010), followed by refinement using REFMAC (CCP4) (Winn et al., 2011) were carried out. All structures were refined with isotropic B-factors. Water and avibactam were added manually by examination of the F_o-F_c and $2F_o$-F_c electron density maps. Coordinates and structure factors were deposited in the PDB with accession codes (4S2I, 4S2J, 4S2K, 4S2N, 4S2P, 4S2O) for CTX-M-15-AVI, OXA-48-AVI6.5, OXA-48-AVI7.5, OXA-48-AVI8.5, native OXA-48, OXA-10-AVI crystal structures. Figures 2, 3, S1, S2, S5, and S7 were designed using PyMol (Schrodinger, 2015) and figures S1 and S4 were created using LIGPLOT$^+$ (Laskowski and Swindells, 2011).

RESULTS

Inhibition of CTX-M-15 by Avibactam.

We have solved the co-crystal structure of avibactam complexed with the CTX-M-15 class A SBL in spacegroup, $P2_1$, at 1.6Å resolution, with two protein chains in the asymmetric unit (ASU) [see Supplemental Table 2-1 in the Supporting Information (SI) for a full list of data collection and refinement statistics]. Recently, Docquier *et al.* presented a 1.1Å resolution x-ray co-crystal structure of the avibactam-CTX-M-15 carbamyl-enzyme complex, which crystallized in space-group $P2_12_12_1$ with a single protein monomer in the ASU (PDB ID: 4HBU). However, a close electrostatic interaction between the bound avibactam sulfate group and R42 on an adjacent monomer was observed as a crystallographic artifact (avibactam N6 sulfate to R42 guanadino η1 distance= 3.0Å) (Lahiri et al., 2013). Despite this difference in avibactam binding we find that the compound itself takes on a nearly identical conformation between the two crystal forms and resulting structures (see Supplemental Figure 2-1a in the SI).

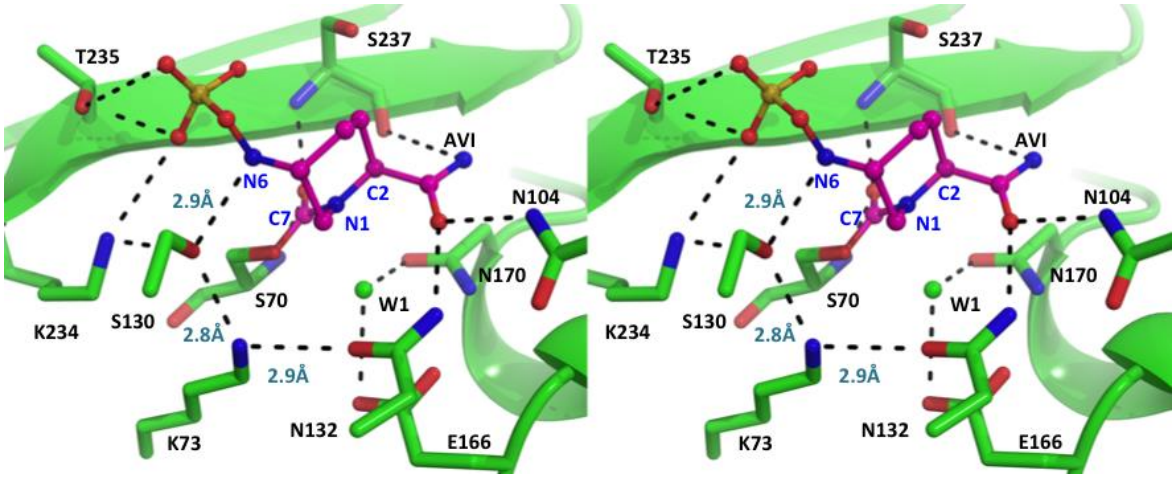

Figure 2-2. Inhibition of CTX-M-15 by avibactam. Stereoview active site close-up of carbamyl-avibactam bound CTX-M-15. The carbon atoms of avibactam are pink and all other atoms are colored by type (N, blue; O, red; S, yellow). The avibactam bound CTX-M-15 protein backbone is displayed as a green cartoon. The catalytic water (W1) is shown as a green sphere. Hydrogen bonding and electrostatic interactions are depicted as black dashes.

From our co-crystal structure, we see that upon carbamylation by the SXXK Ser70, the avibactam C7-N6 amide bond is liberated rather than the C7-N1 bond (Figure 2). The avibactam sulfate projects into an electropositive pocket formed by Lys234 and is stabilized by interactions with T235 and Lys234 on motif iii. The R1 carboxamide is oriented away from the active site core and is within hydrogen bonding distance (3.0Å and 2.7Å) away from the side chain amide nitrogens of N104 and Asn132 (Figure 2, and Supplemental Figure 2-1).

Water (W1), the nucleophile responsible for hydrolytic deacylation of the β-lactams, occupies the typical catalytic position, oriented by hydrogen bonds to the side chains of Glu166 and N170 protruding from the CTX-M-15 Ω-loop motif. We suggest that a major contributing factor to the avoidance of the carbamyl-enzyme to hydrolytic decarbamylation is that the carbamyl carbon is less susceptible to nucleophilic attack than

its ester (acyl-enzyme) counterpart (Alexander and Cravatt, 2005), (Mileni et al., 2010). This stability is presumably due to a resonance effect, in which the lone pair of electrons on the sp^2 hybridized N1 aligns with the carbonyl C=O p-orbitals, thereby increasing electron density at the electrophilic carbonyl carbon (Pattabiraman and Bode, 2011). Carbamyl bond formation is a common feature observed for inhibitors of serine hydrolases, some of which have also been shown to retain the catalytic water in the carbamylated state (Yang et al., 2008), (Mileni et al., 2010).

Carbamylation/decarbamylation kinetics for CTX-M-15 active site mutants.

To evaluate the mechanistic details governing the reversible recyclization reaction of avibactam inhibition, we mutagenized key active site residues within CTX-M-15 and measured enzyme activity using the colorimetric cephalosporin, nitrocefin, as a reporter substrate. We confirmed that mutants adopt a WT fold by dynamic light scattering, and that no hydrolysis of avibactam occurred using liquid chromatography-mass spectrometry (LC-MS) (Supplemental Figure 2-3 and Figures S7-S16) (Ehmann et al., 2013b).

For class A SBLs like CTX-M-15, there are alternative views on the mechanism of Ser70 activation during β-lactam acylation. In one perspective, the Ω-loop Glu166 activates Ser70 for nucleophilic attack by O-γ deprotonation through a water molecule. The second proposal involves Lys73 as the base responsible for Ser70 activation. Here, we find that Glu166Gln has a comparable avibactam carbamylation rate to WT [WT and Glu166Gln carbamylation rates (k_2/K_i) = 1.6 ± 0.2 x 10^5 and 9.3 ± 1.2 x 10^4 $M^{-1}s^{-1}$], suggesting that Glu166 is not directly involved in the carbamylation mechanism. In contrast, Lys73Ala

was almost completely carbamylation deficient ($2.8 \pm 0.1 \times 10^{-1}$ $M^{-1}s^{-1}$) (Table 1). These data support the proposition that Lys73 is the general base responsible for Ser70 activation during avibactam carbamylation. This may in part facilitate avibactam's ability to inhibit all SBL subclasses that each bears the universally conserved SXXK lysine.

During carbamylation, the avibactam N6 nitrogen is protonated following ring opening. We hypothesized that the Ser130 γ-OH is responsible for this protonation event due to its proximity to N6 in the carbamyl-enzyme crystal structure (2.9Å, Figure 2). We observed a dramatic reduction in carbamylation rate for the Ser130Ala mutant [WT and Ser130Ala carbamylation rates (k_2/K_i) = $1.6 \pm 0.2 \times 10^5$ and 3.3 ± 0.4 $M^{-1}s^{-1}$] (Table 1). Therefore, we propose that in an analogous fashion to its role in β-lactam N4 nitrogen protonation during acylation, Ser130 also acts as the general acid responsible for protonation of the avibactam N6 during carbamylation.

Table 2-1. Kinetic values for the carbamylation and decarbamylation of avibactam against a panel of CTX-M-15 active site mutants. The carbamylation and decarbamylation rates were measured using the colorimetric reporter substrate nitrocefin. The K_D values are calculated from the carbamylation and decarbamylation rates.

Parameter	*WT*	*Lys73Ala*	*Asn104Ala*	*Ser130Ala*	*Asn132Ala*	*Glu166Gln*	*Lys234Ala*
On-rate k_2/K_i ($M^{-1}s^{-1}$)	$1.6 \pm 0.2 \times 10^5$	$2.8 \pm 0.1 \times 10^{-1}$	$3.9 \pm 0.2 \times 10^4$	3.3 ± 0.4	$3.7 \pm 0.3 \times 10^5$	$9.3 \pm 1.2 \times 10^4$	$8.0 \pm 0.9 \times 10^2$
Off-rate k_{off} (s^{-1})	$1.5 \pm 0.1 \times 10^{-4}$	$2.1 \pm 0.3 \times 10^{-7}$	$7.1 \pm 0.1 \times 10^{-5}$	$7.7 \pm 0.7 \times 10^{-7}$	$1.6 \pm 0.1 \times 10^{-4}$	$1.8 \pm 0.3 \times 10^{-4}$	$4.0 \pm 0.8 \times 10^{-5}$
Off-rate $t_{1/2}$ (min)	76	6×10^4	160	9×10^3	74	63	292
K_d (μM)	0.001	0.8	0.002	0.2	0.001	0.002	0.05

For subsequent avibactam recyclization to occur, the N6 nitrogen must be deprotonated to facilitate intramolecular attack of the carbamyl linkage reforming the N6-C7 bond. Due to its proximity to the N6 nitrogen in the CTX-M-15 bound structure (2.9Å, Figure 2, Supplemental Figure 2-1b), Docquier *et al.* proposed that Ser130 may potentially act as the general base responsible for reversible-recyclization (Lahiri et al., 2013). To test this, we analyzed the decarbamylation rate for the Ser130Ala CTX-M-15 mutant. The carbamyl enzyme intermediate was virtually unable to decarbamylate in the Ser130Ala mutant [WT and Ser130Ala decarbamylation rates (k_{off}) = 1.5 ± 0.1 x 10^{-4} and 7.7 ± 0.7 x 10^{-7} s^{-1}] (Table 1) consistent with a role of Ser130 as the general base responsible for avibactam recyclization. Despite intensive research on SBLs over the past several decades, this is the first example of Ser130 acting as a general base, a feature that exemplifies the novelty of the avibactam inhibitor and the functional plasticity of this residue.

In the carbamyl avibactam-CTX-M-15 crystal structure, Lys73 and Lys234 are directly hydrogen bonded, 2.8Å away, from the side chain O-γ of Ser130, suggesting that they may be responsible for regulating the protonation state of Ser130 during carbamylation/decarbamylation (Figure 2, Supplemental Figure 2-1b). The Lys73Ala mutant mimic's the effect of Ser130 whereby it is almost completely deficient in decarbamylation (k_{off} = 2.1 ± 0.3 x 10^{-7} s^{-1}). However, Lys234 only displays a moderate reduction in decarbamylation rate as compared to the WT enzyme (Table 1). We therefore suggest that Lys73 may potentially be the base responsible for Ser130 activation during recyclization with Lys234 playing an additional electrostatic role in modulating the pKa depression of Ser130 to facilitate its necessary oxyanion state.

Class A SBL catalyzed hydrolytic deacylation of β-lactams is thought to proceed through Glu166 catalyzed hydrolysis of the acyl-enzyme intermediate, and subsequent protonation of the Ser70 O-γ via an Glu166 coordinated water molecule (Lamotte-Brasseur et al., 1991). However, for avibactam re-cyclization, we find that the Glu166Gln decarbamylation rate is virtually identical to WT suggesting that Glu166 is not required for Ser70 protonation (Table 1). Due to the close proximity of the Lys73 N-ζ to the Ser70 O-γ in the unbound CTX-M-15 crystal structure (2.7 Å) (Lahiri et al., 2013), and the apparent decarbamylation deficiency of the Lys73Ala mutant ($t_{1/2}$= ~1000 hours), we suggest that Lys73 acts as part of a concerted proton shuttle pathway for Ser70 regeneration during avibactam decarbamylation.

In the carbamyl avibactam-CTX-M-15 crystal structure, the side chain amide nitrogen atoms of Asn132 and N104 are within hydrogen bonding distance 2.7 and 3.0 Å away from the avibactam C2 carboxamide oxygen (Figure 2, Supplemental Figure 2-1b). We found that mutant Asn104Ala, but not Asn132Ala, had a 4-fold reduction in carbamylation rate as compared to the WT enzyme but minimal effect on decarbamylation (Table 1). Previous structural and kinetic analysis suggests that the N104 side chain amide nitrogen is also important for the stabilization of the acylamide R1 group of the β-lactam antibiotics in the class A SBLs (Pérez-Llarena et al., 2011; Shimamura et al., 2002). Thus, the role of N104 in class A β-lactamases is likely to contribute to Michaelis complex formation by interacting with the avibactam C2 carboxamide in an analogous fashion to the R1 side chain of β-lactams. Future drug design efforts should seek to maintain a hydrogen bond acceptor at the avibactam C2 carboxamide oxygen position.

Inhibition of the class D SBLs by avibactam.

To understand the structural basis for DBO-mediated inhibition of the class D β-lactamases, we determined co-crystal structures of avibactam bound to OXA-10, and OXA-48 at three different pH values (6.5, 7.5 and 8.5; hereafter called OXA-48-AVI6.5, OXA-48-AVI7.5 and OXA-48-AVI8.5) to 1.7, 2.5, 2.1 and 2.0Å resolution, respectively (Supplemental Table 2-1). Generally, all protein monomers within the ASU contain high structural similarity [with root-mean-square deviations (r.m.s.d.) of <0.2Å for all common alpha-carbon (CA) atoms in all chains in the ASU]. Therefore, we limit our analysis to chain A for each product complex. For simplicity, we further limit our analysis to OXA-48-AVI7.5 unless otherwise stated. All avibactam-bound complexes display clear, and unambiguous ligand omit map F_o-F_c electron density for avibactam within the active site of each protein chain in the ASU (Supplemental Figure 2-2). The carbamyl avibactam molecules were refined at full occupancy, with the exception of the OXA-48-AVI8.5 (Chains A and B), which were refined at an occupancy of 0.7 (Supplemental Table 2-1).

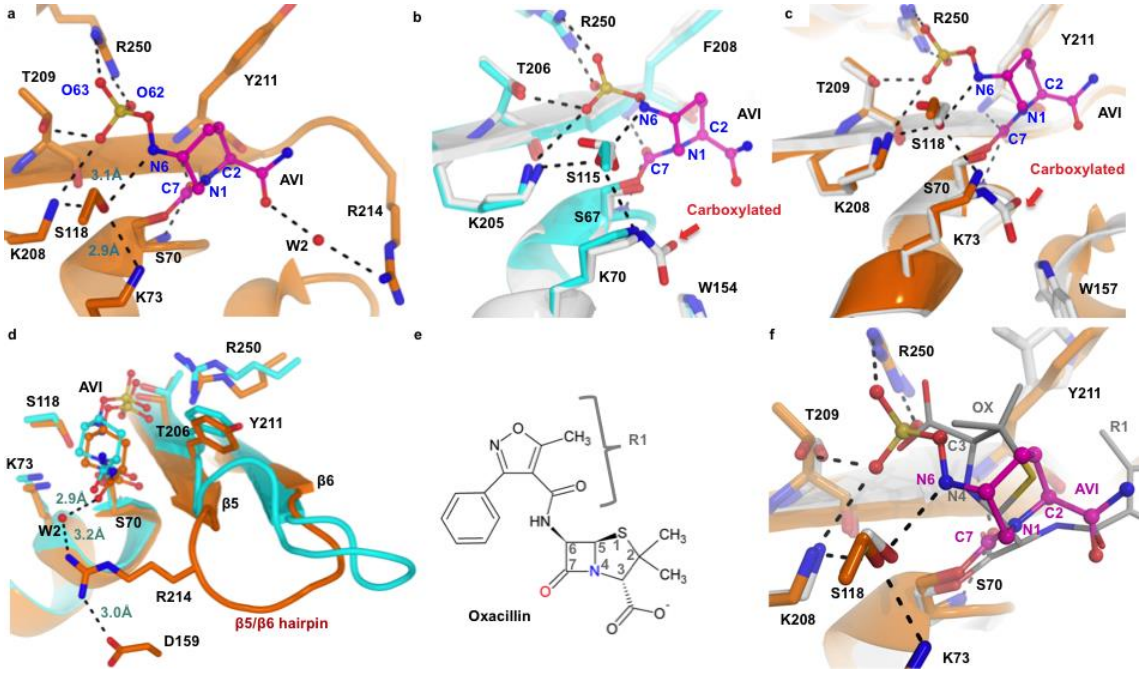

Figure 2-3. Inhibition of OXA-48 and OXA-10 by avibactam. (a) Active site close-up of carbamyl-avibactam OXA-48. The carbon atoms of avibactam are pink with all other non-carbon atoms colored by atom type. The avibactam bound OXA-48 protein chain is displayed in orange cartoon representation, and key active site residues are shown as sticks with atoms colored by type. (b) Active site overlay of carbamyl-avibactam and uncomplexed OXA-10. The avibactam bound and unbound OXA-10 protein chains are illustrated in cyan and white cartoon representation, and key active site residues are depicted as sticks with atoms colored by type (OXA-10 numbering). (c) Active site overlay of carbamyl-avibactam and uncomplexed OXA-48. The carbamyl-avibactam and OXA-48 protein chain are displayed as in A. The unbound OXA-48 protein chain is illustrated in grey cartoon representation, and key active site residues are depicted as sticks with atoms colored by type. (d) Active site overlay of carbamyl-avibactam OXA-48 and OXA-10. The OXA-48 and OXA-10 protein chains, active site residues and bound avibactam are displayed as in a, and b. (e) Structure of oxacillin. (f) Active site overlay of carbamyl-avibactam bound OXA-48 and acyl-oxacillin bound K84D OXA-24 (PDB ID: 4F94). The carbamyl-avibactam bound structure is displayed as in a. The OXA-24 protein backbone is illustrated as a white cartoon, and key active site residues are shown in stick representation with atoms colored by type. The acyl-oxacillin carbon atoms are grey and all other atoms are colored by type. In a, b, c, d and f, all hydrogen bonding and electrostatic interactions are depicted as black dashes.

The high resolution of the models allows us to make detailed observations about key active site interactions. For clarity, we use OXA-48 residue numbering throughout the text when describing both OXA-48 and OXA-10, except in figure 3b whereby we use OXA-10 numbering for consistency with the PDB file. The average temperature-factors for the refined avibactam in the OXA-48 and OXA-10 bound structures are 29.7 and 17.5Å^2

(similar to the average protein B-factors of 27.8 and 22.6Å^2), indicating that the inhibitor is bound in a rigid fashion with little conformational variation and flexibility (Supplemental Table 2-1). In the complexes, the bound avibactam forms a carbamyl bond between the active site Ser70 O-γ and its C7 carbon, as evidenced by the continuous F_o-F_c ligand omit map electron density in this region (Supplemental Figure 2-2). Like the class A and C enzymes (CTX-M-15 and AmpC) (Lahiri et al., 2013), the C7-N6 bond breaks rather the C7-N1 bond upon class D SBL mediated carbamylation. We attribute the C7-N6 bond fission in part to the fact that the N6-$OSO3^-$ is a better leaving group than the corresponding $RR'N1^-$. From a structural standpoint, the location of S118 (equivalent to Ser130 in the class A enzymes), likely also contributes to the observed bond fission as it is ideally positioned to protonate an N6 rather than N1 leaving group (Figures 3a, and 3b).

In the OXA-48 and OXA-10 carbamylated form, the six membered piperidine ring of avibactam adopts a chair-type conformation, with the C4 and N1 atoms located above and below the plane (Figures 3a, and 3b). The C7 carbonyl oxygen of the newly formed carbamyl linkage is located in the oxyanion hole of the enzyme, and is bound by the backbone amide protons of Ser70 and Y211 at 2.7 and 2.8Å, respectively. The avibactam sulfate group projects into a positively charged cavity consisting of R250, T209 and K208, which binds the analogous C3/C4 carboxylate of β-lactams (Figures 3a, 3b and Supplemental Figure 2-4) (Yasuyuki, 2003). OXA-48 and OXA-10 display a strong electrostatic interaction between the avibactam sulfate oxygen's (O62 and O63) and the R250 guanidino group η1 and η2 at 2.8 and 3.2Å, an interaction that is not observed in the class A and C SBL-avibactam complexes. In the OXA-48 and OXA-10 bound structures,

the avibactam C2 carbamate is not stabilized by hydrogen bonding with asparagine residues as observed in the class A and C carbamyl avibactam bound CTX-M-15 and PAO1 AmpC crystal structures (Lahiri et al., 2013).

When aligning the native and avibactam bound OXA-10 and OXA-48 crystal structures, we observe that the protein chains are nearly identical (r.m.s.d. on all common Cα atoms=0.4Å and 0.4Å), with a remarkably similar juxtaposition of active site residues (Figures 3b and 3c). Thus, the class D SBL active site is poised for interaction with avibactam without the need for complicated conformational rearrangements that can substantially slow acylation, as observed for *S. aureus* PBP2a (Eisenmesser et al., 2005; Lim and Strynadka, 2002).

Comparison of carbamyl-avibactam in the class D SBLs OXA-10 and OXA-48.

The OXA-10 and OXA-48 enzymes differ by 2 orders of magnitude in their avibactam carbamylation rates ($1.1 \pm 0.1 \times 10^{1}$ and $1.4 \pm 0.1 \times 10^{3}$ $M^{-1}s^{-1}$), despite having a virtually identical arrangement of catalytic residues (Figure 3d) (Ehmann et al., 2013b). Although carboxylation of Lys73 may be important to the observed carbamylation rates (see discussion below), structural differences between enzymes may also play a role. When overlaying the avibactam bound OXA-48 and OXA-10 crystal structures (49% amino acid sequence identity), we see that the two protein chains align very well (r.m.s.d on 112 common CA atoms= 0.97Å). The only substantial difference between the two proteins is the β-hairpin connecting strands β5 and β6 (Figure 3d), which flanks the active site and is an important feature defining carbapenemase activity via interaction with the carbapenem

hydroxyethyl moiety (De Luca et al., 2011). For OXA-48, the β-hairpin residue R214 interacts electrostatically with D159 on the Ω loop (R214 η1 to D159 δO distance= 3.0Å), bringing the β-hairpin closer to the catalytic core than observed for the elongated OXA-10 β5-β6 hairpin (Figure 3d). From the OXA-48-bound avibactam structure in two out of 4 monomers in the ASU we see that there is a hydrogen bond between the R214 η2 guanidino nitrogen and a water molecule (W2, refined at full occupancy) at 2.9Å, which in turn hydrogen bonds to the amide nitrogen of the avibactam C2 carboxamide at 3.0Å (Figure 3d). Therefore, the β5-β6 hairpin may be important for stabilizing the avibactam C2 carboxamide, and thus future structure-based drug designed efforts should aim to maintain this water-mediated interaction.

Comparison of avibactam and β-lactam binding in the class D SBLs.

When overlaying avibactam-bound OXA-48 onto the 2.4Å resolution crystal structure of acyl-oxacillin bound Lys84Asp OXA-24 (PDB ID: 4F94, unpublished data), we see that the two protein chains align well (r.m.s.d=1.1Å on 80 common CA atoms). Furthermore, the oxacillin and avibactam ligands display analogous overall orientations despite their chemical differences (Figure 3f). In both structures, the acyl/carbamyl carbonyl oxygen interacts with the backbone amides of the oxyanion hole residues Ser70 and Y211 on strand β5 (OXA-48 residue numbering). The electronegative substituent (the avibactam N6 sulfate and penicillin C3 carboxylate) both project toward the basic patch defined by Arg250, Lys208 and Thr209. Additionally, the avibactam C2 carboxamide and the analogous β-lactam R1 functional group orient away from the catalytic core, toward

bulk solvent in both structures (Figure 3f). Taken together, the observed similarities between DBO and β-lactam binding, in part help to explain the broad-spectrum SBL target profile for avibactam, which clearly acts as a substrate analogue. The DBO C2 carboxamide group may be a key site for chemical modification in future drug design efforts, as has been the case for the β-lactam R1 moiety (Chen et al., 2005b).

β-Lactams hydrolytically deacylate from the SBL catalytic serine rather than recyclize to the active antibiotic (Majiduddin et al., 2002). However, both the avibactam N6 and the analogous oxacillin N4 atoms are within hydrogen bonding distance (3.1Å and 3.3Å) from the recyclization general base Ser118 (Figure 3f). We propose that recyclization is prohibited in the β-lactams due to an intrinsically high-energy barrier to cyclize the strained 4-membered lactam ring, as opposed to the 5-membered ring that is formed upon avibactam re-cyclization.

Carboxylation state of lysine 73 in the avibactam carbamyl-enzyme complexes.

The *N*-carboxylation state of Lys73 is sensitive to pH, with carboxylation increasing at higher pH values presumably due to an increased reactivity of Lys73 to carbon dioxide in more basic solutions, and the greater stability of carbamic acid in the anionic form at higher pH (Golemi et al., 2001). OXA-48 with no avibactam present was crystallized at pH 7.5 and displays clear, unambiguous Lys73 omit map F_o-F_c electron density for carboxylated lysine, which was refined at full occupancy for both monomers within the ASU (Supplemental Figure 2-5a). Interestingly, in the avibactam bound OXA-48 structures at both pH 6.5 and 7.5, all monomers display no evidence for carboxylation at Lys73 upon

inspection of the F_o-F_c Lys73 omit electron density maps (Figures S5b and S5c). Therefore, the presence of the bound avibactam appears to disfavor Lys73 carboxylation in the carbamyl-enzyme complexes.

Only in the pH 8.5 structure, OXA-48-AVI8.5, do 2 out of 4 monomers in the ASU (chains A and B) display partial occupancy for *N*-carboxylated Lys73 (Supplemental Table 2-1, and Supplemental Figure 2-5d). At the same time, these are the only chains from all OXA-48 structures that display partial rather than full occupancy for avibactam (Supplemental Table 2-1). However, it should be noted, at pH 8.5 avibactam was shown to degrade when free in solution by LC-MS (Supplemental Figure 2-16), providing an alternative or additional reason for the observed partial occupancy. As an interesting aside, to our knowledge, this is the first report showing that avibactam is not stable at high pH.

Recently, Ehmann et al. have shown by monitoring OXA-10 carbamyl exchange with TEM-1, that OXA-10, like the majority of SBLs tested, undergoes a reversible, rather than hydrolytic route to avibactam decarbamylation (Ehmann et al., 2013b). Taken together, the absence of Lys73 *N*-carboxylation clearly disfavors hydrolytic decarbamylation of avibactam for the class D enzymes. The acyl enzyme crystal structure of OXA-24 bound to tazobactam (which undergoes hydrolytic deacylation rather than decarbamylation), displays a carboxylated Lys73 (PDB ID: 3ZNT, unpublished), further corroborating the notion that motif i lysine carboxylation is a key feature governing hydrolysis in the class D enzymes. However, it is currently unclear whether or not carboxylated-Lys73 is the general base responsible for Ser70 activation during

carbamylation and how this modification affects avibactam carbamylation rates for the class D SBLs.

In the avibactam-bound OXA-48 structure, the de-carboxylated Lys73 is oriented toward S118, rather than W57 as observed in the unbound, carboxylated state (Figure 3c). In the avibactam bound form, the de-carboxylated Lys73 hydrogen bonds to Ser118 at a distance of 2.9Å, which in turn hydrogen bonds to the N6 proton on avibactam at 3.1Å (Figures 3a, and 3c). This conformational switch is reminiscent of the CTX-M-15 avibactam bound structure whereby Lys73 is hydrogen bonded to Ser130 (equivalent to the OXA-48 S118) (Figure 2), yet this interaction is not present in the unbound CTX-M-15 structure (Lahiri et al., 2013). We propose that upon avibactam recyclization, this hydrogen bonding network results in Lys73 mediated deprotonation of Ser118, which in turn removes the avibactam N6 hydrogen facilitating attack on the carbamyl bond and subsequent re-cyclization.

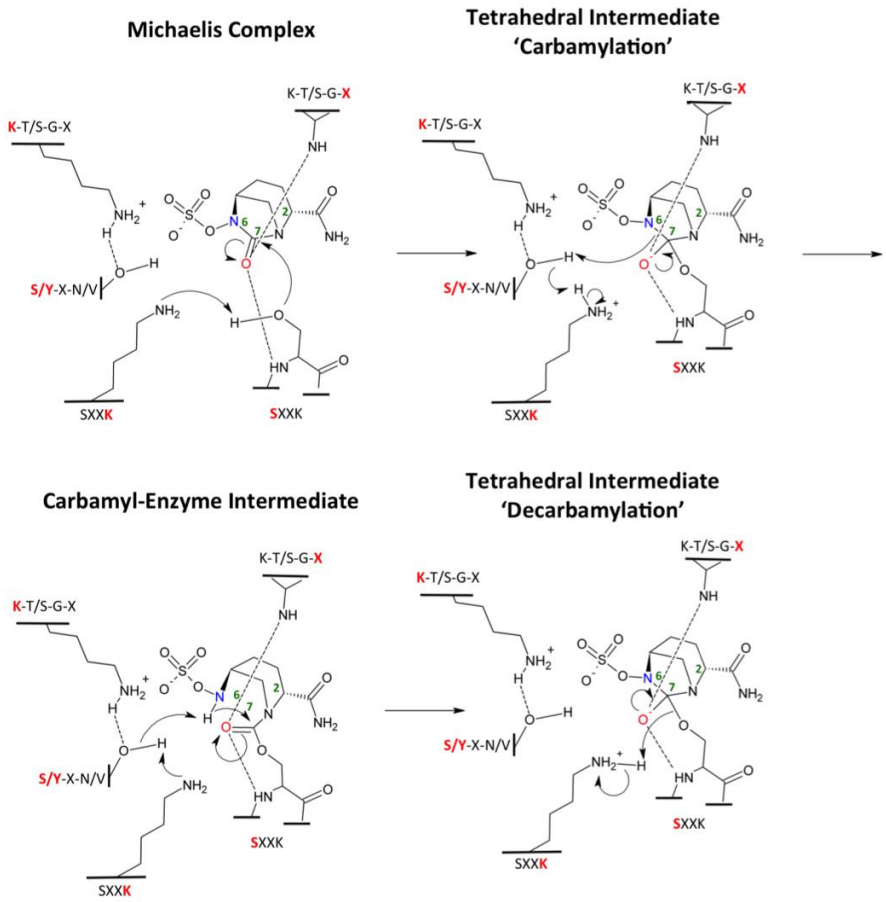

Figure 2-4. Proposed general catalytic mechanism for avibactam mediated SBL inhibition.

Universal mechanism for avibactam mediated SBL inhibition

Analysis of the avibactam-bound carbamyl enzyme crystal structures of the class A, C and D β-lactamases (CTX-M-15, *P. aeruginosa* PA01 AmpC (Lahiri et al., 2013), and OXA-10) reveals that the DBO core takes on a similar orientation with respect to the conserved SBL active site motifs in all three structures (Supplemental Figure 2-6). Taken together, these crystal structures along with the CTX-M-15 mutant kinetic data allows us to propose a universal mechanism for SBL inhibition. Electrostatic stabilization of the N6 sulfate likely helps to orient the bound avibactam in the pre-catalytic Michaelis complex, whereby the sulfate occupies the electropositive pocket formed by the SBL motif iii. The catalytic serine is activated via general base mediated deprotonation (SXX**K**, Figure 4), likely by Lys73 for the class A SBLs, Lys67 for the class C SBLs and Lys73 for the class D enzymes. The subsequent attack of the activated serine O-γ on the avibactam C7 carbonyl results in the formation of a transient tetrahedral intermediate that is stabilized by the oxyanion hole of the enzyme (consisting of the backbone amides of the catalytic serine and residue X from the K-T/S-G-X motif iii). The lone pair of electrons on the C7 oxygen drive back into carbonyl formation expelling the negatively charged N6 nitrogen, which is concomitantly protonated by the motif ii serine (or tyrosine for the class C enzymes), resulting in the formation of a stable carbamyl enzyme complex. The complex resists decomposition by hydrolysis likely due in part to the inherent stability of the carbamyl bond, and/or by removal of the general base involved in β-lactam hydrolytic deacylation (as proposed for the de-carboxylation of the SXXK carboxy-lysine in the class D enzymes). Upon eventual avibactam decarbamylation, a reversible mechanism of recyclization

generally occurs, whereby the SXXK lysine takes part in a concerted acid-base shuffling of protons from the motif ii serine (for class A and D), or tyrosine (for class C), which deprotonates the N6 nitrogen facilitating an intramolecular nucleophilic attack on the electrophilic C7 carbamyl carbon. The decarbamylation results in departure of the catalytic serine-leaving group, which likely abstracts a proton from the N-ζ of the now protonated SXXK lysine to regenerate the active site (Figure 4).

Avibactam binds to the three major classes of SBLs (Class A, C and D) in an overall similar fashion. However, subtle differences in active site hydrogen bonding networks and electrostatic interactions lead to substantial discrepancies in carbamylation rates both between and within these enzyme subclasses. Using CTX-M-15 as a model enzyme we show that the motif ii serine is the likely base required for avibactam's characteristic re-cyclization. The crystal structures of OXA-48 and OXA-10 bound to avibactam uncovers unique binding features that should help to guide prospective synthetic efforts targeted at inhibition of the class D SBLs. It is our hope that this study will serve as a valuable tool for the future design and development of this exciting new class of inhibitors.

SUPPLEMENTAL INFORMATION

Supplemental Methods

Dynamic light scattering.

Dynamic light scattering was performed using a Zetasizer NanoS (Malvern Instruments). All measurements were taken using a 12 µL quartz cell (ZEN2112) at 25°C. Size distribution of the samples was calculated based on the correlation function provided by the Zetasizer Nano S software.

LC-MS analysis of avibactam-CTX-M-15 mutants.

LC-ESI-MS data were obtained by using an Agilent 1100 Series LC system (Agilent Technologies Canada, Inc.) and a QTRAP LC/MS/MS System (Applied Biosystems). The reverse phase HPLC was performed using C_{18} column (SunFire C18 5 µm, 4.6x50 mm, Waters) with Agilent 1100 LC binary pump at a flow rate of 1 mL/min, under the following conditions: isocratic 5% solvent B (0.05% formic acid in acetonitrile) and 95% solvent A (0.05% formic acid in water) for 1 min, followed by a linear gradient to 97% B over 10 min. CTX-M-15 WT, Lys73Ala, Asn104Ala, Ser130Ala, Asn132Ala, Glu166Gln, Lys234Ala; and KPC-2 (7 µM) were incubated with 14 µM avibactam in buffer containing 30 mM HEPES pH 7.5, 300 mM NaCl, and 20 % v/v glycerol and analyzed at both 0 h and 24 h.

Protein expression and purification for crystallographic studies.

The *P. aeruginosa* OXA-10 protein (UniProt ID: P14489) corresponding to the mature sequence (20-266) was cloned, overexpressed and purified as previously described (Paetzel et al., 2000).

The *E. coli* CTX-M-15 and *Klebsiella pneumoniae* OXA-48 expression vectors were constructed as described above. The expression vectors were then transformed into *E. coli* BL21 DE3 cells. The cells were grown in Lauria Bertani (LB) broth at 37°C until an OD_{600} of 0.7 was reached at which point the culture was cooled to room temperature. Protein expression was induced by addition of 1mM isopropyl β-D-1-thiogalactopyranoside (IPTG) and the cultures were grown at 22°C for 12-16 hours. The cells (~20g) were then harvested and resuspended in 50mL lysis buffer (50 mM Tris, pH 7.5, 350 mM NaCl, and one complete, EDTA-free protease inhibitor tablet from Roche). The cells were lysed by two passes on a French Press at ~12,000 p.s.i., and the lysate was centrifuged (45,000 rpm in a Beckman 70 Ti rotor) for 35 minutes. The supernatant was then filtered using a 0.22 μM syringe filter and passed through a 1mL Hi-Trap HP His column, which was pre-equilibrated in lysis buffer. Elution buffer (50 mM Tris, pH 7.5, 350mM NaCl, 1M imidazole) was used to elute the His-tagged proteins from the column with a gradient of imidazole from 0 to 500mM in 50 minutes. Fractions enriched in the protein of interest were pooled and 1U/mL of bovine α-thrombin (Roche) was added and the samples were incubated overnight at 4°C. Samples were then exchanged via a 10 kDa cut-off Amicon centrifugation concentrator into crystallization buffer (20mM Tris, pH 7.5, 100mM NaCl). Samples were passed over a Superdex 200 column using crystallization buffer, as running buffer and pooled fractions were concentrated to 30 mg/mL for CTX-M-15, 50 mg/mL for OXA-48 and 10mg/mL for OXA-10.

Supplemental Tables

Supplementary Table 2-1. Data collection and refinement statistics.

	CTX-M-15-AVI	OXA-10-AVI	OXA-48-AVI8.5	OXA-48-AVI7.5	OXA-48-AVI6.5	OXA-48-Native
Data collection						
Space group	$P2_1$	$P2_12_12_1$	$P3_2$	$P3_2$	$P2_12_12_1$	$P22_12_1$
Cell dimensions						
a, *b*, *c* (Å)	62.0, 60.6, 71.5	48.6, 96.5, 125.7	142.0, 142.0, 52.4	142.8, 142.8, 52.4	64.1, 108.1, 162.8	43.4, 102.9, 124.7
c (°)	90, 104, 90	90, 90, 90	90, 90, 120	90, 90, 120	90, 90, 90	90, 90, 90
Resolution (Å)	34.7-1.6 (1.69-1.60)	52.66-1.70 (1.73-1.70)	46.64-2.00 (2.11-2.00)	52.42-2.10 (2.21-2.10)	65.03-2.54 (2.65-2.54)	41.6-1.70 (1.73-1.70)
R_{merge}	0.052(0.296)	0.040(0.290)	0.090(0.295)	0.096(0.457)	0.065(0.150)	0.055(0.424)
I / I	13.7(3.5)	24.5(5.2)	6.1(2.9)	8.5(2.9)	12.7(6.1)	12.1(2.3)
Completeness (%)	96.7(95.2)	98.0(99.9)	99.2(99.4)	99.8(100.0)	91.2(91.4)	99.7(99.9)
Redundancy	3.9(3.9)	4.8(4.9)	2.5(2.5)	3.4(3.4)	4.0(3.8)	5.0(4.9)
Refinement						
Resolution (Å)	34.7-1.60	52.66-1.70	46.64-2.00	52.42-2.10	65.03-2.54	41.6-1.70
No. reflections	65645(9368)	64493(3478)	76256(11167)	69650(10200)	34471(4158)	62226(3297)
R_{work} / R_{free}	0.165/0.198	0.185/0.230	0.171%/0.205	0.172/0.205	0.184/0.222	0.192/0.226
Avibactam occupancy chainA, chainB, etc.	1.00, 1.00	1.00, 1.00	0.70, 0.70, 1.00, 1.00	1.00, 1.00, 1.00, 1.00	1.00, 1.00, 1.00, 1.00	N/A, N/A
No. atoms						
Protein	3930	3957	8000	8043	7972	3963
Ligand/ion	34	38	68	68	68	N/A
Water	546	438	385	537	185	438
B-factors						
Protein	17.8	22.6	40.2	30.3	34.1	27.2
Ligand/ion	17.8	17.5	36.7	22.4	35.4	N/A
Water	27.4	28.7	37.6	32.3	29.2	35.4
R.m.s. deviations						
Bond lengths (Å)	0.012	0.012	0.014	0.012	0.011	0.014
Bond angles (°)	1.62	1.70	1.72	1.68	1.49	1.53
Favored/allowed/ disallowed (%)[+]	98.2, 1.4, 0.4	97.8, 2.0, 0.2	97.6, 2.4, 0.0	97.2, 2.8, 0.0	97.9, 2.1, 0.0	97.7, 2.3, 0.0

*All datasets correspond to diffraction data collected from a single crystal.
*Values in parentheses are for highest-resolution shell.
*Avibactam (AVI)
[+]phenix.ramalyze; "allowed" is the percentage remaining after "favored" and "outlier" residues are subtracted.

Supplemental Table 2-2. Primers used in this study. Underline shows restriction sites.

Primer	Sequence (5'-3')
CTX-M-15 F	AATATCATATGCAAACGGCGGACGTACAGCA
CTX-M-15 R	TATTAGAATTCTTACCGTCGGTGACGATTTTAGCC
OXA-48 F	GCTTCATATGGAATGGCAAGAAAACAAAAGTTGGAATGCT
OXA-48 R	CGTACTCGAGCTAGGGAATAATTTTTTCCTGTTTGAGCAC
Lys73Ala F	GCGATGTGCAGCACCAGTGCGGTGATGG
Lys73Ala R	CGCTACACGTCGTGGTCACGCCACTACC
Asn104Ala F	CGAGTTGAGATCAAAAAATCTGACCTTGTTGCGTATAATCCGATTGC
Asn104Ala R	GCTCAACTCTAGTTTTTTAGACTGGAACAACGCATATTAGGCTAACG
Ser130Ala F	CGCTACAGTACGCGGATAACGTGGCGATGAATAAGC
Ser130Ala R	GCGATGTCATGCGCCTATTGCACCGCTACTTATTCG
Asn132Ala F	GCTACAGTACAGCGATGCGGTGGCGATGAATAAGC
Asn132Ala R	CGATGTCATGTCGCTACGCCACCGCTACTTATTCG
Glu166Gln F	GCTGGGAGACGAAACGTTCCGTCTCGACC
Glu166Gln R	CGACCCTCTGCTTTGCAAGGCAGAGCTGG
Lys234Ala F	GGTTGTGGGGGATGCGACCGGCAGC
Lys234Ala R	CCAACACCCCCTACGCTGGCCGTCG
T7 terminator	GCTAGTTATTGCTCAGCGG

Supplemental Table 2-3. Kinetic values for the hydrolysis of nitrocefin by CTX-M-15 mutants.

Parameter	***WT***	***Lys73Ala***	***Asn104Ala***	***Ser130Ala***	***Asn132Ala***	***Glu166Gln***	***Lys234Ala***
K_m (μM)	9.9	13	11	33	6.2	8.3	2.6
k_{cat} (s^{-1})	57	4.1	85	270	55	0.06	4.0
k_{cat}/K_m (M^{-1} s^{-1})	5.8×10^6	3.1×10^5	8.2×10^6	8.2×10^6	8.8×10^6	7.9×10^3	1.6×10^6

Supplemental Figures

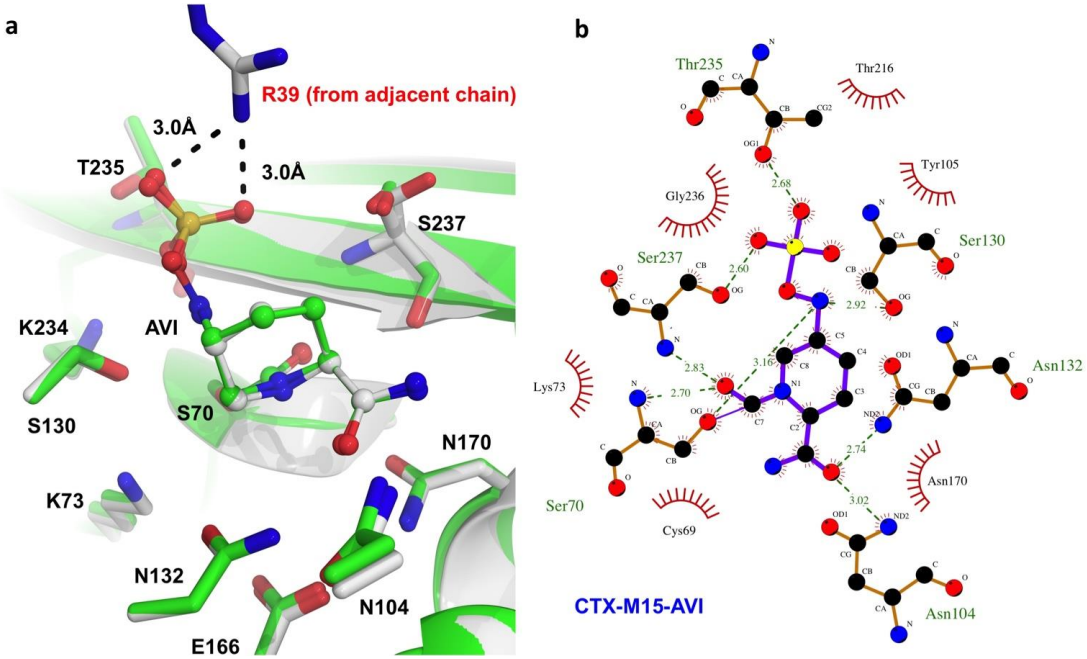

Supplemental Figure 2-1. Carbamyl-avibactam bound CTX-M-15 active site details. (a) Active site overlay of carbamyl-avibactam CTX-M-15 complexes in spacegroups $P2_12_12_1$ (PDB ID: 4HBU) [2], and $P2_1$ (PDB ID: 4S2I). Carbon atoms for the 4HBU and 4S2I active site residues and avibactam are displayed in grey and green, with all other non-carbon atoms colored by type (N, blue; O, red; S, yellow). The 4HBU and 4S2I CTX-M-15 protein backbones are displayed as grey and green cartoons. (b) Protein-ligand interactions between CTX-M-15 and avibactam depicted in monomer A using LigPlot+ [3]. Avibactam and CTX-M-15 are displayed as purple and orange sticks with atoms colored by type. Hydrogen bonding and electrostatic interactions are shown as green dashes. Ligand-protein hydrophobic contacts are shown as curved red combs.

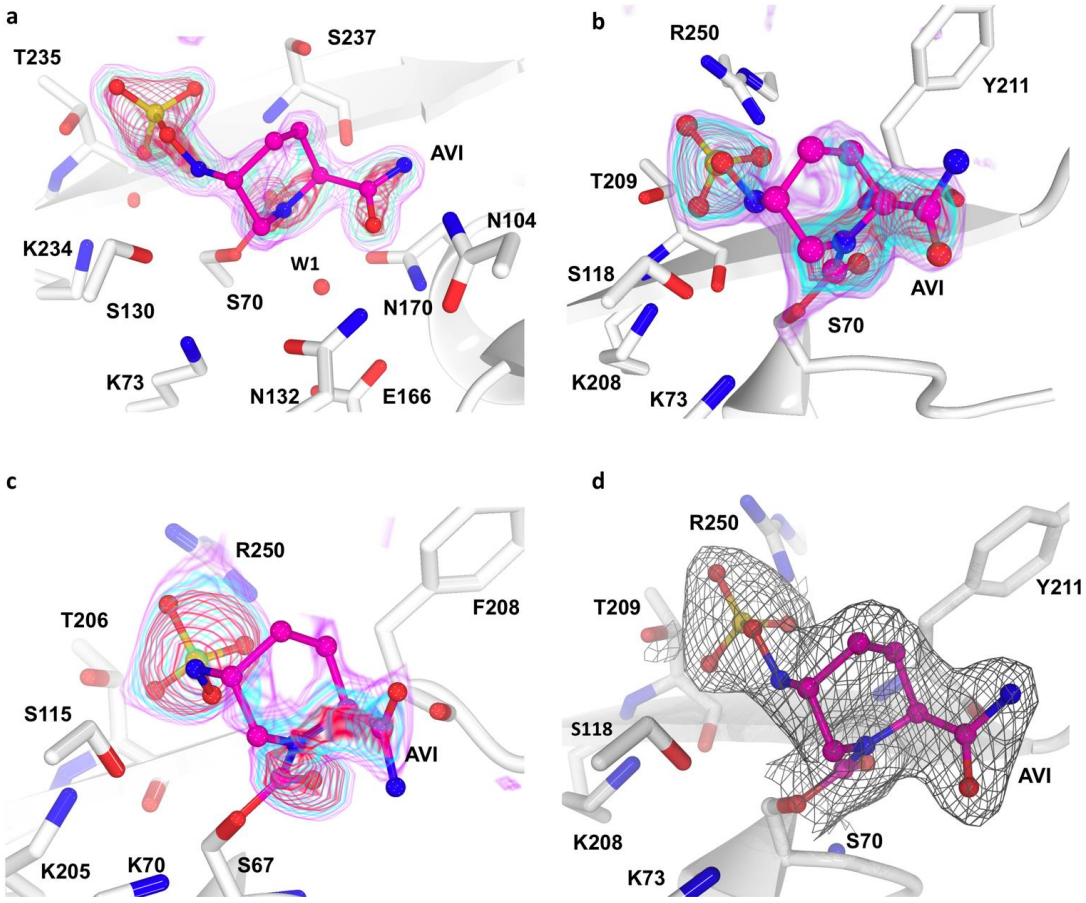

Supplemental Figure 2-2. Avibactam electron density for carbamylated CTX-M-15, OXA-48 and OXA-10 crystal structures. In a-c, the F_o-F_c ligand omit maps are contoured at 3.0, 4.0 and 5.0 σ and are shown as pink, cyan and red transparent surfaces. (a) Carbamyl-avibactam CTX-M-15 ligand omit F_o-F_c electron density. The CTX-M-15 cartoon is shown in white with selected active site residues displayed in stick representation and non-carbon atoms are colored by type. (b) and (c), Carbamyl-avibactam OXA-48-AVI7.5 and OXA-10 ligand omit F_o-F_c electron density. In B and C, the OXA-48-AVI7.5 and OXA-10 protein backbones are shown in white cartoon representation with selected active site residues displayed as white sticks with non-carbon atoms colored by type. In all panels, the carbamyl-avibactam is represented as pink sticks with atoms colored by type. (d) Carbamyl-avibactam OXA-48-AVI7.5 final refined $2F_o$-F_c electron density. The OXA-48-AVI7.5 protein and bound avibactam are displayed as in b. The $2F_o$-F_c electron density map is contoured at 1.0σ and is displayed as a grey mesh.

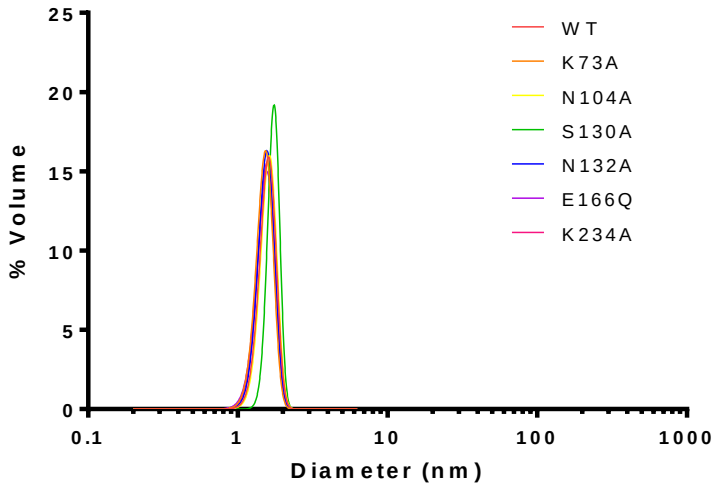

Supplemental Figure 2-3. CTX-M-15 variants are stable in solution. Characterization of the particle size distribution for CTX-M-15 variants using dynamic light scattering.

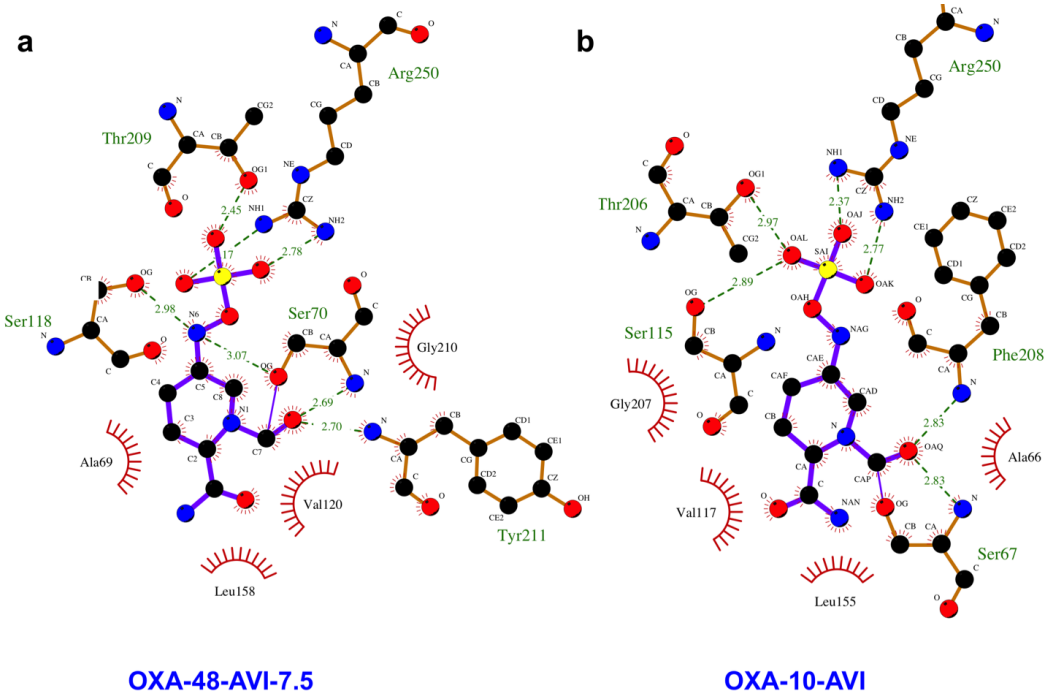

Supplemental Figure 2-4. Interactions between avibactam and active site residues in OXA-48 and OXA-10. (a) and (b), Chain A-avibactam interactions in OXA-48-AVI-7.5 and OXA-10-AVI crystal complexes designed using LigPlot+ [3]. In all panels, the carbamyl-avibactam and active site residues are displayed as purple and orange sticks with atoms colored by type. Hydrogen bonding and electrostatic interactions are shown as green dashes. Ligand-protein hydrophobic contacts are displayed as curved red combs.

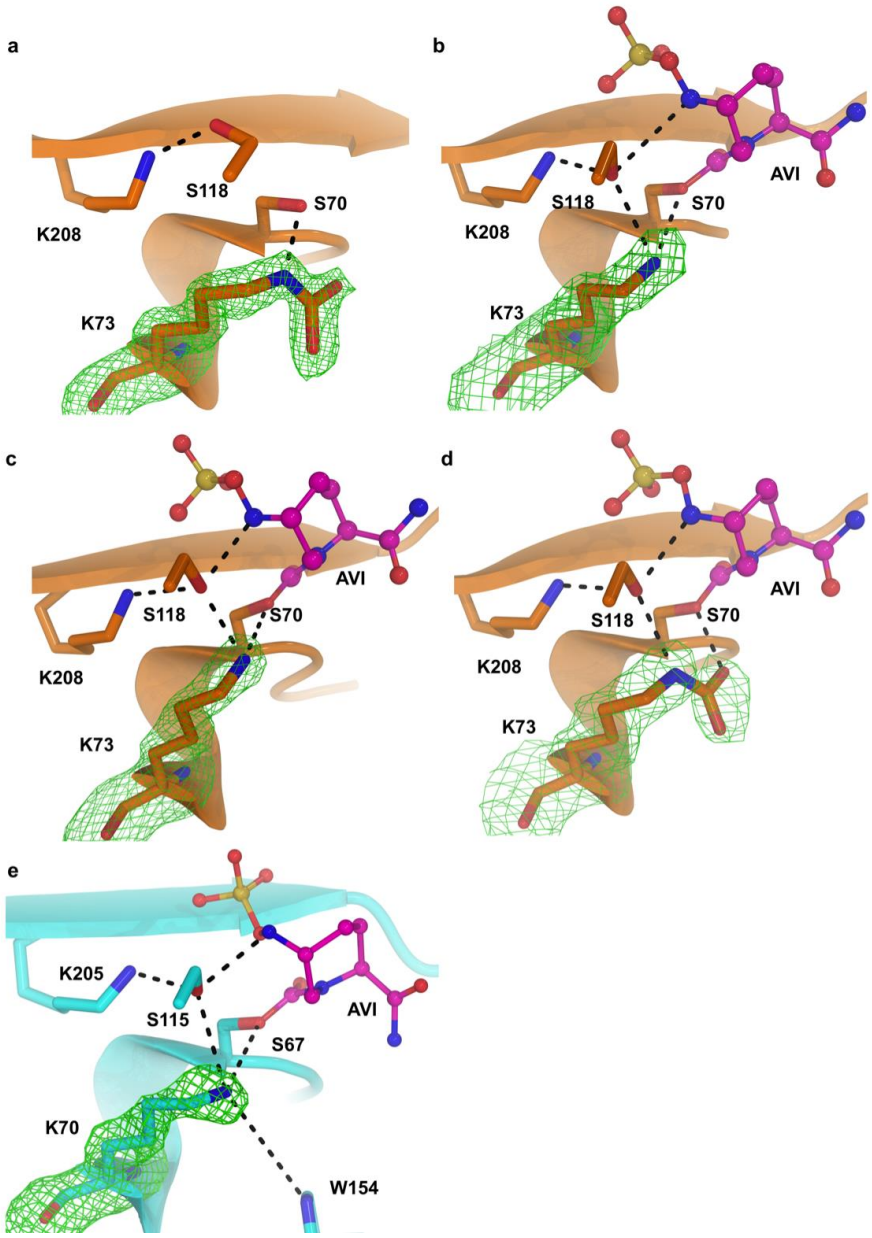

Supplemental Figure 2-5. Carboxylation state of the SXXK lysine in OXA-48 and OXA-10. (a) Native OXA-48 (pH 7.5), chain A Lys73 omit F_o-F_c electron density. The OXA-48 protein backbone is displayed as an orange cartoon with selected active site residues shown as sticks with all non-carbon atoms colored by type. The F_o-F_c Lys73 omit electron density map is contoured at 3.0σ and is shown as a green mesh. (b), (c) and (d) OXA-48-AVI6.5 (pH 6.5), OXA-48-AVI7.5 (pH 7.5) and OXA-48-AVI8.5 (pH 8.5), chain A Lys73 omit F_o-F_c electron density. The OXA-48 protein backbone, active site residues and F_o-F_c Lys73 omit electron density maps are shown as in A. The carbamyl-avibactam is represented as pink sticks with all non-carbon atoms colored by type. (e) OXA-10-AVI (pH 6.5) chain A K70 omit F_o-F_c electron density map. The OXA-10 protein backbone is displayed in cyan cartoon representation with selected active site residues shown as sticks with all non-carbon atoms colored by type. The F_o-F_c K70 omit electron density map is represented as in a. The carbamyl-avibactam is represented as in b.

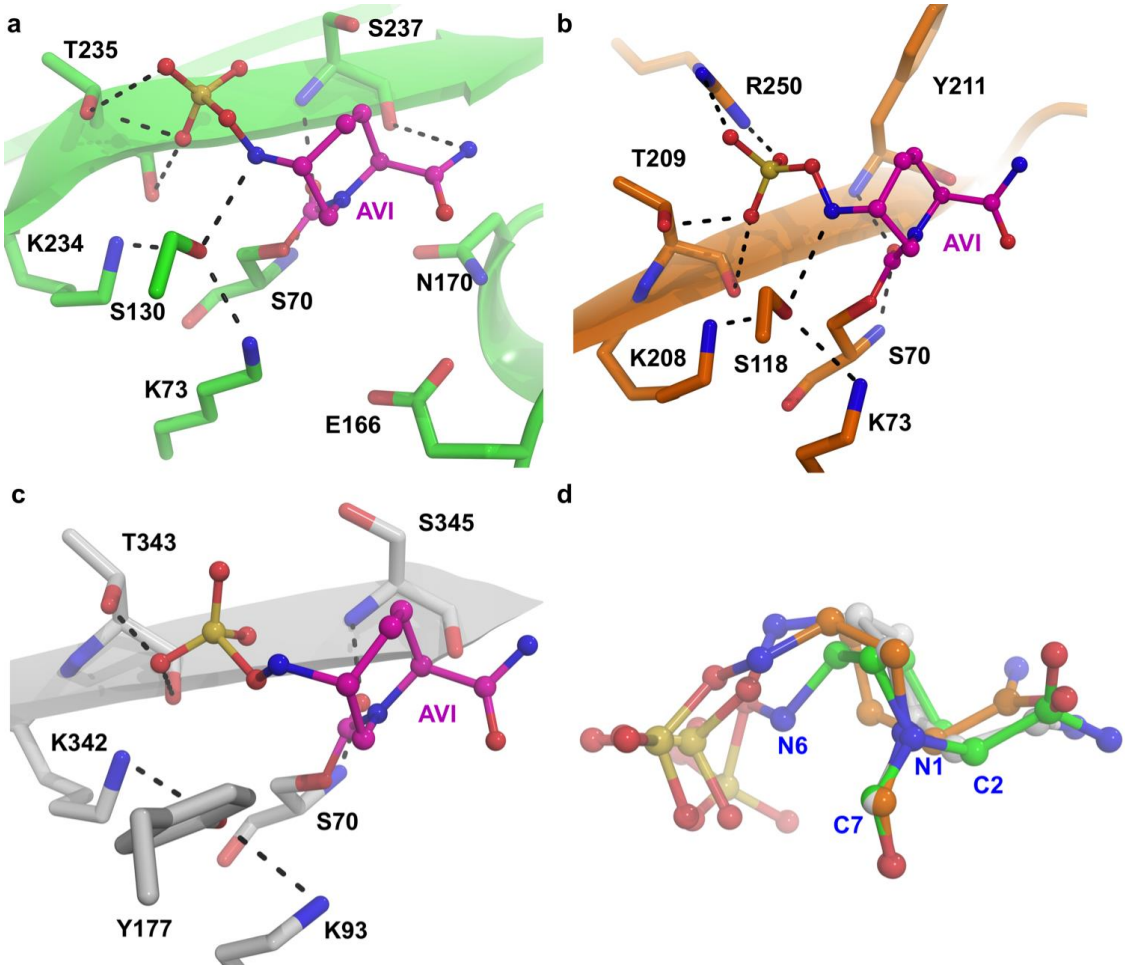

Supplemental Figure 2-6. Comparison of carbamyl-avibactam CTX-M-15, OXA-48 and AmpC co-crystal structures. (a) Active site close-up of carbamyl-avibactam CTX-M-15. The carbon atoms of avibactam are pink with non-carbon atoms colored by atom type. The avibactam bound CTX-M-15 protein chain is represented as a green cartoon, with key active site residues shown as sticks with atoms colored by type. (b) and (c) Active site overlay of carbamyl-avibactam OXA-48, and AmpC (PDB ID: 4HEF) [2]. In b and c, the bound avibactam is represented as in a. The OXA-48 and AmpC protein chains are illustrated as orange and grey cartoons, and active site residues are depicted as sticks with non-carbon atoms colored by type. In a-c, hydrogen bonding and electrostatic interactions are shown as black dashes. (d) Overlay of carbamyl-avibactam from the CTX-M-15, OXA-48 and AmpC co-crystal structures (PDB ID's: 4S2I, 4S2K, 4HEF) [2]. Carbamyl-avibactam from the CTX-M-15, OXA-48 and AmpC structures are displayed as green, orange and white sticks with all non-carbon atoms colored by type. The carbamyl-avibactam C7 carbon, carbonyl oxygen and N1 atoms were fixed in the exact same positions.

Supplemental Figures 2-7 to 2-16. ESI-LC-MS trace overlays of avibactam incubated with β-lactamase as noted at pH 7.5 (Figs S7-S15). Samples were analyzed at 0 hours (red trace) and 24 hours (blue trace). Avibactam remains intact in all samples with the exception of KPC-2 and no enzyme pH 8.5.

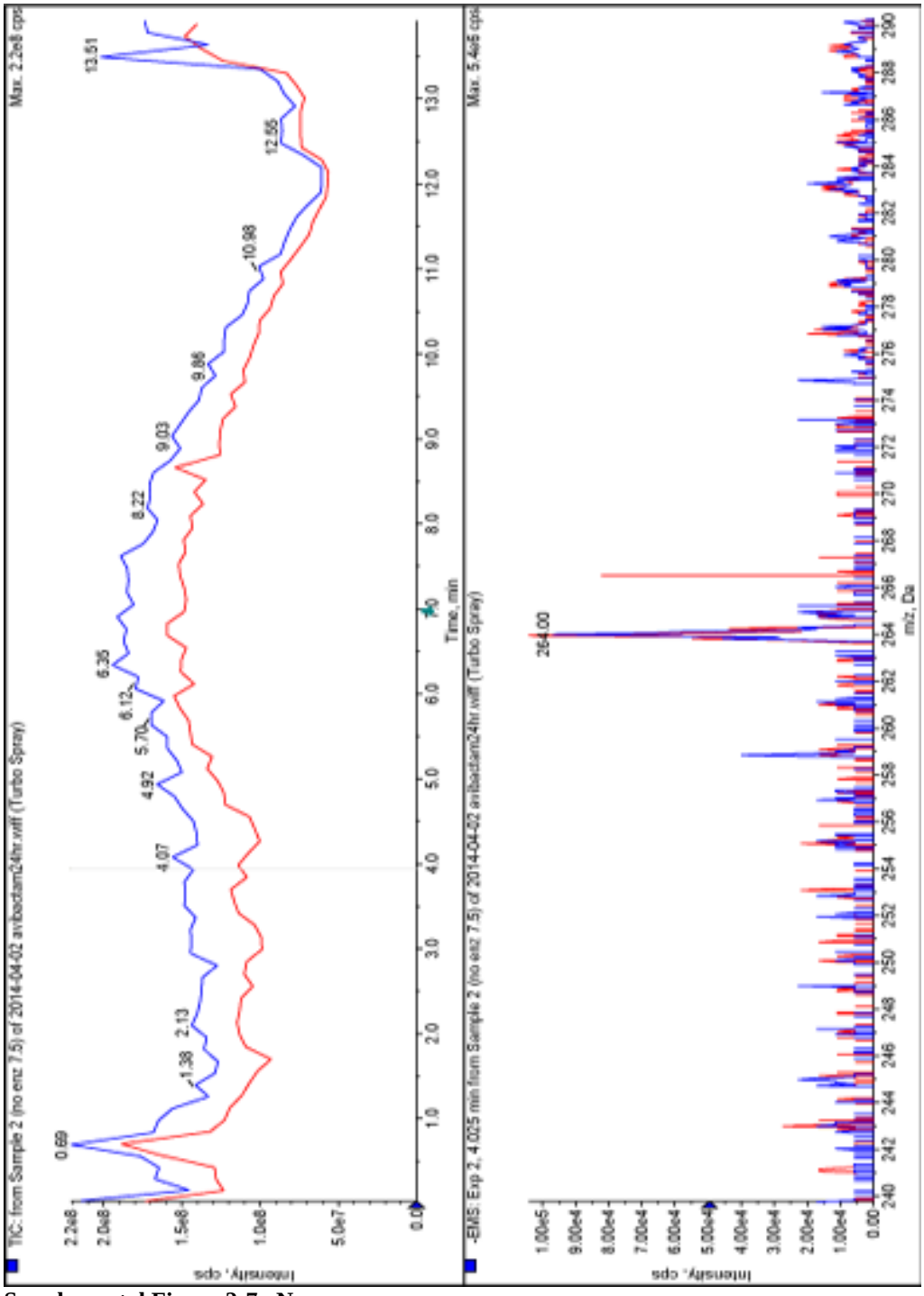

Supplemental Figure 2-7. No enzyme

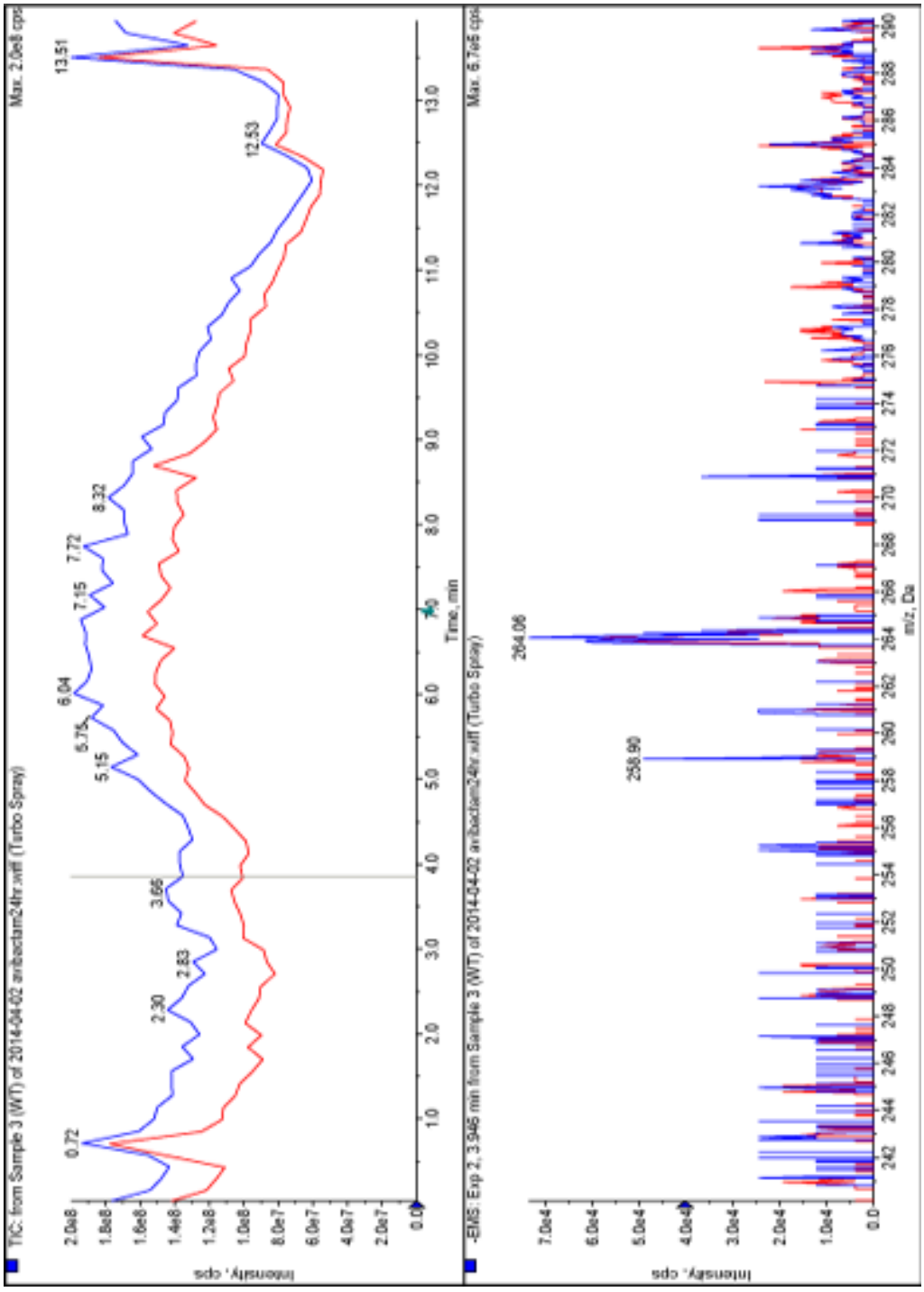

Supplemental Figure 2-8. CTX-M-15

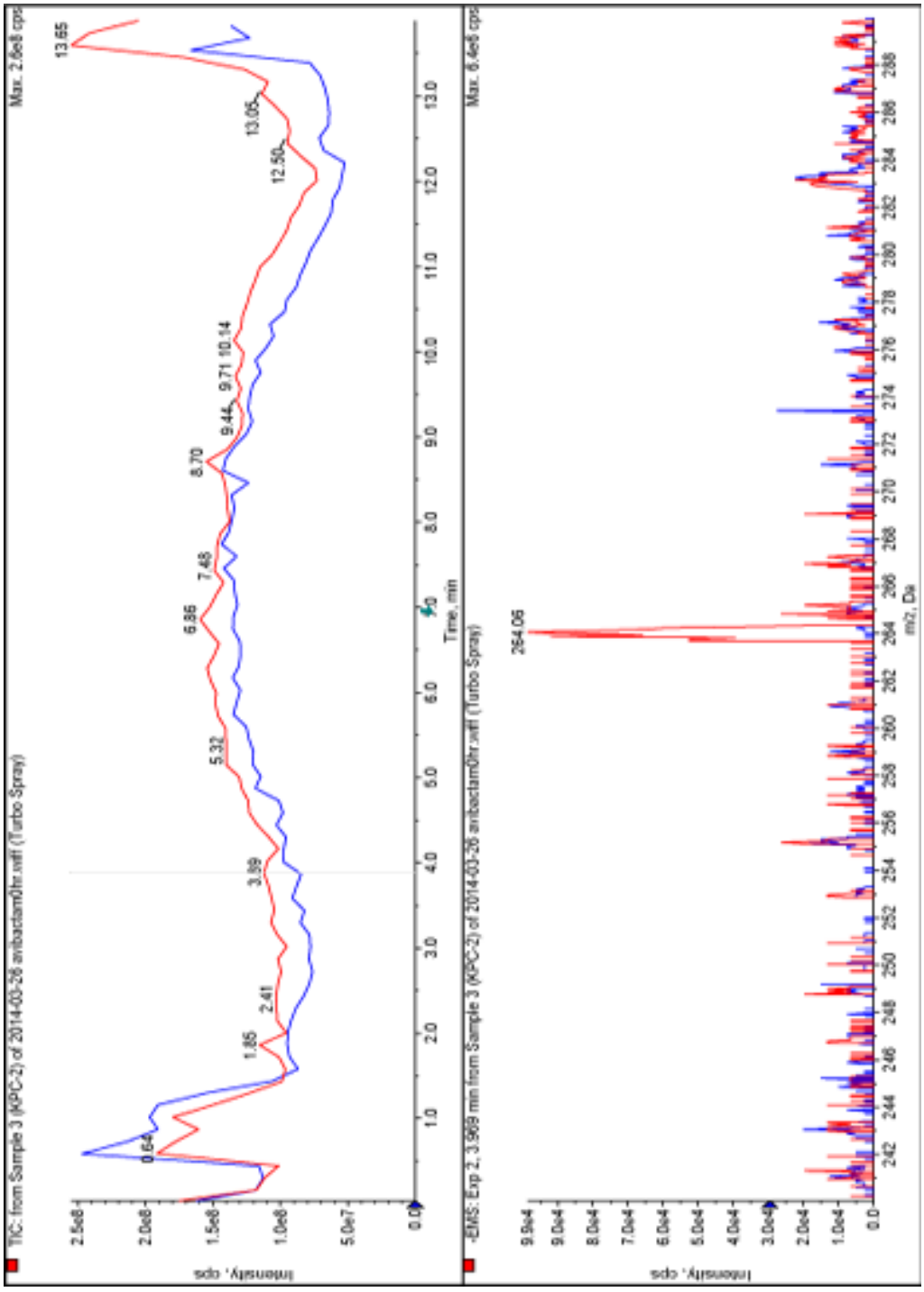

Supplemental Figure 2-9. KPC-2

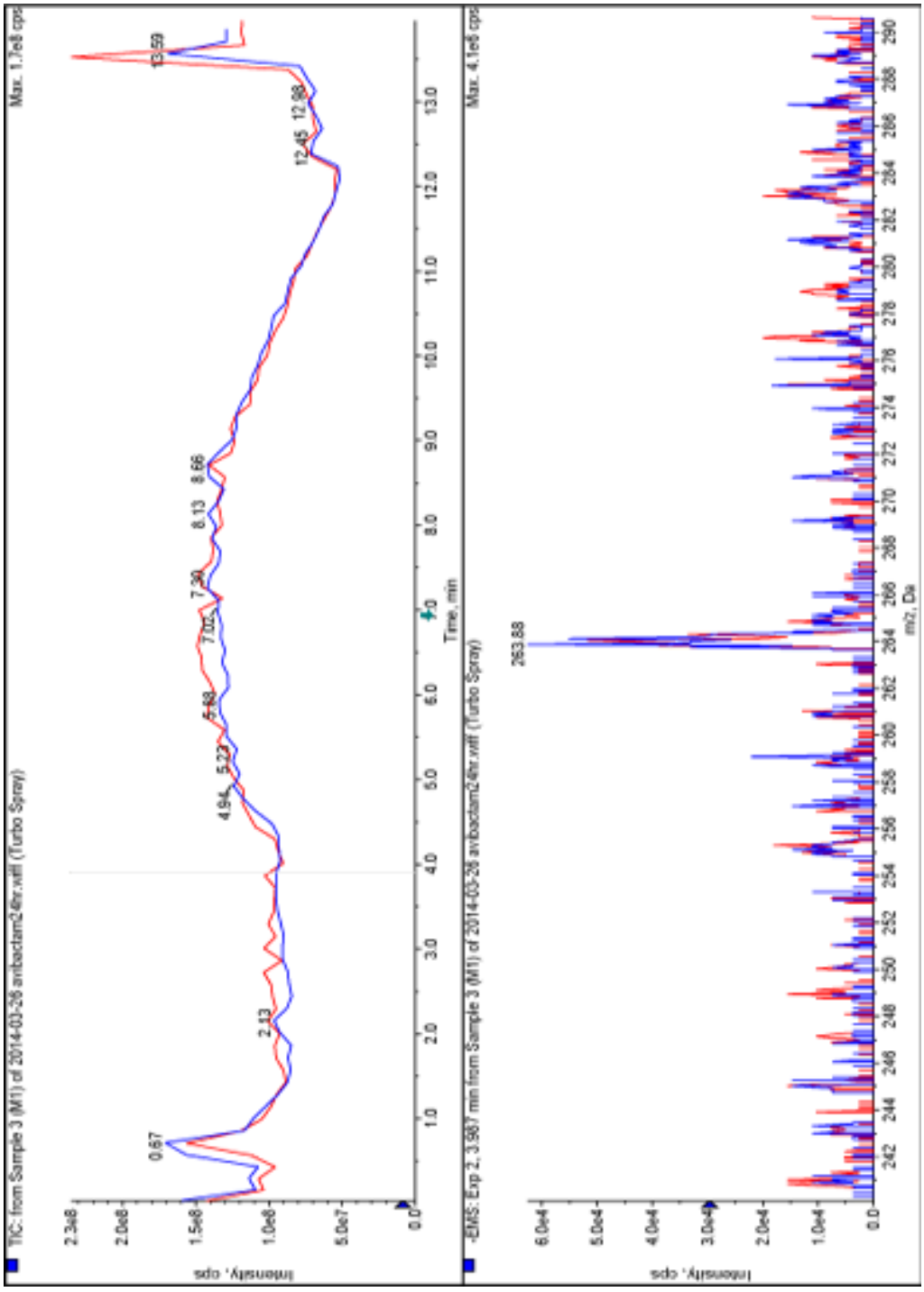

Supplemental Figure 2-10. CTX-M-15 Lys73Ala

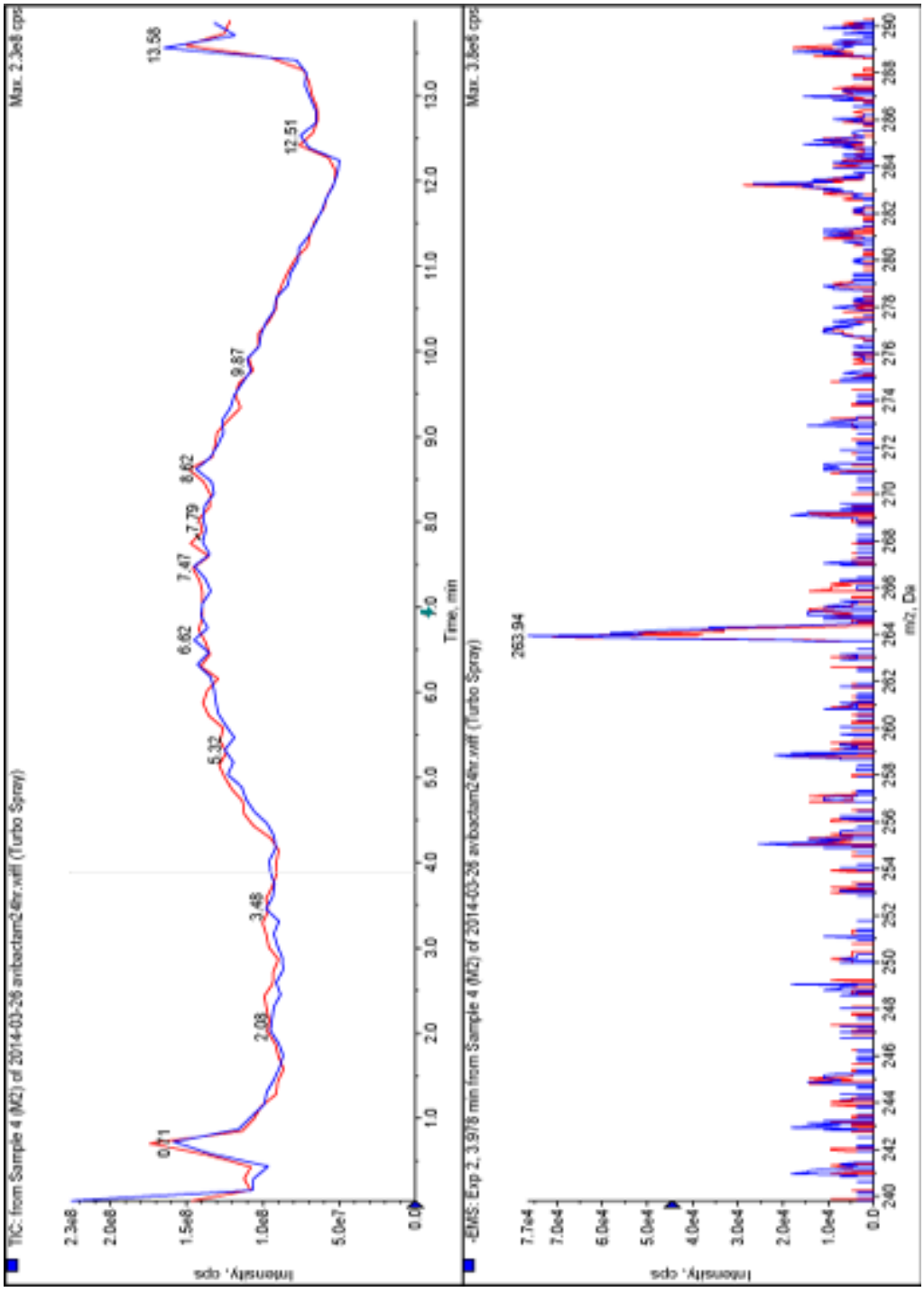

Supplemental Figure 2-11. CTX-M-15 Asn104Ala

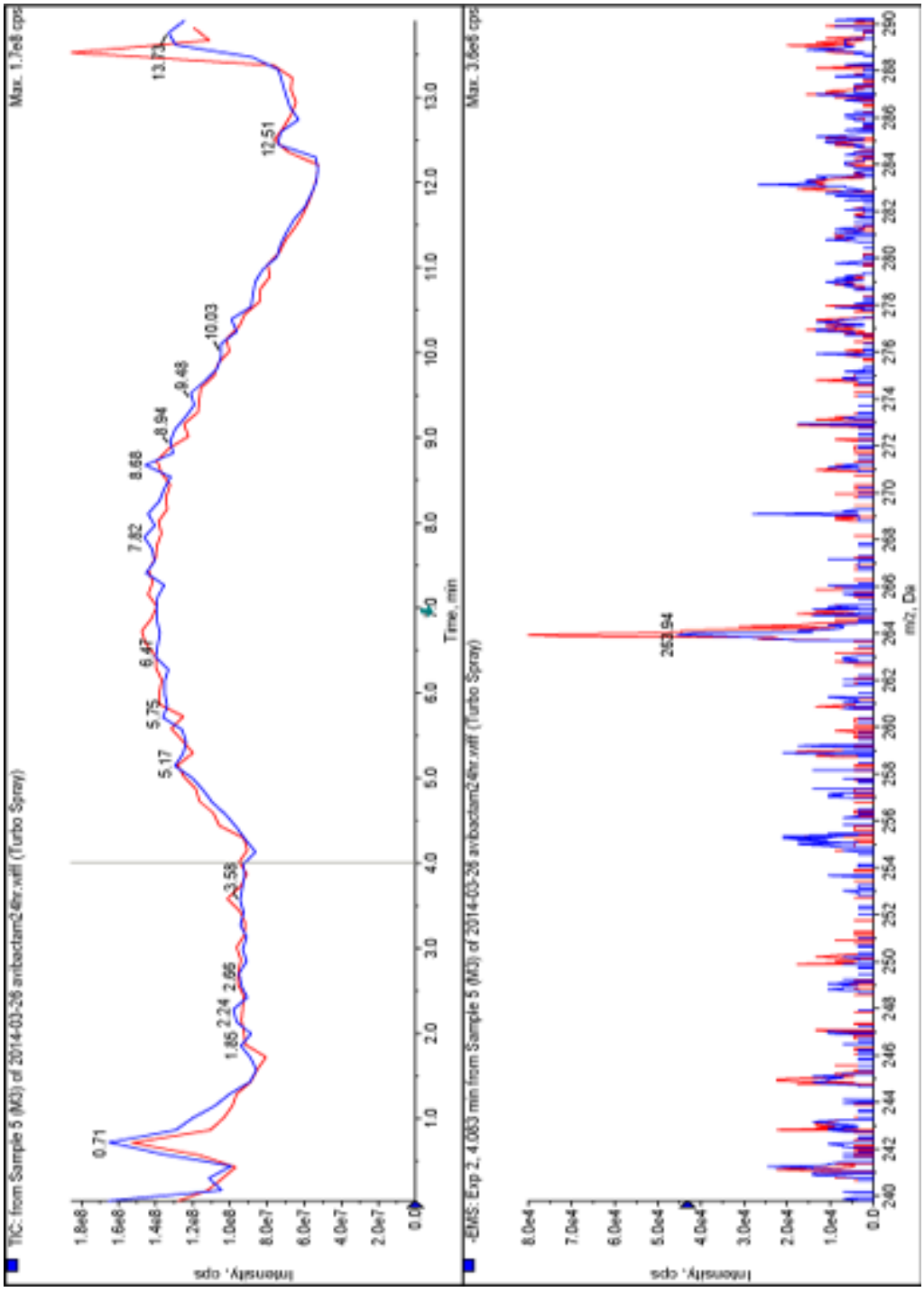

Supplemental Figure 2-12. CTX-M-15 Ser130Ala

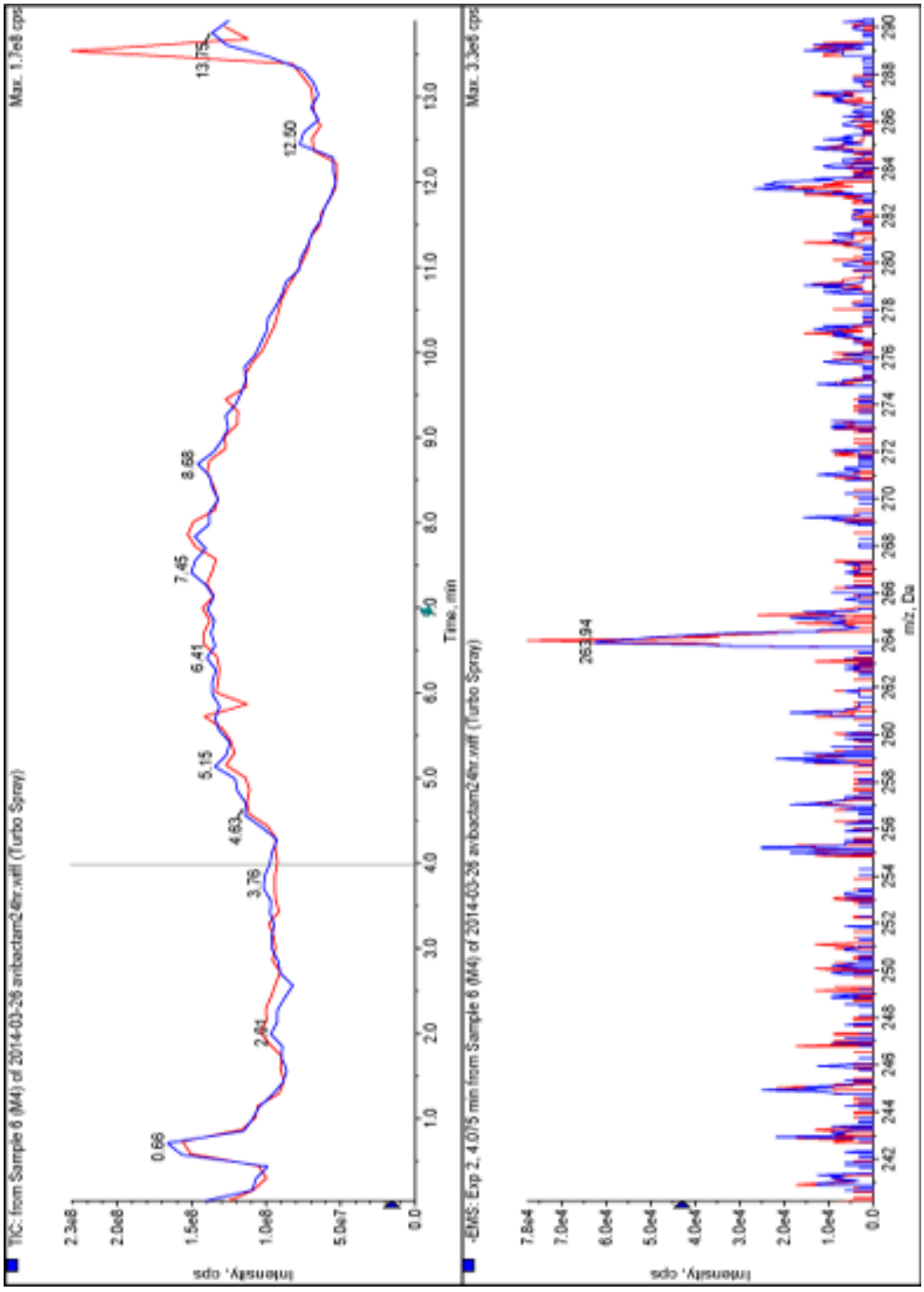

Supplemental Figure 2-13. CTX-M-15 Asn132Ala

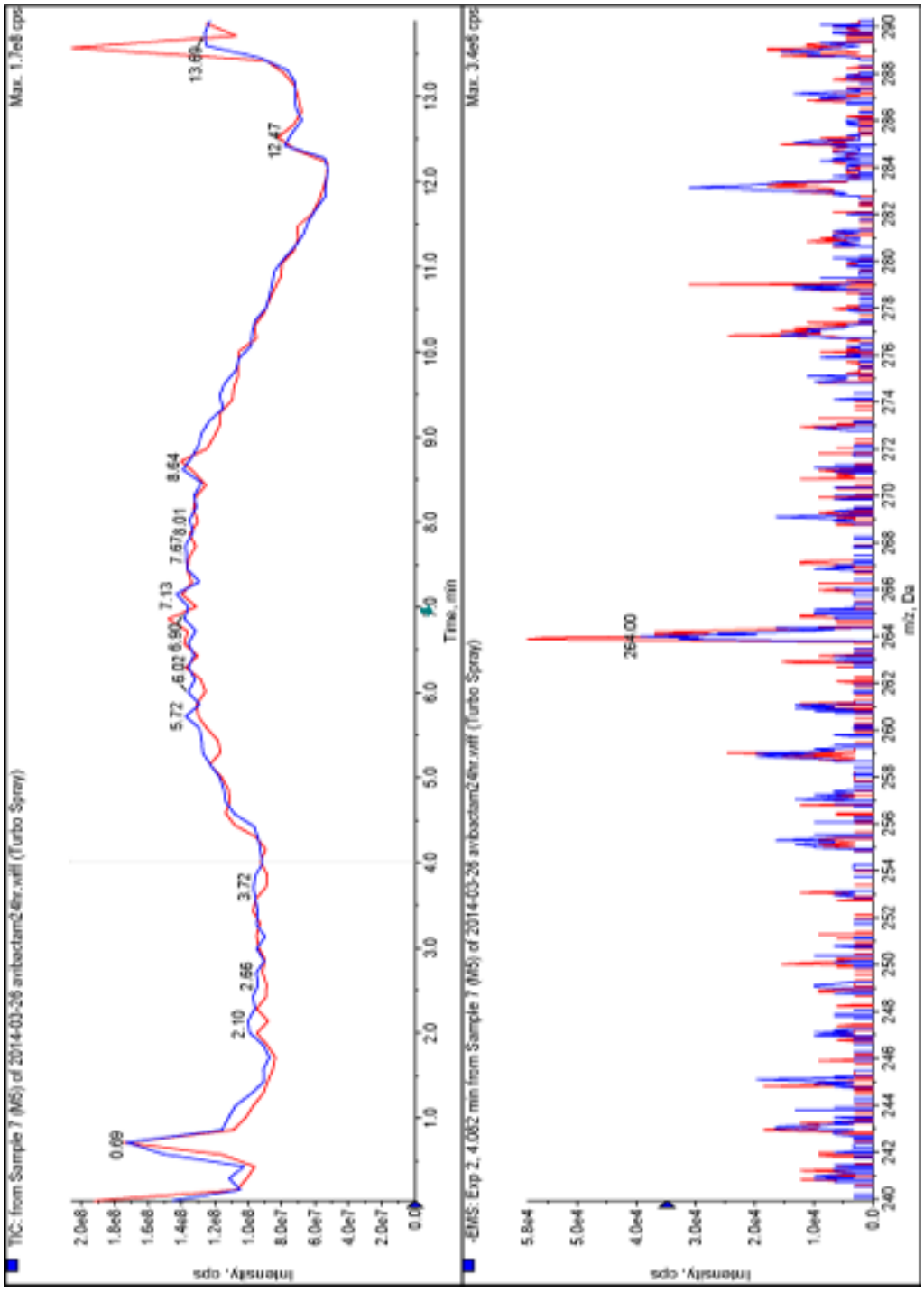

Supplemental Figure 2-14. CTX-M-15 Glu166Gln

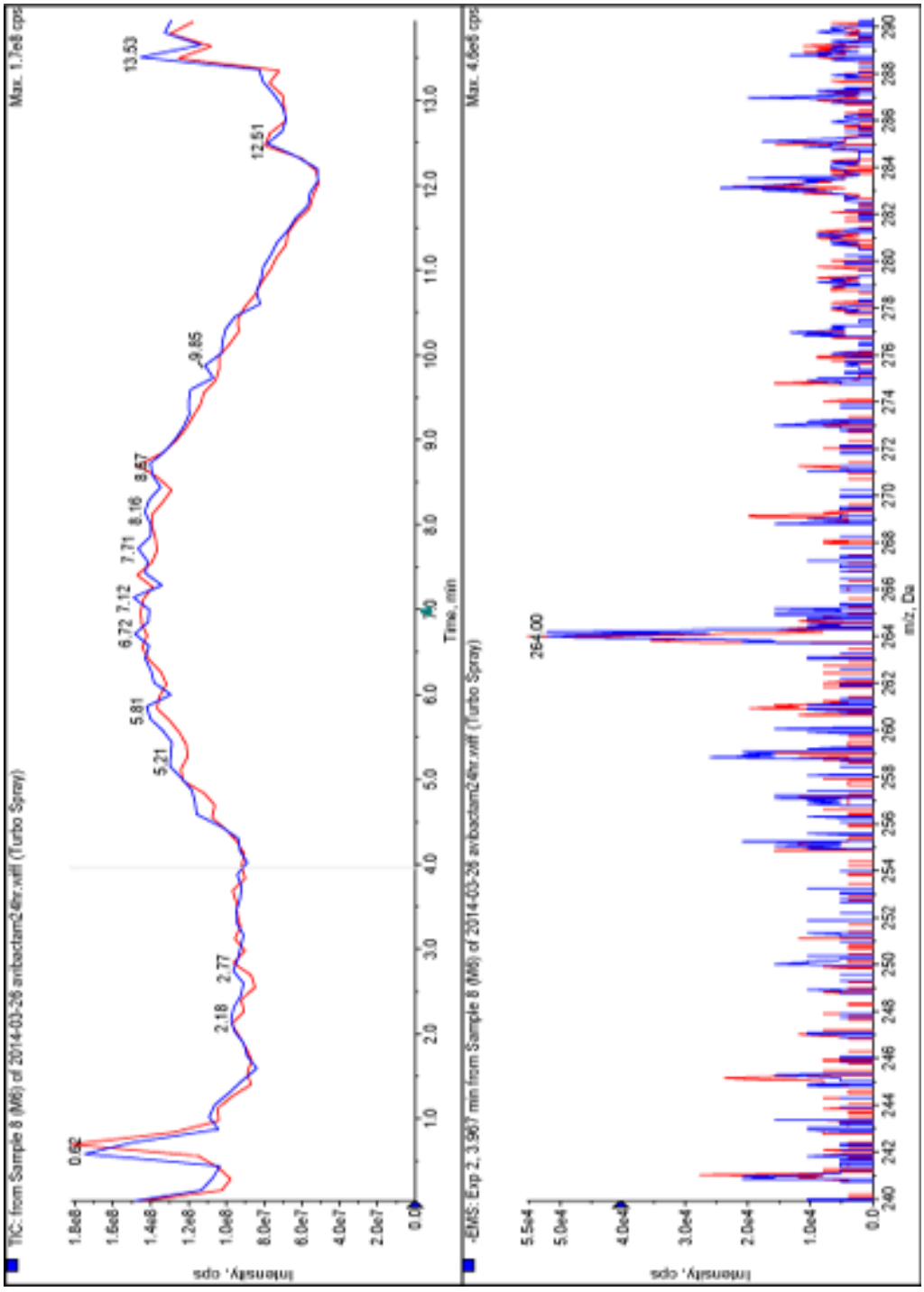

Supplemental Figure 2-15. CTX-M-15 Lys234Ala

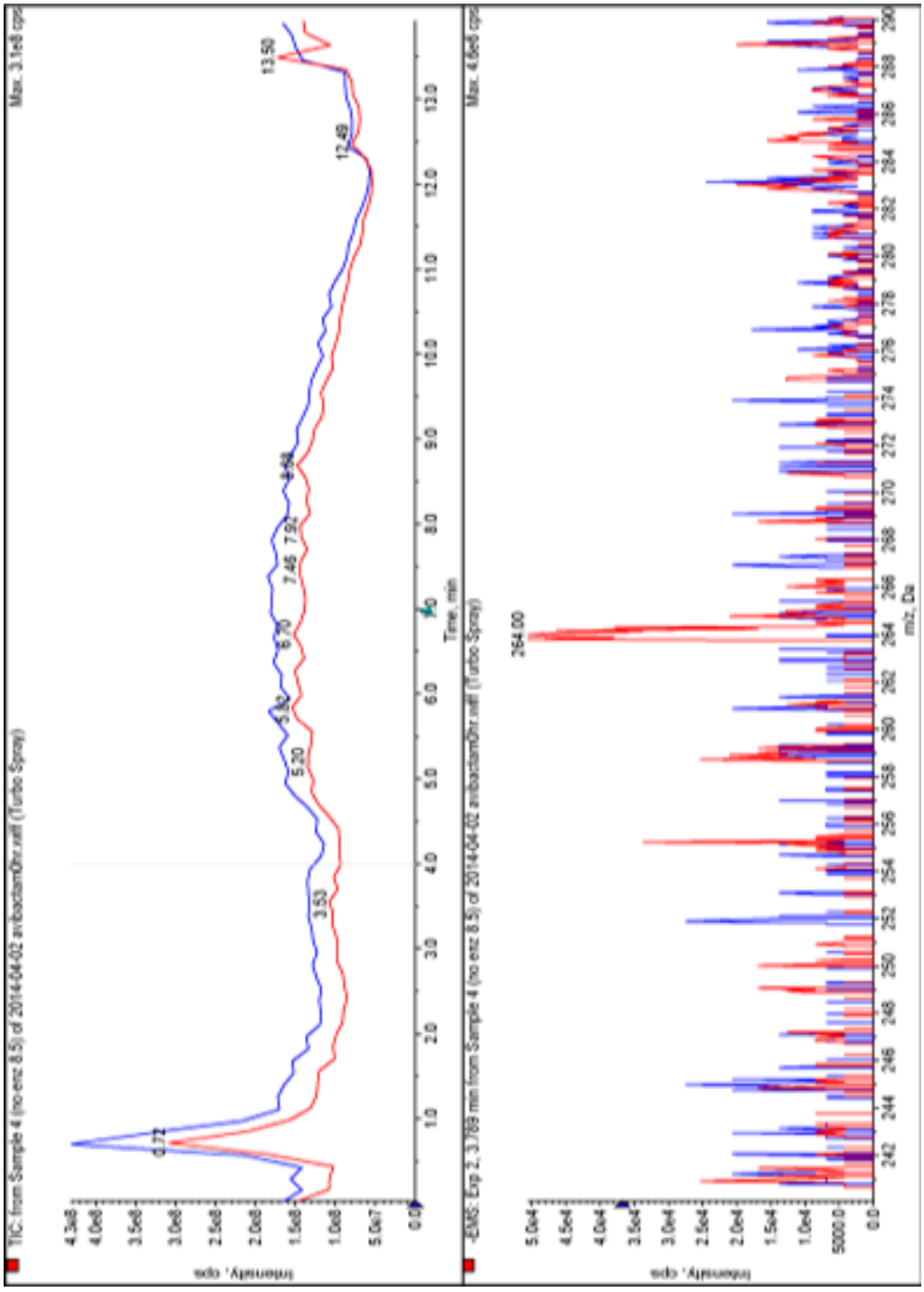

Supplemental Figure 2-16. No enzyme (pH 8.5)

CHAPTER 3

STRUCTURAL AND KINETIC CHARACTERIZATION OF DIAZABICYCLOOCTANES AS DUAL INHIBITORS OF BOTH SERINE-BETA-LACTAMASES AND PENICILLIN-BINDING PROTEINS

CHAPTER 3 PREFACE

The work presented in this chapter was previously published in:

King, A. M.*, King, D. T.*, French, S., Brouillette, E., Asli, A., Alexander, J. A., Vuckovic, M., Maiti, S. N., Parr, T. R., Jr., Brown, E. D., Malouin, F., Strynadka, N. C. and Wright, G. D. Structural and Kinetic Characterization of Diazabicyclooctanes as Dual Inhibitors of Both Serine-beta-Lactamases and Penicillin-Binding Proteins. ACS Chemical Biology 11, 864-868 (2016).

* These authors contributed equally

Copyright © American Chemical Society.

I co-authored this work with Dustin T. King. I conducted cloning, protein purification, enzyme kinetics, MIC experiments and all microbiology.

Acknowledgements:

We acknowledge beamline staff of CMCF-1 at the CLS synchrotron facility (Saskatoon, SK) for assistance with data collection and S. Salama for compound synthesis.

ABSTRACT

Avibactam is a DBO BLI possessing outstanding but incomplete efficacy against multidrug-resistant Gram-negative pathogens in combination with β-lactam antibiotics. Significant pharmaceutical investment in generating derivatives of avibactam warrants a thorough characterization of their activity. We show here through structural and kinetic analysis that select diazabicyclooctane derivatives display effective but varied inhibition of two clinically important β-lactamases (CTX-M-15, and OXA-48). Furthermore, these derivatives exhibit considerable antimicrobial activity (minimum inhibitory concentration (MIC) ≤ 2μg/mL) against clinical isolates of *P. aeruginosa, Escherichia coli* (*E. coli)*, and *Enterobacter spp*. Imaging of cell phenotype along with structural and biochemical experiments unambiguously demonstrate that this activity, in *E. coli*, is a result of targeting PBP 2. Our results suggest that structure-activity relationship studies for the purpose of drug discovery must consider both β-lactamases and PBPs as targets. We believe that this approach will yield next-generation combination or monotherapies with an expanded spectrum of activity against currently untreatable Gram-negative pathogens.

INTRODUCTION

The discovery and semisynthetic modification of the prototypical β-lactam antibiotic, penicillin, revolutionized modern medicine with its unprecedented ability to combat bacterial infection (Kardos and Demain, 2011). β-lactams target the final step in bacterial peptidoglycan biogenesis, wherein they inactivate the transpeptidase activity of PBPs (Waxman and Strominger, 1983). However, the evolution and dissemination of bacterial resistance to β-lactams, primarily mediated by β-lactamase expression, has emerged in response to the selective pressure due in-part to widespread clinical use (Fisher et al., 2005). β-Lactamases are grouped into four classes: the class B enzymes are MBLs that use active site zinc ion(s) during bond cleavage, whereas the more clinically prevalent class A, C and D enzymes are SBLs that employ a serine nucleophile to catalyze hydrolysis (Bush, 2013a).

Two therapeutic strategies have emerged in response to β-lactamase-mediated β-lactam resistance: 1) discovery of additional β-lactam scaffolds and subsequent medicinal chemistry efforts towards evading β-lactamase resistance (Dalhoff and Thomson, 2003) and 2) development of β-lactamase inhibitors (Drawz and Bonomo, 2010a). Avibactam is a reversible, covalent inhibitor possessing a novel DBO core scaffold recently approved by the U.S. Food and Drug Administration in combination with ceftazidime (Avycaz) to treat patients for which there are limited or no alternative therapeutic options (Figure 1a) (Rubin, 2015). Avibactam forms a long-lived carbamyl-linkage with the SBL active site serine. This complex does not dissociate by hydrolysis as do the β-lactam based inhibitors, yet undergoes a reversible recyclization mechanism that reforms intact avibactam (Ehmann et

al., 2012b). Avibactam displays unprecedented inhibitory activity against the class A and C β-lactamases. However, avibactam does not inhibit the MBLs and variable levels of inhibition are observed for the class D SBLs.

Semisynthetic modification of the acyl side-chain of penicillin led to the development of derivatives with a broader spectrum of activity and resistance to β-lactamases, amongst other favorable properties (Rolinson, 1998). Here, we adopt a similar strategy and derivatize the DBO scaffold and thoroughly investigate the inhibitory properties of these novel compounds.

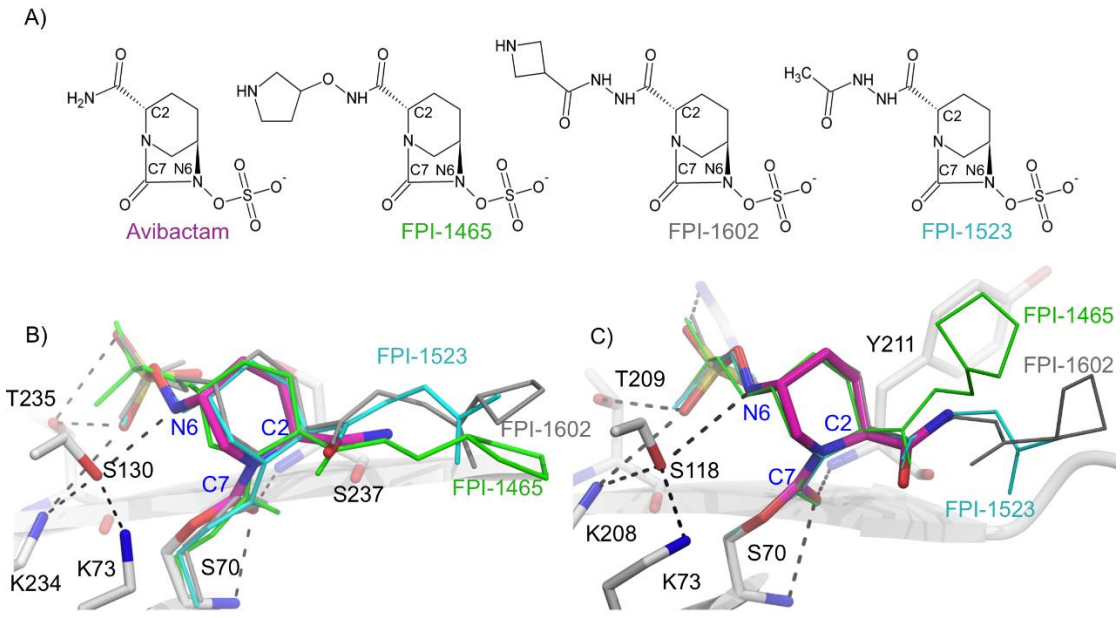

Figure 3-1. (A), Chemical structures of avibactam derivatives used in this study. (B, C) Overlays of carbamyl-avibactam derivatives bound to the class A β-lactamase CTX-M-15 (B) and the class D β-lactamase OXA-48 (C) (rmsd= 0.1Å on all CA atoms).

MATERIALS AND METHODS

Reagents

All chemicals of analytical grade were purchased from Sigma-Aldrich, unless otherwise stated. Nitrocefin was synthesized as described previously (Lee et al., 2005a).

β-Lactamase Protein Expression and Purification

The *E. coli* CTX-M-15 and *Klebsiella pneumonia* OXA-48 constructs include the mature sequences (Q26-L288, and W25-P265) with the signal peptide removed and were prepared as previously described (King et al., 2015). Purified CTX-M-15 (with His-tag cleaved) and OXA-48 (with un-cleaved His-tag) were dialyzed into fresh crystallization buffer (CTX-M-15 buffer: 10mM Tris pH 7.5, 100mM NaCl, 250uM 2-mercaptoethanol, and OXA-48 Buffer: 20mM Tris pH 7.5, 100mM NaCl) and concentrated to ~30mg/mL. For kinetics studies CTX-M-15 and OXA-48 were purified as previously described (King et al., 2014).

PBP Plasmid Construction, Protein Expression, and Purification

The *E. coli* PBP1a, PBP1b, PBP2, and PBP3 DNA corresponding to amino acid residues 1-855, 58-804, 60-633, and 57-577 were amplified from *E. coli* K12 genomic DNA. Restriction free cloning was used to produce pET-41b expression vectors containing each of the PBPs with a thrombin cleavable C-terminal 8XHis tag (van den Ent and Löwe, 2006).

Vectors containing the *E. coli* PBP1b, and PBP1a membrane proteins were transformed into *E. coli* BL21(DE3), and *E. coli* C43(DE3) host cells. The transformed cells were grown at 37°C until an OD_{600} of 0.6 was reached, and the samples were cooled to room temperature for 30 min. Protein expression was induced by addition of 1mM isopropyl β-D-1-thiogalactopyranoside (IPTG) and the cultures were incubated at 25 °C overnight. Cell pellets were resuspended in lysis buffer (PBP1a: 25mM Tris pH 7.5, 10mM $MgCl_2$, 300mM NaCl, 1 EDTA free protease inhibitor tablet from Roche, PBP1b: 20mM Tris pH 8.0, 300 mM NaCl, 1 EDTA free protease inhibitor tablet from Roche) and lysed by 2 passes on a French press at a pressure of 1500 p.s.i. The cell lysate was then centrifuged twice at 14, 600 g for 15 minutes to remove unbroken cells and inclusion bodies. The supernatant was then centrifuged at 200, 000 g for 1 hour in order to pellet the membranes. Membranes were homogenized and incubated for 4 hours in the presence of extraction buffer (lysis buffer + 20mM n-Dodecyl-β-D-maltopyranoside, DDM; Anatrace). The solubilized protein was then purified using nickel chelation chromatography. The column was pre-incubated in the presence of equilibration buffer (PBP1a: 25mM Tris pH 7.5, 300mM NaCl, 1mM DDM, PBP1b: 20mM Tris pH 8.0, 300mM NaCl, 1mM DDM) and eluted using a linear gradient of imidazole from 0-500mM. Fractions containing purified protein were exchanged using a 100 kDa cut-off concentrator into assay buffer [PBP1a: equilibration buffer, PBP1b: 20mM Tris pH 8.0, 300mM NaCl, 4.5 mM n-Decyl-β-D-maltopyranoside (DM), Anatrace].

E. coli BL21(DE3) host cells transformed with the *E. coli* PBP2 and PBP3 expression vectors were grown at 37°C until an OD_{600} of 0.7 was attained. Protein

expression was induced by addition of 1mM IPTG and the cultures (typically 9L) were incubated at 30°C for 16 hrs. Cell pellets were resuspended in lysis buffer [PBP2: 50mM Tris pH 8.0, 300mM NaCl, 1 EDTA free protease inhibitor table from Roche, PBP3: 20mM Tris pH 8.0, 10% glycerol, 300 mM NaCl, 10 mM $MgCl_2$, 40mM 3-[(3-cholamidopropyl)dimethylammonio]-1-propanesulfonate (CHAPS), 1 EDTA free protease inhibitor tablet from Roche] and lysed by 2 passes on a French press at a pressure of 1500 p.s.i. The cell lysate was then centrifuged at 20,000 g for 1 hour. The supernatant was purified using nickel chelation chromatography. The column was pre-incubated in the presence of equilibration buffer (50 mM Tris pH 8.0, 300 mM NaCl, 5% glycerol) and eluted using a linear gradient of imidazole from 0-600mM. Peak fractions containing purified protein were pooled and exchanged into assay buffer (equilibration buffer), using a 50 KDa cutoff Amicon centrifugal concentrator.

Crystallization, Data Collection and Structure Determination

FPI-1465, FPI-1523, and FPI-1602 carbamyl-enzyme complex CTX-M-15 crystals were grown using the sitting drop vapor diffusion method at 24°C. The drops consisted of 1 μL (30mg/mL protein + 2mM FPI-1465, FPI-1523 or FPI-1602), combined with an equal volume of precipitant [0.2M ammonium sulfate, 0.1M 2-(N-morpholino)ethanesulfonic acid (MES) pH6.5, 30% PEG5K monomethyl ether]. Crystals were soaked in cryoprotectant solution for 30s (mother liquor + 25% glycerol), and flash vitrified in liquid nitrogen. The FPI-1465, FPI-1523 and FPI-1602 crystals diffracted to 3.0, 1.67 and 2.70 Å

at beamline CMCF-08B1-1 of the Canadian Light Source in Saskatoon Saskatchewan (CLS).

FPI-1465 and FPI-1523 carbamyl-enzyme complex OXA-48 crystals were grown using the sitting drop vapor diffusion method at 24°C. The drops consisted of 1 μL (30 mg/mL protein + 3.6 mM FPI-1465 or 3.9 mM FPI-1523), combined with an equal volume of precipitant (0.005 M $CoCl_2$, 0.005 M $CdCl_2$, 0.005 M $MgCl_2$, 0.005 M $NiCl_2$, 0.1 M HEPES pH 7.5, 12% w/v PEG 3350). Co-crystallization attempts with FPI-1602 and OXA-48 failed to yield suitable crystals so apo crystals were grown as above but without ligand and soaked in 9.0 mM FPI-1602 for 2 days. Crystals were soaked in cryoprotectant solution for 30s (mother liquor + 29 to 33% (v/v) glycerol, and 3mM inhibitor), and flash vitrified in liquid nitrogen. The FPI-1465, FPI-1523, and FPI-1602 bound OXA-48 crystals diffracted to 1.96, 1.74 and 2.09Å at beamline CMCF 08B1-1 of the CLS.

FPI-1465 carbamyl-enzyme PBP1b crystals were grown using the sitting drop vapor diffusion method at 24°C. Drops contained 1μL (10mg/mL protein + 5mM FPI-1465), combined with an equal volume of precipitant (20% w/v PEG 3350, 0.2M potassium/sodium tartrate, 0.1M Bis Tris pH 8.5). Crystals were soaked in cryoprotectant solution for 4 min (mother liquor + 40% glycerol), and flash vitrified in liquid nitrogen. The FPI-1465-PBP1b crystals diffracted to 2.85Å resolution at beamline CMCF-08B1-1 of the CLS. All crystallographic data in this study was collected at a temperature of 100K and wavelength of 1.00Å.

Data were processed using Xia2.(Winter et al., 2013) During refinement, 5% of reflections were set aside for cross validation. All structures of CTX-M-15, OXA-48, and

PBP1b were solved by molecular replacement using the program Phaser (McCoy et al., 2007), with chain A of the native crystal structures as starting models (PDB ID's, CTX-M-15; 4HBT, OXA-48; 3HBR, PBP1b; 3VMA). Several iterations of manual rebuilding in Coot.(Emsley et al., 2010) followed by refinement using Phenix (Adams et al., 2010) were carried out. All structures were refined using isotropic B-factors, with the notable exception of FPI-1523-CTX-M-15, which was refined using anisotropic B-factors. Water and the appropriate ligands were added manually by examination of the F_o-F_c and $2F_o$-F_c electron density maps. Ligand CIF dictionaries were created using PRODRG.(Schüttelkopf and van Aalten, 2004) In all structures, all ligands were refined at full occupancy. Figs 1b-c, Figure 4-2d, and Supplementary Figure 2-1,2-2 and 2-7 were made using PyMol (Schrodinger, 2015).

Enzyme Assays

For all enzyme assays the buffer consisted of 50 mM HEPES pH 7.5 and Tween20 0.01%. OXA-48 experiments were performed with the addition of 50 mM $NaHCO_3$. Enzyme dilutions were made in BSA to 100 ng/µL. Acylation and deacylation experiments were performed as described previously (Ehmann et al., 2013a; King et al., 2015). For all compounds described, on-rates were determined using a continuous assay with nitrocefin as reporter substrate. For CTX-M-15, 100 µL enzyme (0.2 nM [final]) was added to 100 µL nitrocefin (50 µM [final]; K_m = 10 µM) and inhibitor. The maximum concentration of inhibitor used for CTX-M-15 on-rates was: avibactam, 0.8 µM; FPI-1465, 9 µM; FPI-1523, 4 µM; FPI-1602, 9 µM. The same methods were applied for OXA-48 (0.03 nM [final])

with nitrocefin (100 μM [final]; K_m = 50 μM). For OXA-48, the maximum concentration of inhibitor used was: avibactam, 50 μM; FPI-1465, 100 μM; FPI-1523, 100 μM; FPI-1602, 100 μM.

CTX-M-15 off-rates were determined continuously using the jump dilution method (Ehmann et al., 2013b) where 1 μM enzyme was incubated with 10 μM inhibitor at 37°C for 30 minutes and then diluted 1/400 before adding 20 μL to 180 μL of nitrocefin (400 μM) in assay buffer. For OXA-48 7 μM enzyme was incubated with 10 μM inhibitor and incubated for 1 hour before 1/16000 dilution and addition to substrate (200 μM) as above. For OXA-48, discontinuous sampling was applied for all inhibitors other than FPI-1465.

Concentration-response experiments assay buffer was used as above. All enzymes (1 nM) were incubated with inhibitor for 30 minutes at 37°C before dilution in nitrocefin (20 μM). Metalloenzymes were supplemented with 10 μM $ZnSO_4$. The maximum concentration of avibactam used was 20 μM.

Antimicrobial Susceptibility Testing

MIC testing was done according to the Clinical Laboratory Standards Institute (CLSI, 2012). All experiments were performed in duplicate and strains were grown at 37°C for 18 hours. pGDP constructs were made with the noted gene under control of a *bla* promoter for high-level constitutive expression.

PBP Binding Assays

For bacterial membrane preparation, an overnight culture of *E. coli* K-12 (MG1665) in BHI broth was diluted in a fresh medium and was further incubated at 37°C under agitation to reach an OD_{600} of ~0.6-0.7. The cells were harvested by centrifugation at 3,000 g for 15 min at 4°C, washed and suspended in KPN (20 mM potassium phosphate - 140 mM NaCl, pH 7.5). Cells were first treated with lysozyme (500 µg/mL) for 1h at 37°C, before addition of a protease inhibitor cocktail (Sigma Aldrich Canada, Oakville, ON), deoxyribonuclease (6 µg/mL) and ribonuclease (6 µg/mL). After 30 minutes of treatment, cells were disrupted by a French press and the bacterial lysate was centrifuged at 12,000 g for 10 min to remove unbroken cells. The supernatant was then centrifuged at 150,000 g for 40 min at 4°C using a fixed-angle rotor to collect the membranes. The membranes were suspended in a minimal volume of KPN buffer and stored at -86°C. Protein concentration was estimated by the method of Bradford with the BCA kit (Pierce) using BSA as a standard.

The relative binding affinity of test molecules for bacterial PBPs were assayed in a competition assay with the fluorescent penicillin BOCILLIN FL (Invitrogen, Carlsbad, CA) as the reporter molecule. Increasing concentrations of the test compounds were added to aliquots of the reaction mixture containing 30 µg of bacterial membrane preparation for 10 min at 37°C prior to the addition of BOCILLIN FL (100 µM) for an additional 20 min. Membrane-containing samples were then heated to 95°C for 3 min in electrophoretic loading buffer containing SDS before electrophoresis and separation of proteins on a SDS-polyacrylamide discontinuous gel system (5% stacking and 10% separating gels). After

electrophoresis, the gels were quickly rinsed in water and incubated for 30 min in a fixing solution (50% methanol - 7% acetic acid). Gels were scanned with a Molecular Imager FX Pro instrument (Bio-Rad Laboratories Canada, Mississauga, ON) using the excitation and emission wavelengths of 488 nm and 530 nm, respectively, to collect the image of the PBP profile. The concentration of the test compound needed to block 50% of the subsequent binding of BOCILLIN FL to each PBP represented the IC_{50} value.

BOCILLIN FL Competition Assays using Purified *E. coli* PBPs

To assess the relative inhibition of *E. coli* PBPs by the avibactam derivatives, SDS-PAGE based concentration response experiments were performed in triplicate using BOCILLIN FL as a reporter molecule. All reagents were diluted in assay buffer prior to use. To start the reaction, various concentrations of unlabeled compound and 27.8 μM BOCILLIN FL were simultaneously added to 4.7μM of purified PBP in a final reaction volume of 36 μL. The reaction was incubated at 25°C for 20 min prior to addition of 10X SDS-PAGE loading dye. In contrast, for pre-incubation experiments various amounts of inhibitor compound was pre-incubated with 4.7μM *E. coli* PBP1b for 48 hours prior to an additional 20 min incubation in the presence of 27.8 μM BOCILLIN FL (Supplemental Figure 3-6). The samples were then boiled for 2 min prior to loading 10μL on a 12% SDS-PAGE precast gel (Bio-Rad). Following electrophoresis, gels were imaged under UV light using a Syngene ChemiGenius2 bio imaging System. Densitometry analysis was performed using ImageJ as previously described (Schneider et al., 2012). The individual data points were normalized to the maximum value of the fluorescence intensity, which represents total

saturation of protein by BOCILLIN FL in the absence of unlabeled compound. Benzyl penicillin, and Kanamycin were used as positive and negative controls, respectively. The IC_{50} values are defined as the compound concentration required to reduce the residual binding of BOCILLIN FL by 50% and were calculated using SigmaPlot.

Microscopy

Cells were cultured in a standard MIC curve, then fixed and imaged according to the methods of Czarny et al (Czarny et al., 2014). In brief, after culture densities were recorded using a spectrophotometer, cultures were diluted 1:10 in 2% glutaraldehyde buffered with 25 mM HEPES (pH 6.8) for one hour. Then, 15 uL of this solution was transferred to a 0.17 mm glass-bottom 384-well microplate, along with 5 uL of 1.5% filter-sterilized nigrosin stain. Plates were gently flushed with nitrogen gas, then heat-fixed at 50°C in a humidity-controlled incubator. Finally, plates were imaged under brightfield using a Nikon Eclipse Ti-E inverted microscope. Cell features were quantified with ImageJ (Schneider et al., 2012), using the analysis pipeline in Czarny *et al*. (Czarny et al., 2014). These image features were used to cluster drug treatments using Ward's least variance, as well as compute a correlation map and Pearson correlation values for treatments.

Accession Codes

Coordinates and structure factors for FPI-1465-CTX-M-15, FPI-1523-CTX-M-15, FPI-1602-CTX-M-15, FPI-1465-OXA-48, FPI-1523-OXA-48, FPI-1602-OXA-48 and FPI-1465-PBP1b were deposited in the PDB with accession codes (5FAO, 5FA7, 5FAP, 5FAQ, 5FAS, 5FAT, 5FGZ).

RESULTS AND DISCUSSION

Modification of the avibactam C2 carboxamide yielded three derivatives (FPI-1465, FPI-1523, and FPI-1602, Figure 3-1a), which were synthesized by Fedora Pharmaceuticals as previously described (Maiti et al., 2013). We first characterized interactions of the FPI compounds with the class A β-lactamase CTX-M-15, which is among the most widely disseminated extended-spectrum β-lactamases (ESBLs) worldwide, (Bush, 2013c) and OXA-48, a class D carbapenemase found increasingly in carbapenem-resistant Enterobacteriaceae (CRE) (Evans and Amyes, 2014). Structural analysis of enzyme-derivative interactions was done by solving the x-ray co-crystal structures of FPI-1465, FPI-1523 and FPI-1602 bound to the CTX-M-15 active site to a resolution of 3.00, 1.67 and 2.70Å. Similarly, the crystal structures of FPI-1465, FPI-1523, and FPI-1602 bound to OXA-48 were solved to 1.96, 1.74 and 2.09Å resolution (Supplemental Table 3-1 and 3-2). The CTX-M-15 and OXA-48 proteins crystallized with two protein monomers within the asymmetric unit (ASU). Generally, all chains within the ASU contained high structural similarity [root-mean-square deviations (rmsd's) of ≤ 0.2Å for all α-carbon atoms (CA) in both chains within the ASU]. For simplicity, we limit our analysis to chain A for each complex. We previously determined the co-crystal structures of both CTX-M-15 and OXA-48 bound to avibactam (King et al., 2015), allowing for comparison with the corresponding derivative bound enzyme complexes.

All OXA-48 and CTX-M-15 derivative bound structures display clear and unambiguous F_o-F_c ligand omit map electron density corresponding to a C7-Ser70 O-γ linked carbamyl-enzyme intermediate (Supplemental Figures 3-1 and 3-2), which is

directly analogous to the carbamyl-avibactam complexes (King et al., 2015). An analysis of the overall binding conformation of the DBO core amongst the various derivative complexes reveals a striking resemblance to avibactam (Figure 1b-c). Additionally, these structures have a nearly identical juxtaposition of catalytic residues (Supplemental Figures 3-1 and 3-2).

To evaluate the relative β-lactamase inhibitory activity of the FPI compounds, we kinetically characterized them as previously reported (Ehmann et al., 2013b; Ehmann et al., 2012b). For CTX-M-15, slightly reduced on-rates were observed, likely a consequence of carboxamide modification leading to a lower affinity pre-covalent complex. However, off-rates were also lower, resulting in an overall balance in the dissociation constant (K_d) for these compounds (Table 3-1). The reduced off-rates are likely due in part to stabilization of the carbamyl-enzyme intermediate by hydrogen bonds between the various FPI C2 functional groups and conserved active site residues (Supplemental Figures 3-1D and E).

For OXA-48, all FPI derivatives displayed roughly an order of magnitude slower on-rates as well as faster off-rates, leading to significantly increased K_d values (Table 1). In particular, the FPI-1465-OXA-48 carbamyl-enzyme displayed a very short half-life (off-rate $t_{1/2}$ for avibactam vs. FPI-1465: 1500 ±200 min vs. 22 ±1 min). In the OXA-48 bound FPI co-crystal structures we observe numerous direct and water-mediated hydrogen bonds between the various C2 functional groups and conserved active site residues (Supplemental Figure 3-2D and S2E). The observed higher K_d values may be due in part to an entropic cost associated with ordering the C2 side chain of the derivatives via these hydrogen bonds.

Taken together, the above-mentioned structural and kinetic results demonstrate that C2 avibactam derivatives retain β-lactamase inhibitory properties.

Table 3-1. Kinetic values for the carbamylation and decarbamylation of DBOs compounds against CTX-M-15 and OXA-48.

Enzyme	Parameter	Avibactam	FPI-1465	FPI-1523	FPI-1602
CTX-M-15	On-rate k_2/K_i ($M^{-1}s^{-1}$)	$2.5 \pm 0.1 \times 10^5$	$1.3 \pm 0.1 \times 10^4$	$3.9 \pm 0.1 \times 10^4$	$1.1 \pm 0.1 \times 10^4$
	Off-rate k_{off} (s^{-1})	$5.4 \pm 0.7 \times 10^{-4}$	$1.4 \pm 0.1 \times 10^{-4}$	$1.6 \pm 0.1 \times 10^{-4}$	$1.1 \pm 0.1 \times 10^{-4}$
	Off-rate $t_{1/2}$ (min)	22 ± 3	84 ± 6	72 ± 5	102 ± 5
	K_d (μM)	0.002	0.011	0.004	0.010
OXA-48	On-rate k_2/K_i ($M^{-1}s^{-1}$)	$2.5 \pm 0.2 \times 10^3$	$1.0 \pm 0.1 \times 10^2$	$7.0 \pm 0.2 \times 10^2$	$2.0 \pm 0.1 \times 10^2$
	Off-rate k_{off} (s^{-1})	$7.7 \pm 0.9 \times 10^{-6}$	$5.3 \pm 0.3 \times 10^{-4}$	$2.4 \pm 1 \times 10^{-5}$	$2.1 \pm 0.2 \times 10^{-5}$
	Off-rate $t_{1/2}$ (min)	1500 ± 200	22 ± 1	480 ± 80	560 ± 50
	K_d (μM)	0.003	5.3	0.034	0.11

Previously, FPI-1465 displayed remarkable synergy in combination with β-lactams against MBL-expressing strains (Mendes et al., 2013). We used FPI-1465 as a model DBO compound, and assessed its ability to inhibit a panel of pGDP-2 transformants either with empty vector or expressing different β-lactamases (King et al., 2014). All compounds displayed consistently low MICs irrespective of β-lactamase expression (Supplemental Table 3-3). FPI-1602 demonstrated a remarkably low MIC value of < 0.5 μg/mL and was therefore selected for further MIC experiments against a panel of NDM-1 positive clinical isolates. FPI-1602 displayed marked antimicrobial activity against *P. aeruginosa, E. coli*, and *Enterobacter spp.* (Supplemental Table 3-4). The activity against *P. aeruginosa* is particularly interesting as a recent publication has described a similar compound (OP0595) that does not exhibit antimicrobial activity against *P. aeruginosa* (MIC > 32 μg/mL)

(Morinaka et al., 2015) This data clearly demonstrates that avibactam derivatives act as direct antimicrobial agents, and that their activity is not thwarted by β-lactamase expression.

SBLs and the PBP transpeptidases are thought to have evolved from a common ancestor, and both belong to the penicilloyl serine transferase superfamily and share common active site sequence motifs and an analogous reaction path that proceeds through formation of a covalent acyl-enzyme intermediate (Knox et al., 1996). Previously, the BLIs clavulanic acid and sulbactam were shown to have antibacterial activity due to targeting PBPs in various Gram-negative pathogens including: *E. coli*, *Proteus mirabilis*, *Enterobacter cloacae*, and *Acinetobacter spp* (Moosdeen et al., 1988; Obana and Nishino, 1990). Therefore, we hypothesized that the observed antimicrobial activity of the FPIs may be due to direct inhibition of PBPs in much the same way as β-lactams. We performed gel-based competition assays to assess the relative ability of the derivatives to block binding of the fluorescent penicillin (BOCILLIN FL) to endogenously expressed *E. coli* PBPs using purified membrane extracts. All FPI derivatives tested displayed preferential inhibition of PBP2 in these *in-vitro* binding assays (Figure 3-2a, Supplemental Figure 3-4). BOCILLIN FL competition assays were then performed using purified *E. coli* PBPs (PBP1a, PBP1b, PBP2, and PBP3). The avibactam derivatives specifically inhibit binding of BOCILLIN FL to purified *E. coli* PBP2 (Supplemental Table 3-5). The relative potency of PBP2 inhibition by the derivatives closely mirrors their MIC values against *E. coli* BW25113 pGDP-2 β-lactamase transformants (Supplemental Table 3-3), with FPI-1523 and FPI-1602 displaying more potent inhibition (IC_{50} = 3.2 ± 0.4μM and 3.6 ± 0.3μM), than FPI-1465 and avibactam

(IC_{50} = 15 ± 1μM and 63 ± 6μM, Supplemental Table 3-5). In *E. coli*, PBP2 is intimately involved in cell elongation and consequently its inhibition leads to cell rounding and loss of rod-shaped growth, while inhibition of the cell division specific PBP3 leads to long chains of filamentous cells unable to form septa (Tipper, 1985). Microscopy studies performed on cells treated with sub-MIC concentrations of mecillinam (PBP2 targeting), and ceftazidime (PBP3 targeting) confirmed the expected cell morphology phenotypes (Figure 2b). All FPI derivatives exactly phenocopied the cell rounding effects of mecillinam, further supporting the notion that PBP2 is the cellular target of these compounds (Figure 2b, and Supplemental Figure 3-5). Furthermore, we observed synergy (all fractional inhibitory concentrations < 0.4) when aztreonam (PBP3 targeting) (Hayes and Orr, 1983) was used in combination with FPI-1602 against *E. coli* (Figure 3-2c), similar to a previous report (Sumita and Fukasawa, 1995). Importantly, this combination retained synergy in the presence of any β-lactamase tested. Taken together, these data strongly suggest that PBP2 is the antibacterial target for the FPI compounds in *E. coli*.

In competition experiments in which BOCILLIN FL and the FPIs were added to *E. coli* PBP1b at the same time to start the reaction, no inhibition was observed up to 2mM of the FPIs (Supplemental Table 3-5). However, an extensive 48 hour pre-incubation of FPI-1602 with the purified *E. coli* PBP1b membrane protein prior to addition of BOCILLIN FL resulted in a concentration-dependent inhibition of BOCILLIN FL binding (Supplemental Figure 3-6), indicating that at high concentrations the derivatives can act as slow binding inhibitors of PBP1b. Therefore, due to difficulties in crystallizing *E. coli* PBP2, we reasoned that co-crystallization of *E. coli* PBP1b with the avibactam derivatives would lend

insight into the structural basis of PBP inhibition by these compounds. The co-crystal structure of the single pass bitopic membrane protein *E. coli* PBP1b covalently inhibited by FPI-1465 was solved to 2.85Å resolution in spacegroup $P22_12_1$ with a single protein monomer in the ASU (for ligand electron density maps and crystallographic data statistics see Supplemental Table 3-6). The overall orientation of FPI-1465 in the PBP1b active site is directly analogous to the carbamyl-SBL bound complexes (Figures 3-2d and 3-1b-c). The FPI-1465 N6 sulfate projects toward the conserved motif iii and makes hydrogen bonding contacts with the O-γ of Thr699 and Thr701. Also, the FPI-1465 C7 carbonyl oxygen occupies the canonical oxyanion hole constituted by the backbone amide nitrogens of Thr701 and Ser510. Finally, the C2 side chain projects away from the catalytic core (Figure 2d). This structure represents the first glimpse into DBO-mediated PBP inhibition and demonstrates the ability of avibactam derivatives to interact directly with the conserved active site motifs of PBPs, providing a molecular basis for structure-based drug design efforts.

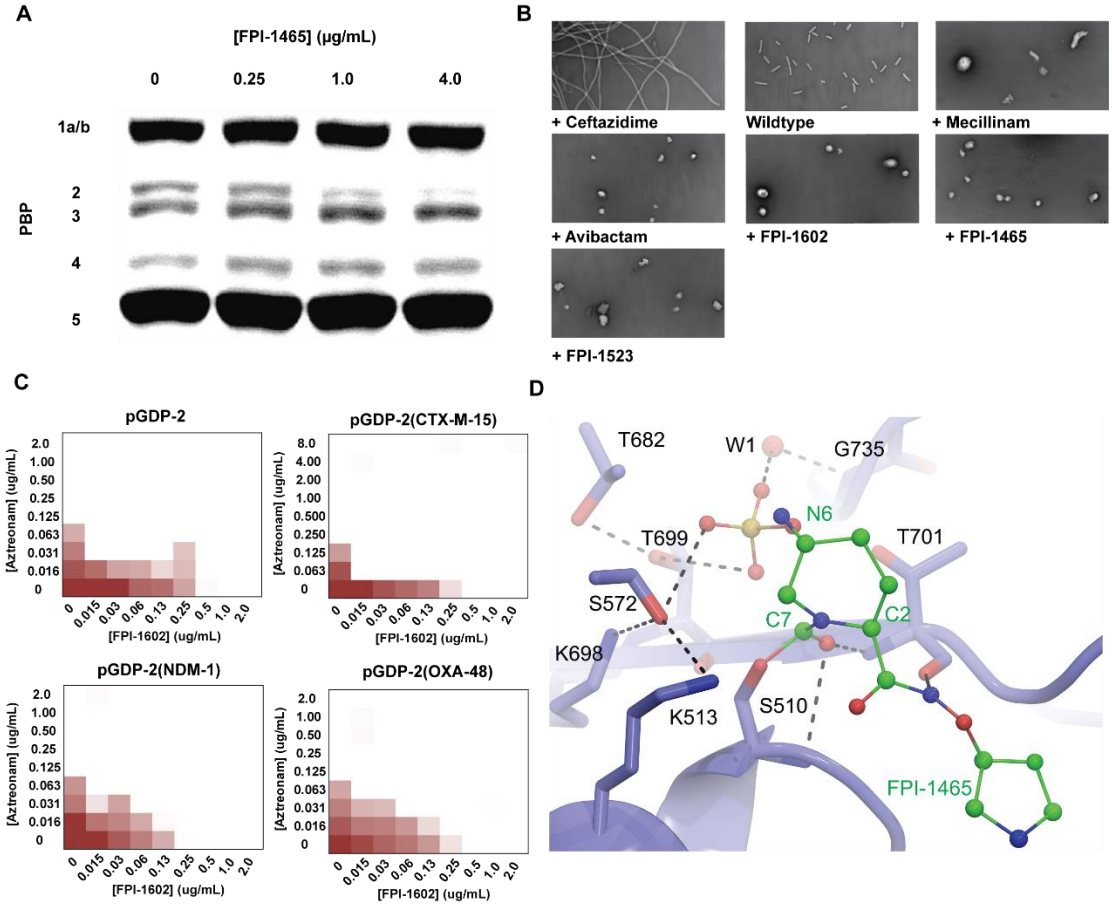

Figure 3-2. PBP2 is the primary cellular target of avibactam derivatives in E. coli. (A) *E. coli* PBP banding profile and PBP binding competition assay for compound FPI-1465 (PBP2 IC_{50} = 1.0 ± 0.6 μg/mL). (B) Brightfield microscopy images of *E. coli*, treated with antibiotics alongside FPI compounds. (C) Microdilution checkerboard analysis demonstrates antimicrobial synergy between aztreonam and FPI-1602 against *E. coli* expressing clinically relevant β-lactamases from class A (CTX-M-15), B (NDM-1), and D (OXA-48). (D) Active site close-up of carbamyl-FPI-1465-*E. coli* PBP1b co-crystal structure. The bound protein backbone is displayed as a blue cartoon with key active site residues shown in stick representation with non-carbon atoms colored by type. Selected hydrogen bonds and electrostatic interactions are depicted as black dashes.

In the FPI-1465-*E. coli* PBP1b crystal structure, the N6 nitrogen is 4.4Å from the S572 O-γ (Figure 2d). In contrast, in the FPI-1465 bound CTX-M-15 and OXA-48 structures, the N6 nitrogen is much closer to the equivalent motif II serine O-γ (3.3Å, and 3.0Å Figures 1b and 1c). The motif II serine has an essential role as the general acid for protonation of the β-lactam or DBO nitrogen leaving group upon formation of the acyl-enzyme covalent intermediate (King et al., 2015). Therefore, we propose that the relatively poor inhibition of *E. coli* PBP1b by the DBO's is likely due to the suboptimal positioning of the general acid required for acylation.

The demonstration that DBO derivatives are potent antibiotics as well as BLIs has far-reaching implications for antibacterial drug discovery. Early DBOs were considered to be poor antibiotics, and were therefore pursued as BLIs and this mindset has continued with the development of avibactam. (Hayes and Orr, 1983) However, there is now significant pharmaceutical investment in this scaffold and it is crucial that any medicinal chemistry efforts acknowledge their potent antimicrobial activity.

SUPPLEMENTAL INFORMATION

Supplemental Tables

Supplemental Table 3-1. Data collection and refinement statistics for CTX-M-15 co-crystal structures

	FPI-1465	FPI-1523	FPI-1602
Data collection			
Space group	$P2_12_12_1$	$P12_11$	$P12_11$
Cell dimensions			
a, *b*, *c* (Å)	43.9, 62.7, 175.5	62.7, 60.3, 76.0	63.1, 61.8, 73.1
α, β, γ (°)	90.0, 90.0, 90.0	90.0, 112.8, 90.0	90.0, 104.0, 90.0
Resolution (Å)	33.28-3.00 (3.16-3.00)*	70.1-1.67 (1.71-1.67)	30.97-2.70 (2.77-2.70)
R_{sym}	0.10 (0.34)	0.053(0.42)	0.06(0.21)
$I/\sigma I$	7.8(2.4)	12.2(1.9)	11.7(3.4)
Completeness (%)	98.3(97.4)	98.4(99.7)	95.4(92.1)
Redundancy	4.4(4.3)	2.9(2.9)	2.5(2.4)
Refinement			
Resolution (Å)	33.28-3.00	70.1-1.67	30.97-2.70
No. reflections	10061(715)	59836(4407)	14478(1010)
R_{work}/ R_{free}	0.223, 0.271	0.166, 0.197	0.187, 0.227
No. atoms			
Protein	3934	3946	3926
Ligand	46	70	48
Water	34	520	85
B-factors (Å^2)			
Protein	30.4	15.3	27.8
Ligand	52.2	14.7	31.1
Water	21.2	27.6	18.1
R.m.s deviations			
Bond lengths (Å)	0.009	0.015	0.011
Bond angles (°)	1.43	1.73	1.48
Favored/allowed/disallowed (%)$^+$	94.9, 4.3, 0.8	97.2, 1.6, 1.2	96.1, 3.1, 0.8

Data corresponds to diffraction from a single crystal for each structure.

*Highest resolution shell is shown in parenthesis.

$^+$phenix.ramalyze; "allowed" is the percentage remaining after "favoured" and "outlier" residues are subtracted.

Supplemental Table 3-2. Data collection and refinement statistics for OXA-48 co-crystal structures

	FPI-1465	FPI-1523	FPI-1602
Data collection			
Space group	$P2_12_12_1$	$P2_12_12_1$	$P2_12_12_1$
Cell dimensions			
a, *b*, *c* (Å)	72.8, 75.5, 107.0	73.0, 75.8, 106.7	73.1, 75.8, 106.7
α, β, γ (°)	90, 90, 90	90, 90, 90	90, 90, 90
Resolution (Å)	43.64-1.96 (2.01-1.96)	43.62-1.74 (1.79-1.74)	47.18-2.09 (2.14-2.09)
R_{merge}	0.071(0.467)	0.04(0.440)	0.072(0.540)
$I/\sigma I$	22.6(4.3)	30.6(4.1)	21.2(3.4)
Completeness (%)	99.7(99.9)	99.9(99.3)	99.7(99.9)
Redundancy	7.3(7.4)	7.4(7.4)	7.3(7.5)
Refinement			
Resolution (Å)	43.64-1.96	43.62-1.74	47.18-2.09
No. reflections	42805(3145)	61458(4464)	35720(2595)
R_{work}/ R_{free}	0.168/0.210	0.157/0.178	0.167/0.216
No. atoms			
Protein	3988	4336	4026
Ligand	46	42	48
Ion	13	13	11
Water	422	457	293
B-factors (Å^2)			
Protein	25.6	25.9	35.5
Ligand	32.7	32.7	51.3
Ion	27.1	26.2	42.6
Water	32.8	34.6	40.6
R.m.s deviations			
Bond lengths (Å)	0.017	0.013	0.010
Bond angles (°)	1.78	1.56	1.59
Favored/allowed/disallowed (%)$^+$	97.9, 2.1, 0.0	98.0, 2.0, 0.0	98.3, 1.7, 0.0

Data corresponds to diffraction from a single crystal for each structure.

*Highest resolution shell is shown in parenthesis.

$^+$phenix.ramalyze; "allowed" is the percentage remaining after "favored" and "outlier" residues are subtracted.

Supplemental Table 3-3. Antimicrobial susceptibility patterns of *E. coli* BW25113 pGDP-2 transformants expressing β-lactamase

	MIC (μg/mL)				
Antibiotic	***CTX-M-15***	***KPC-2***	***NDM-1***	***OXA-48***	***control***
Ampicillin	32	>512	>512	16	4
Avibactam	32	16	16	16	16
FPI-1465	4	4	2	2	2
FPI-1523	2	2	2	1	1
FPI-1602	<0.5	<0.5	<0.5	<0.5	<0.5

Supplemental Table 3-4. Antimicrobial susceptibility patterns of NDM-1-positive clinical isolates to FPI-1602 alone.

Strain	MIC (μg/mL)
E. coli GN688	0.5
E. coli GN610	2
E. cloacae GN574	1
E. cloacae GN579	2
P. aeruginosa PAO1*	2
E. cloacae GN687	8
K. oxytoca GN942	32
C. freundii GN978	64
A. baumanii ATCC 17978*	>128
K. pneumoniae GN629	>128
K. pneumoniae GN529	>128
M. morganii GN575	>128
P. rettgeri GN570	>128
P. stuartii GN576	>128

*Non-NDM-1-expressing strains

Supplemental Table 3-5. Gel based BOCILLIN FL competition assays[a].

	IC_{50}[b] (μM)			
Antibiotic	**PBP2**	**PBP1b**	**PBP1a**	**PBP3**
Avibactam	63 ± 5.5	NI	NI	NI
FPI-1465	14.8 ± 1.1	NI	NI	NI
FPI-1523	3.2 ± 0.4	NI	NI	NI
FPI-1602	3.6 ± 0.3	NI	NI	NI
Benzyl penicillin	318.1 ± 32.3	161.72 ± 8.6	196.9 ± 26.3	35.5 ± 3.27
Mecillinam	0.3 ± 0.1	NI	NI	NI
Kanamycin	NI	NI	NI	NI

[a] The avibactam derivatives were analyzed for the ability to inhibit binding of BOCILLIN FL to purified *E. coli* PBPs. BOCILLIN FL and competitor compound were added at the same time to start the reaction.

NI, no observable inhibition up to 2000 μM competitor compound.

[b] IC_{50} values are taken as averages from three separate experiments and represent the concentration of unlabeled compound required to reduce the residual binding of BOCILLIN FL by 50%

Supplemental Table 3-6. Data collection and refinement statistics for FPI-1465-*E. coli* PBP1b co-crystal structure

	FPI-1465
Data collection	
Space group	$P22_12_1$
Cell dimensions	
a, *b*, *c* (Å)	62.48, 63.22, 293.9
α, β, γ (°)	90, 90, 90
Resolution (Å)	63.22-2.85(2.93-2.85)
R_{merge}	0.040(0.238)
$I/\sigma I$	23.4(4.0)
Completeness (%)	95.1(90.7)
Redundancy	3.9(2.5)
Refinement	
Resolution (Å)	63.22-2.85
No. reflections	26383(1797)
R_{work}/ R_{free}	23.7/29.0
No. atoms	
Protein	5461
Moenomycin	77
FPI-1465	23
Water	59
B-factors (Å^2)	
Protein	63.6
Moenomycin	109.5
FPI-1465	87.0
Water	36.2
R.m.s deviations	
Bond lengths (Å)	0.013
Bond angles (°)	1.65
Favored/allowed/disallowed (%)$^+$	93.9, 6.0, 0.1

Data corresponds to diffraction from a single crystal for each structure.

*Highest resolution shell is shown in parenthesis.

$^+$phenix.ramalyze; "allowed" is the percentage remaining after "favoured" and "outlier" residues are subtracted.

Supplemental Figures

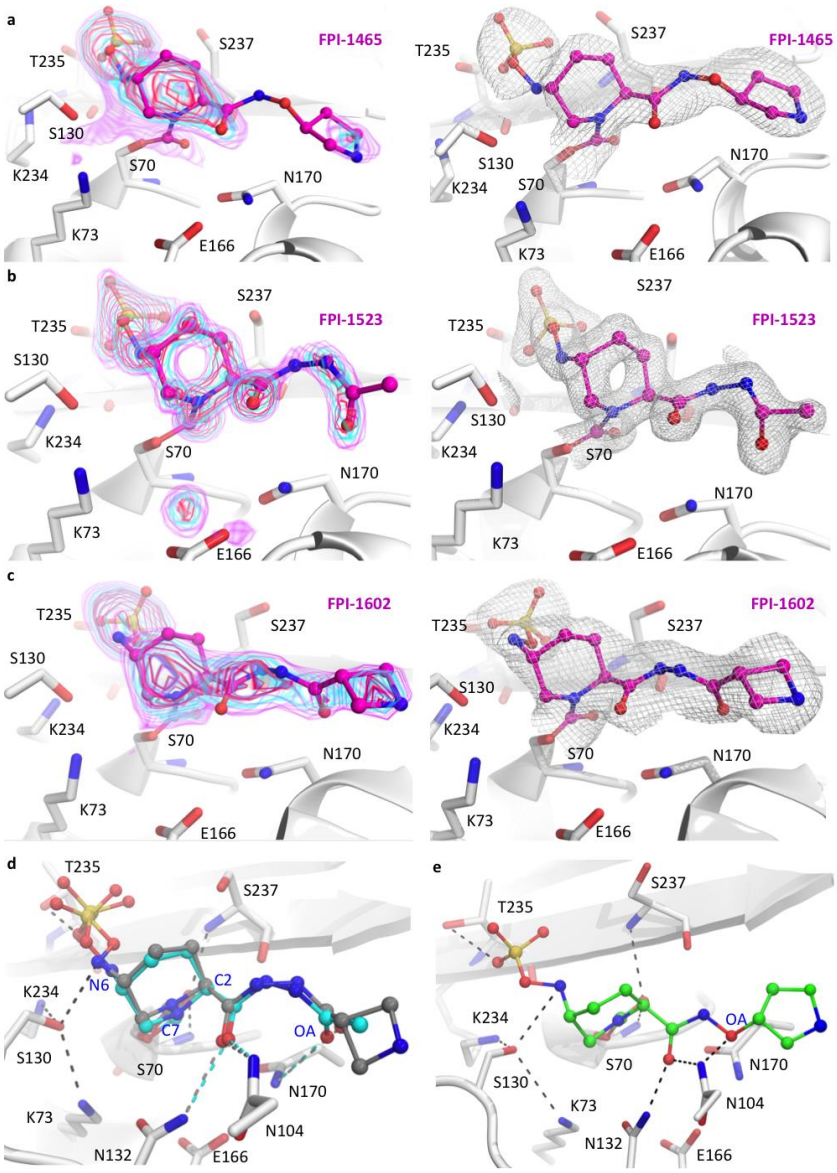

Supplemental Figure 3-1. Avibactam derivative electron density maps and ligand protein interactions for CTX-M-15 co-crystal complexes. a, Carbamyl FPI-1465-CTX-M-15 ligand electron density maps. **b,** Carbamyl FPI-1523-CTX-M-15 ligand electron density maps. **c,** Carbamyl FPI-1602-CTX-M-15 ligand electron density maps. In **(a-c)**, the carbamyl-avibactam derivative is represented as pink sticks with atoms colored by type. The left panel for **(a-c)** shows F_o-F_c ligand omit maps contoured at 3.0, 4.0 and 5.0 σ displayed as pink, cyan and red transparent surfaces. The right panel in **(a-c)** shows final refined $2F_o$-F_c electron density maps for each ligand contoured at 1.0σ. **d,** Active site overlay of FPI-1523 and FPI-1602 bound to CTX-M-15 (rmsd= 0.2Å on all CA atoms). The carbamyl -FPI-1523 and -FPI-1602 are displayed in cyan and grey stick representation with non-carbon atoms colored by atom type. **e,** Active site close-up of FPI-1465 bound to CTX-M-15. The bound FPI-1465 is displayed as green sticks with non-carbon atoms colored by type. In all panels, the CTX-M-15 cartoon is shown in white with selected active site residues displayed in stick representation with all non-carbon atoms colored by type.

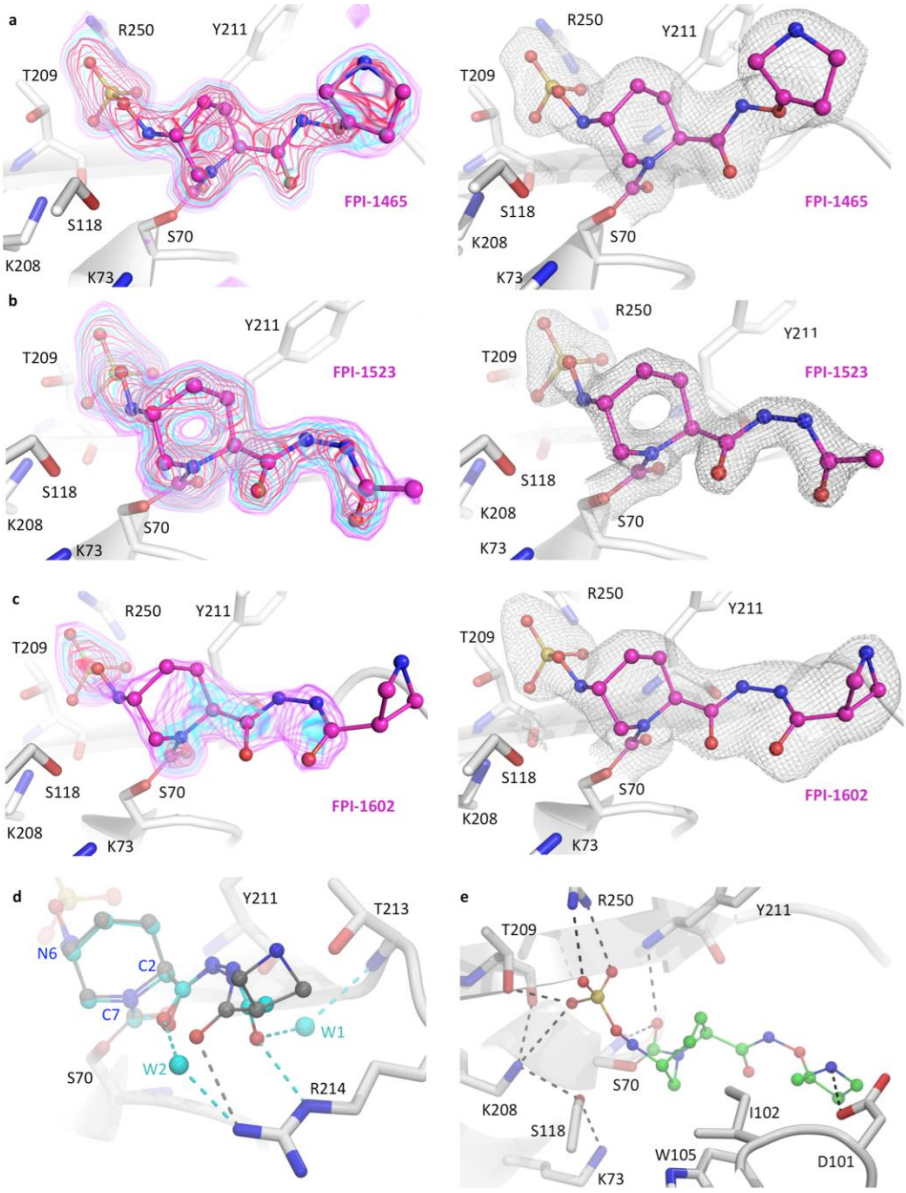

Supplemental Figure 3-2. Avibactam derivative electron density maps and ligand protein interactions for OXA-48 co-crystal complexes. a, Carbamyl FPI-1465-OXA-48 ligand electron density maps. b, Carbamyl FPI-1523-OXA-48 ligand electron density maps. c, Carbamyl FPI-1602-OXA-48 ligand electron density maps. In (a-c), the carbamyl-avibactam derivative is represented as pink sticks with atoms colored by type. The left panel for (a-c) shows Fo-Fc ligand omit maps contoured at 3.0, 4.0 and 5.0 σ and illustrated as pink, cyan and red transparent surfaces. The right panel in (a-c) shows final refined 2Fo-Fc electron density maps for each ligand contoured at 1.0σ. d, Active site overlay of FPI-1523 and FPI-1602 bound to OXA-48 (rmsd= 0.2Å on all CA atoms). The carbamyl -FPI-1523 and -FPI-1602 are displayed in stick representation with non-carbon atoms colored by atom type. e, Active site close-up of FPI-1465 bound to the OXA-48 active site. The bound FPI-1465 is displayed as green sticks with atoms colored by type. In all panels, the OXA-48 cartoon is shown in white with selected active site residues displayed in stick representation with all non-carbon atoms colored by type.

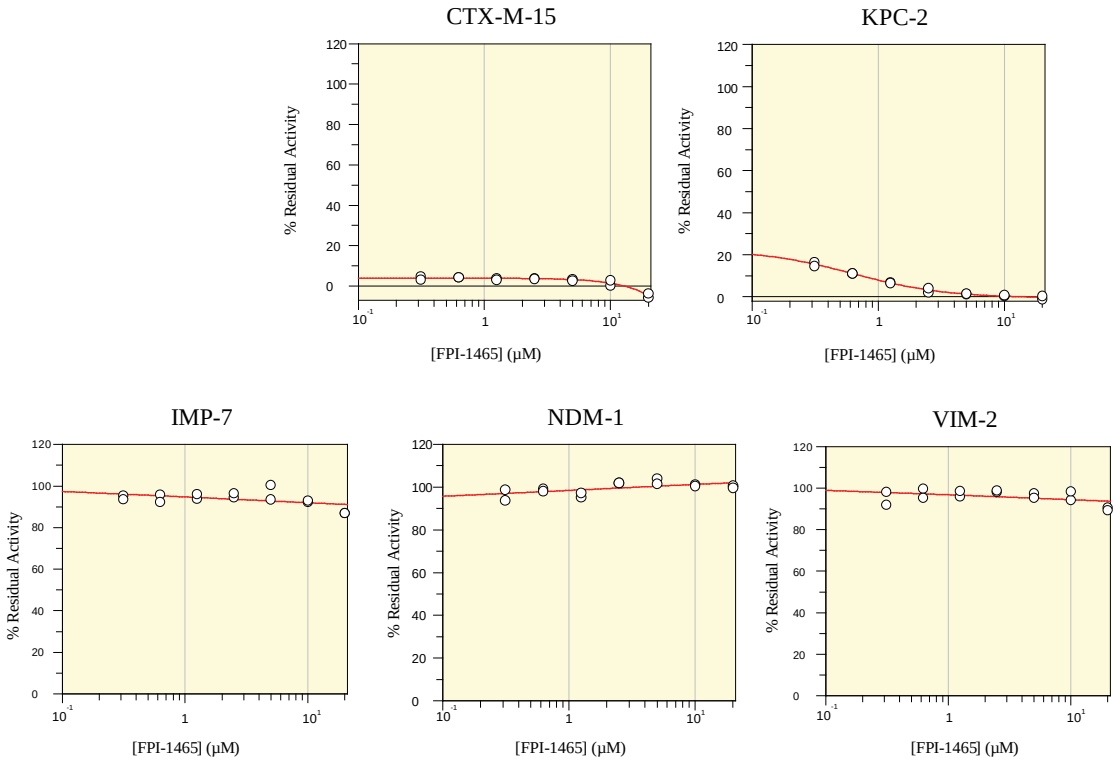

Supplemental Figure 3-3. FPI compounds inhibit SBLs but not MBLs. Concentration-response plots show the SBLs CTX-M-15 and KPC-2 are effectively inhibited by FPI-1465 but not the MBLs IMP-7, NDM-1, or VIM-2.

a)

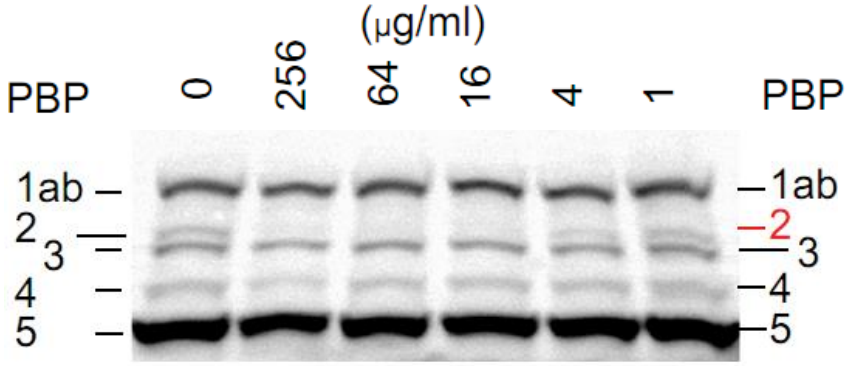

b)

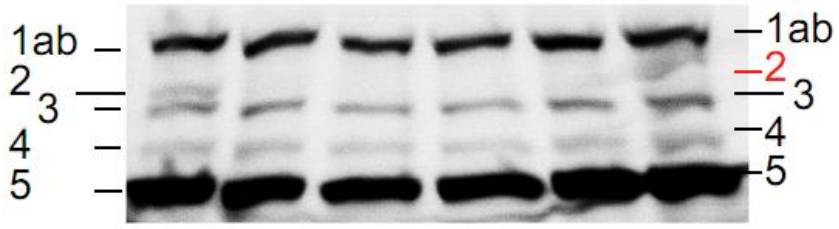

c)

	MIC (μg/ml) for *E. coli* K12	K12 cell shape at 1/2 or 1/4 MIC	K12 PBP2 IC_{50} (μg/ml)
Avibactam	32	Round	2.0 ± 1.2
FPI-1465	4	Round	1.0 ± 0.6
FPI-1523	4	Round	0.4 ± 0.2

Supplemental Figure 3-4. Avibactam and derivatives specifically bind PBP2. *E. coli* PBP banding profile and PBP binding competition assay for **a,** avibactam and **b,** FPI-1523. The banding profile was generated using BOCILLIN FL and the test compound was used at increasing concentrations during the assay. Binding of BOCILLIN FL to PBP2 was specifically decreased by the presence of all DBOs tested. **c,** MICs and PBP2 IC_{50} of avibactam and derivatives for *E. coli* K12. Note that the PBP binding competition assay for FPI-1465 is shown in Figure 3-2.

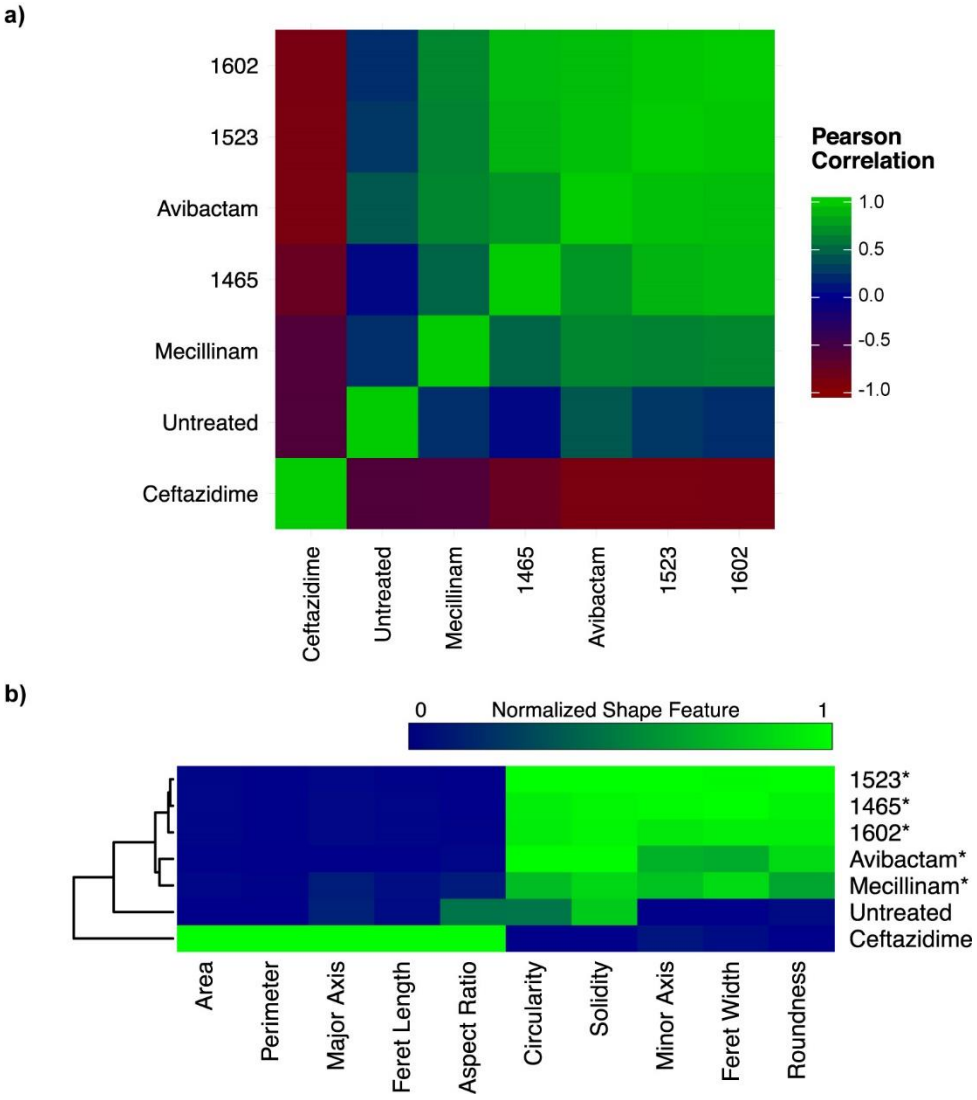

Supplemental Figure 3-5. Pearson correlation map for morphological defects in the presence of select antibiotics. a, The correlation is based on ImageJ features shown in **b,** which were normalized for comparative purposes. It shows clear correlations between derivatives and known drugs avibactam and mecillinam, and a strong negative correlation with ceftazidime.

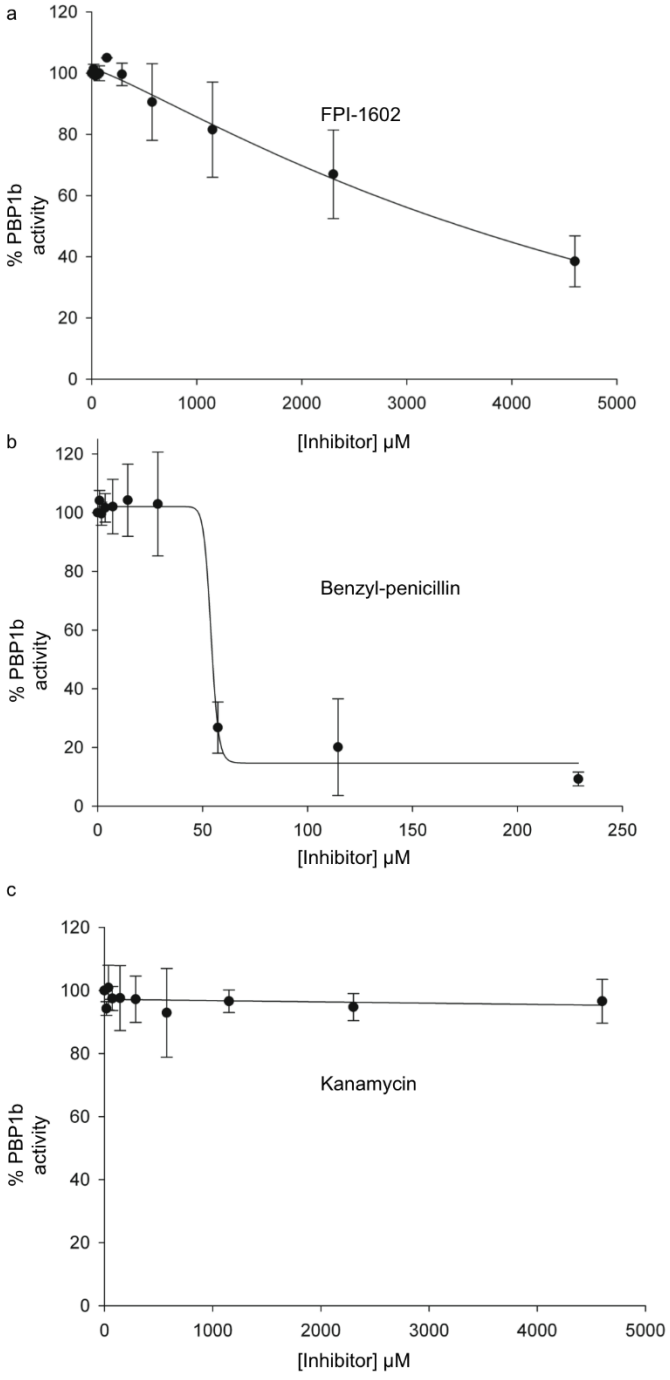

Supplemental Figure 3-6. Gel based BOCILLIN FL competition assays to analyze the ability of unlabeled competitor compounds to bind purified E. coli PBP1b. In **a, b,** and **c,** various amounts of unlabeled FPI-1602, benzyl-penicillin, or kanamycin were pre-incubated with *E. coli* PBP1b for 48 hours prior to addition of BOCILLIN-FL. Error bars represent standard deviations from two separate technical replicates.

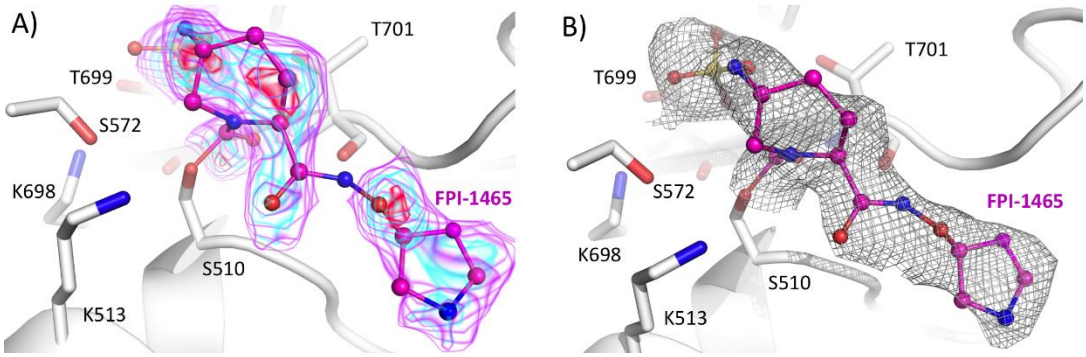

Supplemental Figure 3-7. Avibactam derivative electron density for carbamyl-FPI-1465-E. coli PBP1b. **a,** Carbamyl-FPI-1465 PBP1b ligand omit F_o-F_c electron density. The F_o-F_c ligand omit maps are contoured at 3.0, 4.0 and 5.0 σ and are shown as pink, cyan and red transparent surfaces. **b,** Carbamyl-FPI-1523 final refined $2F_o$-F_c electron density map contoured at 1.0σ. In both panels, the PBP1b cartoon is shown in white with selected active site residues displayed as sticks with all non-carbon atoms colored by type. In all panels, the carbamyl-FPI-1465 is represented as pink sticks with atoms colored by type.

CHAPTER 4

A SYNTHETIC SMALL MOLECULE SCREEN FOR INHIBITORS OF NDM-1

CHAPTER 4 PREFACE

I performed all experiments described in this chapter. None of this work has been published in any form.

Acknowledgements:

I am grateful to both Jenny Wang and Jan Blanchard for their assistance with high-throughput screening method development.

INTRODUCTION

The β-lactam antibiotics are the most valuable assets available to medicine in the treatment of bacterial infection, as evidenced by global consumption (Van Boeckel et al., 2014). In Gram-negative bacteria, the primary mechanism of resistance to β-lactam antibiotics is the evolution and dissemination of β-lactamases, enzymes capable of hydrolyzing the β-lactam bond necessary for antimicrobial activity (Fisher et al., 2005). While SBLs have long been prevalent in clinical settings, it is only recently that MBLs have come to the fore, in particular due to their excellent carbapenemase activity (Bush, 2013b). There is a longstanding history of small molecule inhibitors effective against various SBLs but, to date, there are no clinically used inhibitors of MBLs (Bush, 2013c). This is due to the notable absence of MBLs in clinical settings and the difficulty in discovering broad-spectrum MBL inhibitors with cell-based efficacy (Palzkill, 2013). The emergence and rapid global spread of New Delhi metallo-β-lactamase-1 (NDM-1) propelled MBLs into the spotlight, something that the other clinically relevant subclasses (VIM, IMP) had not done before (Cornaglia et al., 2011; Kumarasamy et al., 2010). Notwithstanding the absence of a clinical inhibitor of MBLs, the rationale for combination therapy of β-lactam antibiotic and BLI is sound and actively being investigated (Buynak, 2013).

High-throughput screening (HTS) is a powerful method for interrogating large chemical collections for any given activity. The development and implementation of any screening process is technically only limited by resources and imagination (Macarron et al., 2011) but most screens can be largely divided between target-based screens, whereby

one screens against purified, recombinant enzyme often monitoring chemical transformations via spectroscopic methods; or cell-based screens, where one screens against whole cells and monitors cell life or death. Another group recently conducted a small target-based screen against purified VIM-2 using the colorimetric cephalosporin, nitrocefin, and found two molecules with activity against both purified enzyme and the ability to restore imipenem sensitivity to VIM-2-expressing laboratory strains of *E. coli* (Minond et al., 2009). We report here a similar target-based screen against NDM-1 and summarize some of the best hits.

MATERIALS AND METHODS

Reagents

All enzymes and chemicals of analytical grade were purchased from Sigma-Aldrich, unless otherwise stated.

DNA manipulations, plasmid construction and protein purification

NDM-1 and CTX-M-15 were cloned, expressed and purified as reported previously (Chapter 5) (King et al., 2014).

Synthesis of nitrocefin

Nitrocefin was synthesized following a published procedure (Scheme 4-1) (Lee et al., 2005b).

Scheme 4-1.

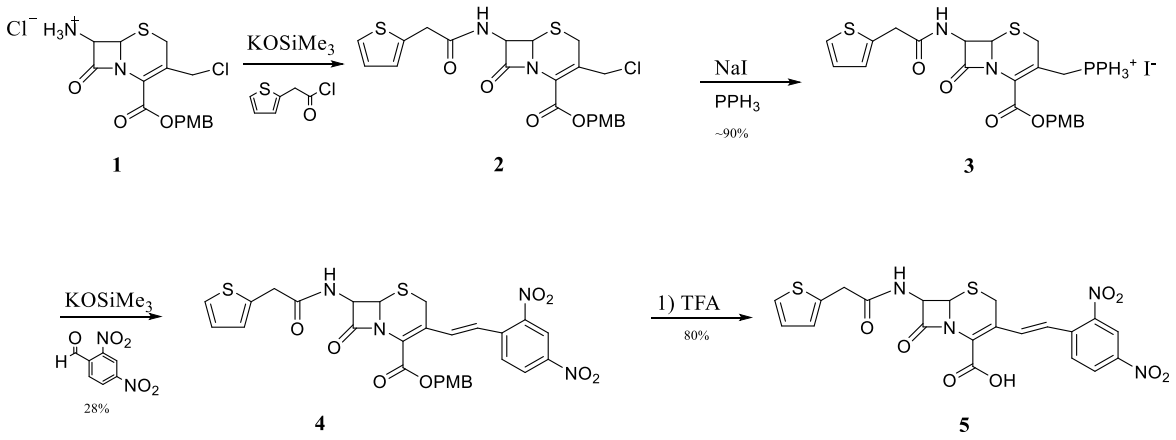

Synthesis of *p*-Methoxybenzyl (6R,7R)-3-Chloromethyl-7β-(2-thienylacetamido)-3-cephem-4-carboxylate (compound 2)

Potassium trimethylsilanolate (4.275 g) in acetonitrile (45 mL) and 2-thiopheneacetyl chloride (1.95 mL) were added simultaneously to a suspension of compound **1** (6 g) in dichloromethane (DCM) (75 mL) over 1.5 hours in an ice-water bath in a 500mL round-bottom flask. The resulting suspension was stirred at room temperature for 1.5 hours. Reaction was monitored by LC-MS (Supplemental Figure 4-6, 4.7). Solvent was evaporated under reduced pressure to give 6.9 g of compound **2.**

Synthesis of *p*-Methoxybenzyl (6R,7R)-3-(2,4-Dinitrostyryl)-7β-(2-thienylacetamido)-3-cephem-4-carboxylate (compound 4)

Compound **2** (6.9 g), sodium iodide (10.5 g), and triphenylphosphine (PPh_3) (6.8 g) were mixed in 2-butanone (105 mL) and stirred overnight in the dark at room temperature. Reaction was monitored by LC-MS (Supplemental Figure 4-8, 4.9). Solvent was evaporated under reduced pressure and purified by normal-phased FLASH chromatography using a gradient of DCM:methanol to give 9 g compound **3** (90% yield) . Compound **3** (9 g) was taken up into DCM (100 mL) and Potassium trimethylsilanolate (1.35 g) in acetonitrile (25 mL) was added at -10°C. Reaction was stirred in the dark for 1 hour. 2,4-dinitrobenzaldehyde (2.1 g) in DCM (50mL) was added drop-wise over 20 minutes then the reaction mixture was brought to room temperature after 2 hours and stirred for an additional 3 hours. Reaction was monitored by LC-MS and solvent was evaporated under reduced pressure. Normal-phased FLASH chromatography purified using a gradient of hexanes:ethyl acetate to give 2.23 g of compound **4** (28% yield).

Synthesis of (6R,7R)-3-Chloromethyl-7β-(2-thienylacetamido)-3-cephem-4-carboxylate (compound 5)

Compound **4** (2.23 g) was taken up in anhydrous DCM (23 mL) and to this was added trifluoroacetic acid (11 mL) and anisole (2.3 mL) for 15 min at ice-water temperature in the dark under inert atmosphere. Aliquots were run on LC-MS to monitor reaction progress. Volatiles were removed rapidly under reduced pressure and residue

was taken up into toluene (10 mL x 4) and again evaporated under reduced pressure. The residue was triturated with cold diethyl ether (15 mL) and filtered to give 1.7 g compound **5** (94% yield). 150 mg compound **5** was taken up in 6 mL of 10% dimethyl sulfoxide (DMSO) in chloroform and stirred at room temperature for 24 hours. Reaction was monitored by ^{1}H NMR. Pure compound **5** (Supplemental Figure 4-6) was obtained using HPLC with a gradient of 40-75% acetonitrile in water over 7 minutes. ^{1}H NMR (700 MHz, DMSO-d_6) δ 3.75, 4.02 (2d, 2H, J = 17.5 Hz, H_2), 3.78 (dd, 2H, J = 15.3 Hz, J = 20.2 Hz, thiophene-CH_2), 5.23 (d, 1H, J = 4.9 Hz, H_6), 5.77 (dd, 1H, J = 4.9 Hz, J = 8.2 Hz, H_7), 6.94-6.97 (m, 2H, thiophene-H), 7.26 (d, 1H, J = 16.0, C=CH), 7.38 (dd, 1H, J = 1.19 Hz, J = 5.1 Hz, thiophene-H), 7.55 (d, 1H, J = 16.0 Hz, C=CH), 7.99 (d, 1H, J = 8.8 Hz, ArH), 8.50 (dd, 1H, J = 2.31 Hz, J = 8.7 Hz, ArH), 8.74 (d, 1H, J = 2.4 Hz, ArH), 9.22 (d, 1H, J = 8.3 Hz, NH).

***In vitro* screen against purified NDM-1**

Enzymatic screening was conducted in 384-well format using a fully automated Beckman/Coulter Core Robotics system. The assay was run under control of SAMI software and all transfers were executed by a Biomek FXP liquid handler. Each well contained 1 nM NDM-1 and 20 μM nitrocefin in 50 mM HEPES pH 7.5, 0.01% Tween20, 50 μM $ZnSO_4$. Compounds were added at an estimated concentration of 12.5 μM for a final DMSO concentration of ~ 2% and absorbance at 480 nm was measured in 1 minute intervals for an 8 minute period. Slopes were calculated by taking points 2 and 8 then % residual activity was determined by comparing to controls.

FIC index determinations

Fractional inhibitory concentration (FIC) values were determined by standard methods (Pillai et al., 2005) setting up checkerboards with 8 concentrations of each meropenem and compound in serial ½ dilutions. Experiments were done in duplicate and the mean used for calculation. The MIC for each compound was the lowest [compound] showing no growth. The FIC for each compound was calculated as the [compound in the presence of co-compound] for a well showing no growth, divided by the MIC for that compound. The FIC index is the sum of the two FICs.

Zinc-dependence in dantrolene concentration-response profiles

Enzyme (NDM-1, 2 nM; CTX-M-15, 1 nM) was mixed with either 40 μM meropenem or nitrocefin after a 60 minute preincubation with dantrolene in serial 2/3 dilutions from 60 μM and the indicated concentration of $ZnSO_4$ at 30°C in 50 mM HEPES pH 7.5. Enzyme dilutions were made with 20 ng/μL BSA. Linear portions of curves were used to analyze data. Assays were read in 96-well microplate format at 490 nm using a Spectramax reader (Molecular Devices) at 30°C.

Spectral characteristics of zinc and dantrolene interaction

Dantrolene (30 μM serial 2/3 dilutions) was incubated with varying concentrations of $ZnSO_4$ in 50 mM HEPES pH 7.5and wavelengths in the range of 260-700 nm were scanned at 0, 10, 30, and 60 minutes.

Benserazide incubation experiments and concentration-response profiles

Benserazide (4mM) was incubated for 24 hours at 4°C in 50 mM HEPES pH 7.5 and 25% DMSO. Aliquots were removed for analysis by LC-MS and to test inhibitory properties. Enzyme (NDM-1, 5 nM; CTX-M-15, 1 nM) was pre-incubated with benserazide in serial ½ dilutions from 100 µM and 50 µM $ZnSO_4$ for 10 minutes at 30°C then mixed with nitrocefin at a final concentration of 20 µM. Enzyme dilutions were made with 20 ng/µL BSA. Linear portions of curves were used to analyze data. Assays were read in 96-well microplate format at 490 nm using a Spectramax reader (Molecular Devices) at 30°C.

For the no HEPES experiments, enzyme (NDM-1 10 µM) was mixed as above but with no buffer present.

HNA concentration-response profiles

Enzyme (NDM-1, 5 nM) was mixed with 20 µM nitrocefin after a 15 minute preincubation with HNA in serial 1/2 dilutions as indicated in 10 µM $ZnSO_4$ at 30°C in 50 mM HEPES pH 7.5. Enzyme dilutions were made with 20 ng/µL BSA. Linear portions of curves were used to analyze data. Assays were read in 96-well microplate format at 490 nm using a Spectramax reader (Molecular Devices) at 30°C.

LC-MS analysis of compounds

LC-ESI-MS data were obtained by using either an Agilent 1100 Series LC system (Agilent Technologies Canada, Inc.) and a QTRAP LC/MS/MS System (Applied Biosystems). The reversed-phase HPLC was performed using C_{18} column (SunFire C18 5

μm, 4.6x50 mm, Waters) with Agilent 1100 LC binary pump at a flow rate of 1 mL/min, under the following conditions: isocratic 5% solvent B (0.05% formic acid in acetonitrile) and 95% solvent A (0.05% formic acid in water) for 1 min, followed by a linear gradient to 97% B over 13 minutes.

RESULTS AND DISCUSSION

Synthesis of nitrocefin

A previously published method was used to synthesize nitrocefin from the cheap and commercially available precursor, 7-ACA (Scheme 4-1). According to this procedure, the last step following deprotection of the para-methoxybenzoate (PMB) moiety is isomerization of the double bond generated after the Wittig reaction of **4**. Supplemental Figure 4-1 shows the ^{1}H spectrum obtained after leaving the reaction mixture in 10% DMSO in chloroform for 24 hours. Peaks at δ 7.1 and δ 6.9 were initially believed to correspond to the Z isomer based on a coupling constant of 8 Hz, however these peaks did not disappear as described previously (Supplemental Figure 4-1) (Lee et al., 2005b). It's more likely that these peaks and additional peaks around δ 3.5 were due to the presence of an impurity resulting from anisole scavenging PMB, which was incompletely removed by trituration with diethyl ether. Triturated material was estimated to be ~ 85% pure. HPLC purified material yielded ^{1}H spectrum identical to commercially available nitrocefin, however (Supplemental Figures 4-6, 4-7). Both HPLC purified and triturated material demonstrated identical behavior in kinetic assays when concentration was normalized (data not shown) and therefore triturated material was used in screening.

Screening of the Canadian Compound Collection

The Canadian Compound Collection (CCC) was chosen to screen against NDM-1 because of the diversity and bioactivity contained within (Supplemental Table 4-1). It is made up of compounds sourced from commercial vendors as well as natural products and synthetic molecules obtained from collaborators. Approximately 1200 of the molecules are off-patent drugs and this is considered to be a privileged subset of the library as these molecules are presumably bioactive and drug-like. A total of 30 205 compounds were screened in duplicate (Figure 4-1A) with good reproducibility. Compounds showing <80% residual activity were then chosen for concentration-response assays (Supplemental Figure 4-8). Based on potency and shape of dose response curves, dantrolene, benserazide, and L-histidine β-naphthylamide (HNA) (Figure 4-1B) were selected for further study.

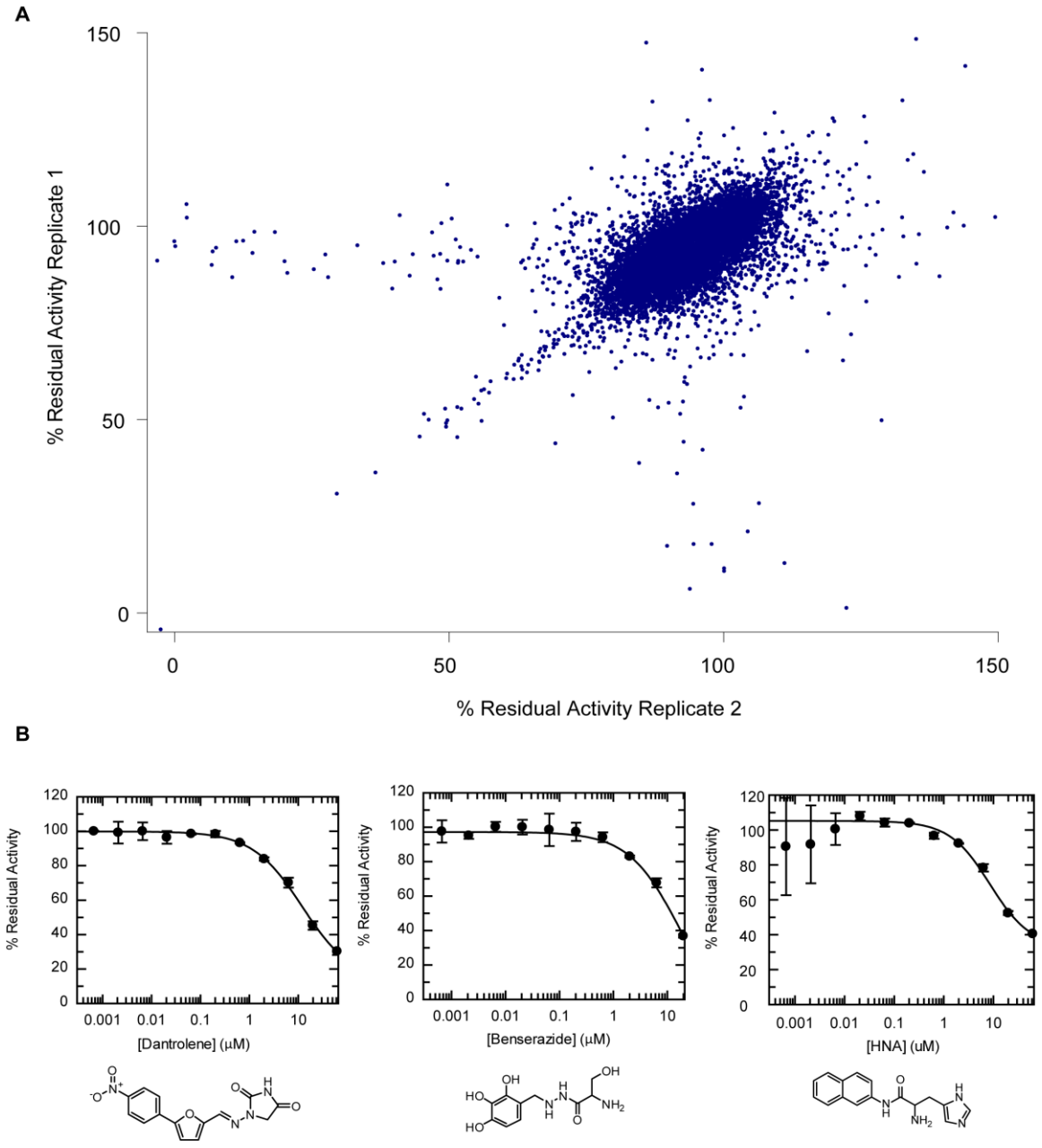

Figure 4-1. HTS of the Canadian Compound Collection yields several hits. (A) Replica plot of % residual enzyme activity in the presence of screened compound. (B) Concentration-response plots for the top hits from screen, left to right: Dantrolene, Benserazide, L-Histidine β-naphthylamide (HNA).

Dantrolene displays Zn-dependent activity and does not synergize with meropenem in cells

After having generated dose-response curves, efforts were made to determine an inhibitor constant (K_i). Dantrolene displayed non-reversible behavior and so a number of reaction conditions were varied, including incubation time (assay for slow-binding (Morrison and Walsh, 1988)) and the effects of varying zinc concentration. It has been well-documented that NDM-1 has significantly varying kinetic parameters depending on the concentration of zinc (Thomas et al., 2011). Surprisingly, when the assay was conducted with no zinc supplementation, dantrolene lost inhibitory activity and therefore a titration experiment was done to determine the contribution of zinc to dantrolene inhibitor efficacy (Figure 4-2A-C). Dantrolene shows significant inhibition of NDM-1 at 50 μM $ZnSO_4$, as expected since this is the same concentration used in screening and follow-up concentration-response. However, increasing the concentration of $ZnSO_4$ lead to even greater reductions in residual activity and the reverse held true when decreasing concentration. This could be seen visually by the generation of color and slight turbidity in wells. As expected, increased concentrations of $ZnSO_4$ led to more significant and rapid spectral shifts when incubated with the same concentration of dantrolene (Figure 4-2D, E). This activity was also shown to be nonspecific, as evidenced by increased activity against the SBL, CTX-M-15, as a function of zinc concentration (Supplemental Figure 4-9). There is another example of a conjugated imine probe that had been developed to detect zinc (Li et al., 2011) and it is likely that a similar binding event and intramolecular charge transfer may occur in dantrolene. The development of turbidity upon increasing zinc addition to

dantrolene may also be indicative of precipitate colloid formation, which can sequester enzyme and show false inhibition profiles (Feng et al., 2005; Feng and Shoichet, 2006). Furthermore, dantrolene did not synergize with meropenem in a cell-based assay targeting NDM-1 in an engineered strain of *E. coli* (King et al., 2014) (Figure 4-2F).

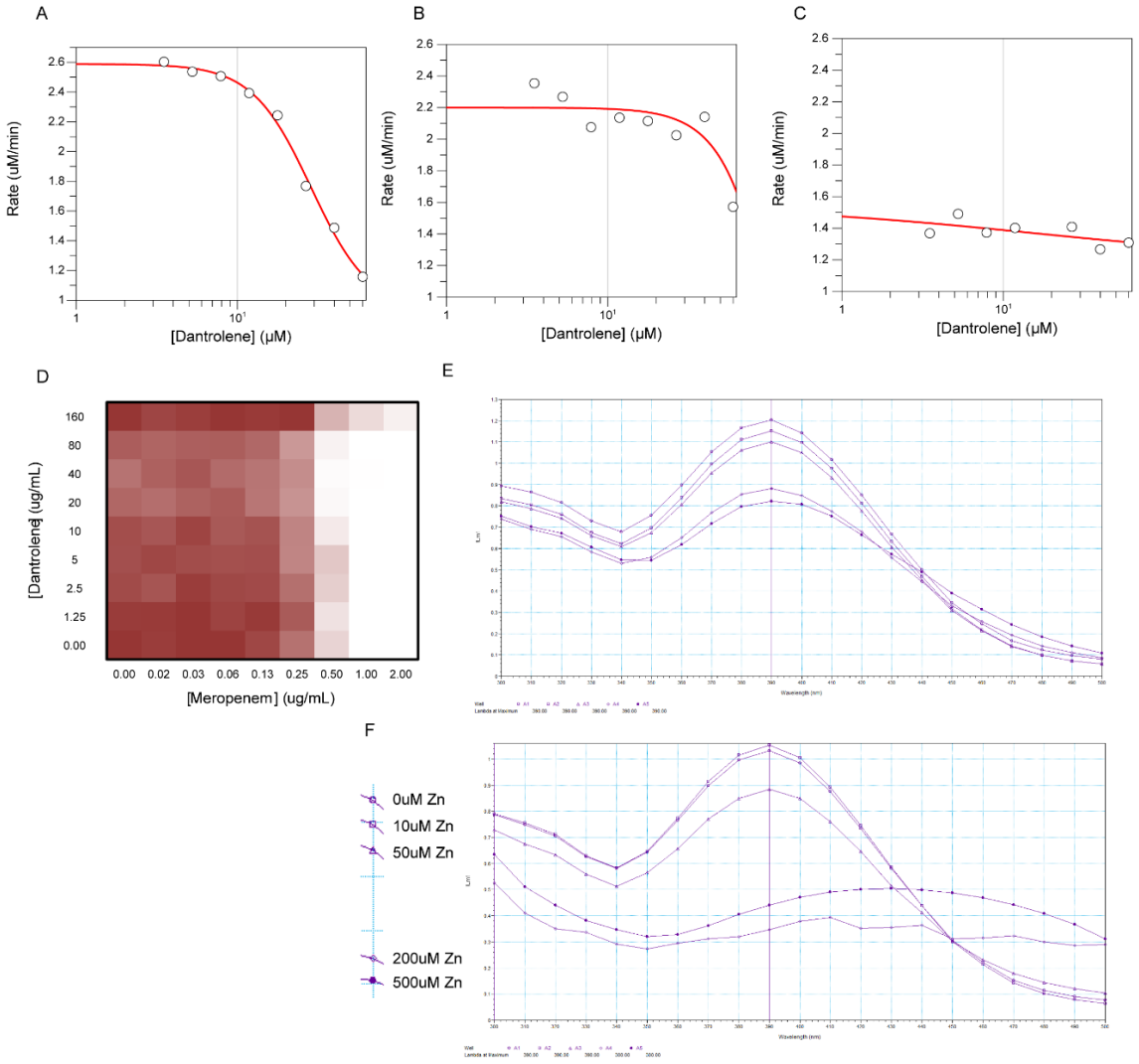

Figure 4-2. Dantrolene is a zinc-dependent inhibitor of NDM-1 that does not synergize with meropenem. (A) Microdilution checkerboard assay demonstrates that dantrolene does not synergize with meropenem in *E. coli* BW25113*ΔbamBΔtolCΔaraDAB::pLac*(bla_{NDM-1}). (B-D) Concentration-response plot demonstrating the zinc-dependent inhibitory activity of dantrolene against NDM-1. (B) 200 µM, (C) 50 µM, (D) 10 µM $ZnSO_4$. (E-F) Time- and concentration-dependent changes in the UV-vis absorption spectra of dantrolene incubated with $ZnSO_4$. (E) 0 minutes, (F) 30 minutes.

Benserazide is unstable in buffered solution, generating breakdown products able to selectively inhibit NDM-1

In similar fashion to dantrolene, benserazide did not yield K_i curves indicative of a classical reversible inhibitor. Furthermore, there was a significant increase in background absorbance over time during enzyme assays in inhibitor alone controls. This increase was present in a number of buffers (HEPES pH 7.5, MOPS pH 7.5, Phosphate pH 7.0, TAPS pH 8.0, TES pH 7.5, Tricine pH 7.5, Tris pH 7.6) but not in unbuffered solution. Indeed, overnight incubation in unbuffered water led to no color development while buffered solutions led to colored solution being developed. Interestingly, the unbuffered benserazide solution was unable to inhibit NDM-1 (Figure 4-3A) while benserazide incubated overnight was able to selectively inhibit NDM-1 and not CTX-M-15 (Figure 4-3B, C). The degradation of benserazide over time was confirmed by LC-MS (Supplemental Figure 4-10). Benserazide has been previously shown to be sensitive to oxidation with the generation of a quinone preceding the generation of colorless compounds (Coello et al., 2000), but these conditions were different from those reported here. The exact mechanism was not investigated any further since benserazide was not active in cells (data not shown) and the reactivity observed here led to its deprioritization in the face of natural product hits ongoing at the same time.

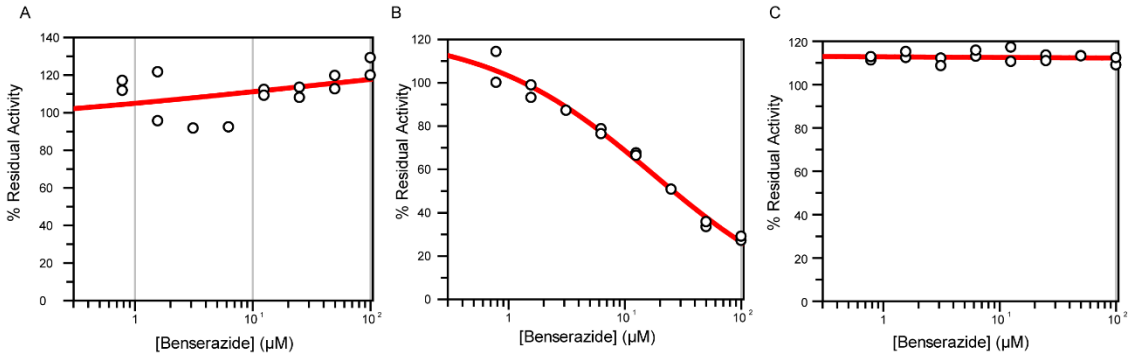

Figure 4-3. Benserazide is unstable in solution and generates breakdown products able to selectively inhibit NDM-1. (A-C) Concentration-response plot demonstrating the zinc-dependent inhibitory activity of benserazide against selected β-lactamases. (A) NDM-1 with benserazide and no buffer, (B) NDM-1 with benserazide in HEPES after 24 hours, (C) CTX-M-15 with benserazide in HEPES after 24 hours.

HNA is not a potent inhibitor of NDM-1 and does not synergize with meropenem

Given the reactivity of dantrolene and benserazide, one more compound from the CCC screen was investigated for its activity against NDM-1. HNA showed a decent IC_{50} value and the shape of the curve was ideal (aside from what must be assumed to be pipetting error at lower concentrations). The structure of HNA also reflects a common trend that has been observed in MBL inhibitors whereby the molecule contains a bulky aromatic group (naphthyl), electrostatic interacting group (amide, free amine), and a metal coordinating group (imidazole) (Oelschlaeger et al., 2010). Unfortunately, HNA did not synergize with meropenem (Figure 4-4A) and, upon reordering the compound from a commercial source, it was found that the activity was significantly reduced (Figure 4-4B,C, Supplemental Figure 4-11, 4-12). Together, these results led to the deprioritization of this molecule.

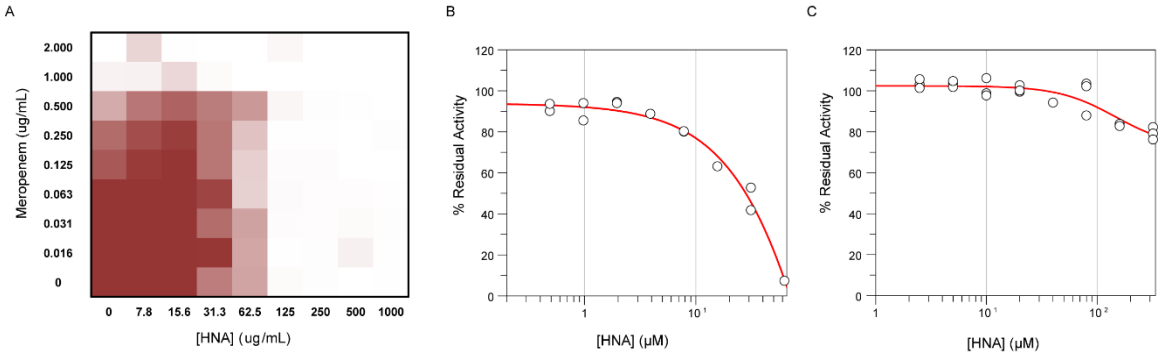

Figure 4-4. HNA is not a potent inhibitor of NDM-1 and does not synergize with meropenem. (A) Microdilution checkerboard assay demonstrates that HNA does not synergize with meropenem in *E. coli* BW25113*ΔbamBΔtolCΔaraDAB::pLac*(bla_{NDM-1}). (B, C) Concentration-response plot demonstrating the activity of (B) HTS stock HNA and (C) re-ordered HNA.

Trends and future directions

The best hits from a 30 000-strong screen against purified enzyme yielded reactive molecules with no activity in cells. Dantrolene is used clinically as a skeletal muscle relaxant in the treatment of human malignant hyperthermia, thought to be a result of inhibiting the ryanodine receptor as is well-summarized by Krause *et. al* (Krause et al., 2004). Here, we have shown that dantrolene binds to zinc, eliciting changes in the UV-vis spectrum and solubility properties of the molecule. It is interesting to note that the exact mechanism of action of dantrolene is unknown but understood to modulate calcium balance either directly or indirectly (Krause et al., 2004), suggesting that its physiological role in mitigating disease may be linked to its metal-binding properties. Such experiments are beyond the scope of this thesis, however.

Benserazide is clinically used as an aromatic L-amino acid decarboxylase (AADC) inhibitor in combination with L-3,4-dihydroxyphenylalanine (L-DOPA) for the treatment

of Parkinson's disease (Shen et al., 2003). AADC is a pyridoxal 5'-phosphate (PLP)-dependent enzyme, with no apparent requirement for zinc in its catalytic mechanism (Ishii et al., 1998). While it is possible that benserazide acts on NDM-1 with some specificity, the data to the contrary are compelling enough to dismiss this notion. The loss of activity in slightly acidic conditions (unbuffered, pH ~ 6.5) is alarming but equally alarming is the fact that, after extended incubations and complete degradation of benserazide, significant inhibitory activity is observed (Figure 4-3, Supplemental Figure 4-10). Coupled with a lack of specific activity in cells, this is not a promising candidate for a clinical inhibitor of MBLs or a useful probe for further study.

HNA, on the other hand, may present an interesting candidate for further study from these experiments. It has not shown strange reactivity but having a low IC_{50} value upon retesting (> 300 μM) and no specific activity in cells led to its dismissal for further study. However, this and other molecules from secondary concentration-response assays may be useful probes and candidates for medicinal chemistry approaches coupled with structure-activity response assays against purified MBLs. In particular, targeting IMP enzymes is particularly appealing for this approach as they are recalcitrant to inhibition from aspergillomarasmine A (AMA) (King et al., 2014; Koteva et al., 2015). It seems likely that a molecule that acts to coordinate one or both zinc ions, possibly a slow, tight-binder, is preferable to molecules able to remove the zinc ions.

Although there were no ideal hits discovered in this process, there still remains potential for exploration. We have created a highly effective workflow that couples *in vitro* enzymology with cell-based inhibitory activity and judicious use of this workflow could

yet yield useful chemistry from these efforts. It is reasonable to assume that any molecules with "real" activity against NDM-1 may share activity against IMP enzymes. An easy filter would be to test the concentration-response plates already generated (Supplementary Figure 4-1) against a strain of *E. coli* expressing an IMP enzyme and look for any molecules able to restore carbapenem susceptibility at ¼ MIC. Any molecules with this activity would be excellent candidates for further testing. If the scaffold is amenable to medicinal chemistry approaches, the infrastructure exists to fine-tune activity to IMP enzymes *in vitro*. It would also be ideal to acquire other clinically relevant enzymes that AMA does not inhibit, like SPM (King et al., 2014). By using a combination of enzymology and cell-based efficacy, one could guide any given compound series to be active against clinically-relevant MBL classes other than NDM and VIM.

SUPPLEMENTAL INFORMATION

Supplemental Tables

Supplemental Table 4-1. Chemical libraries available for screening. The Canadian Compound Collection (highlighted in blue) was chosen for screening against NDM-.

Library name	Source	#Cmds	Overlap with other libraries	Initial Preparation	Comments
P1000	Maybridge	1,000	918 cmds (~92%) also in MA50K	2001	Used primarily for pilot screens.
MA50K (aka MA orig)	Maybridge	50,000	12,631 (~25%) also in CCC	2001	Screening plates in good condition with appropriate volume in 1 mM set for screening.
Chemtura	Chemtura	11,616	Unknown	2002	Cmd identities are unknown. Screened only on approval by GDW.
CH1	ChemBridge	46,480	1,000 cmds (~2%) also in CCC	2003	Have minimal volume of 5 mM only; some foil seals are becoming loose in freezer. This set only ever screened against E. coli.
CH2	ChemBridge	50,000	None	2004	Screening plates in good condition with appropriate volume in 1 mM set for screening. This set only ever screened against DHFR.
Kinase	ChemDiv	1,000	Not yet checked	2004	Screened only on approval by EDB.
Perrin Peptides	Dave Perrin (UBC)	70	None	2006	Screened only on approval by EDB; only 10 uL left.
Gerry & Eric's Excellent Collection (GEEC)	Maybridge	19	7 cmds in CCC; 12 cmds in MA50K	2006	Cmds were sourced from the cherry picking plates of the MA50K and CCC libraries specifically for screens for the EDB & GDW Labs.
	Prestwick	815	100% in CCC		
	BioMol	15	100% in CCC		
	Sigma	77	100% in CCC		
	MicroSource	198	100% in CCC		
Canadian Compound Collection (CCC)	Maybridge	16,000	12,631 cmds (~80%) also in MA50K		
	ChemBridge	9,989	1,000 cmds (~10%) also in CH1		
	Prestwick	1,120	Not yet checked	2006	Bioactive subset (Prestwick, BioMol, MicroSource & Sigma cmds) reformatted from original layout to remove redundant cmds.
	BioMol	361	Not yet checked		
	MicroSource	1,214	Not yet checked		
	Sigma	885	Not yet checked		
	R.T. Tlegenov	26	Unknown	2006	Plant extracts; structures unknown.
	Dennis Hall	690	Not yet checked	2007	Contains lactams, lactones & piperidines.
	Jim McNulty	400	Unknown	2010	Structures unknown; contains anticancer, antifungal, antibacterial cmds.
Johns Hopkins Clinical Compound Library (JHCCL)	Johns Hopkins	562	Not yet checked	2008	Original library was to contain 1,514 cmds, although there were some cmds missing; 956 of these were cherry picked by EDB Lab for GEEC Library. Remaining 562 compounds (with 6 redundant cmds) are distributed over 37 plates.
OICR	Asinex	5,318	Not yet checked	2010	Screened only on approval by OICR.
	ChemDiv	17,420	Not yet checked		
	ChemBridge	27,505	Not yet checked		
	Enamine	91,618	Not yet checked		
OICR Diversity Set	Asinex	1,021	100% in OICR	2011	Cmds were sourced from the master plates of the OICR library. Screened only on approval by OICR.
	ChemDiv	3,950	100% in OICR		
	ChemBridge	4,013	100% in OICR		
	Enamine	11,176	100% in OICR		

Supplemental Figures

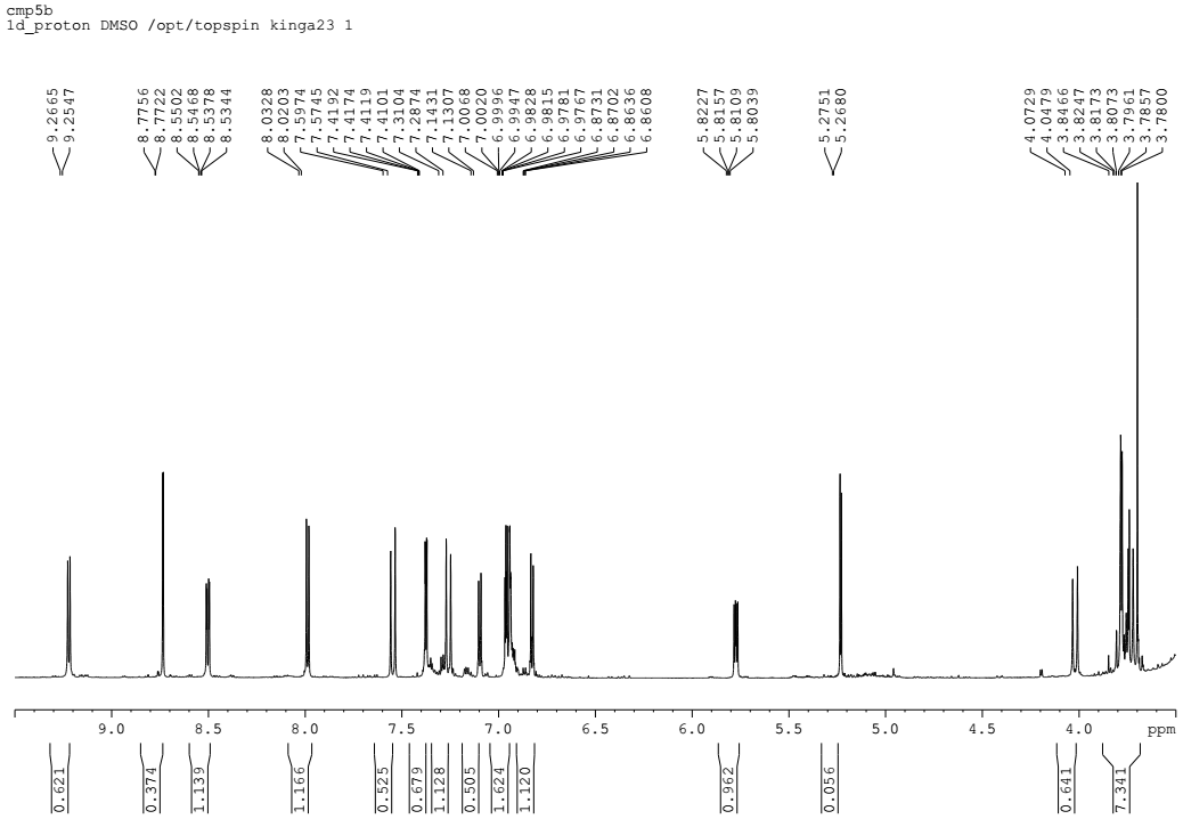

Supplemental Figure 4-1. ^{1}H NMR spectrum for compound 5.

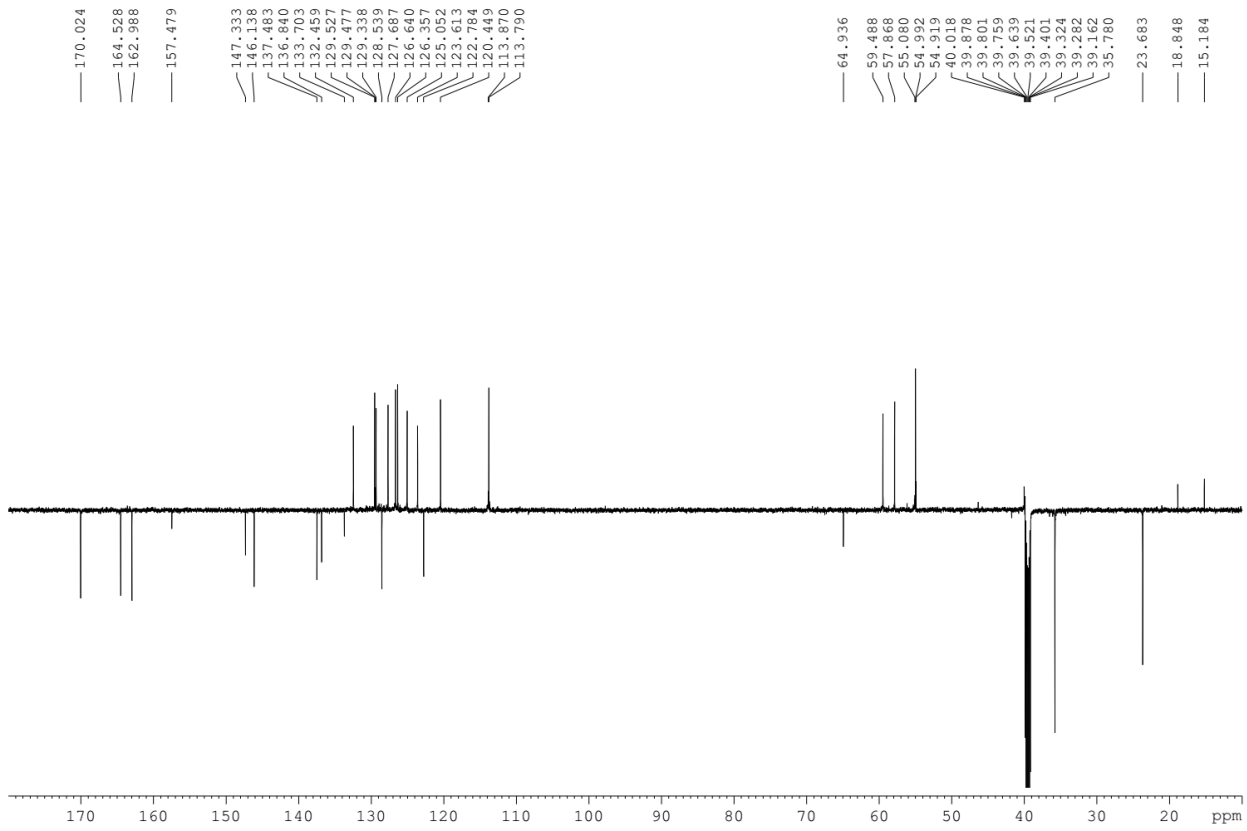

Supplemental Figure 4-2. ^{13}C NMR spectrum for compound 5.

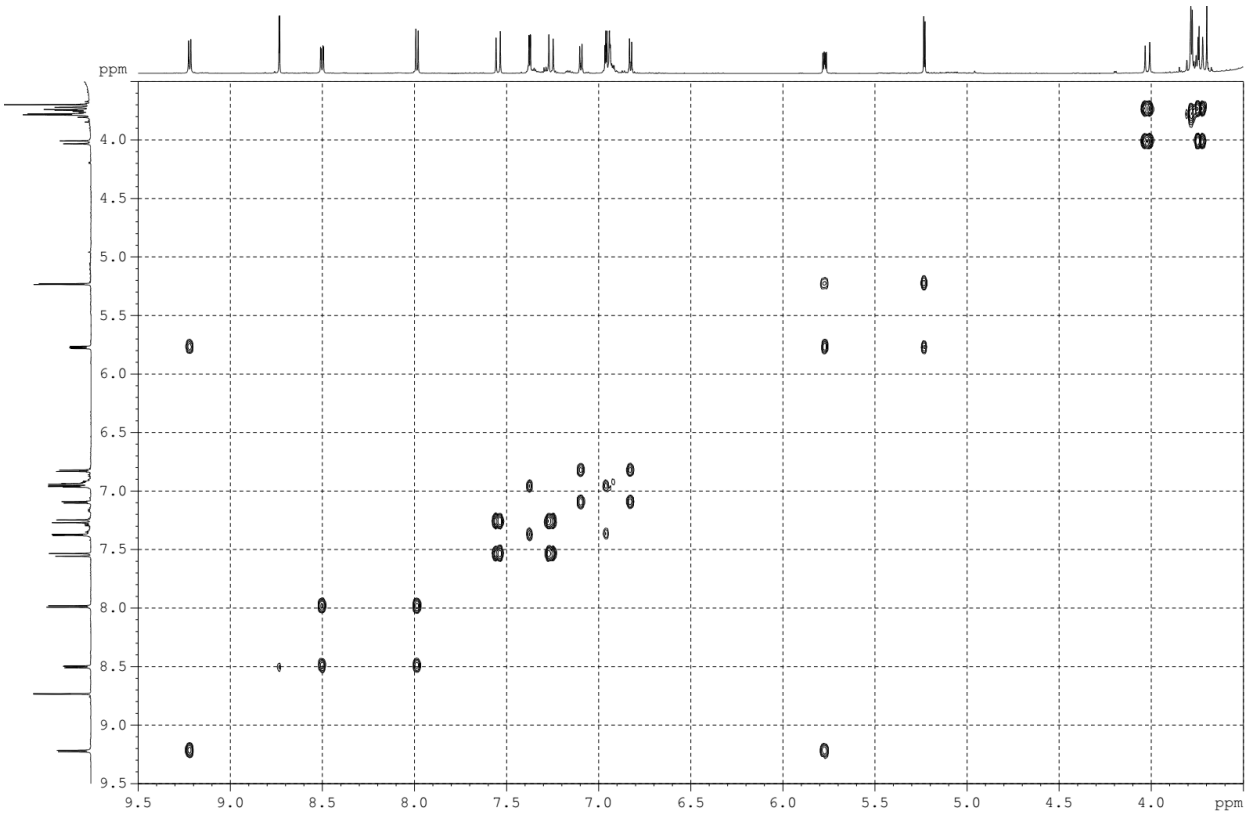

Supplemental Figure 4-3. COSY spectrum for compound 5.

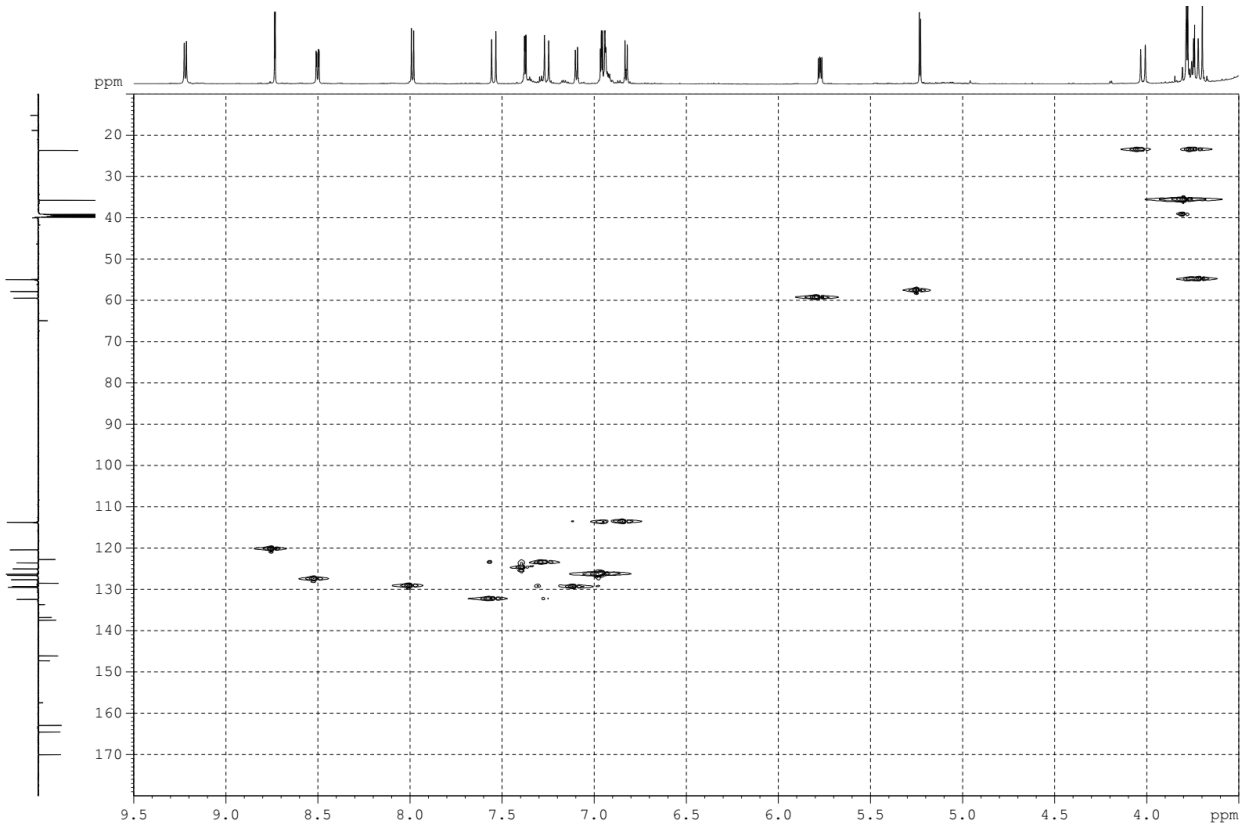

Supplemental Figure 4-4. HSQC spectrum for compound 5.

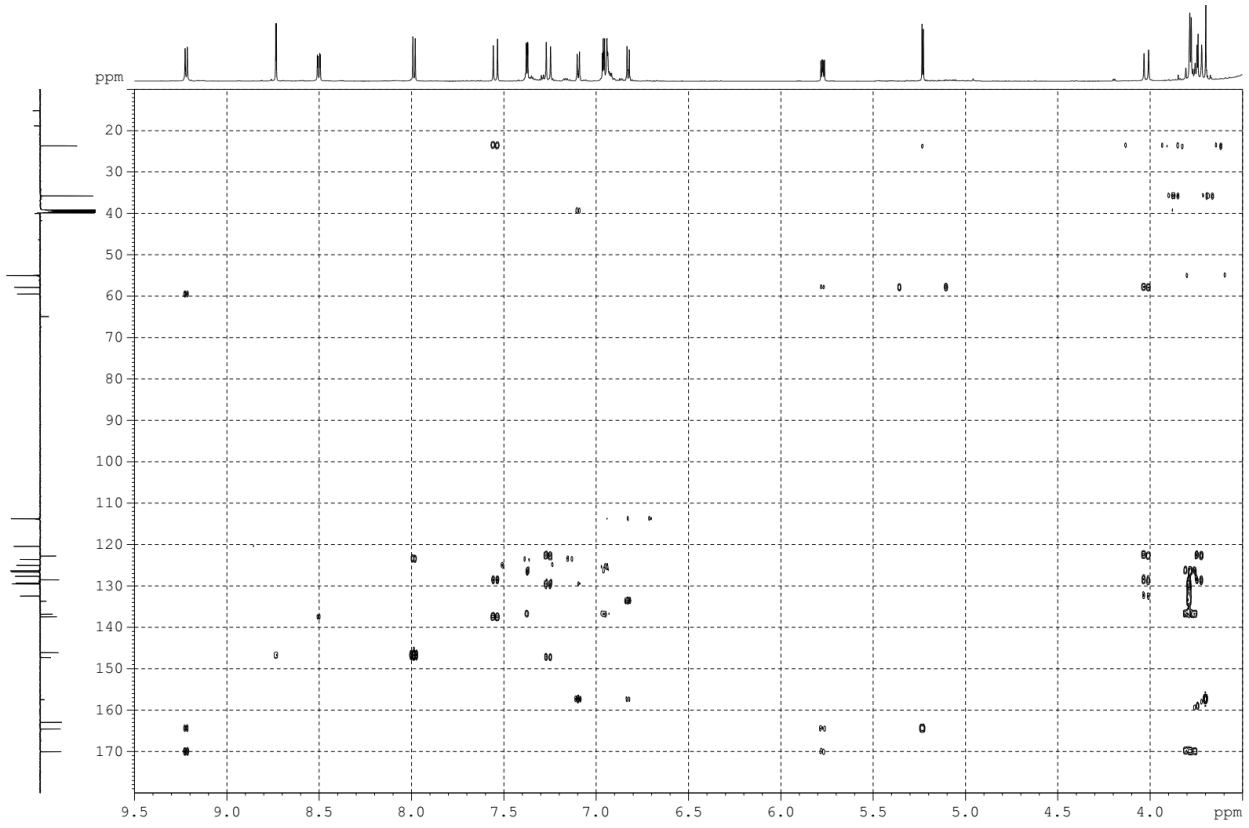

Supplemental Figure 4-5. HMBC spectrum for compound 5.

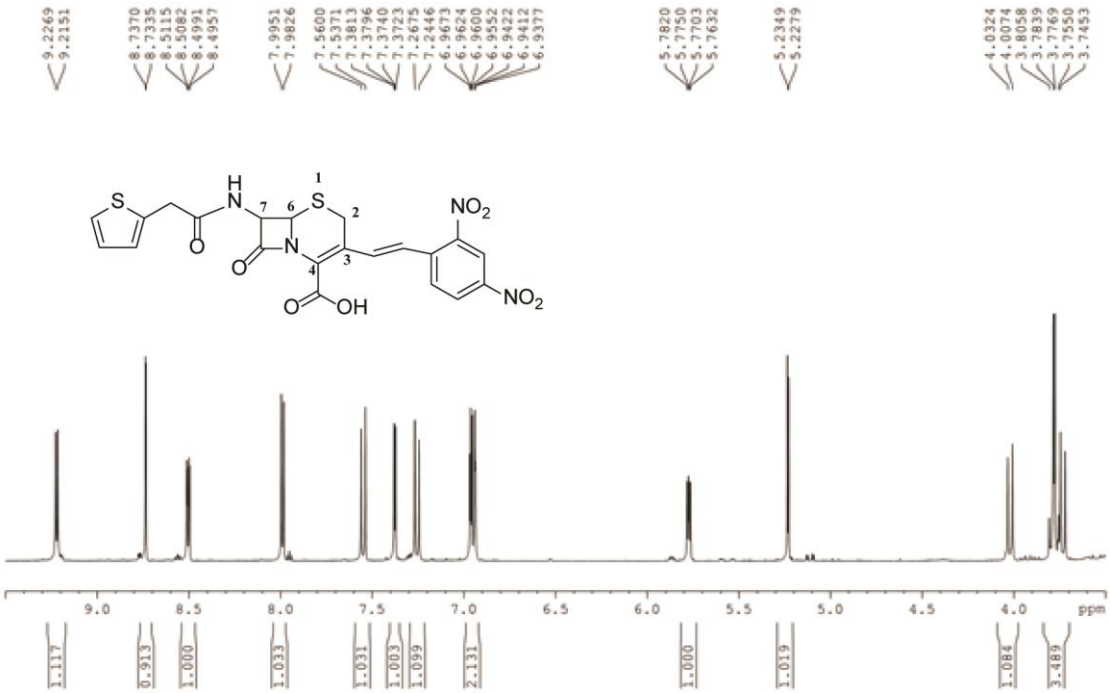

Supplemental Figure 4-6. ^{1}H spectrum for compound 5 after HPLC purification.

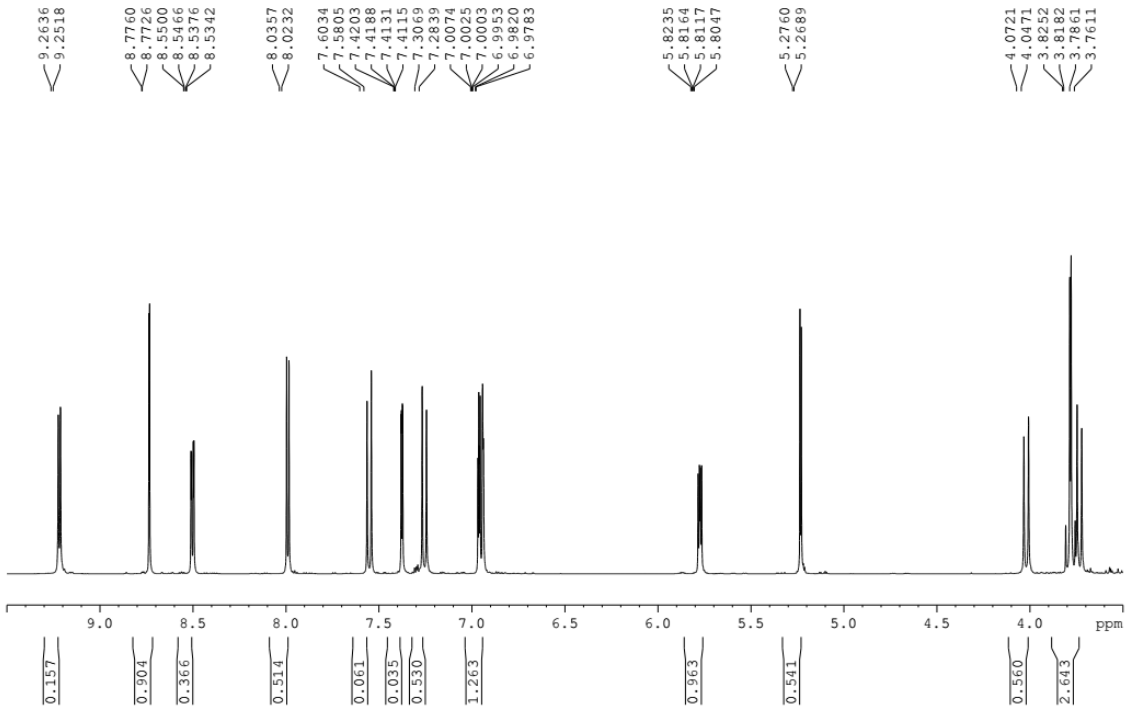

Supplemental Figure 4-7. ^{1}H spectrum for commercially available nitrocefin.

Supplemental Figure 4-8. Chemical structure and concentration-response plots of hits from CCC screen.

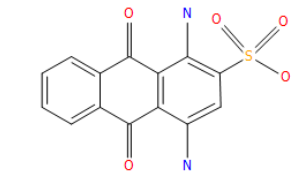

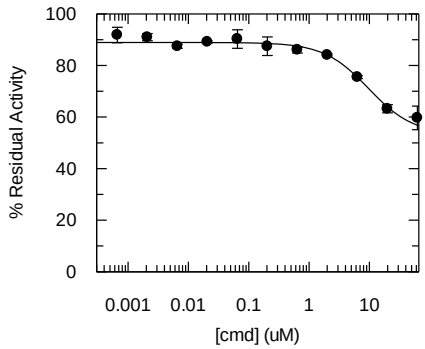

Parameter	Value	Std. Error
Y Range	35.6718	6.2528
IC 50	9.6386	3.0531
Slope factor	1.1715	0.1671
Background	53.2406	6.1757

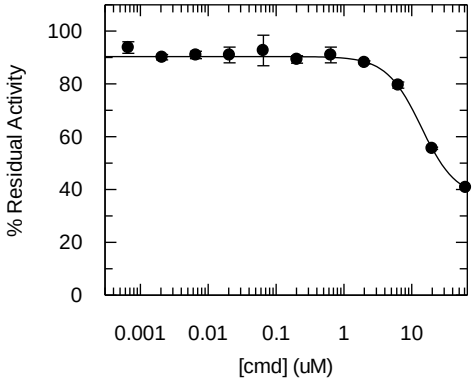

Parameter	Value	Std. Error
Y Range	53.4349	1.1354
IC 50	13.7773	0.3725
Slope factor	1.6931	0.0975
Background	36.9344	0.9061

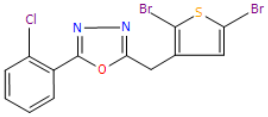

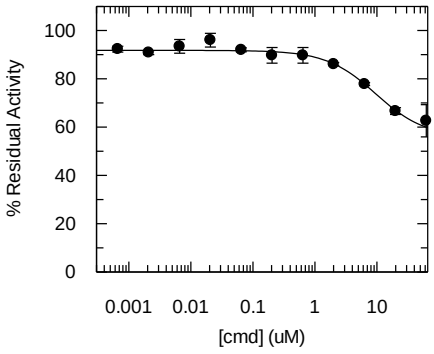

Parameter	Value	Std. Error
Y Range	35.8557	5.9242
IC 50	9.4524	3.0118
Slope factor	1.0926	0.1609
Background	55.9327	5.8160

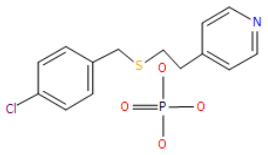

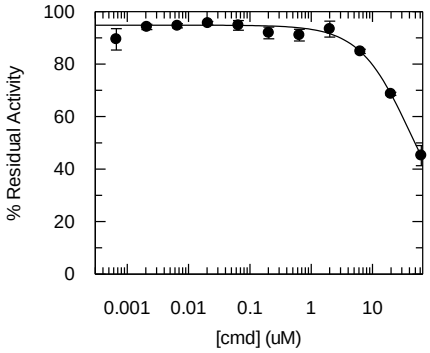

Parameter	Value	Std. Error
Y Range	81.2030	24.6187
IC 50	40.1839	21.1039
Slope factor	1.0578	0.1505
Background	13.6180	24.5525

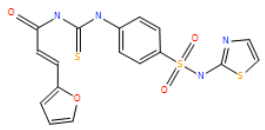

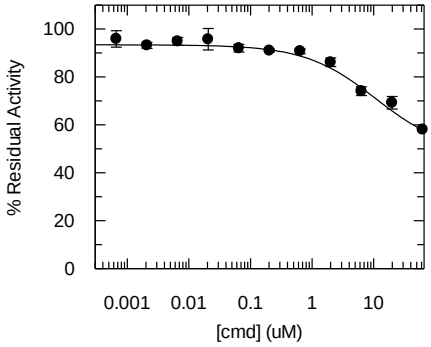

Parameter	Value	Std. Error
Y Range	44.8111	15.0914
IC 50	10.6551	18.9386
Slope factor	0.7633	0.1791
Background	48.6086	14.3568

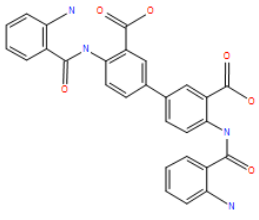

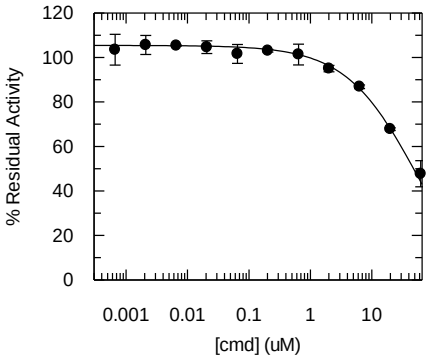

Parameter	Value	Std. Error
Y Range	117.7802	9.5314
IC 50	55.7885	10.4263
Slope factor	0.7426	0.0349
Background	-12.3630	9.5100

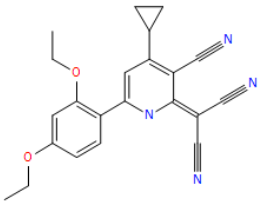

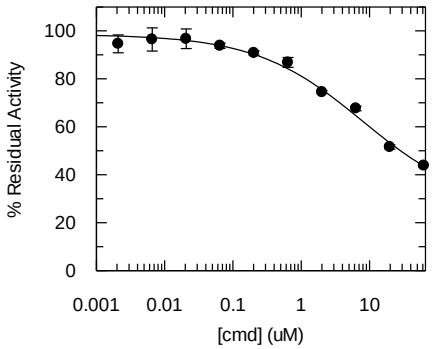

Parameter	Value	Std. Error
Y Range	72.3934	15.4312
IC 50	7.8506	4.4221
Slope factor	0.5557	0.1516
Background	26.1866	12.2536

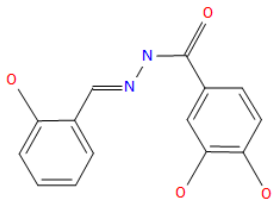

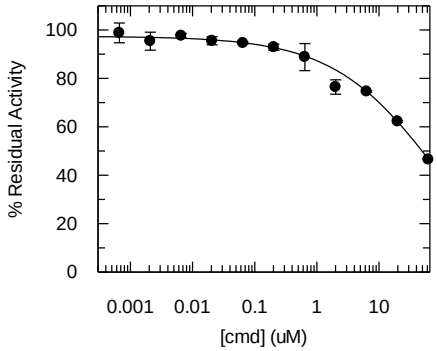

Parameter	Value	Std. Error
Y Range	112.8982	4.5447
IC 50	92.0016	12.9769
Slope factor	0.5124	0.0173
Background	-15.4790	4.4121

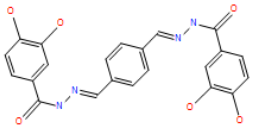

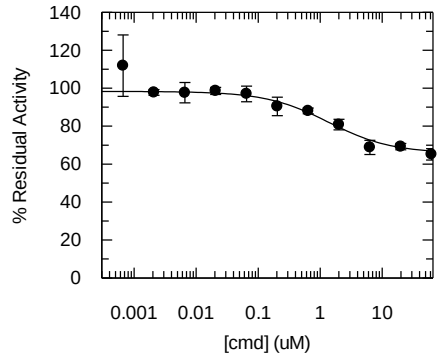

Parameter	Value	Std. Error
Y Range	32.6089	4.6810
IC 50	1.3733	0.9079
Slope factor	0.8533	0.1694
Background	65.6953	4.0925

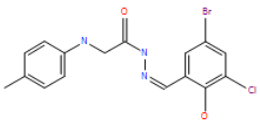

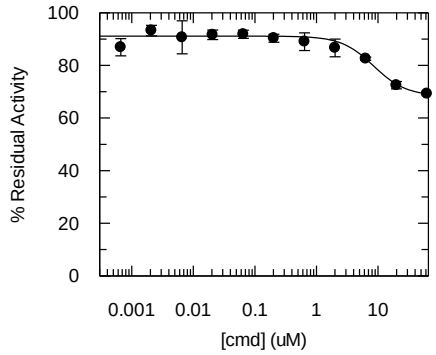

Parameter	Value	Std. Error
Y Range	22.7027	1.1224
IC 50	8.4678	0.9041
Slope factor	1.6600	0.3642
Background	68.4084	0.8641

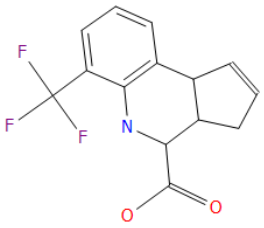

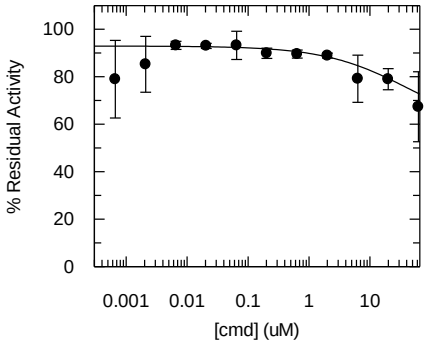

Parameter	Value	Std. Error
Y Range	35.5013	9.2458
IC 50	41.6832	36.5465
Slope factor	0.6312	0.1766
Background	57.4365	9.1614

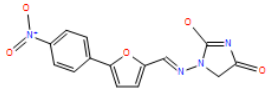

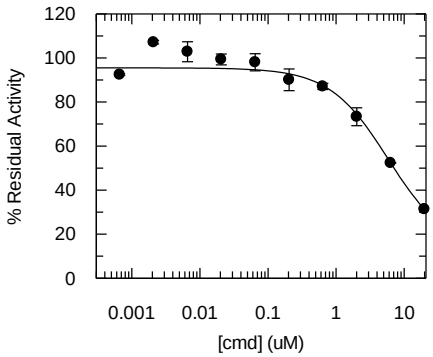

Parameter	Value	Std. Error
Y Range	82.4512	28.0375
IC 50	5.7639	3.5425
Slope factor	1.0110	0.6922
Background	13.0415	27.4705

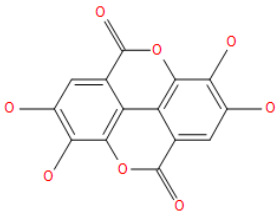

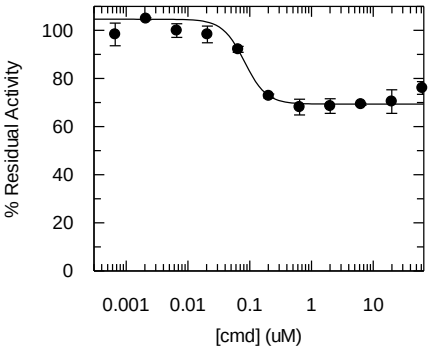

Parameter	Value	Std. Error
Y Range	35.2741	0.7919
IC 50	0.0820	0.0066
Slope factor	2.4351	0.3839
Background	69.3652	0.5546

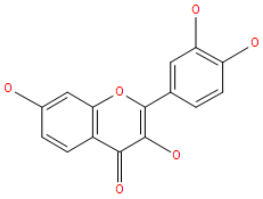

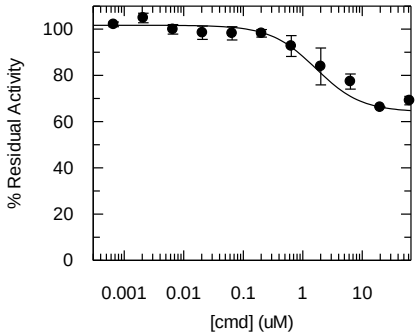

MAC-0179467

Parameter	Value	Std. Error
Y Range	37.4552	3.3729
IC 50	1.6620	0.9285
Slope factor	1.1413	0.3513
Background	64.2294	2.9651

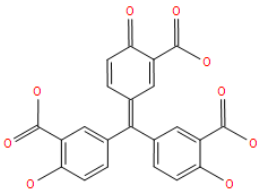

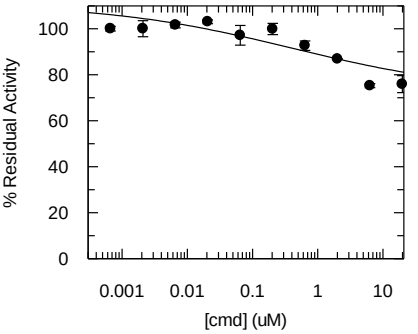

MAC-0179893

Parameter	Value	Std. Error
Y Range	38.7355	1.18194e-007
IC 50	0.4089	6.57454e-009
Slope factor	0.3062	3.08890e-009
Background	72.1690	4.49532e-008

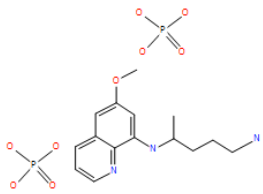

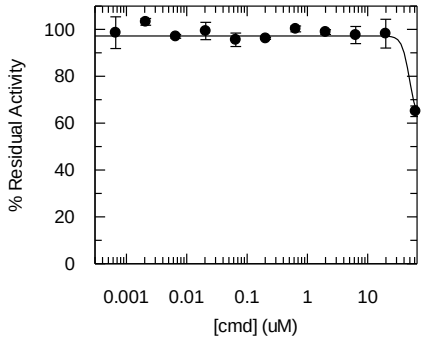

MAC-0179281

Parameter	Value	Std. Error
Y Range	37.0711	492.3321
IC 50	49.2246	527.3855
Slope factor	6.9275	50.7593
Background	60.1390	492.3303

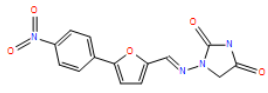

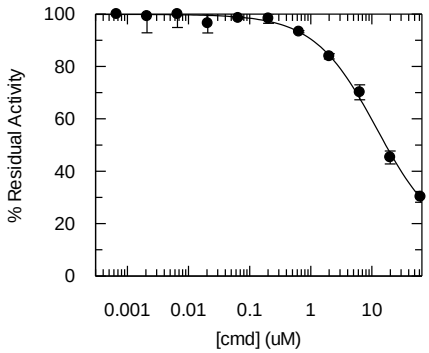

MAC-0180257

Parameter	Value	Std. Error
Y Range	87.5627	4.9963
IC 50	12.0828	2.2239
Slope factor	0.8475	0.0429
Background	12.3132	4.9395

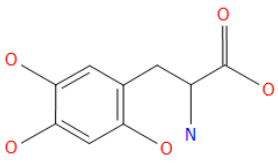

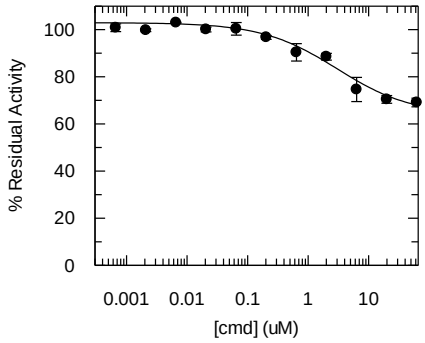

MAC-0180463

Parameter	Value	Std. Error
Y Range	39.0856	10.8802
IC 50	2.9822	3.4146
Slope factor	0.7040	0.2868
Background	63.8994	10.2297

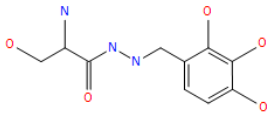

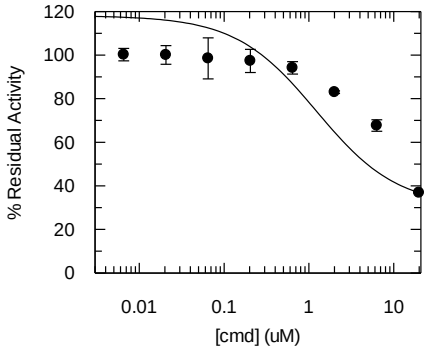

MAC-0179054

Parameter	Value	Std. Error
Y Range	87.6781	9.4871
IC 50	1.2247	0.1632
Slope factor	0.9097	0.0432
Background	30.4258	0.7154

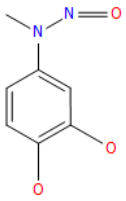

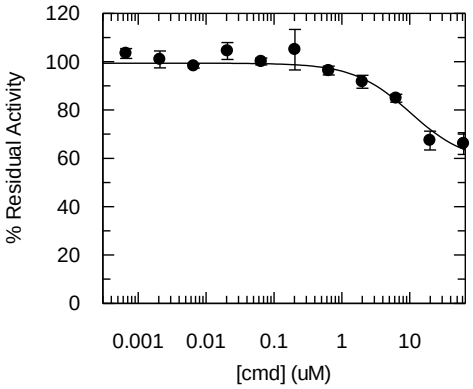

MAC-0180698

Parameter	Value	Std. Error
Y Range	40.9544	12.4343
IC 50	10.1468	6.9295
Slope factor	1.0464	0.4385
Background	58.4241	12.2018

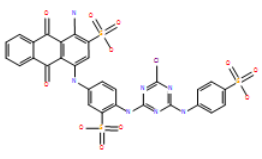

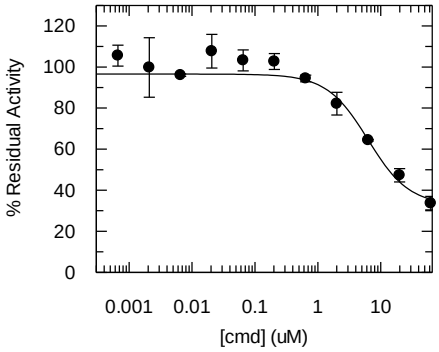

MAC-0180881

Parameter	Value	Std. Error
Y Range	63.8263	5.8712
IC 50	6.2473	0.8458
Slope factor	1.3289	0.3157
Background	32.7251	5.6845

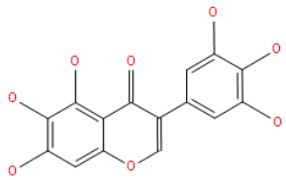

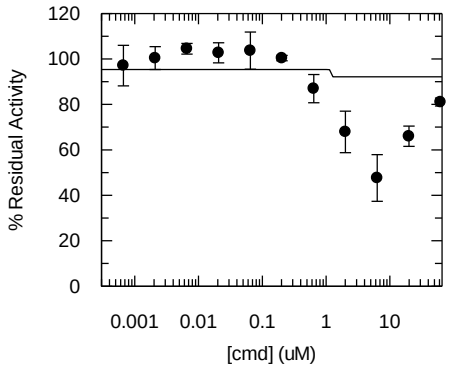

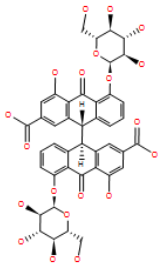

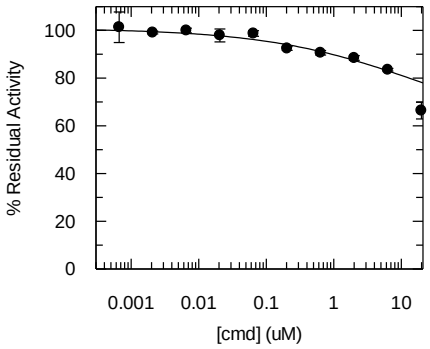

Parameter	Value	Std. Error
Y Range	45.6006	14.2724
IC 50	20.4489	25.5247
Slope factor	0.3755	0.1150
Background	55.2930	13.7862

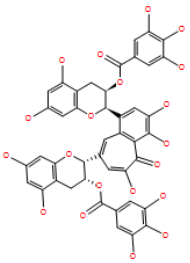

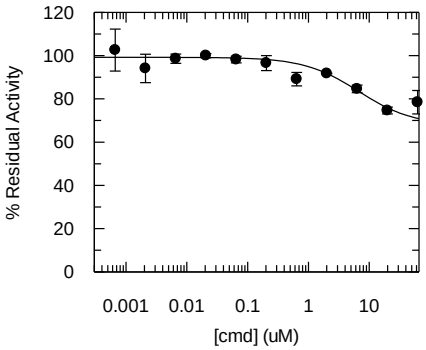

Parameter	Value	Std. Error
Y Range	31.4256	11.1630
IC 50	6.6500	6.1358
Slope factor	0.9709	0.3573
Background	67.7793	10.8078

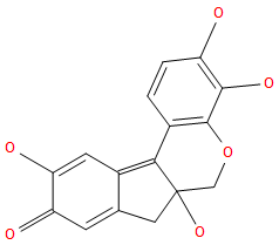

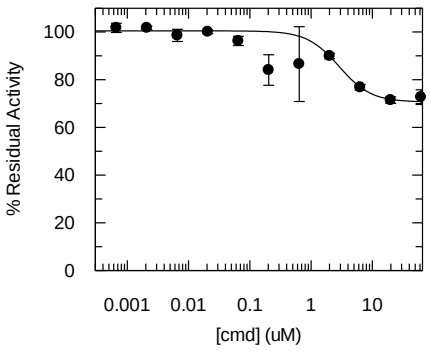

Parameter	Value	Std. Error
Y Range	29.8355	2.9426
IC 50	2.8524	0.5680
Slope factor	1.6673	0.5207
Background	70.6515	2.8191

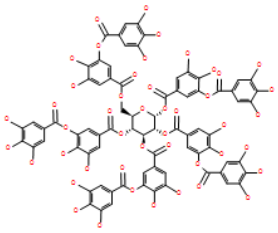

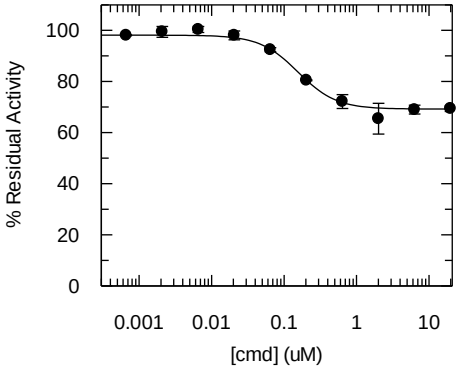

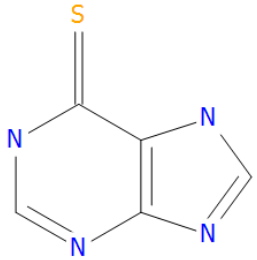

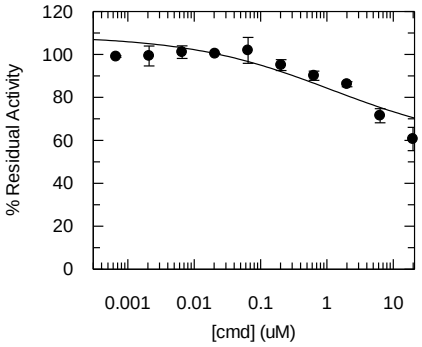

Parameter	Value	Std. Error
Y Range	50.3274	8.37714e-008
IC 50	1.1680	2.93124e-008
Slope factor	0.4012	2.49465e-009
Background	58.3622	6.99218e-008

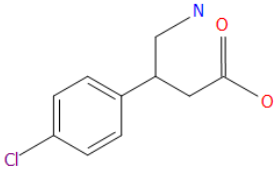

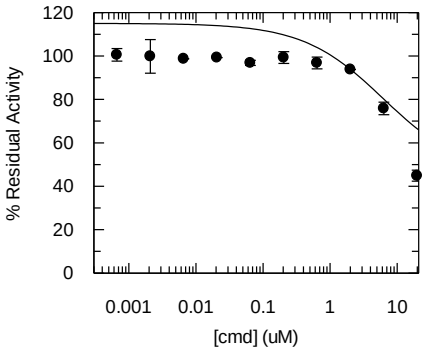

Parameter	Value	Std. Error
Y Range	69.0802	0.0111
IC 50	6.1261	0.0044
Slope factor	0.7299	0.0005
Background	45.9483	0.0077

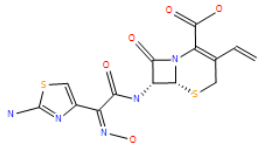

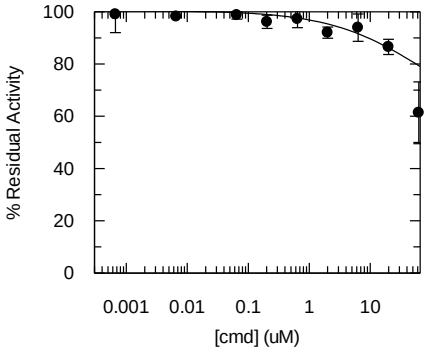

Parameter	Value	Std. Error
Y Range	44.5966	0.7080
IC 50	75.2257	81.4883
Slope factor	0.5601	0.1494
Background	55.8917	0.7014

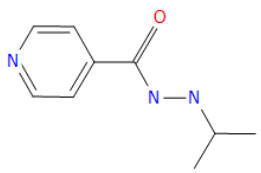

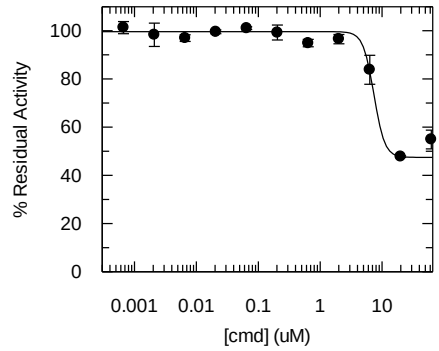

Parameter	Value	Std. Error
Y Range	52.1858	1.3512
IC 50	7.3610	1.4418
Slope factor	5.0146	2.4594
Background	47.4584	1.2320

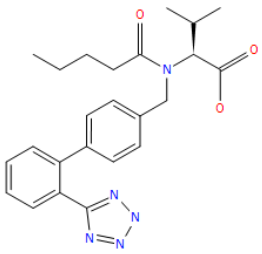

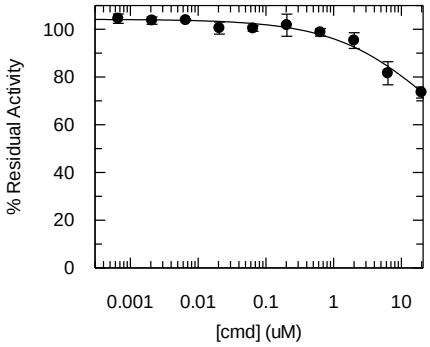

Parameter	Value	Std. Error
Y Range	67.9179	13.1400
IC 50	28.2569	16.9551
Slope factor	0.5941	0.0950
Background	36.2894	13.0457

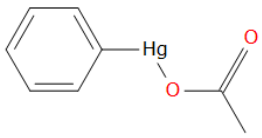

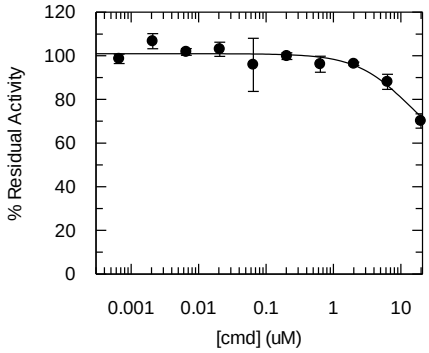

Parameter	Value	Std. Error
Y Range	46.2920	12.4117
IC 50	12.7530	6.2515
Slope factor	1.1097	0.3401
Background	54.6343	12.1815

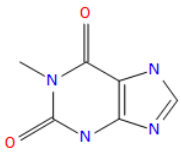

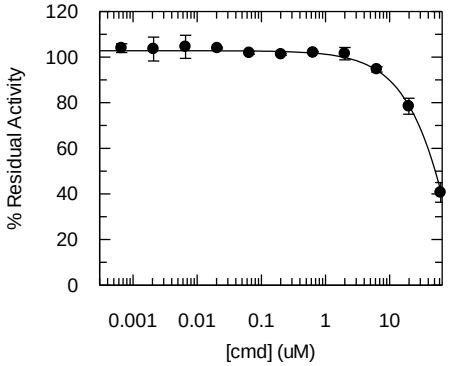

Parameter	Value	Std. Error
Y Range	331.0377	253.8369
IC 50	302.1801	339.5774
Slope factor	0.9368	0.1425
Background	-228.2555	253.7607

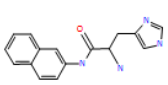

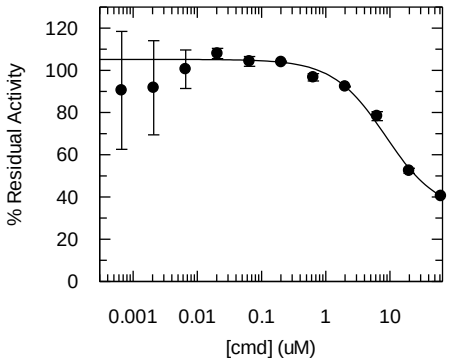

Parameter	Value	Std. Error
Y Range	72.4455	2.7540
IC 50	8.4874	1.0622
Slope factor	1.0636	0.0832
Background	32.7274	2.3550

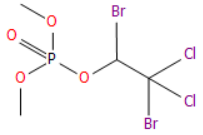

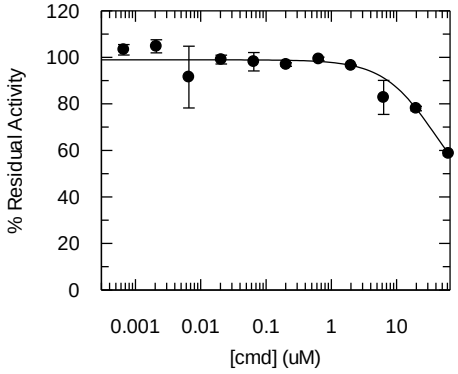

Parameter	Value	Std. Error
Y Range	62.9248	16.6679
IC 50	37.2089	18.3797
Slope factor	1.1057	0.2293
Background	35.9940	15.9708

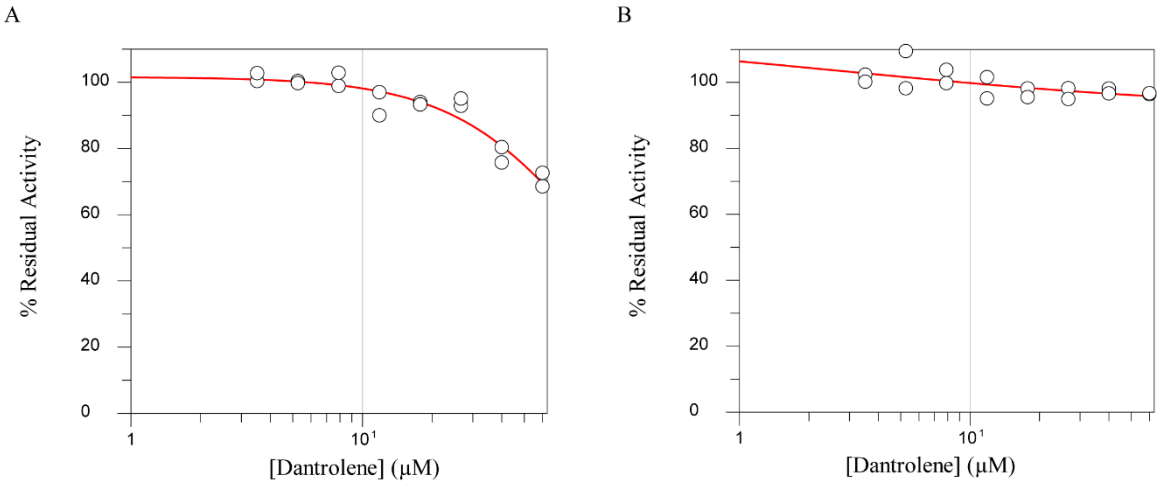

Supplemental Figure 4-9. Dantrolene loses inhibitory specificity as a function of ZnSO4 concentration. Concentration-response plots for (A) CTX-M-15 in the presence of 150 μM $ZnSO_4$ and (B) CTX-M-15 in the presence of 50 μM $ZnSO_4$.

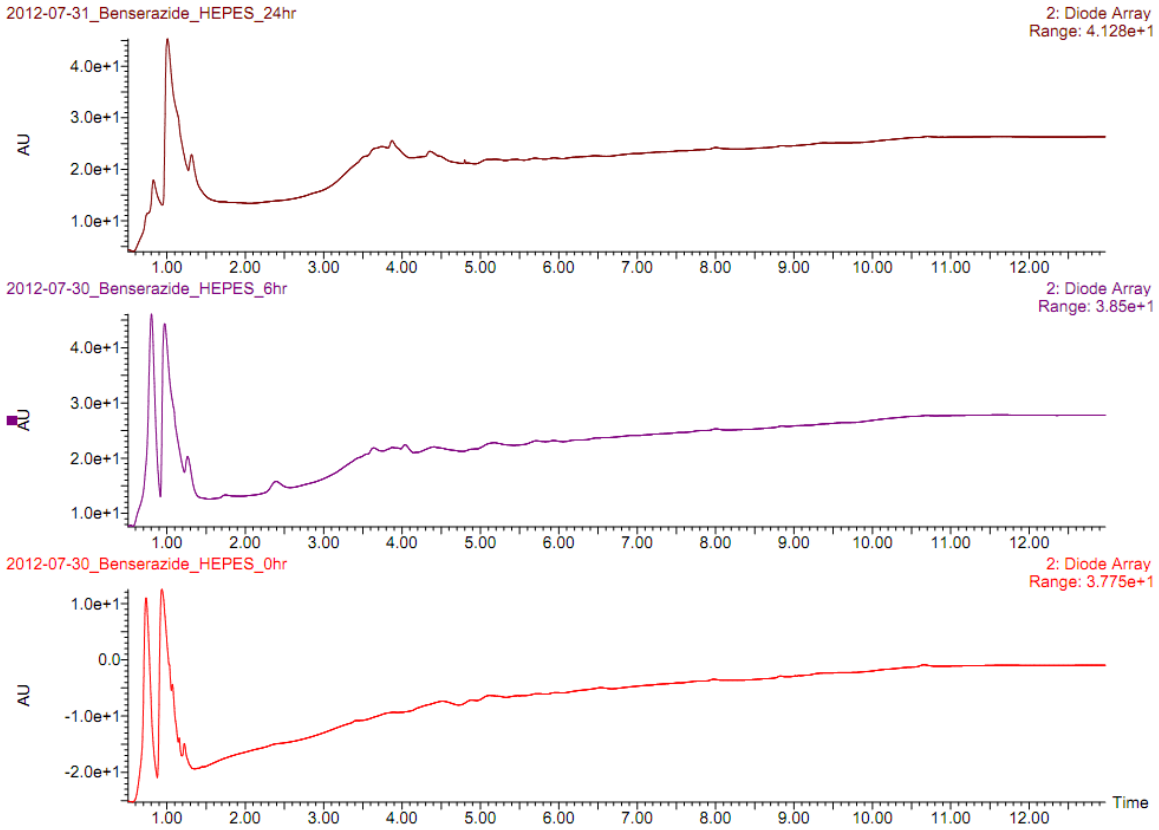

Supplemental Figure 4-10. Benserazide degrades over time in HEPES buffer. Liquid chromatography traces after both 0, 6, and 24 hour incubation periods, a number of peaks appear, corresponding to random breakdown products.

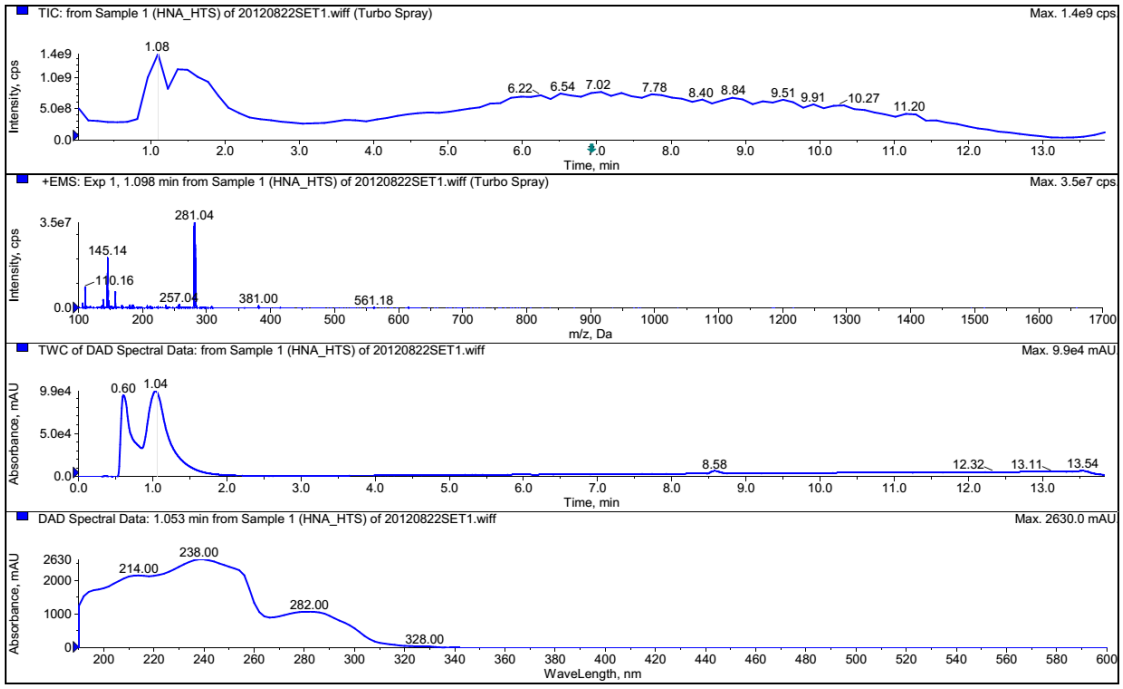

Supplemental Figure 4-11. HNA from HTS stock. HNA predicted m/z 281.34

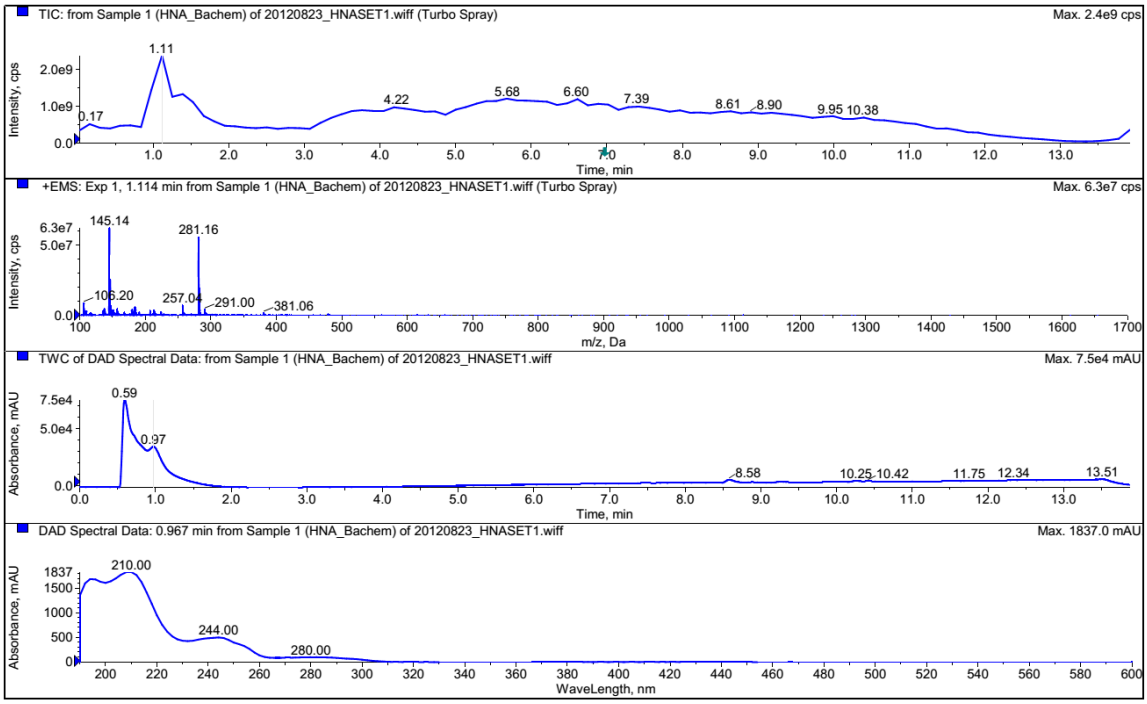

Supplemental Figure 4-12. HNA from commercial source. HNA predicted m/z 281.34

CHAPTER 5

AMA OVERCOMES ANTIBIOTIC RESISTANCE BY NDM AND VIM METALLO-ß-LACTAMASES

CHAPTER 5 PREFACE

The work presented in this chapter was previously published in:

King, A.M., Reid-Yu, S.A., Wang, W., King, D.T., De Pascale, G., Strynadka, N.C., Walsh, T.R., Coombes, B.K., and Wright, G.D. (2014). Aspergillomarasmine A overcomes metallo-beta-lactamase antibiotic resistance. Nature 510, 503-506.

Copyright © Nature Publishing Group.

AMK, GDW, SAR, BKC, TRW, and NCS designed experiments, GDP and AMK designed and engineered the *E. coli* strains and screened extracts, AMK synthesized nitrocefin, AMK cloned constructs, AMK and DTK purified enzymes, AMK performed enzyme kinetics, WW and AMK fermented WAC-138 and purified AMA, WW elucidated AMA structure, AMK performed FIC experiments, DTK performed ICP-MS, SAR and BKC designed the animal studies, SAR and AMK performed animal experiments, TRW performed clinical isolate screen, AMK and GDW principally wrote the manuscript with input from all.

Acknowledgements:

We thank Dr. Michael Mulvey (Public Health Agency of Canada) and Dr. Roberto Melano (Public Health Ontario) for clinical strains. We thank Laura Rossi for her work in constructing *E. coli* BW25113*ΔbamBΔtolCΔaraDAB::pLac*($bla_{\text{NDM-1}}$)

ABSTRACT

The emergence and spread of carbapenem-resistant Gram-negative pathogens is a global public health problem. The acquisition of MBLs such as NDM-1 is a principle contributor to the emergence of carbapenem-resistant Gram-negative pathogens that threatens the use of penicillin, cephalosporin, and carbapenem antibiotics to treat infections. So far a clinical inhibitor of MBLs that could reverse resistance and re-sensitize resistant Gram-negative pathogens to carbapenems does not exist. Here we have identified a fungal natural product, aspergillomarasmine A (AMA) that is a rapid and potent inhibitor of the NDM-1 enzyme and another clinically relevant MBL, VIM-2. AMA also fully restored the activity of meropenem against Enterobacteriaceae, *Acinetobacter* spp. and *Pseudomonas* spp. possessing either VIM or NDM-type alleles. In mice infected with NDM-1-expressing *Klebsiella pneumoniae,* AMA efficiently restored meropenem activity, demonstrating that a combination of AMA and a carbapenem antibiotic has therapeutic potential to address the clinical challenge of MBL positive carbapenem-resistant Gram-negative pathogens.

INTRODUCTION

The ß-lactams (penicillins, cephalosporins, carbapenems & monobactams) are one of the most important and frequently used classes of antibiotics in medicine and are essential in the treatment of serious Gram-negative infections. Since the clinical introduction of penicillins and cephalosporins over 60 years ago, the emergence of β-lactamases, enzymes that hydrolyse the ß-lactam ring that is essential for cell-killing activity of the antibiotics, has been an ongoing clinical problem (Frère, 2011). Antibiotic resistance has intensified medicinal chemistry efforts to broaden antibacterial spectrum while shielding the core ß-lactam scaffold from ß-lactamase-catalyzed hydrolysis. The result has been multiple generations of ß-lactams with improved efficacy and tolerance to existing ß-lactamases. However, pathogenic bacteria have in turn evolved further resistance mechanisms primarily by acquiring new or modified ß-lactamases. This is typified by the emergence of ESBLs that inactivate many of the latest generation cephalosporins and penicillins (but not carbapenems) (Pitout and Laupland, 2008). Consequently, the past two decades have seen substantial increases in the utilization of carbapenems such as imipenem and meropenem. Predictably, this increase in carbapenem consumption has been accompanied by the emergence of resistant Gram-negative pathogens (Centers for Disease and Prevention, 2013; Edelstein et al., 2013). In particular, carbapenem-resistant *Enterobacteriaceae* (CRE) is a growing crisis across the globe (Patel and Bonomo, 2013) as witnessed by recent outbreaks in Chicago (Frias et al., 2014) and British Columbia (Chang, 2013).

Carbapenemases, ß-lactamases that inactivate carbapenems, can be divided into two categories based on their mechanism of ß-lactam ring hydrolysis. The first deploy an active site Serine residue that covalently attacks the ß-lactam ring e.g. KPC and OXA-48 types (Yigit et al., 2001a). The second are MBLs that use Zn^{2+} atoms to activate a nucleophilic water molecule that opens the ring e.g. VIM and NDM types (Bush, 2013b). Several inhibitors of SBL are clinically available as co-drugs where the inhibitor is formulated with a ß-lactam antibiotic in order to overcome resistance (e.g. clavulanic acid with amoxicillin, tazobactam-piperacillin, sulbactam-ampicillin and the more recent SBL inhibitor avibactam, which is in phase III clinical trials paired with various cephalosporins) (Drawz and Bonomo, 2010b). Despite ongoing efforts (Buynak, 2013; Fast and Sutton, 2013), there are no equivalent inhibitors for MBLs in the clinic for practical and technical reasons. First, until recently, MBL-derived CRE was not thought to be a major clinical problem and its rapid increase has outpaced MBL-inhibitor development. Second, the development of a single inhibitor to neutralise key clinically important MBLs (VIM and NDM) has been deemed too technically challenging, and overcoming *in vivo* toxicity associated with cross reactivity with human metallo-enzymes has been a concern. With the recent emergence of MBLs as a significant clinical threat, a potent and safe inhibitor of MBLs particularly against VIM and NDM would greatly benefit infectious disease management.

MATERIALS AND METHODS

Methods Summary

E. coli strain BW25113 was modified by deletion of the *bamB* and *tolC* genes so as to increase permeability to and reduce efflux of small molecules. This strain was then further modified by the single-copy chromosomal insertion of the bla_{NDM-1} gene under control of the *pLac* promoter. Microbial natural product extracts were screened against this strain in the presence of sublethal ¼ MIC meropenem. AMA was purified from a hit extract and its structure elucidated by NMR, mass spectrometry and polarimetry. IC_{50} values for AMA were determined using nitrocefin (for MBLs and Ser BLs) and furanacryloyl-L-phenylalanylglycylglycine (for ACE) (Holmquist et al., 1979) as reporter substrates against the following purified enzymes: MBLs IMP-7, VIM-2, and NDM-1; SBLs CTX-M-15, KPC-2, OXA-48, and TEM-1; as well as ACE from rabbit lung. IC_{50}, reversibility, Zn^{2+} restoration, and inactivation enzyme assays were performed in 50 mM HEPES pH 7.5 and measured using a SpectraMax reader (Molecular Devices). ICP-MS experiments were conducted using purified NDM-1 at 5 mg/mL and varying concentrations of AMA with subsequent dilution and transfer by nebulization into a NexION 3000 ICP mass spectrometer (Perkin Elmer). FIC values were determined using standard methods (Pillai et al., 2005). Various concentrations of AMA were tested in combination with 2 mg/L meropenem against 200+ MBL-expressing clinical isolates including *Pseudomonas spp*., *Acinetobacter spp.,* and Enterobacteriaceae. A dose of $2x10^6$ forming units (cfu) of *Klebsiella pneumoniae* N11-2218 was used for all organ bacterial load experiments and a

dose of $5x10^7$cfu for all survival experiments. For all experiments, mice were treated with compound 30 minutes post infection.

Reagents

All enzymes and chemicals of analytical grade were purchased from Sigma-Aldrich, unless otherwise stated. Proton and carbon NMR spectra were recorded on a Bruker 700 MHz spectrometer. Nitrocefin was synthesized as reported previously (Lee et al., 2005b)

DNA manipulations and plasmid construction

Plasmid DNA purification and gel extraction were performed using the PureLink Quick plasmid miniprep and PureLink Quick gel extraction kits (Invitrogen), respectively. Restriction enzymes were purchased from Fermentas. Primers for PCR DNA amplification were purchased from IDT (Coralville, Iowa). PCR was performed using Phusion High-Fidelity DNA polymerase (Thermo Scientific) using reaction conditions specified by the manufacturer. All ligation reactions were performed using T4 DNA ligase (Thermo Scientific) according to manufacturer's instructions. All β-lactamase overexpression constructs were generated without the leader peptide in a pET-28b plasmid containing a N-terminal His Tag. Leader peptide sequences were determined using SignalP 4.0 (Petersen et al., 2011) All vectors were transformed in *E. coli* TOP10 chemically competent cells.

Protein purification

VIM-2, IMP-7, CTX-M-15, TEM-1, and OXA-48: An *E. coli* BL21(DE3) colony transformed with its respective β-lactamase construct was inoculated into LB medium

containing 50 µg/mL kanamycin and grown at 37°C. Protein expression was induced with 1 mM IPTG at OD_{600} 0.7 and cultures were incubated overnight at 16°C. Cells were harvested by centrifugation and cell paste from 1 L of culture expressing β-lactamase was washed with 8 mL 0.85 % NaCl, resuspended in buffer containing 20 mM HEPES pH 7.5, 500 mM NaCl, 20 mM imidazole and 20 µM $ZnSO_4$ (for metalloenzymes) then lysed by sonication. Lysate was centrifuged using a Beckman JA 25.50 rotor at 20 000 RPM (48 254 x g) for 45 min at 4°C. The supernatant was applied to a 5-mL HiTrap Ni-NTA column (GE Lifesciences) at a constant flow rate of 3 mL/min. The column was washed with 5 column volumes of the same buffer and step gradients of increasing imidazole were used for wash and elution steps. Fractions containing purified β-lactamase, based on SDS-PAGE, were pooled and dialyzed overnight at 4°C in buffer containing 20 mM HEPES pH 7.5, 150 mM NaCl, 20% glycerol and 20 µM $ZnSO_4$ for metalloenzymes. NDM-1 was purified as above with the addition of 84 µg SUMO protease. Protease and uncleaved NDM-1 were removed by applying dialyzed solution to a 5-mL HiTrap Ni-NTA column and collecting the flow through fractions. All purified enzymes were verified to be >95% pure as assessed by SDS-PAGE and stored at -20°C.

Cell-based screen

~500 natural product extracts were screened against *E. coli* BW25113*ΔbamBΔtolCΔaraDAB::pLac*(bla_{NDM-1}) in combination with 0.125 µg/mL meropenem. Screen was conducted in 96-well plates in duplicate using cation-adjusted Mueller-Hinton broth (CAMHB). Low growth control was 2X MIC meropenem (1 µg/mL)

and growth control was ¼ MIC meropenem (0.125 µg/mL). Z' was determined to be 0.77, indicating an excellent screening window (Zhang et al., 1999).

Purification of AMA

WAC-138 (*Aspergillus versicolor*) (4L) was evaporated under reduced pressure with 2% (W/V) HP-20 resin (Diaion) to give a residue, WAC138-E. The crude mixture was applied on a HP-20 (100g) column eluting with H_2O (1L), 10% MeOH (1L), 25% MeOH (1L), 60% MeOH (1L), and 100% MeOH (1L) to yield five fractions, WAC138-E-1~5. The active fraction WAC138-E-1 was applied to reverse-phase CombiFlash ISCO (RediSep Rf C18, Teledyne) and eluted with a Water-Acetonitrile linear gradient system (0-100% Acetonitrile) to give 65 fractions WAC138-E-1-1~65. The active subfractions WAC138-E-1-5 were passed through a Sephadex LH-20 column (100 ml), eluting with 25% MeOH, to yield 12 subfractions. The active subfractions WAC138-E-1-5-6~8 were combined and recrystallized in 5 ml 1% acetic acid (V/V) to give AMA as white crystals. 1 L of culture yielded ~ 200 mg AMA. $\alpha_D^{20} = -48.9^\circ$ (previously reported value = -48°)[15]. Predicted *m/z* = 308.1094. Exact *m/z* = 308.1094. Optical rotations were determined on a Perkin-Elmer 241 polarimeter. Mass spectrometry experiments were conducted using a Bruker Maxis 4G Q/TOF, ESI MS Direct infusion (3 µL/min) in positive ion mode.

IC_{50} enzyme inhibition assays

Enzyme (NDM-1, 5 nM; VIM-2, 500 pM; CTX-M-15, 500 pM; KPC-2, 5 nM; OXA-48, 1 nM; TEM-1, 100 pM; ACE, 50 nM) was mixed with 30 µM nitrocefin (100 µM nitrocefin for TEM-1; 250 µM furanacryloyl-L-phenylalanylglycylglycine [FAPGG]

for ACE[24]) after a 5-10 minute preincubation with AMA and linear portions of curves were used to analyze data. Metallo-β-lactamases were supplemented with 10 μM $ZnSO_4$. Assays were read in 96-well microplate format at 490 nm using a Spectramax reader (Molecular Devices) at 30-37°C.

Incubation of AMA with metalloenzymes

For Supplemental Table 5-2, Enzyme (500 nM) was incubated with AMA (500 μM) for 10 minutes. 20 μL of the above was diluted with 180 μL nitrocefin or FAPGG substrate for the following final concentrations: Enzyme (50 nM), FAPGG (50 μM)/nitrocefin (20 μM), AMA (50 μM). Buffer (50 mM HEPES pH 7.5, 300 mM NaCl) was stirred overnight with 2 g/100 mL Chelex-100 (Biorad; Richmond, CA). Assays were read in 96-well microplate format at 490 nm using a Spectramax reader (Molecular Devices) at 37°C.

Reversibility assays

5 mL NDM-1 (500 nM) was incubated either with AMA (100 μM) or without on ice for 1 hour. No enzyme control was buffer alone (Chelex-treated 50 mM HEPES pH 7.5). 2.5 mL was passed through a PD-10 spin column (GE healthcare) following column equilibration with buffer and centrifuged at 2,000xg for 2 minutes. Pre-PD-10 (+ AMA, - AMA, - NDM-1), Post-PD-10 ((+ AMA, - AMA, - NDM-1), and nitrocefin were equilibrated to 30°C. 20 μL of the enzyme solution was added to 180 μL nitrocefin for final enzyme concentration of 50 nM, and nitrocefin of 100 μM and AMA of 10μM. Assays were read in 96-well microplate format at 490 nm using a Spectramax reader (Molecular Devices) for 1 hr at 30°C.

Zn^{2+} restoration assays

NDM-1 (5 nM) supplemented with 10 μM $ZnSO_4$ was incubated with 20 μM AMA for 15 minutes at 30°C. Nitrocefin (30 μM) and $ZnSO_4$ from 500 nM-40 μM were added to a final volume of 100 μL and absorbance at 490 nm was monitored using a Spectramax reader (Molecular Devices) for 30 minutes at 30°C. Percent residual activity was calculated from no AMA control. Slightly negative percent residual activity was reported as 0.

Inactivation kinetics

NDM-1 (50 nM) was added to 20 μM nitrocefin containing AMA in serial ½ dilutions from 8 μM. Assay was performed in 50 mM HEPES pH 7.5, 200 μL final volume. Assay was read in 96-well microplate format at 490 nm using a Spectramax reader (Molecular Devices) for 10 minutes at 37°C. VIM-2 (10 nM) was added to 20 μM nitrocefin containing AMA in serial ½ dilutions from 16 μM. Assay was performed in 50 mM HEPES pH 7.5, 200 μL final volume. Assay was read in 96-well microplate format at 490 nm using a Spectramax reader (Molecular Devices) for 10 minutes at 37°C. For all assays experiments the offset between reaction initiation and the first read was ~ 6s.

Rate constants characterizing the inactivation of enzyme were calculated based on the dependence of the pseudo-first order rate constant, k_i, upon AMA concentration according to the following model*:*

$$E \bullet Zn^{2+} + AMA \overset{K_i}{\rightleftharpoons} E \bullet Zn^{2+} \bullet AMA \overset{k_{+2}}{\rightleftharpoons} E + Zn^{2+} \bullet AMA$$

Where E•Zn, A, E•Zn•A, and Zn•A are the active metalloenzyme, AMA, the ternary metalloenzyme-AMA complex, and AMA-metal complex, respectively. K_i represents the dissociation constant of the ternary complex and k_{+2} is the rate constant for dissociation of ternary complex into inactivated enzyme and AMA-Zn complex. Steady-state progress curves were fit to the integrated equation:

$$P = \frac{v_0}{k_i}\left(1 - e^{-k_i t}\right) \qquad (1)$$

Where v_0 is the initial rate of reporter substrate turnover and k_i is the pseudo-first-order inactivation rate constant. The individual values of K_i and k_{+2} were determined by fitting the value of k_i to equation 2 as described previously (Hernandez Valladares et al., 1997):

$$k_i = \frac{k_{+2}.[A]}{K_i(1 + [S]/K_M) + [A]} \qquad (2)$$

Where [A] is the concentration of AMA and [S] and K_M were the concentration and K_M of the reporter substrate, respectively.

ICP Mass Spectrometry

Inductively coupled mass spectrometry (ICP-MS) was used to analyze the ability of AMA to chelate Zn^{66} from purified NDM-1 (27-270). The NDM-1 protein was purified as previously described (King et al., 2012) and freshly exchanged using a 15 kDa cutoff dialysis tubing into ICP-MS buffer (20mM HEPES, 100mM NaCl, pH 7.5) overnight at

4°C in order to remove any contaminating metals. The protein was concentrated to ~5 mg/mL and varying concentrations of AMA were incubated with the protein samples in triplicate for 3 hours at room temperature with gentle shaking. The protein-AMA samples were again dialyzed overnight at 4°C into ICP-MS buffer using 12-14kDa cutoff D-tube dialyzer mini (EMD biosciences) microdialysis cassettes. The final protein was diluted to 1mg/mL in ICP-MS buffer, followed by a 1/40 dilution in an internal standard (10ug/L Sc^{45}, 1% nitric acid, Inorganic Ventures). Prior to sample analysis, the ICP MS was calibrated using a standard solution containing the metal isotopes of interest (Inorganic Ventures). The protein sample was then transferred by nebulization into a NexION 3000 ICP mass spectrometer (Perkin Elmer). Quantitative analysis was performed in triplicate for each sample with 60 sweeps per reading using the peak-hopping mode with a 50ms/AMU dwell time for each element. Instrument settings were: rf power (1600 W), integration time (35s), collision gas (Ar^{40}), RPQ voltage (25V) and sample flow rate (4 rpm). Isotope abundance was determined by integrating peak areas using the NexION software program, and the data was represented graphically using Microsoft Excel.

FIC index determination

FIC values were determined by standard methods (Pillai et al., 2005) setting up checkerboards with 8 concentrations of each meropenem and AMA in serial ½ dilutions. Experiments were done in duplicate and the mean used for calculation. The MIC for each compound was the lowest [compound] showing no growth. The FIC for each compound was calculated as the [compound in the presence of co-compound] for a well showing no growth, divided by the MIC for that compound. The FIC index is the sum of the two FICs.

Clinical isolate screening

Various concentrations of AMA were chosen in combination with 2mg/L of meropenem which is the EUCAST breakpoint for resistance (EUCAST, 2014) Synergistic properties of the two compounds were examined in a micro-titre tray using BHI as the growth medium (Oxford Science Park, England) and an inoculum of 0.5 MacFarland. All plates contained the control strains *E. coli* ATCC 25922 and *P. aeruginosa* ATCC 27853. Overall, 226 non-clonal clinical isolates (Enterobacteriaceae, P. *aeruginosa* and *Acinetobacter* spp.) were challenged containing one of the following MBLs: SPM-1 (n = 17), AIM-1 (n = 8), NDM-1 (n = 67), VIM-type (n = 114) or IMP-type (n = 20). Three *E. coli* and 5 *K. pneumoniae* carrying VIM-1 also carried the serine carbapenemase KPC; and 4 *E. coli* and one *K. pneumoniae* carrying NDM-1 also possessed the carbapenemase OXA-181. Plates were incubated at 37 ^{o}C and read after 18 hrs. A sub-set of strains (48) were repeated to examine reproducibility and showed no deviation from the original data.

Animal studies

All animals were housed in specific pathogen-free unit in the Central Animal Facility at McMaster University. All experimental protocols were approved by, and performed in accordance with the McMaster Animal Research Ethics Board. Female, 7-9 week old CD1 mice were purchased from Charles River. Animals were randomized to cages of 5 per group for each experiment. Sample sizes were chosen based on empirical data from pilot experiments and to maximize statistical power. The preparation of treatments, animal infections, and tissue processing was performed by two independent investigators to maximize blinding.

Bacterial Infections

Experiments were based on previously established murine models of infection with β-lactamase-expressing Enterobacteriaceae (Endimiani et al., 2011; Marra et al., 2012). Mice were infected intraperitoneally (ip) with a dose of $2x10^6$ colony forming units (cfu) of *Klebsiella pneumoniae* N11-2218 for all organ bacterial load experiments, or with a dose of $5x10^7$cfu for all survival experiments. For all organ bacterial load experiments, mice were euthanized 48 hours post infection, and spleen and liver were harvested. Organs were placed into 1mL sterile PBS on ice, and then homogenized (Mixer Mill 400; Retsch). Organ homogenates were then serially diluted in PBS, and plated on Brilliant Green agar (Oxoid) for cfu enumeration. For survival curves, mice were monitored for endpoint until day 4 post infection. For all experiments, mice were treated 30 minutes post infection with a specified subcutaneous dose of either PBS, meropenem, AMA inhibitor, or a combination of both antibiotic and inhibitor.

RESULTS AND DISCUSSION

Cell-based screen for inhibitors of NDM-1

We initiated a cell-based screen for inhibitors of the NDM-1 MBL using our in-house collection of DMSO-dissolved natural product extracts derived from environmental microorganisms. To increase the sensitivity of the screen to MBL inhibitor discovery we generated a test strain of *E. coli* BW25113 in which the *bamB* and *tolC* genes were independently deleted (*E. coli* BW25113*ΔbamBΔtolC*). BamB is essential to outer membrane porin assembly and disruption results in increased permeability to small

molecules(Ricci and Silhavy, 2012) and TolC is a key component of tripartite small molecule efflux systems such as AcrA-AcrB-TolC that serve to actively eliminate small molecules from the cell (Blair and Piddock, 2009). Therefore, *E. coli* BW25113*ΔbamBΔtolC* increases the sensitivity of the screen to discovery of "hits". This strain was further modified by integrating the bla_{NDM-1}ß-lactamase gene under control of the *pLac* promoter into the chromosome (*E. coli* BW25113*ΔbamBΔtolCΔaraDAB::pLac*(bla_{NDM-1})). We screened this strain in the presence of a sub-lethal concentration of meropenem (¼ of the minimum inhibitory concentration 0.125 µg/mL) in combination with ~500 natural product extracts.

The screen generated one reproducible hit from an extract of a strain of *Aspergillus versicolor* (as identified by 18S rRNA gene sequence) with excellent ability to restore meropenem antibiotic activity against the *E. coli* screening strain. The selectivity of the extract to neutralise NDM-1 activity *in vitro* was confirmed using purified enzyme and the colorimetric ß-lactamase substrate nitrocefin and with the carbapenem drug meropenem. Activity-guided purification of the active compound from the fermentation broth of *A. versicolor* and subsequent detailed chemical characterization identified the MBL inhibitor as aspergillomarasmine A (AMA; Figure 5-1a, Supplemental Table 5-1 and Supplemental Figures 5-1 to 5-5), a fungus-derived molecule that was discovered and reported in the early 1960s for its wilting and necrotic activity on plant leaves (Haenni et al., 1965). This molecule was re-evaluated in the 1980s as an inhibitor of angiotensin-converting enzyme (ACE) (Mikami and Suzuki, 1983) and in the early 1990s as a pre-clinical candidate for the inhibition of activation of human endothelin (Arai et al., 1993), a peptide that modulates

blood vessel muscle contraction. The activation of this vasoconstricting peptide requires endothelin-converting enzyme, which, like angiotensin-converting enzyme, is a metalloproteinase that shares some mechanistic similarities with MBLs. This previous work demonstrated that AMA was well-tolerated and had low toxicity in mice (LD_{50} 159.8 mg/kg, i.v. compared to EDTA at 28.5 mg/kg) and had no effect on mean atrial blood pressure (Matsuura et al., 1993a).

AMA is a potent inactivator of MBLs

AMA showed potent *in vitro* dose-dependent inhibition of NDM-1 and the related MBL VIM-2 (Figure 5-1b), with weaker activity against the IMP-7 MBL. AMA had no effect on the Serine ß-lactamases TEM-1 and CTX-M-15 as well as the Serine-carbapenemases KPC-2 and OXA-48 (Figure 5-1b and Supplemental Figure 5-6B). The fact that AMA was identified as an inhibitor of unrelated mammalian metalloproteinases in the past suggested that the compound interacts with the MBL metal centres. Inhibition of NDM-1 was shown to be irreversible after removal of AMA by gel filtration (Figure 5-1c), but enzymatic activity could be restored by addition of excess $ZnSO_4$ consistent with a metal depletion mechanism (Figure 5-1d). The inhibition of mammalian metalloenyzmes could be seen as a potential side effect however AMA was only able to reduce the activity of rabbit lung ACE by ~ 35% in concentration-response assays (Supplemental Figure 5-6a). Extended incubation of the metalloenzymes NDM-1, VIM-2, IMP-7, and ACE at high concentrations of AMA (0.5 mM) in Zn^{2+}-depleted buffer prepared as previously described (Hernandez Valladares et al., 1997) led to complete inactivation of NDM-1 and VIM-2, and ~ 70% and ~50% inhibition of activity in IMP-7 and ACE, respectively demonstrating

selectivity toward NDM and VIM MBLs (Supplemental Table 5-2). Time-dependent inactivation was shown to be saturable for NDM-1 (K_i = 11 nM, k_{+2} = 0.0062 s^{-1}) and VIM-2 (K_i = 7 nM, k_{+2} = 0.0065 s^{-1}) (Figure 5-1e), consistent with an inactivation mechanism whereby AMA removes Zn^{2+} ions similar to known *in vitro* chelators that interact with subclass B1 MBLs (Docquier et al., 2003b). This mechanism of action was confirmed by inductively coupled mass spectrometry that showed a loss of ~ 1.8 Zn equivalents in NDM-1 inactivated by AMA (Figure 5-1f).

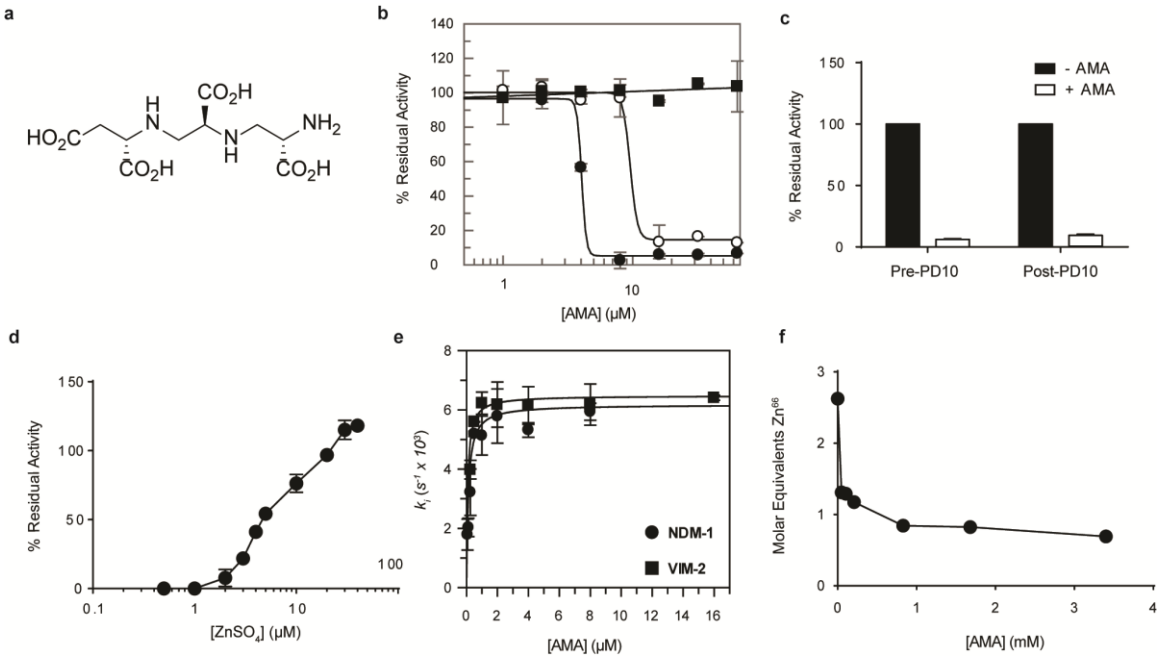

Figure 5-1. AMA inactivates MBLs. (a) Chemical structure of AMA * revised according to (Koteva et al., 2015; Liao et al., 2015). (b) AMA inhibits NDM-1 (●) (IC_{50} 4.0 ± 1.0 μM) and VIM-2 (○) (IC_{50} of 9.6 ± 2.4 μM). Activity of OXA-48 (■) was unaffected by AMA. (c) Removal of AMA via PD10 column does not restore NDM-1 activity, confirming irreversible inactivation. (d) Addition of excess $ZnSO_4$ restores activity post-inactivation. (e) The rate of inactivation of NDM-1 and VIM-2 is saturable with [AMA]. (f) ICP-MS confirms depletion of Zn from NDM-1. For all experiments error bars denote standard deviation of three technical replicates.

Systematic titration of AMA and meropenem concentrations against our engineered *E. coli* and a panel of clinical CRE strains demonstrated that AMA restored meropenem activity consistent with NDM inhibition. Checkerboard MIC studies confirmed the expected synergy between meropenem and AMA only in NDM-1 expressing CRE and not in carbapenem sensitive strains (Figure 5-2a, b). Fractional inhibitory concentration (FIC) index values were determined to be < 0.1 for a panel of 16 clinical CRE isolates tested against meropenem and AMA combinations (FIC values of ≤ 0.5 are defined as synergistic (Pillai et al., 2005)) (Supplemental Table 5-3). Potentiation of AMA (8 µg/ml) with meropenem was further investigated using 229 MBL positive (SPM-1, IMP, NDM, AIM and VIM) non-clonal clinical isolates (Enterobacteriaceae, *Acinetobacter* spp. and *Pseudomonas* spp.) (Figure 5-2c). 76 isolates were also tested that possessed serine carbapenemases, or MBLs and serine carbapenemases. Strains were amassed over a 10 year period as part of a global MBL collection including isolates from Russia, India, Pakistan, Australia, North Africa, and South America. AMA restored meropenem sensitivity (2 µg/ml) in 88% of NDM positives isolates and 90% of VIM positive isolates. Importantly, AMA was active in *Pseudomonas* spp. (mainly *P. aeruginosa*), which are viewed as a highly challenging model for new antibiotics. AMA showed very little potentiation with SPM-1, IMP and AIM but these MBLs are less numerous than the "global" VIM and NDM MBLs and therefore deemed to be less clinically relevant. The lack of potentiation with IMP-expressing strains correlates well with biochemical data showing less potent inactivation of purified IMP-7 compared to NDM-1 or VIM-2 (Supplemental Table 5-2).

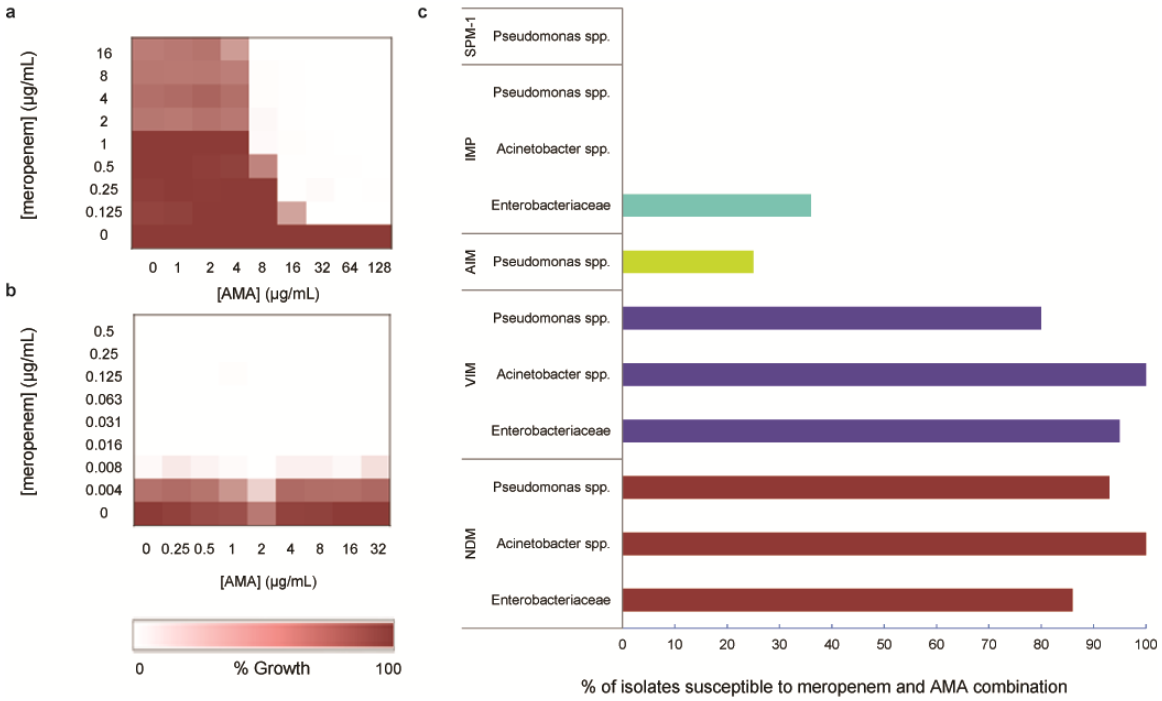

Figure 5-2. AMA potentiates the activity of meropenem against CRGNP. (a, b) Microdilution checkerboard analysis showing the combined effect of AMA and meropenem selectively against CRE (a, *K. pneumoniae* N11-2218 MIC meropenem = 32 µg/ml) but not a carbapenem sensitive strain (b, *E. coli* BW25113 MIC = 0.008-0.016 µg/ml). Heat plots shows the average of two technical replicates. (c) VIM- and NDM-expressing Gram negative pathogens were highly susceptible to meropenem/AMA combination (respectively 2µg/ml and 8 µg/ml) while AIM-, IMP-, and SPM-1-expressing isolates remained resistant.

AMA reverses carbapenem resistance *in vivo*

The resistance profile of NDM-1-positive clinical CRE and the efficacy with which AMA potentiated meropenem activity against NDM-1-positive clinical CRE suggested that AMA would reverse NDM-1-mediated resistance to meropenem *in vivo* and restore clinical efficacy of this antibiotic. To test this, CD1 mice were infected intraperitoneally with a lethal dose of NDM-1-positive *K. pneumoniae* N11-2218 to initiate a lethal systemic infection and the effects of meropenem or AMA monotherapy or antibiotic-inhibitor combination therapy was evaluated. Preliminary dosing experiments determined empirically that the bacterial load of NDM-1-positive *K. pneumoniae* in tissues was unaffected by treatment with AMA alone, and that this strain was resistant to meropenem monotherapy at doses below 50 mg/kg, leading to lethal infection (Supplemental Figure 5-7). However, combination therapy with AMA and meropenem significantly reduced the bacterial load in the spleen (Figure 5-3a) and to a lesser extent in the liver (Figure 5-3b) after a single intraperitoneal dose. Remarkably, while meropenem or AMA alone were unable to prevent lethal infection by NDM-1-positive *K. pneumoniae,* a single dose of combination therapy led to >95% survival at 5 days following infection (Figure 5-3c).

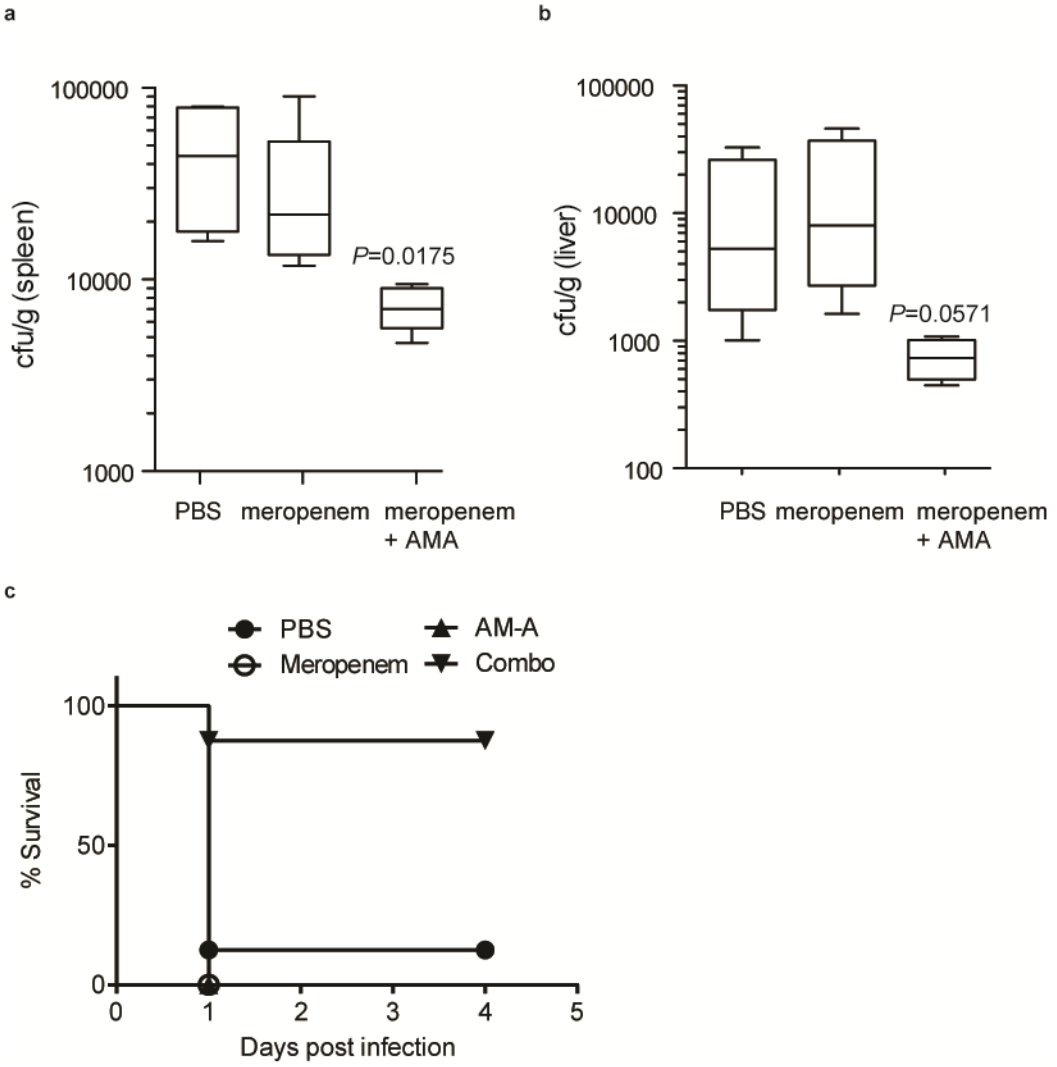

Figure 5-3. AMA rescues meropenem activity in vivo. CD-1 mice were given a sub-lethal dose of *K. pneumoniae* N11-2218 (meropenem MIC 32 µg/mL) by i.p. injection. (a, b) Groups of mice were treated with a single dose of meropenem (10 mg/kg), a combination of meropenem (10 mg/kg) + AMA (10 mg/kg), or PBS by s.c. injection. Bacterial load in the spleen (a) and liver (b) was determined by selective plating. Data are the means with standard error from two separate experiments (n=7 per group). (c) For survival experiments, CD-1 mice were given a lethal dose of *K. pneumoniae* N11-2218, and treated with a single dose of meropenem (10 mg/kg), a combination of meropenem (10 mg/kg) + AMA (30 mg/kg), AMA alone (30mg/kg), or PBS by s.c. injection. Data are the means with standard error from four separate experiments (n=12 per group, except AMA only treatment where n=13). Groups were analyzed using a non-parametric Mann-Whitney U-test. *P*-values <0.05 were considered statistically significant.

AMA presents a non-toxic candidate for an antibiotic adjuvant that can overcome resistance mediated by NDM and VIM MBLs and re-sensitize carbapenem-resistant Gram-negative pathogens to carbapenems. Active drug/inhibitor combinations continue to be highly successful in the clinic with inhibitors targeted to Ser-ß-lactamases (Shlaes, 2013). AMA presents for the first time, *in vitro* and *in vivo*, complementary activity against key MBLs that have become rapidly global and result in significant human morbidity particularly in developing countries. In combination with a ß-lactam antibiotic such as meropenem as we show here, resistance can be overcome and antibiotic activity fully restored. AMA, or semi-synthetic derivatives, is therefore an excellent lead for an antibiotic adjuvant co-therapy to address the recent emergence of MBLs in the clinic.

SUPPLEMENTAL INFORMATION

Supplemental Tables

Supplemental Table 5-1. ^{1}H and ^{13}C NMR Data of Aspergillomarasmine in D_2O

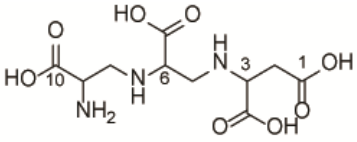

No.	δ_H	δ_C	No.	δ_H	δ_C
1		176.6	8	3.19 (dd, *J* = 13.5, 5.7 Hz) 2.80 (dd, *J* = 13.5, 4.1 Hz)	46.4
2	2.73 (dd, *J* = 17.9, 3.6 Hz) 2.61 (dd, *J* = 17.9, 9.1 Hz)	35.0	9	3.74 (dd, *J* = 5.7, 4.1 Hz)	53.8
3	3.75 (dd, *J* = 9.1, 3.6 Hz)	58.7	10		176.2
5	3.21 (dd, *J* = 12.8, 4.5 Hz) 3.06 (dd, *J* = 12.8, 9.5 Hz)	47.2	3-COOH		172.5
6	3.35 (dd, *J* = 9.5, 4.5 Hz)	59.0	6-COOH		172.4

Supplemental Table 5-2. Percent Residual Activity following metalloenzyme incubation with AMA. Initial rates of reporter substrate hydrolysis following incubation of enzyme with AMA over time. % residual activity values are calculated by using a no inhibitor and no enzyme sample as high and low controls, respectively. Error values are the standard deviations of 3 technical replicates

Enzyme	% Residual Activity (0 min)	% Residual Activity (60 min)
NDM-1	84.3 ± 5.5	0.3 ± 0.2
VIM-2	59.3 ± 3.6	1.0 ± 0.2
IMP-7	87.4 ± 5.1	35.6 ± 2.0
ACE	53.1 ± 8.4	46.9 ± 8.9

Supplemental Table 5-3. FIC indices against select clinical isolates of CRE. Values are from single assay according to CLSI protocols.

Strain	FIC index
M. morganii N10-3295	0.09
K. pneumoniae N11-0306	0.08
K. pneumoniae N11-0459	0.07
K. pneumoniae N11-2218	0.07
K. pneumoniae GN529	0.05
P. rettgeri GN570	0.06
E. cloacae GN574	0.06
M. morganii GN575	0.06
P. stuartii GN576	0.09
E. cloacae GN579	0.09
E. coli GN610	0.08
K. pneumoniae GN629	0.08
E. cloacae GN687	0.06
E. coli GN688	0.06
K. oxytoca GN942	0.05
C. freundii GN978	0.09

Supplemental Figures

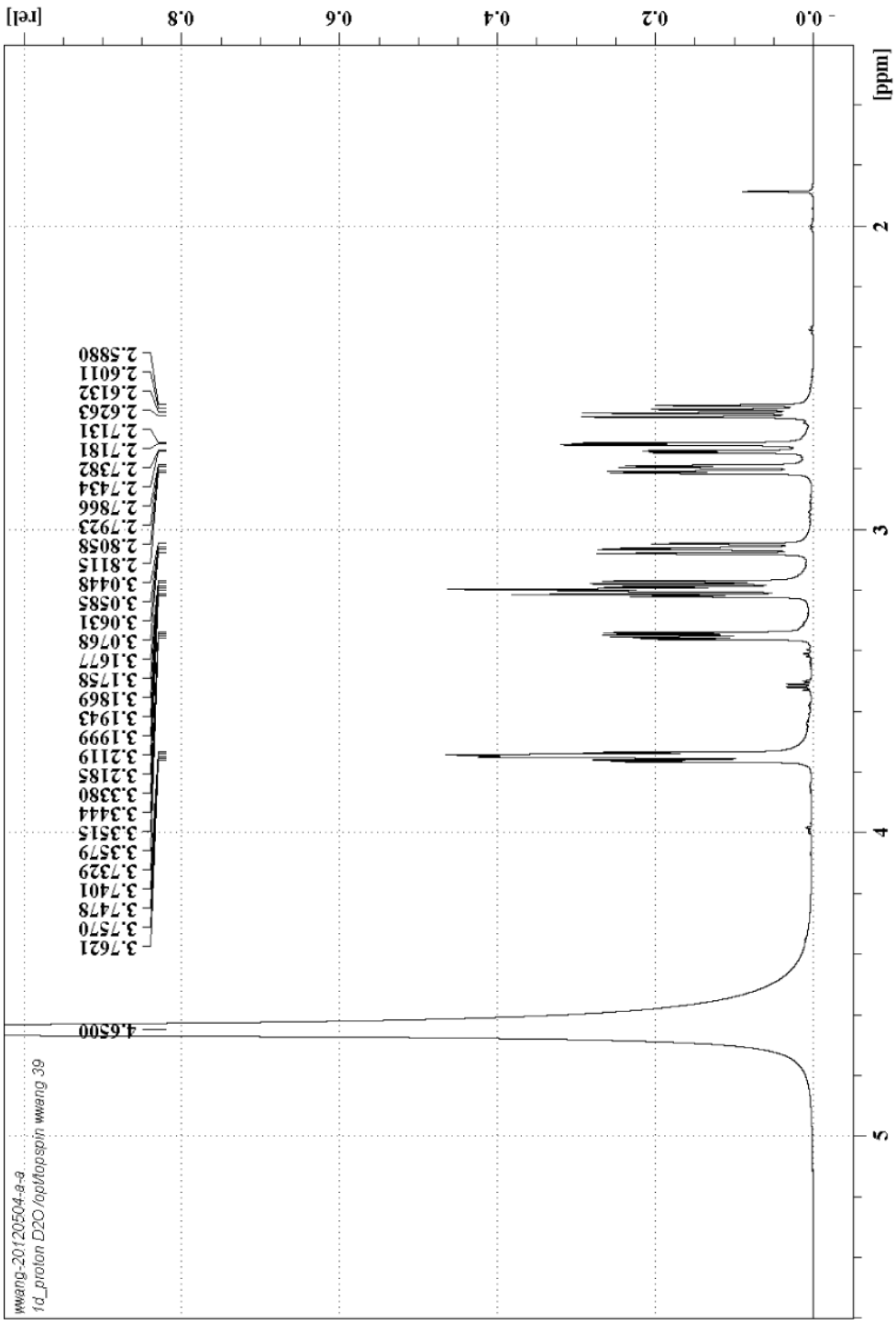

Supplemental Figure 5-1. ^{1}H NMR spectrum of AMA in D_2O

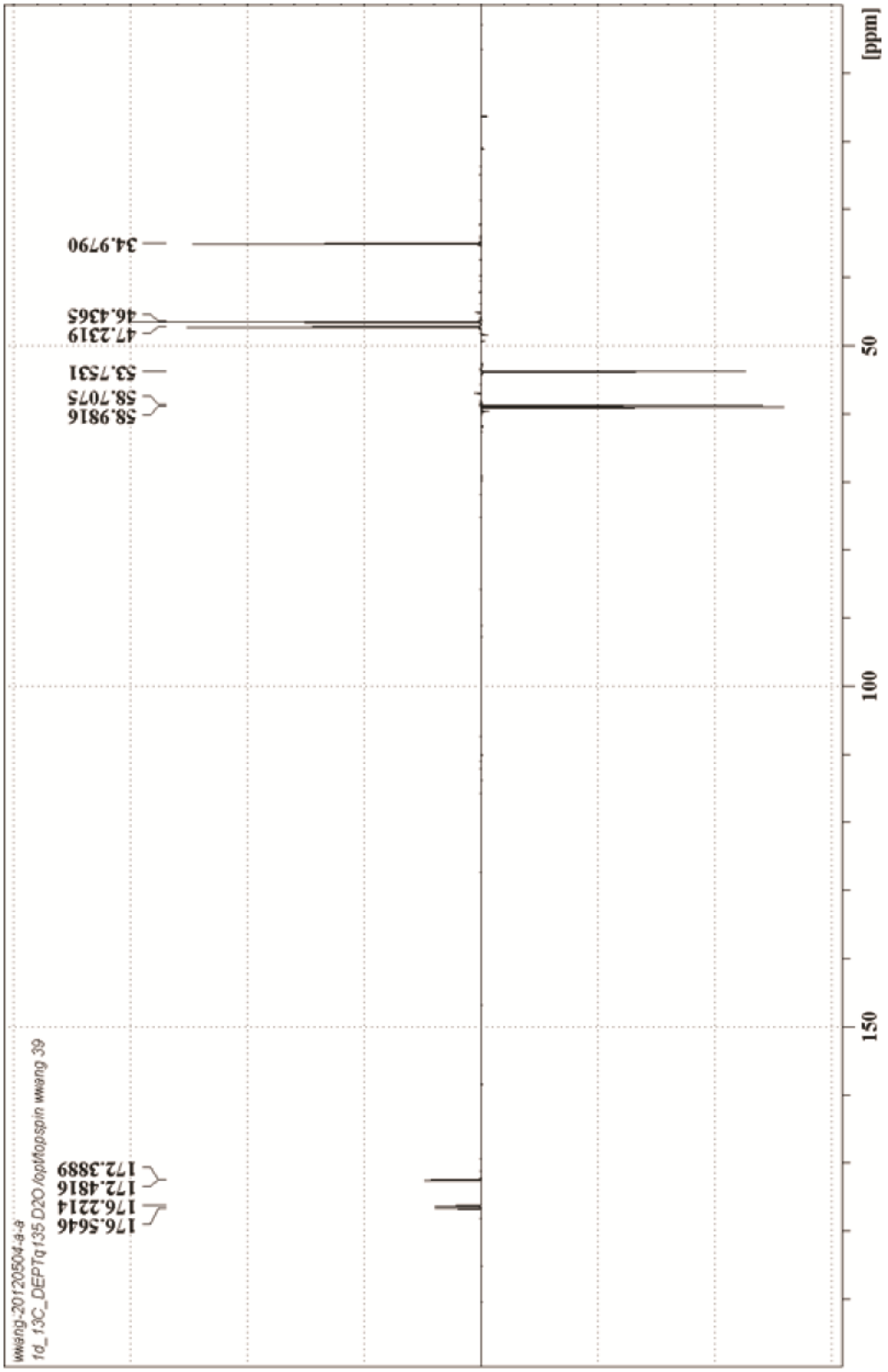

Supplemental Data Figure 5-2. ^{13}C NMR spectrum of AMA in D_2O

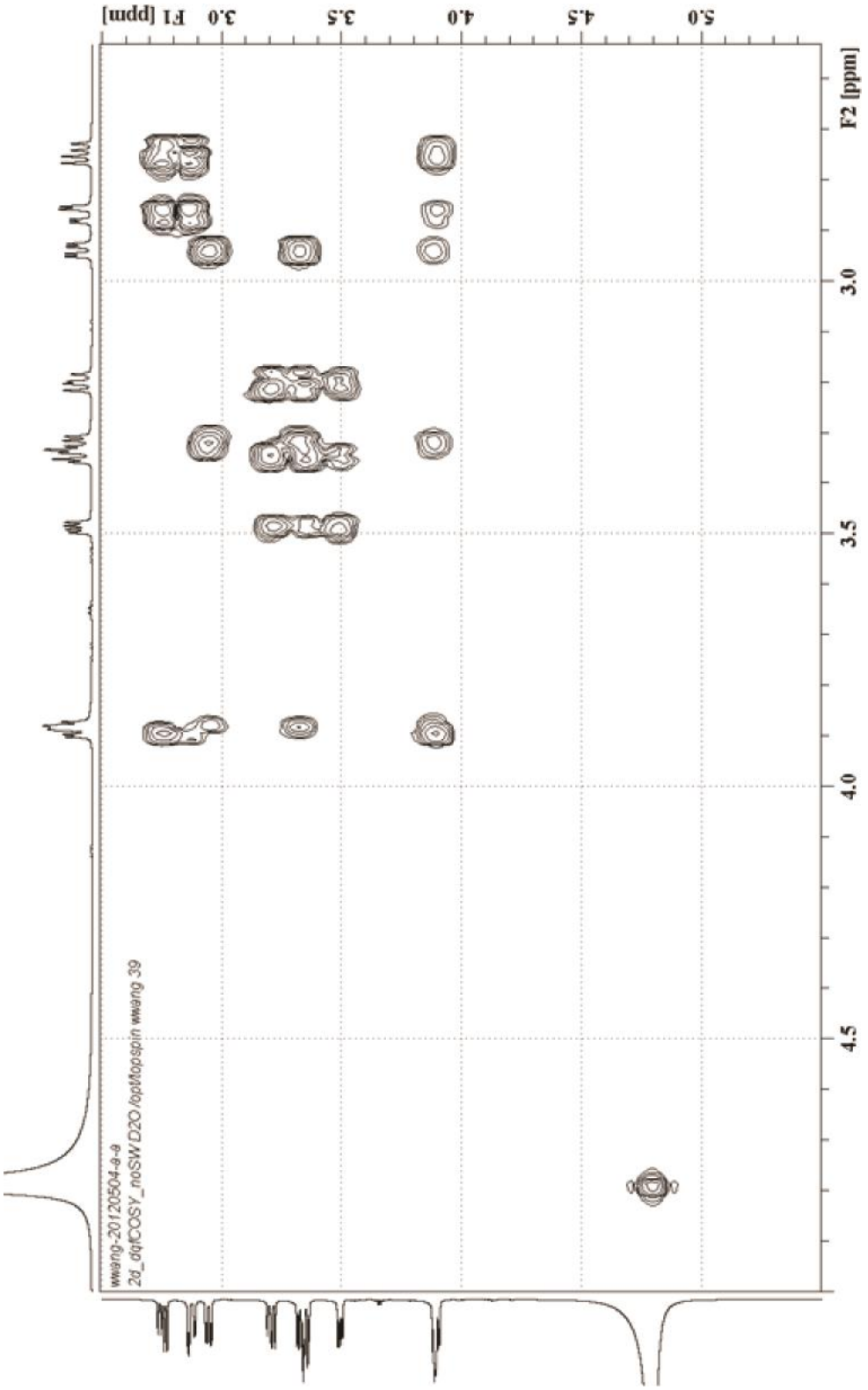

Supplemental Data Figure 5-3. ^{1}H-^{1}H COSY NMR spectrum of AMA in D_2O

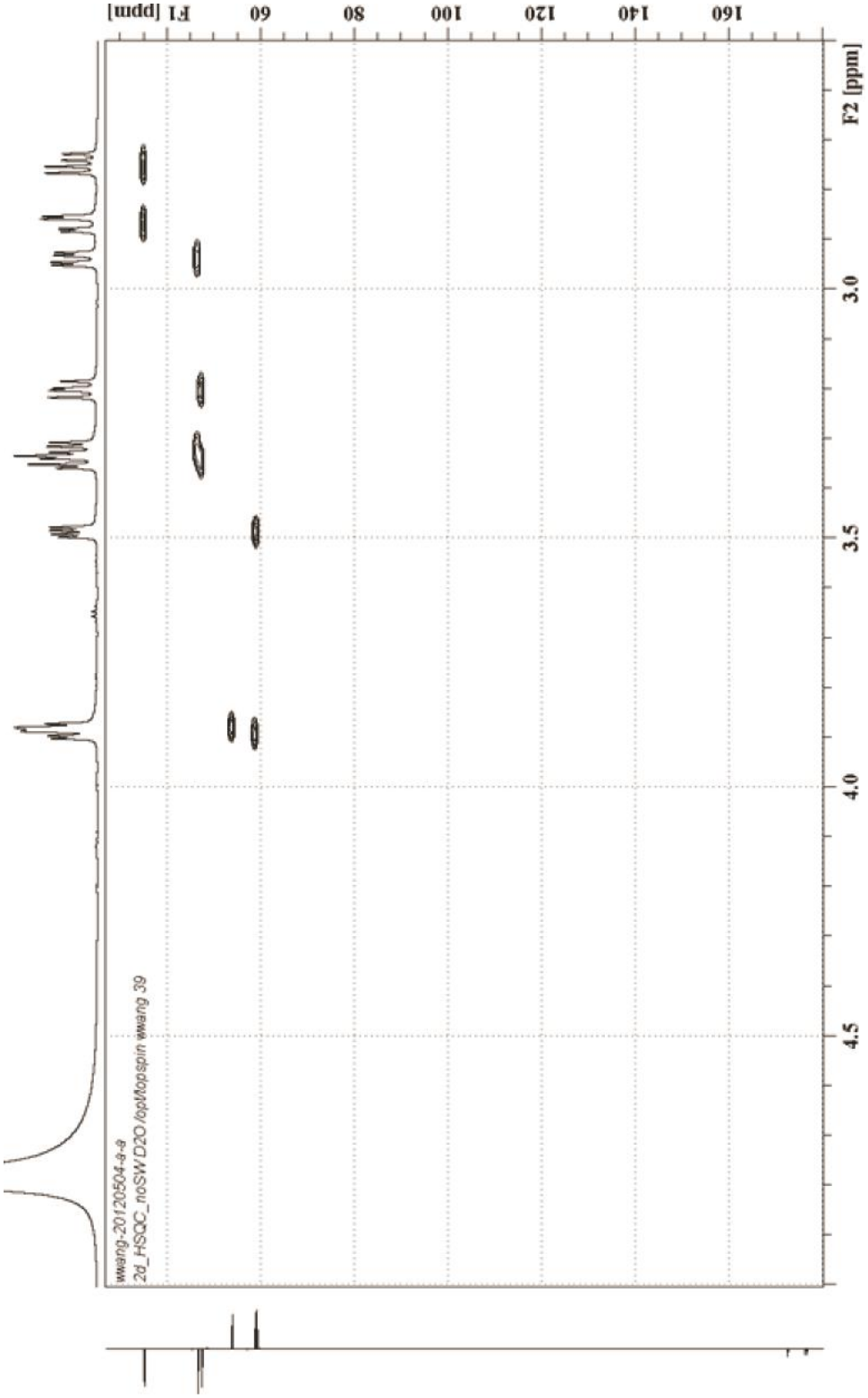

Supplemental Data Figure 5-4. ^{1}H-^{13}C HSQC NMR spectrum of AMA in D_2O

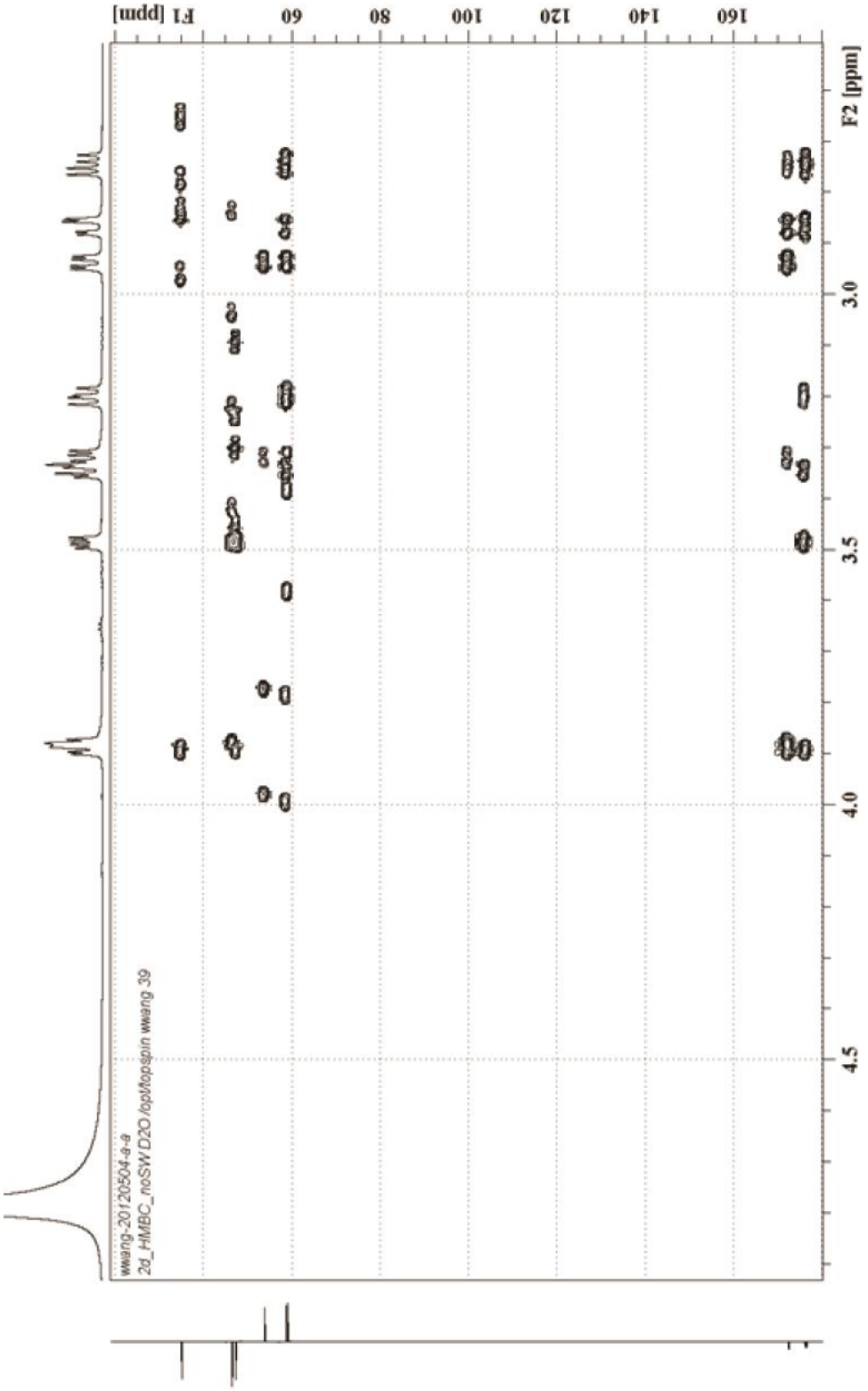

Supplemental Data Figure 5-5. ^{1}H-^{13}C HMBC NMR spectrum of AMA in D_2O

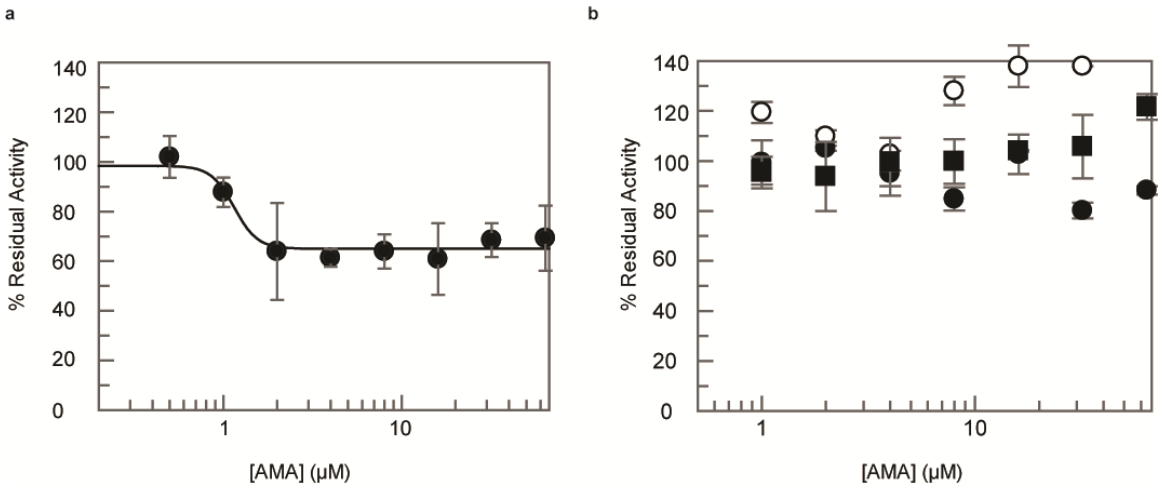

Supplemental Data Figure 5-6. IC50 inhibition profiles for select SBLs and ACE. Experiments were done as in Figure 5-1b for (a) ACE and (b) CTX-M-15 (●), KPC-2 (○), and TEM-1 (■). Error bars denote standard deviation of at least two replicates.

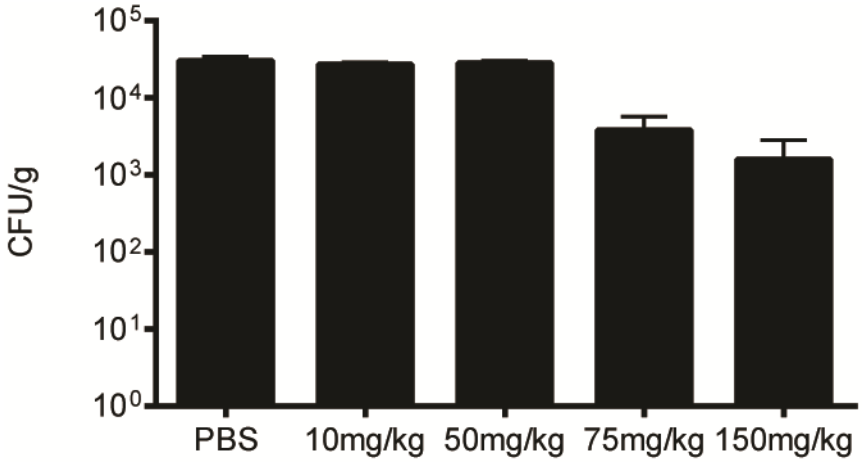

Supplemental Data Figure 5-7. Effects of meropenem dosage on spleen burden. CD-1 mice were infected with *K. pneumoniae* N11-2218 by i.p. injection. Mice were treated with either PBS (n=6), or various doses of meropenem (n=3 per group) by s.c. injection. Mice were euthanized 48 h after infection, and the bacterial load in the spleen was determined by selective plating. Data are the means with standard error.

CHAPTER 6

DISCUSSION AND FUTURE DIRECTIONS

DISCUSSION

Despite impressive strides in the past decade, there is still an outstanding clinical need for novel BLIs (Bush, 2015a). Thanks to global surveillance systems (i.e. SENTRY) (Sader et al., 2014), those studying β-lactamases are able to track the molecular epidemiology of frequently isolated enzymes and also discover new variants with concerning properties, well exemplified by the discovery and retrospective analysis of NDM-1-positive isolates (Castanheira et al., 2011; Kumarasamy et al., 2010). This is important in dictating which β-lactamases warrant the most attention in inhibitor development, however the discovery of new inhibitor scaffolds remains a daunting task. The two most promising 'new' scaffolds for inhibitors of SBLs, the DBOs and boronic acid-based inhibitors, have actually been in varying stages of development for quite some time; DBOs were investigated in the 1990s as potential PBP inhibitors (but they were better BLIs, in fact) (Coleman, 2011) and boronic acid was reported to inhibit SBLs as early as the late 1970s (Kiener and Waley, 1978). Notwithstanding the discovery of AMA and the recent report of a boronic acid BLI with activity against SBLs and MBLs (Hecker, 2015), pan-MBL inhibitors remain elusive. Here, we have provided evidence to support the notion that BLI scaffold discovery via HTS relies on two main considerations: 1) the choice of chemical space together with biological context interrogated and 2) understanding mechanism of target inhibition in the context of cellular activity.

Chemical space, biological context, and library generation

The choice of chemical space from which one screens a target or selection of targets is restricted by whatever library is accessible. Most compounds active against bacteria were discovered using the Waksman platform – systematic growth and screening of soil bacteria for bioactive compounds (Lewis, 2012). This was a successful pharmaceutical drug discovery platform but due to factors like the dereplication problem (grappling with the frequent rediscovery of known compounds) and new technologies enabling high-throughput synthesis of chemical libraries, the industry shifted their source of chemical space from which to screen. Instead, they began to rely on large libraries of synthetic molecules and screening purified enzyme targets proposed to be essential (Brown and Wright, 2016). Furthermore, these libraries eventually began to be crafted according to Lipinski's Rule of 5, a computational rule set that factored in molecular mass and lipophilicity, amongst other variables, to improve pharmacokinetic properties in screening libraries (Lipinski et al., 2001). Retrospective analyses from both GlaxoSmithKline (Payne et al., 2007) and AstraZeneca (Tommasi et al., 2015) have commented on the different chemical space that bacterial-active molecules occupy. It should be noted that these reviews were considering HTS campaigns directed at essential enzyme targets for the development of antibiotics. While we have not been screening for antibiotics, per se, the same set of rules should apply in BLI identification as we are looking for enzyme targets in the context of whole cells. Since our work has focused almost exclusively on targeting Gram-negative pathogens, it's also important to note the trends in physicochemical properties that distinguish Gram-negative-active compounds. When compared with a set

of commercially available "comprehensive medicinal chemistry" set, it was found that antibacterials occupy significantly different regions of chemical space in terms of molecular weight, lipophilicity, and polar surface area (O'Shea and Moser, 2008). Natural products tend to cover this space beyond the Rule of 5 much better than combinatorial chemistry libraries (Dobson, 2004; Harvey et al., 2015). The simple answer to the question why natural products occupy a more bioactive region of chemical space could be that they're products of evolution that are synthesized on chiral catalysts. The myriad factors that contribute to this "privileged" chemical space are far from well understood but in the context of Gram-negative bacteria, permeation undoubtedly plays a large role (Tommasi et al., 2015).

Here, we screened ~ 30 000 small molecules against a purified, recombinant target (NDM-1) in very similar fashion to the GlaxoSmithKline and AstraZeneca screens mentioned above. The few hits that were prioritized for follow-up study were found to have either artefactual or chemically intractable activity (Chapter 4). Copeland has suggested a workflow for profiling hits from HTS and this workflow should be adhered to if possible (Figure 6-1) (Copeland, 2005). A common and serious mistake is to assume classical reversible inhibition before properly interrogating the nature of inhibition. Testing for reversibility is best done by a simple jump-dilution analysis and much information can be gleaned from a single experiment (Copeland et al., 2011). Another important consideration is the presence of PAINS (**P**an **A**ssay **IN**terference compound**S)** (Baell and Holloway, 2010). Some of these molecules can be triaged by inspection but there also now exists software and databases to filter out these frequent hit compounds that are

nonspecifically reactive. In this case, both benserazide and dantrolene were found to be noncovalent inhibitors with non-ideal and nonspecific mechanisms of action. Significant time and effort could have been saved by proper mechanistic investigation from the beginning of follow-ups. These molecules also had no cell-based efficacy in the inhibition of their target, however, it's interesting to note that the other hit, HNA, was cytotoxic before it reached any level of cell-based enzyme inhibition. Given that the target resides in the periplasm, this is strong evidence that the molecule could penetrate cells but was simply a poor inhibitor.

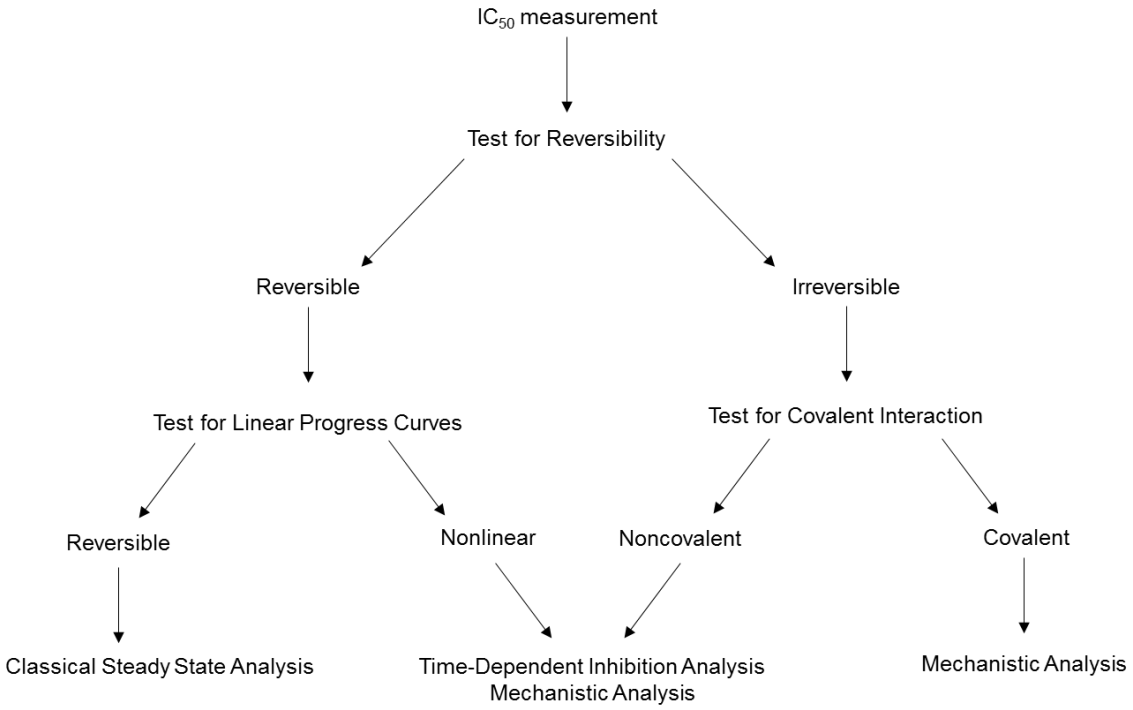

Figure 6-1. A workflow for HTS compound characterization. Adapted from (Copeland et al., 2006)

In contrast, ~500 natural product extracts were screened in a cell-based assay and a promising hit extract yielded a candidate lead with strong bioactivity and good specificity (Chapter 5). It's interesting to note that this particular hit was found in the culture supernatant, or spent media, extract. Here one would expect to find compounds with high polar surface area and hydrophilicity, exactly the type of compound that is expected to have favorable bioactivity against Gram-negative pathogens (Tommasi et al., 2015). This begs the question: how does one generate a natural product library that will enrich for these sorts of molecules? Natural product library preparation is a massive undertaking and has, out of pragmatism, historically favored the fractionation of moderately hydrophobic compounds (i.e. those that elute from a C18 stationary phase within a percentage range of mobile phase (acetonitrile or comparable solvent)). This has the advantage of eliminating highly water-soluble and greasy fractions, which have the propensity to interfere with assays and display nonspecific inhibition (Wagenaar, 2008). It's apparent that there are significant advantages to pre-fractionation of natural product extracts but there is no all-encompassing strategy to maximize bioactivity whilst minimizing cost (Harvey et al., 2015). It may be that labs invested in natural product research have to take stock of their goals and fractionate accordingly to enrich for certain areas of chemical space.

Both pharmaceutical screening campaigns mentioned above focused heavily on a genes-to-target approach, fueled by recent technological advances (Brown and Wright, 2016; Payne et al., 2007; Tommasi et al., 2015). Purified enzyme was screened against chemical libraries using reporter substrate in artificial conditions, a method that appears to have failed. Here, we have displayed the power of combining a target-based approach with

a systems-based approach by engineering the expression of a target enzyme in a cell-based context (Chapter 5). The literature currently divides target-based approaches from cell-based approaches (Eder et al., 2014) but it stands to reason that, given the rapid rate at which technology is enabling organism/cell engineering, a combination of the two is the best way forward. We anticipate that this platform will enable the discovery of resistance enzyme inhibitors active in the context of whole cells. The outstanding question remains the best library from which to screen, however.

Understanding target mechanism

From the above discussion, it's clear that an understanding of mechanism is crucial to progress from a hit molecule to lead in HTS workflows. This dissertation has detailed a significant amount of work on understanding the mechanism of inhibition for a previously discovered compound, avibactam, and SAR for some derivatives. There is now recognition that drug-target residence time can be a powerful predictor of *in vivo* efficacy for a drug (Copeland, 2016). This model prioritizes compounds that display slow-binding kinetics (Morrison and Walsh, 1988) and argues that, *in vivo*, classical reversible inhibitors are limited by their physiological distribution as a result of pharmacokinetics and pharmacodynamics (PK/PD). What this means is that equilibrium measurements done *in vitro* in a closed system (IC_{50}, for example) may not correlate well with inhibitory efficacy in an open system where concentrations are in flux. The single most important kinetic parameter is the off-rate of drug-target complex, or the drug-target residence time. This model has been applied to the discovery and series optimization of competitive inhibitors

of UDP-3-O-acyl-N-acetylglucosmine deacetylase (LpxC) in *P. aeruginosa* (Walkup et al., 2015). In the case of avibactam, incomplete understanding of the mechanism led to the report of incorrect kinetic parameters, since experimental conditions were set up under the assumption that avibactam was a covalent, irreversible inhibitor (Stachyra et al., 2010). The demonstration that avibactam is in fact a covalent, reversible inhibitor changed experimental design and yielded different kinetic parameters (Ehmann et al., 2012a; Ehmann et al., 2013b). This experimental design has allowed us to quantify the on- and off-rates of acyl-enzyme formation and it is anticipated that this workflow will be an effective way to optimize SAR development of the DBO scaffold. It should be noted, however, that off-rates are not the sole kinetic parameter that must be considered. The OXA enzymes, for instance, demonstrate exceptionally slow deacylation rates but that is combined with very slow acylation rates (Ehmann et al., 2013b). This translates into mixed efficacy against the class D enzymes in cell-based experiments (Drawz et al., 2014). It will be interesting to see if SAR using these parameters as guides might lead to the discovery of effective derivatives against all classes of SBLs. Lastly, it will be important to delineate PBP binding in any series optimization via MIC/FIC experiments since DBO derivatives can display potent PBP inhibition.

The mechanism by which AMA inactivates certain MBLs remains less clear. The observation that AMA could inactivate both NDM-1 and VIM-2 in a time and concentration-dependent manner with saturation kinetics suggested reversible complex formation between enzyme and AMA (Chapter 5) (Docquier et al., 2003a; Laraki et al., 1999). However, as described in Chapter 1, the exact mechanism and zinc content in these

enzymes is still a matter of debate. As with all compounds discussed in this thesis, the goal for AMA is to understand mechanism of inhibition and use that as a basis for semisynthetic modification. Without a sound understanding of enzyme mechanism, however, it's difficult to properly assess inhibitor efficacy *in vitro* and hope to see predictive correlations *in vivo*. In this instance, selective derivatization of the molecule will hopefully lead to an understanding of what functional groups are required for AMA to inactivate its targets. With that knowledge in hand, it may be possible to prepare derivatives with higher specificity and favorable PK/PD properties. As always, these experiments will require both *in vitro* enzymology and cell-based assays to properly assess the effects of SAR.

Lastly, we feel that AMA combined with avibactam represents an excellent opportunity for investigating the efficacy of triple combinations to deal with pan-drug resistant Gram-negative pathogens. The two inhibitors combined with an appropriate β-lactam antibiotic (meropenem, aztreonam, or ceftazidime, for instance) should be able to treat any infection caused by problematic pathogens in the clinic, with the possible exception of IMP-expressing bacteria (Chapter 5). Triple combinations are a mainstay in other disease treatments (i.e. Complera for HIV) and given the clinical difficulties presented by drug-resistant organisms expressing multiple β-lactamases, it may be time to look into this as an option.

Future Directions

1. Determine the mechanism of AMA inactivation of MBLs
2. Conduct SAR studies with AMA
3. Investigate triple combinations of AMA, avibactam, and β-lactam antibiotics
4. Establish a workflow for cell-based screening of resistance determinants

Concluding remarks

Antibiotic resistance has and always will be associated with our current clinical practice of chemotherapeutic treatment of bacterial infections. History has shown, however, that nature can provide excellent new chemical scaffolds with biological activity; clever methodologies are what is required to tease out what is no longer "low-hanging fruit". We have shown through cell-based screening of natural products for inhibitors of resistance that one can discover compounds with clinical potential. However, in order to guide subsequent derivatization of lead molecules an understanding of target mechanism and biological context is essential. The longstanding paradigm of scaffold derivatization to evade resistance and increase efficacy of bioactive molecules is still valid in modern times. Furthermore, rapid advances in technology coupled with retrospective analysis of both failures and successes in targeting Gram-negative pathogens should facilitate the discovery of chemotherapeutics to counter antibiotic resistance in these organisms.

REFERENCES

Abraham, E.P. (1987). Sir Robert Robinson and the early history of penicillin. Nat Prod Rep *4*, 41-46.

Abraham, E.P., and Chain, E. (1940). An enzyme from bacteria able to destroy penicillin. Nature *146*, 837.

Abraham, E.P., Chain, E., Fletcher, C.M., Gardner, A.D., Heatley, N.G., Jennings, M.A., and Florey, H.W. (1941). FURTHER OBSERVATIONS ON PENICILLIN. The Lancet *238*, 177-189.

Abraham, E.P., and Newton, G.G. (1961). The structure of cephalesporin C. The Biochemical journal *79*, 377-393.

Adams, P.D., Afonine, P.V., Bunkóczi, G., Chen, V.B., Davis, I.W., Echols, N., Headd, J.J., Hung, L.W., Kapral, G.J., Grosse-Kunstleve, R.W., *et al.* (2010). PHENIX: a comprehensive Python-based system for macromolecular structure solution. Acta Crystallogr D Biol Crystallogr *66*, 213-221.

Alexander, J.P., and Cravatt, B.F. (2005). Mechanism of carbamate inactivation of FAAH: implications for the design of covalent inhibitors and in vivo functional probes for enzymes. Chem Biol *12*, 1179-1187.

Ambler, R.P. (1980). The structure of beta-lactamases. Philos Trans R Soc Lond B Biol Sci *289*, 321-331.

Antunes, N.T., Lamoureaux, T.L., Toth, M., Stewart, N.K., Frase, H., and Vakulenko, S.B. (2014). Class D β-lactamases: are they all carbapenemases? Antimicrob Agents Chemother *58*, 2119-2125.

Arai, K., Ashikawa, N., KNakakita, Y., Matsuura, A., Ashikawa, N., and Munekata, M. (1993). Aspergillomarasmine A and B, potent microbial inhibitors of endothelin-converting enzyme. Biosci Biotech Biochem *57*, 1944.

Aronoff, S.C., Jacobs, M.R., Johenning, S., and Yamabe, S. (1984). Comparative activities of the beta-lactamase inhibitors YTR 830, sodium clavulanate, and sulbactam combined with amoxicillin or ampicillin. Antimicrob Agents Chemother *26*, 580-582.

Badarau, A., and Page, M.I. (2006). Enzyme deactivation due to metal-ion dissociation during turnover of the cobalt-beta-lactamase catalyzed hydrolysis of beta-lactams. Biochemistry *45*, 11012-11020.

Baell, J.B., and Holloway, G.A. (2010). New substructure filters for removal of pan assay interference compounds (PAINS) from screening libraries and for their exclusion in bioassays. J Med Chem *53*, 2719-2740.

Battye, T.G., Kontogiannis, L., Johnson, O., Powell, H.R., and Leslie, A.G. (2011). iMOSFLM: a new graphical interface for diffraction-image processing with MOSFLM. Acta Crystallogr D Biol Crystallogr *67*, 271-281.

Bauernfeind, A., Grimm, H., and Schweighart, S. (1990). A new plasmidic cefotaximase in a clinical isolate of Escherichia coli. Infection *18*, 294-298.

Bebrone, C., Garau, G., Garcia-Saez, I., Chantalat, L., Carfi, A., and Dideberg, O. (2012). X-ray Structures and Mechanisms of Metallo-beta-lactamases. In Beta-lactamases, J.M. Frere, ed. (Nova Science Publishers), pp. 41-77.

Bebrone, C., Lassaux, P., Vercheval, L., Sohier, J.S., Jehaes, A., Sauvage, E., and Galleni, M. (2010). Current challenges in antimicrobial chemotherapy: focus on ß-lactamase inhibition. Drugs *70*, 651-679.

Blair, J.M., and Piddock, L.J. (2009). Structure, function and inhibition of RND efflux pumps in Gram-negative bacteria: an update. Current opinion in microbiology *12*, 512-519.

Bonnefoy, A., Dupuis-Hamelin, C., Steier, V.r., Delachaume, C., Seys, C., Stachyra, T.r.s., Fairley, M., Guitton, M.l., and Lampilas, M. (2004). In vitro activity of AVE1330A, an innovative broad-spectrum non-β-lactam β-lactamase inhibitor. Journal of Antimicrobial Chemotherapy *54*, 410-417.

Boucher, H.W., Talbot, G.H., Bradley, J.S., Edwards, J.E., Gilbert, D., Rice, L.B., Scheld, M., Spellberg, B., and Bartlett, J. (2009). Bad Bugs, No Drugs: No ESKAPE! An Update from the Infectious Diseases Society of America. Clinical Infectious Diseases *48*, 1-12.

Bradford, P.A. (2001). Extended-spectrum beta-lactamases in the 21st century: characterization, epidemiology, and detection of this important resistance threat. Clin Microbiol Rev *14*, 933-951, table of contents.

Brown, E.D., and Wright, G.D. (2016). Antibacterial drug discovery in the resistance era. Nature *529*, 336-343.

Bryskier, A. (2000). Perfecting the ring and extending the antibacterial spectrum: 'the multiple generations'. Clinical Microbiology and Infection *6*, 13-21.

Bush, K. (1988). Recent developments in beta-lactamase research and their implications for the future. Rev Infect Dis *10*, 681-690.

Bush, K. (2010). Alarming β-lactamase-mediated resistance in multidrug-resistant Enterobacteriaceae. Curr Opin Microbiol *13*, 558-564.

Bush, K. (2013a). The ABCD's of β-lactamase nomenclature. J Infect Chemother *19*, 549-559.

Bush, K. (2013b). Proliferation and significance of clinically relevant beta-lactamases. Annals of the New York Academy of Sciences *1277*, 84-90.

Bush, K. (2013c). Proliferation and significance of clinically relevant β-lactamases. Annals of the New York Academy of Sciences *1277*, 84-90.

Bush, K. (2015a). A resurgence of beta-lactamase inhibitor combinations effective against multidrug-resistant Gram-negative pathogens. Int J Antimicrob Agents *46*, 483-493.

Bush, K. (2015b). ß-Lactamase Classification and Amino Acid Sequences for TEM, SHV and OXA Extended-Spectrum and Inhibitor Resistant Enzymes.

Bush, K., and Fisher, J.F. (2011). Epidemiological Expansion, Structural Studies, and Clinical Challenges of New β-Lactamases from Gram-Negative Bacteria. Annual Review of Microbiology *65*, 455-478.

Bush, K., Macalintal, C., Rasmussen, B.A., Lee, V.J., and Yang, Y. (1993). Kinetic interactions of tazobactam with beta-lactamases from all major structural classes. Antimicrob Agents Chemother *37*, 851-858.

Buynak, J.D. (2013). beta-Lactamase inhibitors: a review of the patent literature (2010 - 2013). Expert Opin Ther Pat *23*, 1469-1481.

Canton, R., Gonzalez-Alba, J.M., and Galan, J.C. (2012). CTX-M Enzymes: Origin and Diffusion. Front Microbiol *3*, 110.

Cantón, R., Morosini, M.I., Martín, O., de la Maza, O.M., and de la Pedrosa, E.G. (2008). IRT and CMT beta-lactamases and inhibitor resistance. Clin Microbiol Infect *14 Suppl 1*, 53-62.

Castanheira, M., Deshpande, L.M., Mathai, D., Bell, J.M., Jones, R.N., and Mendes, R.E. (2011). Early dissemination of NDM-1- and OXA-181-producing Enterobacteriaceae in Indian hospitals: report from the SENTRY Antimicrobial Surveillance Program, 2006-2007. Antimicrob Agents Chemother *55*, 1274-1278.

Centers for Disease, C., and Prevention (2013). ANTIBIOTIC RESISTANCE THREATS in the United States.

Chain, E., Florey, H.W., Gardner, A.D., Heatley, N.G., Jennings, M.A., Orr-Ewing, J., and Sanders, A.G. (1940). PENICILLIN AS A CHEMOTHERAPEUTIC AGENT. The Lancet *236*, 226-228.

Chang, Y. (2013). Laboratory Trends, December 17 (Vancouver, BC: BC Public Health Microbiology & Reference Laboratory), pp. 8.

Chen, Y., Delmas, J., Sirot, J., Shoichet, B., and Bonnet, R. (2005a). Atomic resolution structures of CTX-M beta-lactamases: extended spectrum activities from increased mobility and decreased stability. J Mol Biol *348*, 349-362.

Chen, Y., McReynolds, A., and Shoichet, B.K. (2009). Re-examining the role of Lys67 in class C beta-lactamase catalysis. Protein Sci *18*, 662-669.

Chen, Y., Shoichet, B., and Bonnet, R. (2005b). Structure, function, and inhibition along the reaction coordinate of CTX-M beta-lactamases. J Am Chem Soc *127*, 5423-5434.

Cho, H., Uehara, T., and Bernhardt, T.G. (2014). Beta-lactam antibiotics induce a lethal malfunctioning of the bacterial cell wall synthesis machinery. Cell *159*, 1300-1311.

Cimermancic, P., Medema, M.H., Claesen, J., Kurita, K., Wieland Brown, L.C., Mavrommatis, K., Pati, A., Godfrey, P.A., Koehrsen, M., Clardy, J., *et al.* (2014). Insights into secondary metabolism from a global analysis of prokaryotic biosynthetic gene clusters. Cell *158*, 412-421.

Clarke, A.M., Zemcov, S.J.V., and Wright, J.M. (1985). HR 810 and BMY-28142, two new cephalosporins with broad-spectrum activity:an in-vitro comparison with other β-lactam antibiotics. Journal of Antimicrobial Chemotherapy *15*, 305-310.

CLSI (2012). Methods for Dilution: Antimicrobial Susceptibility Testing of Bacteria that Grow Aerobically (Wayne, PA: Clinical and Laboratory Standards Institute).

Coello, J., Maspoch, S., and Villegas, N. (2000). Simultaneous kinetic-spectrophotometric determination of levodopa and benserazide by bi- and three-way partial least squares calibration. Talanta *53*, 627-637.

Coleman, K. (2011). Diazabicyclooctanes (DBOs): a potent new class of non-β-lactam β-lactamase inhibitors. Curr Opin Microbiol *14*, 550-555.

Concha, N.O., Janson, C.A., Rowling, P., Pearson, S., Cheever, C.A., Clarke, B.P., Lewis, C., Galleni, M., Frere, J.M., Payne, D.J., *et al.* (2000). Crystal structure of the IMP-1 metallo beta-lactamase from Pseudomonas aeruginosa and its complex with a mercaptocarboxylate inhibitor: binding determinants of a potent, broad-spectrum inhibitor. Biochemistry *39*, 4288-4298.

Copeland, R.A. (2005). Evaluation of Enzyme Inhibitors in Drug Discovery (New Jersey: John WIley & Sons, Inc.).

Copeland, R.A. (2016). The drug-target residence time model: a 10-year retrospective. Nat Rev Drug Discov *15*, 87-95.

Copeland, R.A., Basavapathruni, A., Moyer, M., and Scott, M.P. (2011). Impact of enzyme concentration and residence time on apparent activity recovery in jump dilution analysis. Analytical biochemistry *416*, 206-210.

Copeland, R.A., Pompliano, D.L., and Meek, T.D. (2006). Drug-target residence time and its implications for lead optimization. Nat Rev Drug Discov *5*, 730-739.

Cornaglia, G., Giamarellou, H., and Rossolini, G.M. (2011). Metallo-beta-lactamases: a last frontier for beta-lactams? The Lancet Infectious diseases *11*, 381-393.

Corvec, S., Poirel, L., Decousser, J.W., Allouch, P.Y., Drugeon, H., and Nordmann, P. (2006). Emergence of carbapenem-hydrolysing metallo-beta-lactamase VIM-1 in Pseudomonas aeruginosa isolates in France. Clin Microbiol Infect *12*, 941-942.

Cosgrove, S.E., Kaye, K.S., Eliopoulous, G.M., and Carmeli, Y. (2002). Health and economic outcomes of the emergence of third-generation cephalosporin resistance in Enterobacter species. Arch Intern Med *162*, 185-190.

Crowfoot, D.B., C. W.; Rogers-Low, B. W.; Turner-Jones, A. (1949). The X-Ray Crystallographic Investigation of the Structure of Penicillin. (Princeton, NJ: Princeton University Press).

Czarny, T.L., Perri, A.L., French, S., and Brown, E.D. (2014). Discovery of novel cell wall-active compounds using P ywaC, a sensitive reporter of cell wall stress, in the model gram-positive bacterium Bacillus subtilis. Antimicrob Agents Chemother *58*, 3261-3269.

D'Costa, V.M., King, C.E., Kalan, L., Morar, M., Sung, W.W., Schwarz, C., Froese, D., Zazula, G., Calmels, F., Debruyne, R., *et al.* (2011). Antibiotic resistance is ancient. Nature *477*, 457-461.

Dalhoff, A., and Thomson, C.J. (2003). The art of fusion: from penams and cephems to penems. Chemotherapy *49*, 105-120.

Datta, N., and Kontomichalou, P. (1965). Penicillinase synthesis controlled by infectious R factors in Enterobacteriaceae. Nature *208*, 239-241.

Davies, R.B., and Abraham, E.P. (1974). Metal cofactor requirements of beta-lactamase II. The Biochemical journal *143*, 129-135.

De Luca, F., Benvenuti, M., Carboni, F., Pozzi, C., Rossolini, G.M., Mangani, S., and Docquier, J.D. (2011). Evolution to carbapenem-hydrolyzing activity in noncarbapenemase class D β-lactamase OXA-10 by rational protein design. Proc Natl Acad Sci U S A *108*, 18424-18429.

De Pascale, G., and Wright, G.D. (2010). Antibiotic Resistance by Enzyme Inactivation: From Mechanisms to Solutions. ChemBioChem *11*, 1325-1334.

Delmas, J., Chen, Y., Prati, F., Robin, F., Shoichet, B.K., and Bonnet, R. (2008). Structure and dynamics of CTX-M enzymes reveal insights into substrate accommodation by extended-spectrum beta-lactamases. J Mol Biol *375*, 192-201.

Dobson, C.M. (2004). Chemical space and biology. Nature *432*, 824-828.

Docquier, J.-D., Lamotte-Brasseur, J., Galleni, M., Amicosante, G., Frere, J.-M., and Rossolini, G.M. (2003a). On functional and structural heterogeneity of VIM-type metallo- β-lactamases. Journal of Antimicrobial Chemotherapy *51*, 257-266.

Docquier, J.D., Calderone, V., De Luca, F., Benvenuti, M., Giuliani, F., Bellucci, L., Tafi, A., Nordmann, P., Botta, M., Rossolini, G.M., *et al.* (2009). Crystal structure of the OXA-48 beta-lactamase reveals mechanistic diversity among class D carbapenemases. Chem Biol *16*, 540-547.

Docquier, J.D., Lamotte-Brasseur, J., Galleni, M., Amicosante, G., Frere, J.M., and Rossolini, G.M. (2003b). On functional and structural heterogeneity of VIM-type metallo-beta-lactamases. The Journal of antimicrobial chemotherapy *51*, 257-266.

Drawz, S., and Bonomo, R. (2010a). Three decades of beta-lactamase inhibitors. Clinical microbiology reviews *23*, 160-201.

Drawz, S.M., and Bonomo, R.A. (2010b). Three decades of beta-lactamase inhibitors. Clinical microbiology reviews *23*, 160-201.

Drawz, S.M., Papp-Wallace, K.M., and Bonomo, R.A. (2014). New beta-lactamase inhibitors: a therapeutic renaissance in an MDR world. Antimicrob Agents Chemother *58*, 1835-1846.

Edelstein, M.V., Skleenova, E.N., Shevchenko, O.V., D'Souza J, W., Tapalski, D.V., Azizov, I.S., Sukhorukova, M.V., Pavlukov, R.A., Kozlov, R.S., Toleman, M.A., *et al.* (2013). Spread of extensively resistant VIM-2-positive ST235 Pseudomonas aeruginosa in Belarus, Kazakhstan, and Russia: a longitudinal epidemiological and clinical study. The Lancet infectious diseases *13*, 867-876.

Eder, J., Sedrani, R., and Wiesmann, C. (2014). The discovery of first-in-class drugs: origins and evolution. Nat Rev Drug Discov *13*, 577-587.

Ehmann, D.E., Jahić, H., Ross, P.L., Gu, R.-F., Hu, J., Kern, G., Walkup, G.K., and Fisher, S.L. (2012a). Avibactam is a covalent, reversible, non–β-lactam β-lactamase inhibitor. Proceedings of the National Academy of Sciences *109*, 11663-11668.

Ehmann, D.E., Jahic, H., Ross, P.L., Gu, R.F., Hu, J., Durand-Reville, T.F., Lahiri, S., Thresher, J., Livchak, S., Gao, N., *et al.* (2013a). Kinetics of avibactam inhibition against Class A, C, and D beta-lactamases. The Journal of biological chemistry *288*, 27960-27971.

Ehmann, D.E., Jahic, H., Ross, P.L., Gu, R.F., Hu, J., Durand-Réville, T.F., Lahiri, S., Thresher, J., Livchak, S., Gao, N., *et al.* (2013b). Kinetics of avibactam inhibition against Class A, C, and D β-lactamases. J Biol Chem *288*, 27960-27971.

Ehmann, D.E., Jahić, H., Ross, P.L., Gu, R.F., Hu, J., Kern, G., Walkup, G.K., and Fisher, S.L. (2012b). Avibactam is a covalent, reversible, non-β-lactam β-lactamase inhibitor. Proc Natl Acad Sci U S A *109*, 11663-11668.

Eisenmesser, E.Z., Millet, O., Labeikovsky, W., Korzhnev, D.M., Wolf-Watz, M., Bosco, D.A., Skalicky, J.J., Kay, L.E., and Kern, D. (2005). Intrinsic dynamics of an enzyme underlies catalysis. Nature *438*, 117-121.

Emsley, P., Lohkamp, B., Scott, W.G., and Cowtan, K. (2010). Features and development of Coot. Acta Crystallogr D Biol Crystallogr *66*, 486-501.

Endimiani, A., Hujer, K.M., Hujer, A.M., Pulse, M.E., Weiss, W.J., and Bonomo, R.A. (2011). Evaluation of Ceftazidime and NXL104 in Two Murine Models of Infection Due to KPC-Producing Klebsiella pneumoniae. Antimicrobial Agents and Chemotherapy *55*, 82-85.

English, A.R., Retsema, J.A., Girard, A.E., Lynch, J.E., and Barth, W.E. (1978). CP-45,899, a beta-lactamase inhibitor that extends the antibacterial spectrum of beta-lactams: initial bacteriological characterization. Antimicrob Agents Chemother *14*, 414-419.

Evans, B.A., and Amyes, S.G. (2014). OXA beta-lactamases. Clin Microbiol Rev *27*, 241-263.

EUCAST (2014). Breakpoint tables for interpretation of MICs and zone diameters. Version 4.0, 2014.

Fast, W., and Sutton, L.D. (2013). Metallo-beta-lactamase: inhibitors and reporter substrates. Biochimica et biophysica acta *1834*, 1648-1659.

Feng, B.Y., Shelat, A., Doman, T.N., Guy, R.K., and Shoichet, B.K. (2005). High-throughput assays for promiscuous inhibitors. Nat Chem Biol *1*, 146-148.

Feng, B.Y., and Shoichet, B.K. (2006). A detergent-based assay for the detection of promiscuous inhibitors. Nat Protoc *1*, 550-553.

Fink, A.L., and Page, M.I. (2012). The Mechanisms of Catalysis by Beta-Lactamases. In Beta-lactamases, J.M. Frere, ed. (Nova Science Publishers), pp. 161-198.

Fisher, J.F., Meroueh, S.O., and Mobashery, S. (2005). Bacterial Resistance to β-Lactam Antibiotics: Compelling Opportunism, Compelling Opportunity. Chemical reviews *105*, 395-424.

Fleming, A. (1922). On a remarkable bacteriolytic element found in tissues and secretions. Proceedings of the Royal Society of London B: Biological Sciences *93*, 306-317.

Fleming, A. (1929). On the antibacterial action of a *Penicillin*, with special reference to their use in the isolation of *B. influenza*. Brit J Exp Pathol, 226-236.

Forsberg, K.J., Reyes, A., Wang, B., Selleck, E.M., Sommer, M.O., and Dantas, G. (2012). The shared antibiotic resistome of soil bacteria and human pathogens. Science *337*, 1107-1111.

Frère, J.M., ed. (2011). beta-Lactamases (New York: Nova Science Publishers).

Frias, M., Tsai, V., Moulton-Meissner, H., Avillan, J., Epstein, L., Hunter, J., and Arwady, M.A. (2014). New Delhi Metallo-β-Lactamase–Producing *Escherichia coli* Associated with Endoscopic Retrograde Cholangiopancreatography — Illinois, 2013. MMWR *62*, 1051.

Ghuysen, J.M. (1991). Serine beta-lactamases and penicillin-binding proteins. Annu Rev Microbiol *45*, 37-67.

Golemi, D., Maveyraud, L., Vakulenko, S., Samama, J.P., and Mobashery, S. (2001). Critical involvement of a carbamylated lysine in catalytic function of class D beta-lactamases. Proc Natl Acad Sci U S A *98*, 14280-14285.

Gonzalez, J.M., Meini, M.R., Tomatis, P.E., Medrano Martin, F.J., Cricco, J.A., and Vila, A.J. (2012). Metallo-beta-lactamases withstand low Zn(II) conditions by tuning metal-ligand interactions. Nat Chem Biol *8*, 698-700.

Haenni, A.L., Robert, M., Vetter, W., Roux, L., Barbier, M., and Lederer, E. (1965). Structure chimique des aspergillomarasmines A et B. Helvetica Chimica Acta *48*, 729-750.

Hall, L.M., Livermore, D.M., Gur, D., Akova, M., and Akalin, H.E. (1993). OXA-11, an extended-spectrum variant of OXA-10 (PSE-2) beta-lactamase from Pseudomonas aeruginosa. Antimicrob Agents Chemother *37*, 1637-1644.

Harvey, A.L., Edrada-Ebel, R., and Quinn, R.J. (2015). The re-emergence of natural products for drug discovery in the genomics era. Nat Rev Drug Discov *14*, 111-129.

Hawkey, P.M., and Jones, A.M. (2009). The changing epidemiology of resistance. The Journal of antimicrobial chemotherapy *64 Suppl 1*, i3-10.

Hayes, M.V., and Orr, D.C. (1983). Mode of action of ceftazidime: affinity for the penicillin-binding proteins of Escherichia coli K12, Pseudomonas aeruginosa and Staphylococcus aureus. The Journal of antimicrobial chemotherapy *12*, 119-126.

Hecker, S.D., et al. (2015). Discovery of a New Series of Broad-spectrum Carbapenemase Inhibitors (BCIs) with Activity vs Serine and Metallo Beta-lactamases. In ICAAC 2015 (San Diego).

Helfand, M.S., Totir, M.A., Carey, M.P., Hujer, A.M., Bonomo, R.A., and Carey, P.R. (2003). Following the reactions of mechanism-based inhibitors with beta-lactamase by Raman crystallography. Biochemistry *42*, 13386-13392.

Hernandez Valladares, M., Felici, A., Weber, G., Adolph, H.W., Zeppezauer, M., Rossolini, G.M., Amicosante, G., Frere, J.M., and Galleni, M. (1997). Zn(II) dependence of the Aeromonas hydrophila AE036 metallo-beta-lactamase activity and stability. Biochemistry *36*, 11534-11541.

Heymes, R., Lutz, A., and Schrinner, E. (1977). Experimental evaluation of HR756, a new cephalosporin derivative: pre-clinical study. Infection *5*, 259-260.

Holmquist, B., Bunning, P., and Riordan, J.F. (1979). A continuous spectrophotometric assay for angiotensin converting enzyme. Anal Biochem *95*, 540-548.

Ishii, S., Hayashi, H., Okamoto, A., and Kagamiyama, H. (1998). Aromatic L-amino acid decarboxylase: conformational change in the flexible region around Arg334 is required during the transaldimination process. Protein Sci *7*, 1802-1810.

Jacoby, G.A. (2009). AmpC beta-lactamases. Clin Microbiol Rev *22*, 161-182, Table of Contents.

Kahan, J.S., Kahan, F.M., Goegelman, R., Currie, S.A., Jackson, M., Stapley, E.O., Miller, T.W., Miller, A.K., Hendlin, D., Mochales, S., *et al.* (1979). Thienamycin, a new beta-lactam antibiotic. I. Discovery, taxonomy, isolation and physical properties. J Antibiot (Tokyo) *32*, 1-12.

Kardos, N., and Demain, A.L. (2011). Penicillin: the medicine with the greatest impact on therapeutic outcomes. Applied microbiology and biotechnology *92*, 677-687.

Kerff, F., Sauvage, E., Vercheval, L., and Carlier, P. (2012). Structures of Class D Beta-lactamase. In Beta-lactamases, J.M. Frere, ed. (Nova Science Publishers), pp. 103-135.

Kiener, P.A., and Waley, S.G. (1978). Reversible inhibitors of penicillinases. Biochemical Journal *169*, 197-204.

King, A.M., Reid-Yu, S.A., Wang, W., King, D.T., De Pascale, G., Strynadka, N.C., Walsh, T.R., Coombes, B.K., and Wright, G.D. (2014). Aspergillomarasmine A overcomes metallo-beta-lactamase antibiotic resistance. Nature *510*, 503-506.

King, D., and Strynadka, N. (2011). Crystal structure of New Delhi metallo- β-lactamase reveals molecular basis for antibiotic resistance. Protein Science *20*, 1484-1491.

King, D.T., King, A.M., Lal, S.M., Wright, G.D., and Strynadka, N.C.J. (2015). Molecular Mechanism of Avibactam-Mediated β-Lactamase Inhibition. ACS Infect Dis *1*, 175-184.

King, D.T., Worrall, L.J., Gruninger, R., and Strynadka, N.C. (2012). New Delhi metallo-beta-lactamase: structural insights into beta-lactam recognition and inhibition. Journal of the American Chemical Society *134*, 11362-11365.

Kliebe, C., Nies, B.A., Meyer, J.F., Tolxdorff-Neutzling, R.M., and Wiedemann, B. (1985). Evolution of plasmid-coded resistance to broad-spectrum cephalosporins. Antimicrob Agents Chemother *28*, 302-307.

Knox, J.R., Moews, P.C., and Frere, J.M. (1996). Molecular evolution of bacterial beta-lactam resistance. Chem Biol *3*, 937-947.

Koteva, K., King, A.M., Capretta, A., and Wright, G.D. (2015). Total Synthesis and Activity of the Metallo-beta-lactamase Inhibitor Aspergillomarasmine A. Angew Chem Int Ed Engl.

Krause, T., Gerbershagen, M.U., Fiege, M., WeiBhorn, R., and Wappler, F. (2004). Dantrolene - A review of its pharmacology, therapeutic use and new developments. Anaesthesia *59*, 364-373.

Kumarasamy, K.K., Toleman, M.A., Walsh, T.R., Bagaria, J., Butt, F., Balakrishnan, R., Chaudhary, U., Doumith, M., Giske, C.G., Irfan, S., *et al.* (2010). Emergence of a new antibiotic resistance mechanism in India, Pakistan, and the UK: a molecular, biological, and epidemiological study. The Lancet Infectious Diseases *10*, 597-602.

Kuwabara, S., and Abraham, E.P. (1967). Some properties of two extracellular beta-lactamases from Bacillus cereus 569/H. The Biochemical journal *103*, 27C-30C.

Lagacé-Wiens, P., Walkty, A., and Karlowsky, J.A. (2014). Ceftazidime-avibactam: an evidence-based review of its pharmacology and potential use in the treatment of Gram-negative bacterial infections. Core Evid *9*, 13-25.

Lahiri, S.D., Mangani, S., Durand-Reville, T., Benvenuti, M., De Luca, F., Sanyal, G., and Docquier, J.D. (2013). Structural insight into potent broad-spectrum inhibition with reversible recyclization mechanism: avibactam in complex with CTX-M-15 and Pseudomonas aeruginosa AmpC β-lactamases. Antimicrob Agents Chemother *57*, 2496-2505.

Lahiri, S.D., Mangani, S., Jahić, H., Benvenuti, M., Durand-Reville, T.F., De Luca, F., Ehmann, D.E., Rossolini, G.M., Alm, R.A., and Docquier, J.D. (2014). Molecular Basis of Selective Inhibition and Slow Reversibility of Avibactam against Class D Carbapenemases: A Structure-Guided Study of OXA-24 and OXA-48. ACS Chem Biol.

Lamotte-Brasseur, J., Dive, G., Dideberg, O., Charlier, P., Frère, J.M., and Ghuysen, J.M. (1991). Mechanism of acyl transfer by the class A serine beta-lactamase of Streptomyces albus G. Biochem J *279 (Pt 1)*, 213-221.

Laraki, N., Franceschini, N., Rossolini, G.M., Santucci, P., Meunier, C., de Pauw, E., Amicosante, G., Frere, J.M., and Galleni, M. (1999). Biochemical Characterization of the Pseudomonas aeruginosa 101/1477 Metallo-beta-Lactamase IMP-1 Produced byEscherichia coli. Antimicrobial Agents and Chemotherapy *43*, 902-906.

Laskowski, R.A., and Swindells, M.B. (2011). LigPlot+: multiple ligand-protein interaction diagrams for drug discovery. J Chem Inf Model *51*, 2778-2786.

Lauretti, L., Riccio, M.L., Mazzariol, A., Cornaglia, G., Amicosante, G., Fontana, R., and Rossolini, G.M. (1999). Cloning and characterization of blaVIM, a new integron-borne metallo-beta-lactamase gene from a Pseudomonas aeruginosa clinical isolate. Antimicrob Agents Chemother *43*, 1584-1590.

Lee, M., Hesek, D., and Mobashery, S. (2005a). A practical synthesis of nitrocefin. J Org Chem *70*, 367-369.

Lee, M., Hesek, D., and Mobashery, S. (2005b). A Practical Synthesis of Nitrocefin. The Journal of organic chemistry *70*, 367-369.

Lewis, K. (2012). Antibiotics: Recover the lost art of drug discovery. Nature *485*, 439-440.

Li, L., Liu, F., and Li, H.-W. (2011). Selective fluorescent probes based on CN isomerization and intramolecular charge transfer (ICT) for zinc ions in aqueous solution. Spectrochimica Acta Part A: Molecular and Biomolecular Spectroscopy *79*, 1688-1692.

Liao, D., Yang, S., Wang, J., Zhang, J., Hong, B., Wu, F., and Lei, X. (2015). Total Synthesis and Structural Reassignment of Aspergillomarasmine A. Angew Chem Int Ed Engl.

Lim, D., and Strynadka, N.C. (2002). Structural basis for the beta lactam resistance of PBP2a from methicillin-resistant Staphylococcus aureus. Nat Struct Biol *9*, 870-876.

Lipinski, C.A., Lombardo, F., Dominy, B.W., and Feeney, P.J. (2001). Experimental and computational approaches to estimate solubility and permeability in drug discovery and development settings. Adv Drug Deliv Rev *46*, 3-26.

Liu, Y.Y., Wang, Y., Walsh, T.R., Yi, L.X., Zhang, R., Spencer, J., Doi, Y., Tian, G., Dong, B., Huang, X., *et al.* (2015). Emergence of plasmid-mediated colistin resistance mechanism MCR-1 in animals and human beings in China: a microbiological and molecular biological study. The Lancet Infectious diseases.

Llarrull, L.I., Fabiane, S.M., Kowalski, J.M., Bennett, B., Sutton, B.J., and Vila, A.J. (2007). Asp-120 Locates Zn2 for Optimal Metallo-β-lactamase Activity. Journal of Biological Chemistry *282*, 18276-18285.

Macarron, R., Banks, M.N., Bojanic, D., Burns, D.J., Cirovic, D.A., Garyantes, T., Green, D.V., Hertzberg, R.P., Janzen, W.P., Paslay, J.W., *et al.* (2011). Impact of high-throughput screening in biomedical research. Nat Rev Drug Discov *10*, 188-195.

Maiti, S.N., Nguyen, D., Khan, J., and Ling, R. (2013). New bicyclic compounds and their use as antibacterial agents and beta-lactamase inhibitors (U.S.: NAEJA PHARMACEUTICAL INC.).

Majiduddin, F.K., Materon, I.C., and Palzkill, T.G. (2002). Molecular analysis of beta-lactamase structure and function. Int J Med Microbiol *292*, 127-137.

Marra, A., Lamb, L., Medina, I., George, D., Gibson, G., Hardink, J., Rugg, J., Van Deusen, J., and O'Donnell, J.P. (2012). Effect of linezolid on the 50% lethal dose and 50% protective dose in treatment of infections by Gram-negative pathogens in naive and immunosuppressed mice and on the efficacy of ciprofloxacin in an acute murine model of septicemia. Antimicrob Agents Chemother *56*, 4671-4675.

Matsuura, A., Okumura, H., Asakura, R., Ashizawa, N., Takahashi, M., Kobayashi, F., Ashikawa, N., and Arai, K. (1993a). Pharmacological profiles of aspergillomarasmines as endothelin converting enzyme inhibitors. Japanese journal of pharmacology *63*, 187-193.

Matsuura, A., Okumura, H., Asakura, R., Ashizawa, N., Takahashi, M., Kobayashi, F., Ashikawa, N., and Arai, K. (1993b). Pharmacological Profiles of Aspergillomarasmines as Endothelin Converting Enzyme Inhibitors. The Japanese Journal of Pharmacology *63*, 187-193.

Mazzariol, A., Mammina, C., Koncan, R., Di Gaetano, V., Di Carlo, P., Cipolla, D., Corsello, G., and Cornaglia, G. (2011). A novel VIM-type metallo-beta-lactamase (VIM-14) in a Pseudomonas aeruginosa clinical isolate from a neonatal intensive care unit. Clin Microbiol Infect *17*, 722-724.

McCoy, A.J., Grosse-Kunstleve, R.W., Adams, P.D., Winn, M.D., Storoni, L.C., and Read, R.J. (2007). Phaser crystallographic software. J Appl Crystallogr *40*, 658-674.

McQuarrie, E., Liebmann, A., Kluener, R., and Venosa, A. (1944). Studies on penicillinase. Arch Biochem *5*, 307-315.

Meini, M.R., Llarrull, L.I., and Vila, A.J. (2015). Overcoming differences: The catalytic mechanism of metallo-beta-lactamases. FEBS Lett *589*, 3419-3432.

Mendes, R.E., Rhomberg, P.R., Becker, H.K., and Jones, R.N. (2013). β-lactam Activity Tested in Combination with β-lactamase Inhibitor Candidates against Enterobacteriaceae Producing Class A, B and D Carbapenemases Paper presented at: ICAAC (Denver, CO).

Meroueh, S.O., Fisher, J.F., Schlegel, H.B., and Mobashery, S. (2005). Ab initio QM/MM study of class A beta-lactamase acylation: dual participation of Glu166 and Lys73 in a concerted base promotion of Ser70. J Am Chem Soc *127*, 15397-15407.

Mikami, Y., and Suzuki, T. (1983). Novel microbial inhibitors of angiotensin-converting enzyme, aspergillomarasmines A and B. Agric Biol Chem *47*, 2693-2695.

Mileni, M., Kamtekar, S., Wood, D.C., Benson, T.E., Cravatt, B.F., and Stevens, R.C. (2010). Crystal structure of fatty acid amide hydrolase bound to the carbamate inhibitor URB597: discovery of a deacylating water molecule and insight into enzyme inactivation. J Mol Biol *400*, 743-754.

Minasov, G., Wang, X., and Shoichet, B.K. (2002). An ultrahigh resolution structure of TEM-1 beta-lactamase suggests a role for Glu166 as the general base in acylation. J Am Chem Soc *124*, 5333-5340.

Minond, D., Saldanha, S.A., Subramaniam, P., Spaargaren, M., Spicer, T., Fotsing, J.R., Weide, T., Fokin, V.V., Sharpless, K.B., Galleni, M., *et al.* (2009). Inhibitors of VIM-2 by screening pharmacologically active and click-chemistry compound libraries. Bioorganic & medicinal chemistry *17*, 5027-5037.

Mojica, M.F., Bonomo, R.A., and Fast, W. (2015). B1-Metallo-beta-Lactamases: Where do we stand? Curr Drug Targets.

Moosdeen, F., Williams, J.D., and Yamabe, S. (1988). Antibacterial characteristics of YTR 830, a sulfone beta-lactamase inhibitor, compared with those of clavulanic acid and sulbactam. Antimicrob Agents Chemother *32*, 925-927.

Morar, M., and Wright, G.D. (2010). The genomic enzymology of antibiotic resistance. Annu Rev Genet *44*, 25-51.

Morin, R.B., Jackson, B.G., Flynn, E.H., and Roeske, R.W. (1962). Chemistry of Cephalosporin Antibiotics. I. 7-Aminocephalosporanic Acid from Cephalosporin C. Journal of the American Chemical Society *84*, 3400-3401.

Morinaka, A., Tsutsumi, Y., Yamada, M., Suzuki, K., Watanabe, T., Abe, T., Furuuchi, T., Inamura, S., Sakamaki, Y., Mitsuhashi, N., *et al.* (2015). OP0595, a new

diazabicyclooctane: mode of action as a serine beta-lactamase inhibitor, antibiotic and beta-lactam 'enhancer'. The Journal of antimicrobial chemotherapy.

Morrison, J.F., and Walsh, C.T. (1988). The behaviour and significance of slow-binding enzyme inhibitors. Advances in Enzymology and Related Areas of Molecular Biology *61*, 201.

Munoz-Price, L.S., Poirel, L., Bonomo, R.A., Schwaber, M.J., Daikos, G.L., Cormican, M., Cornaglia, G., Garau, J., Gniadkowski, M., Hayden, M.K., *et al.* (2013). Clinical epidemiology of the global expansion of Klebsiella pneumoniae carbapenemases. The Lancet Infectious diseases *13*, 785-796.

Murphy, T.A., Catto, L.E., Halford, S.E., Hadfield, A.T., Minor, W., Walsh, T.R., and Spencer, J. (2006). Crystal structure of Pseudomonas aeruginosa SPM-1 provides insights into variable zinc affinity of metallo-beta-lactamases. J Mol Biol *357*, 890-903.

Murphy, T.A., Simm, A.M., Toleman, M.A., Jones, R.N., and Walsh, T.R. (2003). Biochemical characterization of the acquired metallo-beta-lactamase SPM-1 from Pseudomonas aeruginosa. Antimicrob Agents Chemother *47*, 582-587.

Nagarajan, R., Boeck, L.D., Gorman, M., Hamill, R.L., Higgens, C.E., Hoehn, M.M., Stark, W.M., and Whitney, J.G. (1971). Beta-lactam antibiotics from Streptomyces. J Am Chem Soc *93*, 2308-2310.

Neu, H.C. (1982). The new beta-lactamase-stable cephalosporins. Ann Intern Med *97*, 408-419.

Neu, H.C., and Fu, K.P. (1978). Clavulanic acid, a novel inhibitor of beta-lactamases. Antimicrob Agents Chemother *14*, 650-655.

Newton, G.G., and Abraham, E.P. (1956). Isolation of cephalosporin C, a penicillin-like antibiotic containing D-alpha-aminoadipic acid. The Biochemical journal *62*, 651-658.

Nukaga, M., Mayama, K., Hujer, A.M., Bonomo, R.A., and Knox, J.R. (2003). Ultrahigh resolution structure of a class A beta-lactamase: on the mechanism and specificity of the extended-spectrum SHV-2 enzyme. J Mol Biol *328*, 289-301.

O'Shea, R., and Moser, H.E. (2008). Physicochemical properties of antibacterial compounds: implications for drug discovery. J Med Chem *51*, 2871-2878.

Obana, Y., and Nishino, T. (1990). In-vitro and in-vivo activities of sulbactam and YTR830H against Acinetobacter calcoaceticus. The Journal of antimicrobial chemotherapy *26*, 677-682.

Oelschlaeger, P., Ai, N., DuPrez, K.T., Welsh, W.J., and Toney, J.H. (2010). Evolving Carbapenemases: Can Medicinal Chemists Advance One Step Ahead of the Coming Storm? Journal of medicinal chemistry *53*, 3013-3027.

Paetzel, M., Danel, F., de Castro, L., Mosimann, S.C., Page, M.G., and Strynadka, N.C. (2000). Crystal structure of the class D beta-lactamase OXA-10. Nat Struct Biol *7*, 918-925.

Palzkill, T. (2013). Metallo-beta-lactamase structure and function. Ann N Y Acad Sci *1277*, 91-104.

Patel, G., and Bonomo, R.A. (2013). "Stormy waters ahead": global emergence of carbapenemases. Frontiers in microbiology *4*, 48.

Pattabiraman, V.R., and Bode, J.W. (2011). Rethinking amide bond synthesis. Nature *480*, 471-479.

Payne, D.J., Gwynn, M.N., Holmes, D.J., and Pompliano, D.L. (2007). Drugs for bad bugs: confronting the challenges of antibacterial discovery. Nat Rev Drug Discov *6*, 29-40.

Peirano, G., and Pitout, J.D.D. (2010). Molecular epidemiology of Escherichia coli producing CTX-M β-lactamases: the worldwide emergence of clone ST131 O25:H4. International Journal of Antimicrobial Agents *35*, 316-321.

Pérez-Llarena, F.J., Kerff, F., Abián, O., Mallo, S., Fernández, M.C., Galleni, M., Sancho, J., and Bou, G. (2011). Distant and new mutations in CTX-M-1 beta-lactamase affect cefotaxime hydrolysis. Antimicrob Agents Chemother *55*, 4361-4368.

Petersen, T.N., Brunak, S., von Heijne, G., and Nielsen, H. (2011). SignalP 4.0: discriminating signal peptides from transmembrane regions. Nature methods *8*, 785-786.

Pillai, S.K., Moellering Jr, R.C., and Eliopoulos, G.M. (2005). Antimicrobial combinations. In Antibiotics in Laboratory Medicine V. Lorian, ed. (Philadelphia, PA: Williams & Wilkins, Philadelphia), pp. 365-440.

Pitout, J.D., and Laupland, K.B. (2008). Extended-spectrum beta-lactamase-producing Enterobacteriaceae: an emerging public-health concern. The Lancet infectious diseases *8*, 159-166.

Poirel, L., Dortet, L., Bernabeu, S., and Nordmann, P. (2011). Genetic features of blaNDM-1-positive Enterobacteriaceae. Antimicrob Agents Chemother *55*, 5403-5407.

Poirel, L., Heritier, C., Tolun, V., and Nordmann, P. (2004). Emergence of oxacillinase-mediated resistance to imipenem in Klebsiella pneumoniae. Antimicrob Agents Chemother *48*, 15-22.

Poirel, L., Nordmann, P., Ducroz, S., Boulouis, H.J., Arné, P., and Millemann, Y. (2013). Extended-spectrum β-lactamase CTX-M-15-producing Klebsiella pneumoniae of sequence type ST274 in companion animals. Antimicrob Agents Chemother *57*, 2372-2375.

Pratt, R.F. (2012). Beat-lactamase Inhibitors: Non-Beta-Lactams. In Beta-lactamases, J.M. Frere, ed. (Nova Science Publishers), pp. 259-292.

Queenan, A.M., and Bush, K. (2007). Carbapenemases: the Versatile β-Lactamases. Clinical microbiology reviews *20*, 440-458.

Reading, C., and Cole, M. (1977). Clavulanic Acid: a Beta-Lactamase-Inhibiting Beta-Lactam from Streptomyces clavuligerus. Antimicrobial Agents and Chemotherapy *11*, 852-857.

Ricci, D.P., and Silhavy, T.J. (2012). The Bam machine: a molecular cooper. Biochimica et biophysica acta *1818*, 1067-1084.

Rodríguez-Martínez, J.-M., Poirel, L., and Nordmann, P. (2009). Molecular Epidemiology and Mechanisms of Carbapenem Resistance in Pseudomonas aeruginosa. Antimicrobial Agents and Chemotherapy *53*, 4783-4788.

Rolinson, G.N. (1998). Forty years of beta-lactam research. The Journal of antimicrobial chemotherapy *41*, 589-603.

Rubin, R. (2015). New Antibacterial Drug Approved. JAMA *313*.

Sader, H.S., Farrell, D.J., Flamm, R.K., and Jones, R.N. (2014). Antimicrobial susceptibility of Gram-negative organisms isolated from patients hospitalized in intensive care units in United States and European hospitals (2009-2011). Diagn Microbiol Infect Dis *78*, 443-448.

Samson, R.A., Hadlok, R., and Stolk, A.C. (1977). A taxonomic study of the Penicillium chrysogenum series. Antonie Van Leeuwenhoek *43*, 169-175.

Schneider, C.A., Rasband, W.S., and Eliceiri, K.W. (2012). NIH Image to ImageJ: 25 years of image analysis. Nat Methods *9*, 671-675.

Schneider, K.D., Karpen, M.E., Bonomo, R.A., Leonard, D.A., and Powers, R.A. (2009). The 1.4 A crystal structure of the class D beta-lactamase OXA-1 complexed with doripenem. Biochemistry *48*, 11840-11847.

Schrodinger, LLC (2015). The PyMOL Molecular Graphics System, Version 1.8.

Schüttelkopf, A.W., and van Aalten, D.M. (2004). PRODRG: a tool for high-throughput crystallography of protein-ligand complexes. Acta Crystallogr D Biol Crystallogr *60*, 1355-1363.

Shen, H., Kannari, K., Yamato, H., Arai, A., and Matsunaga, M. (2003). Effects of Benserazide on L-DOPA-Derived Extracellular Dopamine Levels and Aromatic L-Amino Acid Decarboxylase Activity in the Striatum of 6-Hydroxydopamine-Lesioned Rats. The Tohoku journal of experimental medicine *199*, 149-159.

Shimamura, T., Ibuka, A., Fushinobu, S., Wakagi, T., Ishiguro, M., Ishii, Y., and Matsuzawa, H. (2002). Acyl-intermediate structures of the extended-spectrum class A beta-lactamase, Toho-1, in complex with cefotaxime, cephalothin, and benzylpenicillin. J Biol Chem *277*, 46601-46608.

Shlaes, D.M. (2013). New beta-lactam-beta-lactamase inhibitor combinations in clinical development. Annals of the New York Academy of Sciences *1277*, 105-114.

Sidjabat, H.E., Paterson, D.L., Qureshi, Z.A., Adams-Haduch, J.M., O'Keefe, A., Pascual, A., Rodriguez-Bano, J., and Doi, Y. (2009). Clinical features and molecular epidemiology of CMY-type beta-lactamase-producing Escherichia coli. Clin Infect Dis *48*, 739-744.

Simona, F., Magistrato, A., Dal Peraro, M., Cavalli, A., Vila, A.J., and Carloni, P. (2009). Common Mechanistic Features among Metallo-β-lactamases: A COMPUTATIONAL STUDY OF AEROMONAS HYDROPHILA CphA ENZYME. Journal of Biological Chemistry *284*, 28164-28171.

Spanogiannopoulos, P., Waglechner, N., Koteva, K., and Wright, G.D. (2014). A rifamycin inactivating phosphotransferase family shared by environmental and pathogenic bacteria. Proc Natl Acad Sci U S A *111*, 7102-7107.

Spellberg, B. (2014). The future of antibiotics. Crit Care *18*, 228.

Spellberg, B., Bartlett, J.G., and Gilbert, D.N. (2013). The future of antibiotics and resistance. N Engl J Med *368*, 299-302.

Spellberg, B., and Taylor-Blake, B. (2013). On the exoneration of Dr. William H. Stewart: debunking an urban legend. Infect Dis Poverty *2*, 3.

Spratt, B.G. (1980). Biochemical and genetical approaches to the mechanism of action of penicillin. Philos Trans R Soc Lond B Biol Sci *289*, 273-283.

Stachyra, T., Péchereau, M.-C., Bruneau, J.-M., Claudon, M., Frère, J.-M., Miossec, C., Coleman, K., and Black, M.T. (2010). Mechanistic Studies of the Inactivation of TEM-1 and P99 by NXL104, a Novel Non-β-Lactam β-Lactamase Inhibitor. Antimicrobial Agents and Chemotherapy *54*, 5132-5138.

Strynadka, N.C., Adachi, H., Jensen, S.E., Johns, K., Sielecki, A., Betzel, C., Sutoh, K., and James, M.N. (1992). Molecular structure of the acyl-enzyme intermediate in beta-lactam hydrolysis at 1.7 A resolution. Nature *359*, 700-705.

Sumita, Y., and Fukasawa, M. (1995). Potent activity of meropenem against Escherichia coli arising from its simultaneous binding to penicillin-binding proteins 2 and 3. The Journal of antimicrobial chemotherapy *36*, 53-64.

Sykes, R.B., and Matthew, M. (1976). The beta-lactamases of gram-negative bacteria and their role in resistance to beta-lactam antibiotics. The Journal of antimicrobial chemotherapy *2*, 115-157.

Thomas, P.W., Zheng, M., Wu, S., Guo, H., Liu, D., Xu, D., and Fast, W. (2011). Characterization of Purified New Delhi Metallo- β-lactamase-1. Biochemistry *50*, 10102-10113.

Tioni, M.F., Llarrull, L.I., Poeylaut-Palena, A.A., Marti, M.A., Saggu, M., Periyannan, G.R., Mata, E.G., Bennett, B., Murgida, D.H., and Vila, A.J. (2008). Trapping and

characterization of a reaction intermediate in carbapenem hydrolysis by B. cereus metallo-beta-lactamase. J Am Chem Soc *130*, 15852-15863.

Tipper, D.J. (1985). Mode of action of beta-lactam antibiotics. Pharmacology & therapeutics *27*, 1-35.

Tipper, D.J., and Strominger, J.L. (1965). Mechanism of action of penicillins: a proposal based on their structural similarity to acyl-D-alanyl-D-alanine. Proc Natl Acad Sci U S A *54*, 1133-1141.

Tommasi, R., Brown, D.G., Walkup, G.K., Manchester, J.I., and Miller, A.A. (2015). ESKAPEing the labyrinth of antibacterial discovery. Nat Rev Drug Discov *14*, 529-542.

Van Boeckel, T.P., Gandra, S., Ashok, A., Caudron, Q., Grenfell, B.T., Levin, S.A., and Laxminarayan, R. (2014). Global antibiotic consumption 2000 to 2010: an analysis of national pharmaceutical sales data. The Lancet Infectious diseases *14*, 742-750.

van den Ent, F., and Löwe, J. (2006). RF cloning: a restriction-free method for inserting target genes into plasmids. J Biochem Biophys Methods *67*, 67-74.

Wagenaar, M.M. (2008). Pre-fractionated microbial samples--the second generation natural products library at Wyeth. Molecules *13*, 1406-1426.

Walkup, G.K., You, Z., Ross, P.L., Allen, E.K., Daryaee, F., Hale, M.R., O'Donnell, J., Ehmann, D.E., Schuck, V.J., Buurman, E.T., *et al.* (2015). Translating slow-binding inhibition kinetics into cellular and in vivo effects. Nat Chem Biol *11*, 416-423.

Walsh, C. (2003). Where will new antibiotics come from? Nat Rev Microbiol *1*, 65-70.

Walsh, T.R., Weeks, J., Livermore, D.M., and Toleman, M.A. (2011). Dissemination of NDM-1 positive bacteria in the New Delhi environment and its implications for human health: an environmental point prevalence study. The Lancet Infectious Diseases *11*, 355-362.

Wang, Z., Fast, W., and Benkovic, S.J. (1999). On the mechanism of the metallo-beta-lactamase from Bacteroides fragilis. Biochemistry *38*, 10013-10023.

Watanabe, M., Iyobe, S., Inoue, M., and Mitsuhashi, S. (1991). Transferable imipenem resistance in Pseudomonas aeruginosa. Antimicrob Agents Chemother *35*, 147-151.

Waxman, D.J., and Strominger, J.L. (1983). Penicillin-binding proteins and the mechanism of action of beta-lactam antibiotics. Annu Rev Biochem *52*, 825-869.

Waxman, D.J., Yocum, R.R., and Strominger, J.L. (1980). Penicillins and Cephalosporins are Active Site-Directed Acylating Agents: Evidence in Support of the Substrate Analogue Hypothesis. Philosophical Transactions of the Royal Society of London B: Biological Sciences *289*, 257-271.

Winn, M.D., Ballard, C.C., Cowtan, K.D., Dodson, E.J., Emsley, P., Evans, P.R., Keegan, R.M., Krissinel, E.B., Leslie, A.G., McCoy, A., *et al.* (2011). Overview of the CCP4 suite and current developments. Acta Crystallogr D Biol Crystallogr *67*, 235-242.

Winter, G., Lobley, C.M., and Prince, S.M. (2013). Decision making in xia2. Acta Crystallogr D Biol Crystallogr *69*, 1260-1273.

Wommer, S., Rival, S., Heinz, U., Galleni, M., Frere, J.M., Franceschini, N., Amicosante, G., Rasmussen, B., Bauer, R., and Adolph, H.W. (2002). Substrate-activated zinc binding of metallo-beta -lactamases: physiological importance of mononuclear enzymes. The Journal of biological chemistry *277*, 24142-24147.

Wouters, J., and Bauvois, C. (2012). Structures of Class C beta-lactamases and Perspectives in Drug Design. In Beta-lactamases, J.M. Frere, ed. (Nova Science Publishers), pp. 79-101.

Wright, G.D. (2011). Molecular mechanisms of antibiotic resistance. Chem Commun (Camb) *47*, 4055-4061.

Xu, H., Hazra, S., and Blanchard, J.S. (2012). NXL104 irreversibly inhibits the β-lactamase from Mycobacterium tuberculosis. Biochemistry *51*, 4551-4557.

Yang, H., Aitha, M., Hetrick, A.M., Richmond, T.K., Tierney, D.L., and Crowder, M.W. (2012). Mechanistic and spectroscopic studies of metallo-beta-lactamase NDM-1. Biochemistry *51*, 3839-3847.

Yang, Q., Li, Y., Dou, D., Gan, X., Mohan, S., Groutas, C.S., Stevenson, L.E., Lai, Z., Alliston, K.R., Zhong, J., *et al.* (2008). Inhibition of serine proteases by a new class of cyclosulfamide-based carbamylating agents. Arch Biochem Biophys *475*, 115-120.

Yasuyuki, F., Noriaki, O., Masayuki, H., Tetsu, N., Kenji, Y., Ryutaro, S., Atsushi, S., Noriyuki, F., Takahiro, K., Hideaki, F., Atsushi, K., Toshikazu, E., Saburo, N., Tyuji, H. (2003). Molecular Dynamics Study on Class A β-Lactamase: Hydrogen Bond Network among the Functional Groups of Penicillin G and Side Chains of the Conserved Residues in the Active Site (*J. Phys. Chem.*), pp. 10274-10283.

Yigit, H., Queenan, A.M., Anderson, G.J., Domenech-Sanchez, A., Biddle, J.W., Steward, C.D., Alberti, S., Bush, K., and Tenover, F.C. (2001a). Novel carbapenem-hydrolyzing beta-lactamase, KPC-1, from a carbapenem-resistant strain of Klebsiella pneumoniae. Antimicrobial agents and chemotherapy *45*, 1151-1161.

Yigit, H., Queenan, A.M., Anderson, G.J., Domenech-Sanchez, A., Biddle, J.W., Steward, C.D., Alberti, S., Bush, K., and Tenover, F.C. (2001b). Novel Carbapenem-Hydrolyzing ß-Lactamase, KPC-1, from a Carbapenem-Resistant Strain of Klebsiella pneumoniae. Antimicrobial Agents and Chemotherapy *45*, 1151-1161.

Yigit, H., Queenan, A.M., Anderson, G.J., Domenech-Sanchez, A., Biddle, J.W., Steward, C.D., Alberti, S., Bush, K., and Tenover, F.C. (2008). Novel Carbapenem-Hydrolyzing β-Lactamase, KPC-1, from a Carbapenem-Resistant Strain of Klebsiella pneumoniae. Antimicrobial Agents and Chemotherapy *52*, 809.

Yong, D., Toleman, M.A., Giske, C.G., Cho, H.S., Sundman, K., Lee, K., and Walsh, T.R. (2009). Characterization of a New Metallo-{beta}-Lactamase Gene, blaNDM-1, and a Novel Erythromycin Esterase Gene Carried on a Unique Genetic Structure in Klebsiella pneumoniae Sequence Type 14 from India. Antimicrobial Agents and Chemotherapy *53*, 5046-5054.

Zhang, J.H., Chung, T.D., and Oldenburg, K.R. (1999). A Simple Statistical Parameter for Use in Evaluation and Validation of High Throughput Screening Assays. Journal of biomolecular screening *4*, 67-73.

Zhang, L., Lü, X., and Zong, Z. (2013). The emergence of blaCTX-M-15-carrying Escherichia coli of ST131 and new sequence types in Western China. Ann Clin Microbiol Antimicrob *12*, 35.

Zhao, W.H., and Hu, Z.Q. (2011). IMP-type metallo-beta-lactamases in Gram-negative bacilli: distribution, phylogeny, and association with integrons. Crit Rev Microbiol *37*, 214-226.